DOE/CH/10435-02

# RESEARCH AND DEVELOPMENT OF PROTON-EXCHANGE-MEMBRANE (PEM) FUEL CELL SYSTEM FOR TRANSPORTATION APPLICATIONS



PHASE I. FINAL REPORT

CONTRACT NO. DE-AC02-90CH10435

January 1996

PREPARED FOR:

U.S. DEPARTMENT OF ENERGY
OFFICE OF TRANSPORTATION TECHNOLOGIES

PREPARED BY:

ALLISON GAS TURBINE DIVISION
GENERAL MOTORS CORPORATION
INDIANAPOLIS, IN 46206

## DISCLAIMER



Reproduced from the best available copy.

Available to DOE and DOE contractors from the
Office of Scientific and Technical Information
P.O. Box 62
Oak Ridge, TN 37831
Prices available from (423) 576-8401

Available to the public from the
National Technical Information Service
U.S. Department of Commerce
5285 Port Royal Road
Springfield, VA 22161

DOE/CH/10435-02

# RESEARCH AND DEVELOPMENT OF PROTON-EXCHANGE-MEMBRANE (PEM) FUEL CELL SYSTEM FOR TRANSPORTATION APPLICATIONS

PHASE I. FINAL REPORT

CONTRACT NO. DE-AC02-90CH10435

January 1996

Prepared for:

U.S. Department of Energy
Office of Transportation Technologies

Prepared by:

Allison Gas Turbine Division
General Motors Corporation
Indianapolis, IN 46206

## FOREWORD

This report documents the results of "Research and Development of Proton-Exchange-Membrane (PEM) Fuel Cell System for Transportation Applications" performed by the Allison Gas Turbine Division of General Motors Corporation under contract DE-AC02-90CH10435. The objective during Phase I was to develop a methanol-fueled 10-kW fuel cell power source and evaluate its feasibility for transportation applications. Specifically, this report documents research on component (fuel cell stack, fuel processor, power source ancillaries and system sensors) development and the 10-kW power source system integration and test. The conceptual design study for a PEM fuel cell powered vehicle was documented in an earlier report (DOE/CH/10435-01) and is summarized herein.

Major achievements in the program include development of advanced membrane and thin-film low Pt-loaded electrode assemblies that in reference cell testing with reformate-air reactants yielded performance exceeding the program target (0.7 V at 1000 amps/$ft^2$); identification of oxidation catalysts and operating conditions that routinely result in very low CO levels ($\leq$10 ppm) in the fuel processor reformate, thus avoiding degradation of the fuel cell stack performance; and successful integrated operation of a 10-kW fuel cell stack on reformate from the fuel processor.

The General Motors (GM) team which carried out this work is as follows:

- Allison Gas Turbine Division of GM served as prime contractor and provided the system integration and advanced power system design
- GM's North American Operations Research and Development (NAO R&D) Center provided membrane and electrode research, and hybrid electric vehicle and electrical power train expertise for the vehicle conceptual design studies
- GM's AC Rochester Division provided catalyst expertise, fuel metering hardware, and sensor development
- Los Alamos National Laboratory (LANL), through the Joint Development Center staffed by both Allison and LANL personnel, provided the expertise and facilities for fuel processor development and the system integration and testing of the 10-kW fuel cell system
- Ballard Power Systems provided the fuel cell stacks
- Dow Chemical Company supplied advanced membranes and electrodes
- The Analytic Sciences Corporation and DAKO Services provided input to the conceptual design studies

The preparation of this report represents a joint effort between Allison, LANL, and NAO R&D Power Systems Research Department.

This work was funded by the U.S. Department of Energy (DOE), Energy Efficiency and Renewable Energy, Office of Transportation Technologies, Office of Propulsion Systems, Electric/Hybrid Propulsion Division. Project and technical management was provided by Dr. Pandit Patil and Mr. Robert Kost of DOE's Electric/Hybrid Propulsion Division with technical oversight and advice provided by Mr. Clinton Christianson and Dr. James Miller of Argonne National Laboratory. Dr. Howard Creveling and Dr. Robert Sutton of Allison Gas Turbine Division of General Motors were the Program Manager and the Technical Director, respectively, for this project.

Steven G. Chalk
Manager, Fuel Cell Systems R&D
Office of Transportation Technologies
U.S. Department of Energy

# Table of Contents

# List of Illustrations

# List of Tables

# I. INTRODUCTION AND EXECUTIVE SUMMARY

## 1.1 PROGRAM BACKGROUND, SCOPE, AND SCHEDULE

### 1.1.1 Background And Functional Organization

Increasing environmental and strategic fuel concerns and a potentially changing fuel base continue to dictate the need for advanced vehicular power plants that exhibit improved fuel efficiency, reduced emissions, and alternative fuel capability. The electric vehicle has been suggested as one means of decoupling petroleum from the transportation sector and dramatically reducing vehicular environmental emissions. Some form of a hybrid power system could be beneficial in extending the overall range and load carrying capacity of today's battery-powered electric vehicles. Among the candidate power plants for the engine/charging component within the hybrid system, the indirect methanol PEM fuel cell is potentially the most efficient, as the device is unrestricted by heat engine (Carnot cycle) limitations. GM, under contract to the U.S. DoE, has completed the first phase of a program to develop and test an electrochemical engine (ECE), a methanol-powered reformate-air PEM fuel cell power plant. The intent of this overall program is to define the feasibility of such an engine for future transportation applications. The planned overall program includes proof-of-concept testing in vehicles of a selected type.

The ECE in this program is an electrical power producing machine formed by integration of components including: (1) a fuel processor which converts liquid methanol to a hydrogen rich gas, (2) PEM fuel cell power stacks fueled by reformate and air as the oxidant for electrochemical conversion, (3) ancillary equipment (air turbocompressor, pumps and heat exchangers, etc), and (4) an ECE control system. Similar to an internal combustion engine this ECE consumes a liquid fuel, but the ECE converts the fuel energy directly to electrical energy. The ECE is projected to feature sharply lowered emissions, high thermodynamic efficiency with concurrent decreased carbon dioxide production, and convenient refueling.

The first phase contract effort has emphasized the development of critical technologies necessary for success of this propulsion system concept. The program has used expertise at GM, LANL, Dow, Ballard, and other vendors. The functional organization of the Phase I program team, in which GM is depicted acting through its Allison Gas Turbine Division as prime contractor, is presented in Figure 1.1.1-1. A key element of this effort involved the system engineering and integration of all components into a 10-kW power plant.

### 1.1.2 Program Scope and Achievements

Phase I effort was set forth in detail in the Program Management Plan (Allison EDR 15105) and has included:

- System Conceptual Design Study
- Component Research and Development
- Fuel Cell Stack and Methanol Fuel Processor Development
- Power Source Ancillaries, Sensors, and Control Development
- Integration and Evaluation of a 10-kW Power Source

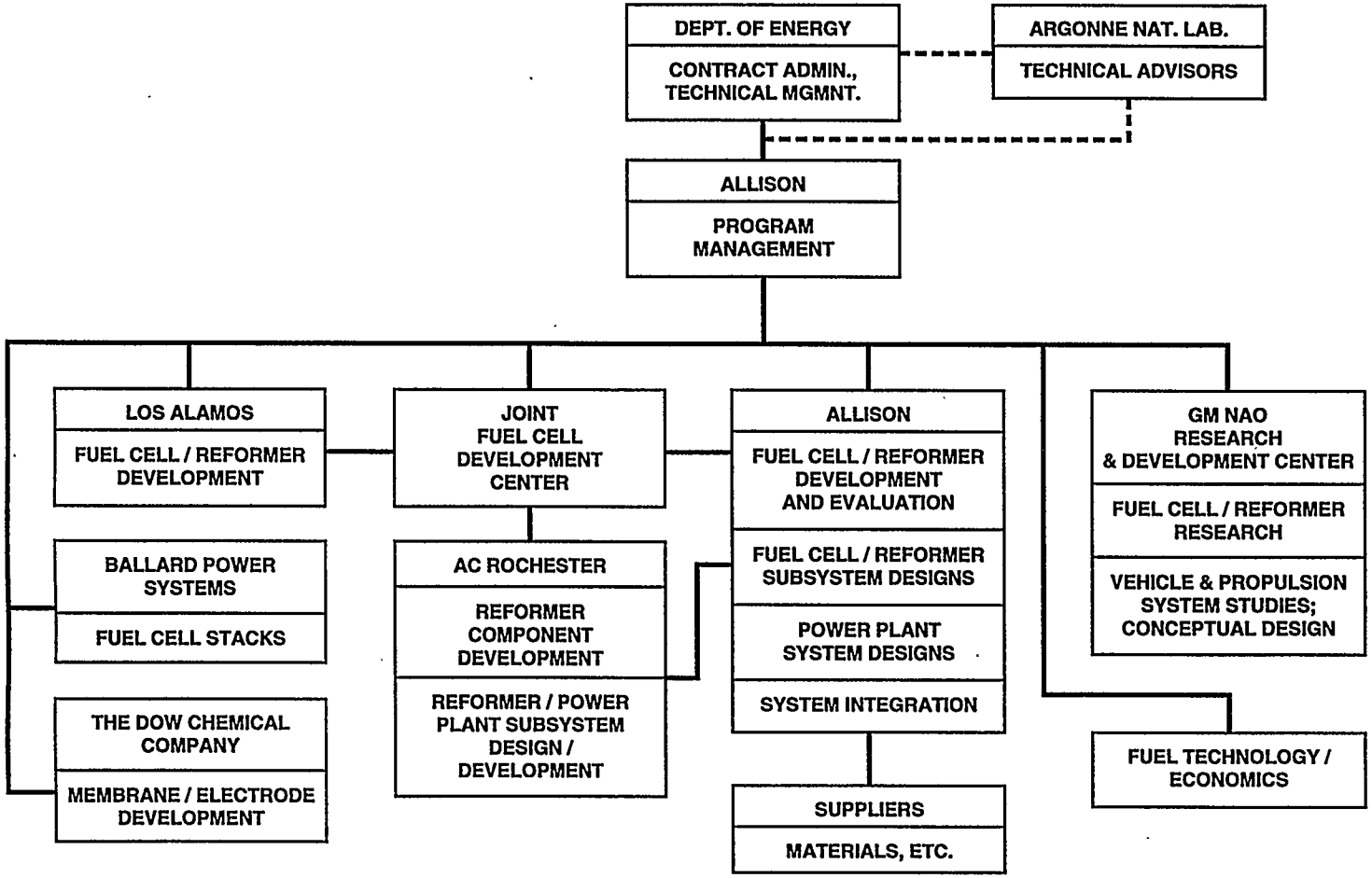


VS93-1638
TE94-1825

Figure 1.1.1-1. Functional organization of the Phase I program team.

The Phase I effort also includes Allison's construction of experimental facilities in part of its Plant 8 Research Laboratories in Indianapolis, Indiana. This construction is in preparation for Phase II building of test bench/test cell facilities and Phase II testing and evaluation of advanced technology fuel cell hardware. Additionally, Phase I effort was applied to a Facilities and Development Plan that identifies the steps required to scale-up to a full-size system.

Phase I effort in the program has produced the Mark II 10-kW fuel cell power system now operational at the GM/Los Alamos JDC, plus a broad base of system component development activity, including control system and ancillary equipment development. Major elements of system development have involved the incorporation of automotive type fuel injection techniques and controls, the fabrication and demonstration of monolithic catalyst supports and component research, and the development of catalyst modules for use in the fuel processor. More basic activity produced improvements in membrane and electrode performance and strength, plus reductions in catalyst loadings in advanced reference type fuel cells. In addition, the first phase of the contract effort pursued a comprehensive system conceptual design study, resulting in integration of an ECE system model into GM's proprietary hybrid vehicle simulator code. The resultant capability was central to vehicle mission studies and analysis, which in turn resulted in a conceptual design report and the recommendation of a mini-van vehicle configuration for further parametric trade-off studies. These studies also resulted in a reference power train design to be updated as the follow-on effort progresses. The Phase I effort has also included an on-going commercialization study which has addressed and documented a wide variety of issues including energy economics and infrastructures, fuel issues, regulatory factors, consumer choices, and development of competitive technologies.

### 1.1.3 Program Schedule and Milestones

Initial efforts were formulated in a first phase contract written between the DoE, Office of Transportation Technologies, and the Allison Gas Turbine Division of General Motors Corporation. This Phase I, which was initiated 1 September 1990, continued through 31 October 1993. The contract focus was a 10-kW fuel cell power source (ECE) which included one or more fuel cell stacks, a fuel processor, battery subsystem, and controls. The ECE is considered to be used as part of a fuel cell powered vehicle system, designed to handle automotive load profiles. In general, the ECE serves as the energy source and the battery serves to supply or accept power surges.

The original 32-month program (which subsequently was extended to 38 months) was planned to address all of the goals defined in the contract. The original elements of effort and the approximate time-schedule for the original Phase I program are summarized in Figure 1.1.3-1.

All of the tasks and major milestones in Figure 1.1.3-1 were completed with the exception of the "Mark III" system. This proposed system differed from the Mark II system in that it included a combustion driven fuel processing section (the Mark II system fuel processor is electrically heated), an integral oil free compressor/expander unit, and more sophisticated controls linking the battery subsystems to the fuel cell system permitting fully transient capable operation. As described later in this report, many of the anticipated technical problems associated with the

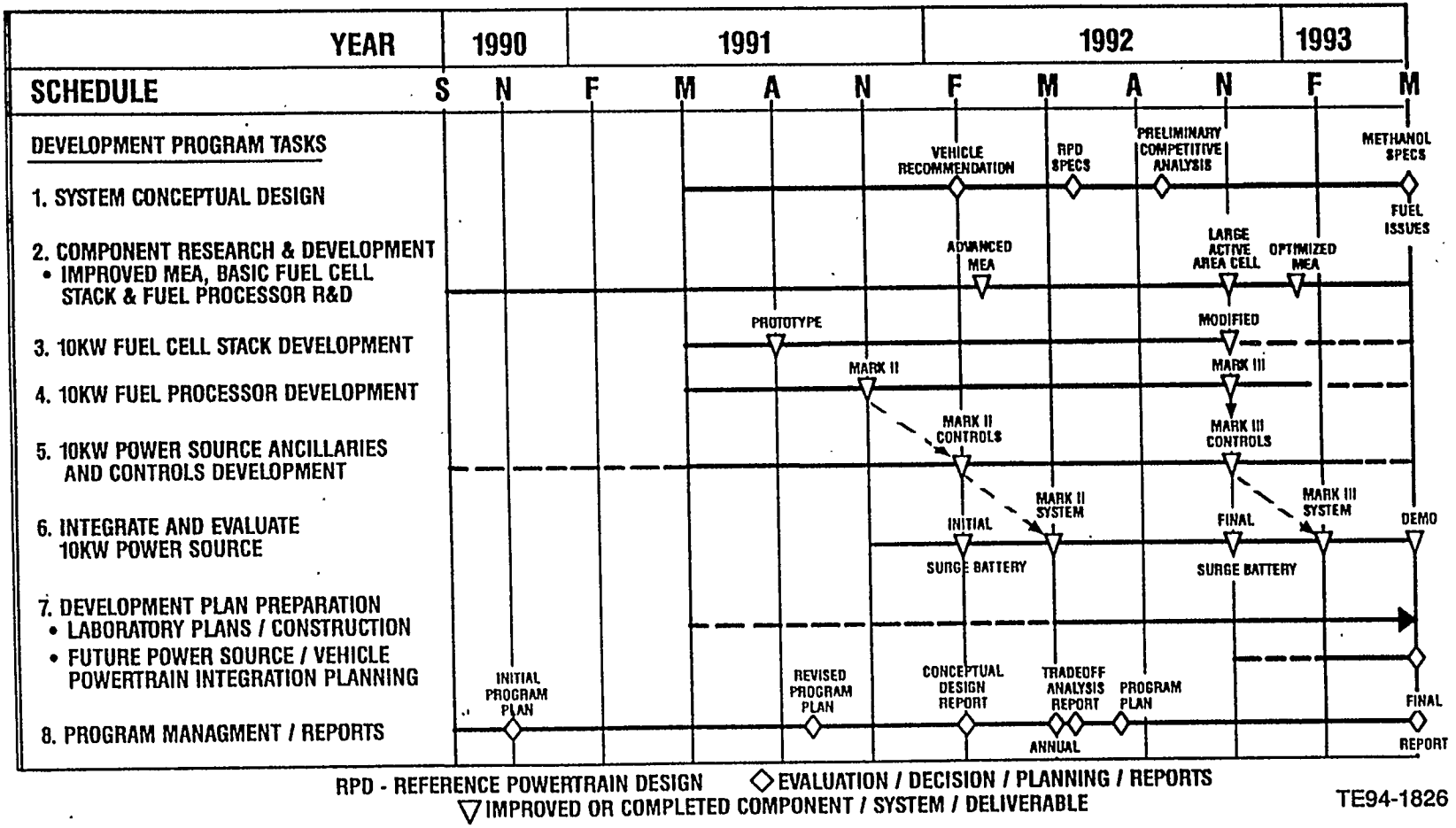


Figure 1.1.3-1. Master milestone schedule for all tasks.

power system components never materialized or were readily solved; however, in some cases unforeseen problems, such as the effects of $CO_2$ on stack anode electrode performance and the development of stable preferential oxidation (PROX) devices capable of transient operation, arose and required substantial effort to resolve. Thus, in concurrence with the DoE, the development of an optimized 10-kW system incorporating both a fuel processor, utilizing a mixed anode vent gas/methanol driven combustor, and an integrated air compression system were deferred until the first part of Phase II.

As described in subsection 1.1.2, a highly modified, sophisticated Mark II fuel cell power source system was successfully operated on 26 March 1993 and is now fully operational at the GM/Los Alamos JDC. The activity (test hours) accumulated to date on this device and the components which comprise it are summarized in Figure 1.1.3-2. To date the Mark II system itself has accumulated 38 hours of operation, while some of the components have over 1600 hours of operation. The terms (F.S.) and (T.B.) refer to full scale and test bench, respectively.

## 1.2 PHASE 1 PROGRAM TECHNICAL ELEMENTS, ISSUES, AND SUMMARY OF ACCOMPLISHMENTS

Program Phase I activities were organized into seven technical tasks. These tasks are summarized below; specified technical accomplishments and remaining technical issues are emphasized following the outline of each task. Only the major results achieved during the Phase I effort are summarized in this section.

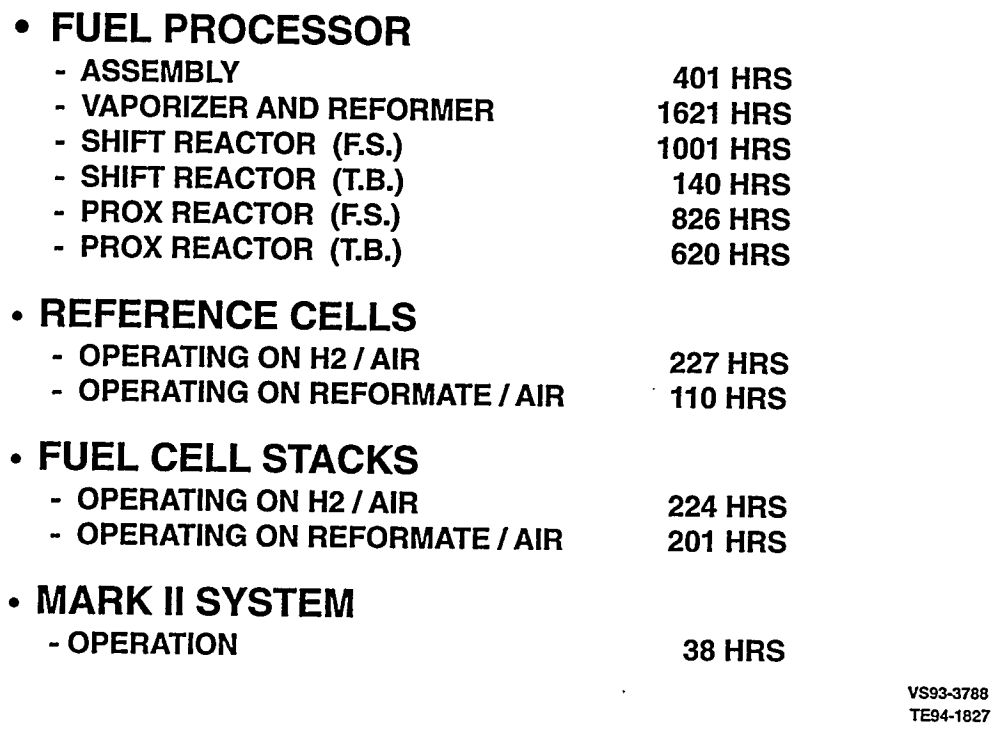


Figure 1.1.3-2. Component and System Test Activity at the JDC.

## Task 1 – System Conceptual Design Study

Any new power generating source must integrate into a system in a manner that meets system requirements. The ECE is intended to function as part of a vehicular system and these system requirements dictate ECE performance. Task 1 included a lengthy series of calculations beginning with projected performance of an ECE. Results of these calculations were then transferred to TASC, an engineering analysis group under contract to Allison. Staff at TASC and General Motors NAO Research and Development Center established vehicle mission requirements and utilized the calculating ECE performance as input to a vehicular performance code used by GM to model several classes of fuel cell-powered vehicles. This established the required performance of ECE/battery power plants in vehicles, and thus characterized the ECE/battery systems. Importantly, the calculations highlighted important technical issues, suggesting the focus of continued development work. The ECE code solves the energy and mass flows in a system comprising four major components:

- Fuel processing including the vaporizer, catalytic reformer, and two sequential gas clean-up operations, the shift zone and PROX. A mixed fuel combustor provides the thermal energy for the endothermic portions of the conceptual design.

- Power production, including the fuel cell stack as the power producing component of the ECE. The model considers details of flow quantities, as measured by the stack stoichiometries which are the ratio of the actual reactant flow rate to the theoretical reactant flow rate required to maintain the electrochemical reactions within the stack at a given power level.

- Air management in which pressurization is accomplished by a high efficiency, wide load range compressor. Pressurized air supplies the cathode feed, combustor air, and the PROX air. Exhaust air is fed through an expander unit that partly recovers the work required for air pressurization .

- Thermal and water management which captures heat loss occurring as part of the conversion processes in the fuel cell stack. Most of this heat is rejected at the stack operating temperature. Overboard heat rejection occurs through the use of a liquid-air heat exchanger similar to a contemporary automobile radiator. The ECE also produces water; this system recycles some of the water for use in the fuel processing and humidification streams.

The ECE model yields steady-state solutions to a complex series of functions. This flexible code can be utilized to analyze various performance cases, for example, a system operating at a single design point (i.e., a 50-kW system operating at 50,000 watts) or at an off-design point (i.e., a 50-kW system operating at part load or 20-kW). The code also solves heat flow through heat exchangers and includes a rudimentary solution that sizes those heat exchangers for operation at rated engine output.

Results from the use of the electrochemical engine system (ECESYS) code include:

- Conversion efficiency - Computational results, using a projected fuel cell stack polarization curve achieved in reference cells and verified effectiveness coefficients and efficiencies for all other components, indicate a thermal conversion

efficiency of 55% at part load (20-25%) operating conditions (20-25% of maximum continuous load)

- Thermal integration - Computations also indicate that stack waste heat is useful for methanol vaporization under conditions where the cathode and anode operate at different pressures. This mode of operation can increase system efficiency by 3 to 5 percentage points.

- Autothermal operation - Computational results indicate that an autothermal fuel processing approach (using an internal oxidation process that partially consumes the fuel to generate fuel processing heat) degrades system efficiency. This steady-state conclusion does not, however, preclude advantages that could ensue with short-term use of autothermal fuel processing, for example, the achievement of a more rapid start-up.

The ECESYS code, integrated into GM's hybrid electric vehicle performance code, was used in vehicle mission studies to determine required ECE/battery sizes. Various vehicle designs were evaluated using a subjective scoring system. When factors such as performance, system packaging, range, and consumer acceptance were considered the all-purpose mini-van was recommended to the government for further study. An ECE/battery-powered vehicle can provide equal performance comparable to vehicles powered by existing internal combustion engines, and can also yield more than double the thermal efficiency in fuel usage. Very low projected emissions suggest such a vehicle can exceed future projected ULEV emissions requirements. These conclusions are presented in the Initial Conceptual Design Report, as a deliverable in this task.

**Task 2 – Component Research and Development**

Although the overall emphasis of this project is on system engineering, it is understood that in transportation applications such systems will require improvements in a number of components; excellent component performance is essential to achieve acceptable system performance. GM placed special emphasis on the research and development activities of this task as significant advances in membranes, electrodes, fuel cell stacks and fuel processing components were expected at the beginning of the program. In fact, these component R&D efforts have resulted in advanced stack and fuel processor concepts considerably different from those presently in use by others. Consequently, GM committed a substantial portion of the contractual effort to this task.

One developmental focus was on improved membrane and electrode assemblies (MEA). These studies were performed by team members at Dow, who prepared advanced and improved membrane and electrode materials, and team members at GM NAO R&D Center who used expertise in custom surface treatments of graphite to form high-performance thin-film Pt loaded electrodes. JDC personnel also conducted thin-film low Pt loaded electrode studies in coordination with the LANL Core Technology Group and GM's NAO R&D Center. However, the JDC's primary task involved the reference cell testing portion of this effort. During this first phase, electrochemical reference cell testing using synthetic reformate and air yielded performance exceeding 0.700V at 1000 amps/ft$^2$, the initial design target. Considerable emphasis was placed on understanding causes and remedies for the adverse effects noted following the admission of carbon dioxide to PEM anodes. These adverse ef-

fects are still not totally understood and some technical issues remain. No work was accomplished on bipolar plate development; large active area advanced cells/stacks were designed but not fabricated, as primary emphasis was placed on understanding the effects of reformate reactant on Ballard stack operation. Bipolar plate development and low cost membrane and electrode assemblies still remain as critical technical and economic issues.

Commercial methanol fuel processing is typically completed in large-scale, steady-state reactors. The necessary focus for transportation applications directs attention toward compact, transient-capable designs. Much of that emphasis is on the design of unique heterogeneous catalyst reactors. These tasks were accomplished jointly between the JDC, which performed the analytical modeling design work and catalyst testing, and the AC Rochester Division of GM, which developed new catalyst formulations and geometries. Two major catalyst types were explored: reforming catalysts prepared on monolithic supports for mechanical stability, reduced volume, and low flow resistance; and oxidation catalysts, prepared on similar monolithic supports. The latter oxidation catalysts are used in the PROX operation, cleaning the product gas of CO through preferential oxidation of CO in the presence of $H_2$. Success in these tasks involved identifying conditions that routinely accomplish the required removal of CO to levels <10 ppm that do not degrade fuel cell stack performance. Transient operation of these PROX devices is still a technical issue; further development work is required.

**Task 3 – 10-kW Fuel Cell Stack Development**

The majority of the fabrication effort of this task was accomplished at Ballard. Six stacks were delivered for utilization in Phase I activities. Four stacks were early delivered prototypes, while two (2) additional stacks, representing a modified and improved design, were delivered during the final months of Phase I. These were all supplied with membrane materials synthesized by Dow; electrodes were supplied by Ballard.

Task 3 activities at the JDC concentrated on performance and reliability testing of the Ballard stacks. The intent of these tests was to determine optimum operational conditions using synthetic reformate (a mixture consisting of 75% $H_2$ – 25% $CO_2$) and air. Parameters, including pressure, temperature, water coolant flow rate, humidification section design, flow stoichiometry, current, and voltage were varied during these tests. Tests involved each stack, on separate test, up to power levels exceeding 5-kW. Detailed stack tests revealed optimum conditions for operation of contemporary stacks. During this program phase, work at Ballard also resulted in improved manufacturing operations, evidenced by more consistent results in cell-to-cell repeatability. The best reformate-air performance was evident in the last stack delivered; an average cell voltage of 0.60V at 1000 amps/ft$^2$ using reformate/air reactants was achieved. Approximately 500 hours of operational experience was obtained during various stack tests at the JDC.

Similar to the reference cell tests, control tests indicated performance degradation following $CO_2$ feed to the anode compartment. Unlike the rapid performance loss resulting from CO poisoning, $CO_2$ poisoning results in slow voltage degradation over an hour or more. It was concluded that this is the result of a COH-type intermediate species adsorbate that tends to block access of hydrogen to active anode sites. The addition of a small quantity of air to the anode stream was one successful

method of removing this performance degradation; particularly when anode alloy catalyst mixtures were utilized. The optimum alloy and anode air addition contents are still being investigated.

### Task 4 – 10-kW Fuel Processor Development

This ECE system concept includes an on-board methanol-to-hydrogen converter. A useful system must have such a component that achieves both power density and performance targets. Activities focused on the design, fabrication, assembly, and testing of a fuel processor that could be used to conduct preliminary system tests. This major program emphasis resulted in several key breakthroughs which are summarized below in the following paragraphs.

Injection of methanol vapor and steam into the catalytic reformer was accomplished using newly-developed fuel injection hardware specially designed for methanol and deionized water operation. These components, and the required 12-volt automotive drive and control circuits, were provided by AC Rochester. The fuel metering hardware also consists of a JDC-designed pool boiler in which liquid water and methanol are sprayed into the boiler resulting in rapid vaporization. The result is careful control of fuel flow with a minimum methanol inventory. This results in both safe reformer operation and high transient capability. Idle-to-full power reformer operational transients were accomplished in less than 3 seconds.

Two major contaminating constituents are present in the reformer efflux; these constituents are breakthrough methanol and carbon monoxide. The shift zone acts to remove nearly all of the breakthrough methanol and significantly reduce the carbon monoxide level. The shift zone hardware consists of two catalyst beds that operate in series. The first zone, operating at reformer temperatures, converts breakthrough methanol; under successful conditions, residual, unreacted methanol is undetectable. The second zone accepts additional water, operates at lower temperatures, and results in significant CO control. The CO contaminant is reduced by the water-gas shift reaction, forming additional $H_2$ fuel and $CO_2$. Forty to sixty percent of the CO is removed in this second-stage shift operation.

The final fuel processing stage cleans the residual CO to levels required for efficient fuel cell operation, <10 ppm. The PROX hardware mixes air into the stream prior to introduction to a controlled-residence-time reaction zone. Under appropriate conditions, this device has proven very successful; consistent results of under 10 ppm CO are readily achieved during steady-state operation. As previously described, transient operation of these devices requires additional development work; variable geometry may be required to achieve similar residence times for varying flow conditions.

### Task 5 – 10-kW Power Source Ancillaries and System Sensors/Controls Development

Both steady-state and transient operation of the ECE system requires adequate ancillaries, sensors, and controls. The ancillaries designed during Phase I include those devices necessary to operate the breadboard 10-kW ECE system. These include: heat exchangers, condensers, cooling water circulation pumps, pumps and injectors for methanol and water delivery to the vaporizer, and air injection metering valves to the various PROX stages. One of the major ancillary developments to

date involves the acquisition of commercial oil-free scroll compressor and expander units (Powerex Corporation). These units require some modification to provide adequate air flow at the pressures required by the cathode portion of the fuel cell stacks, and are presently undergoing bench testing prior to modification.

Steady-state and transient system operation also requires adequate sensors and controls. Varying the load point requires provision for changing both fuel and cooling flows. This task involves a broadly based activity on both sensor development and on the integration of those sensors into a working control environment. Both computer software and rack-mounted hardware development are included in this task. Sensor development has been a continuing activity during Phase I. Some sensors, such as thermocouples, are off-the-shelf; even so, selection, calibration, and measurement are essential. Other sensors require special design and fabrication. Chemical sensors, that would replicate and eventually replace gas chromatographic measurements are still in very early design phases.

The initial system data acquisition (DACQ) of control computer software was based on a commercial instrument, the Hewlett Packard VXI hardware. This reliable system initially controlled most of the laboratory measurements and accomplished both experimental DACQ and some low level of experimental control. Importantly, safety features are also controlled using this equipment. Development of an automotive-based control environment has been proceeding throughout Phase I. That activity has proceeded in parallel; an off-the-shelf real-time operating system (RTOS) has been used. The system has been designed to parallel and exceed the control functions now provided by the Hewlett Packard VXI hardware. Successful operation of the system has been demonstrated.

### Task 6 – Integration and Evaluation of a 10-kW Power Source

The key Phase I deliverable is the integrated ECE system demonstrating both the technical feasibility of various system components and that of the total system, itself. This Phase I Mark II system deliverable maintains some utility connections. For example, the device presently utilizes power from electrical connections to provide the electric resistance heating necessary to drive the, vaporizer, endothermic (steam) reformer, and first stage shifter. System air is also presently supplied from a laboratory air source, rather than from an integrally-driven air compressor. Consequently, the current emphasis has been on components and controls, and on the ability of the control system to control system operating transients. Activities in later program phases will focus more on vehicle-compatible system configurations.

Work progressed continuously during Phase I to build a comprehensive ECE test stand. Because the ECE involves simultaneous operation of both the reformer and the fuel cell stack, the test stand has provision to operate either of these components independently of the other. During the last half of Phase I, considerable emphasis was placed on the design of full-scale shifter and PROX components. The complete Mark II fuel processing system operated well in excess of 200 hours on this test stand. During repeated tests, the data indicated that the shift zone components deliver a gas stream containing nearly undetectable methanol breakthrough concentrations and carbon monoxide that is in near equilibrium with the rest of the mixture of hydrogen, water, and carbon dioxide. The PROX units, using short-residence-time designs, deliver acceptably low carbon monoxide levels. The other half of the ECE test stand supports fuel cell stack operation. Either one of the two 5-kW

Ballard stacks, or both, can be operated to meet the 10-kW electrical target (20-kW when combined with a 10-kW surge battery subsystem).

The first successful ECE system test occurred on 26 March 1993. The test involved simultaneous operation of the stack on synthetic reformate-air and the Mark II fuel processor at a flow rate required for the fuel cell stack current. After several hours of stable fuel processor operation with measured low carbon monoxide contamination, the anode feed was switched from the utility anode gas feed to the feed emanating from the fuel processor subsystem. The average cell voltage on actual reformate contrasted to synthetic reformate is virtually identical. Stable operation of 0.740V at 400 amps/ft$^2$ was measured until the test was terminated. Current density operations up to 800 amps/ft$^2$ (on each of two stacks) have now been achieved. In general, the results closely followed data obtained with synthetic reformate.

### Task 7 – Development Plan

This plan calls for the contractor to initiate the construction of a new fuel cell power source system laboratory at the contractor's main plant facility, to identify future research and development (R&D) requirements and prepare a plan for scale-up to full system size, and to evaluate system cost reductions. These items were accomplished, a Government solicitation including a statement of work was issued for a proposed follow-on effort focusing on a 60-kW brassboard system. The technical approach to accomplish the proposed statement of work for Phase II is described in the next section.

## 1.3 PHASE II FOLLOW-ON EFFORT

The Phase II proposal was submitted in response to the DoE's sole-source solicitation for a 30-month follow-on effort to build on the results of the first phase of work done under Contract No. DE-AC01-90CH10435, *Research and Development of a Proton Exchange Membrane (PEM) Fuel Cell System for Transportation Applications.* First-phase work began in September 1990, and was scheduled for completion 30 September 1994. The Phase II program team was proposed to include General Motors Corporation, acting through its Allison Gas Turbine Division, as prime contractor, and principal subcontractors LANL, Dow, E.I. DuPont & Co., and Ballard. Functional organization of the program team is shown in Figure 1.3-1.

This on-going cost-shared program is a multiphase effort extending thorough late 1998, culminating in the test and evaluation of proof-of-concept fuel cell powered vehicles incorporating PEM power systems designed and built in this program. The elements of effort and the approximate time-schedule for the multiphase program are summarized in Figure 1.3-2.

The primary objective of the Phase II effort will be a nominal 60-kW rated brassboard system (30-kW fuel cell stack, etc., plus a nominal 30-kW battery pack). Advanced fuel cell and fuel processor technology will be utilized at the JDC in producing components for the brassboard system. In addition, comprehensive evaluation of available and proposed fuel cell/stack technologies will be conducted as a basis for selecting and subsequently testing additional advanced fuel cell short stacks for comparison with the design built at the JDC. Following a down-select, two short stacks will be scaled up to 30-kW stack size, tested, and incorporated into the brassboard system.

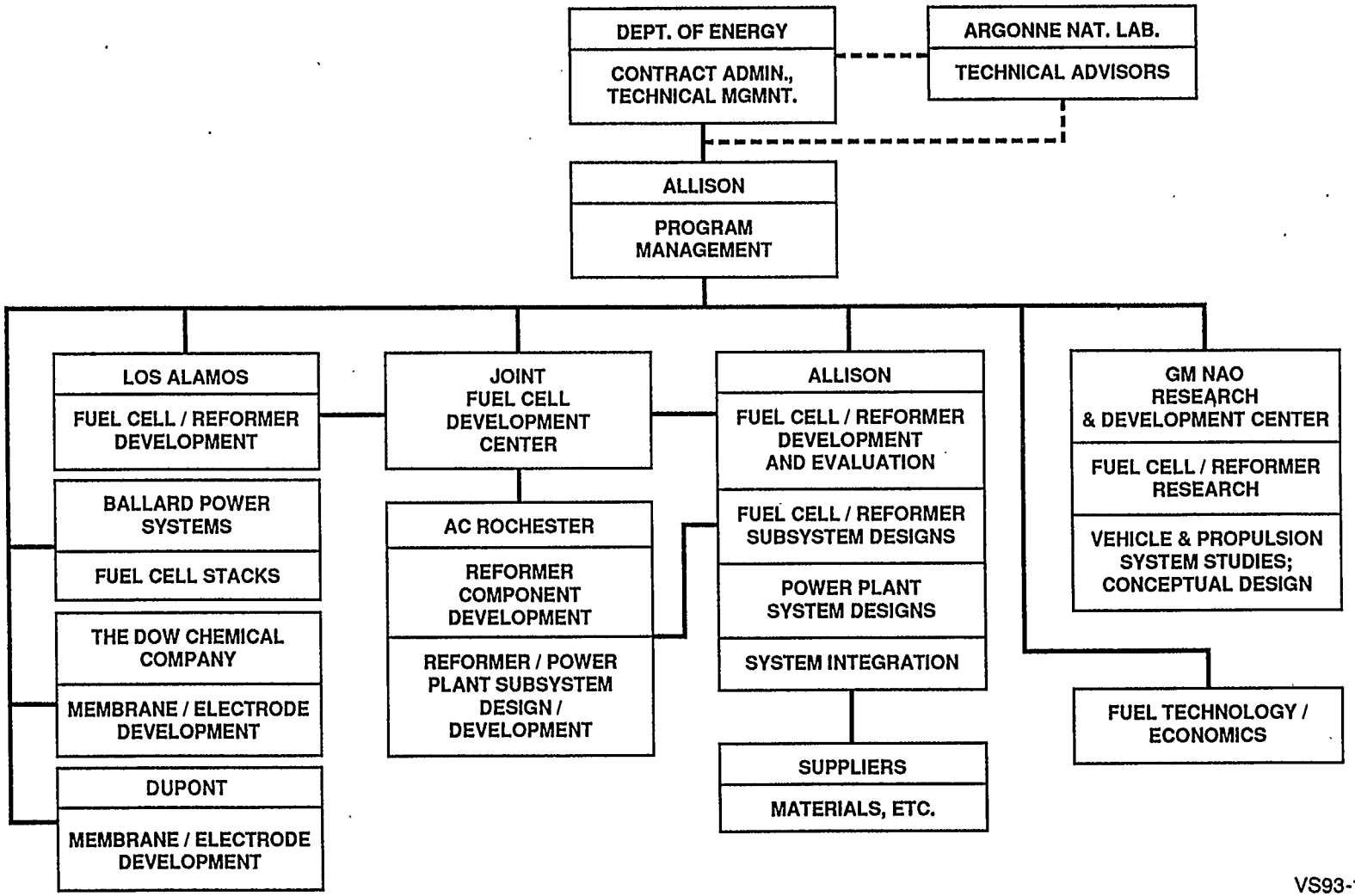


VS93-1638A
TE93-877

Figure 1.3-1. Functional organization of the Phase II program team.

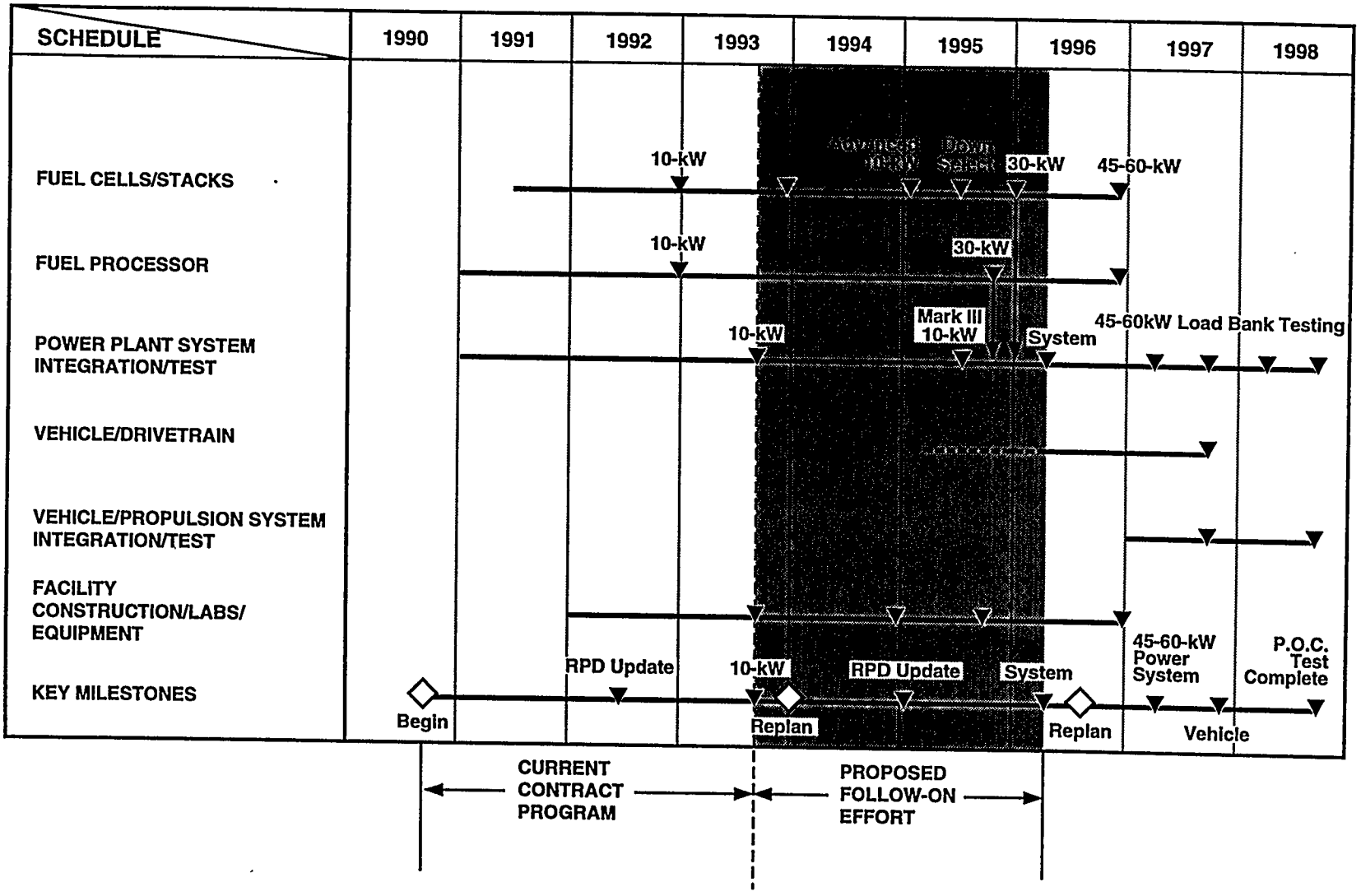


Figure 1.3-2. Preliminary multiphase milestone schedule.

VS93-1138A
TE93-878

Concurrent with stack technology selection and development, the JDC will design and develop an advanced methanol fuel processor for use in the brassboard system. Phase II program efforts to optimize the Phase I 10-kW power system will result in early system integration, operation, and control knowledge which will be a basis for design and integration of the brassboard system. Component research and development will continue in Phase II and serve as a basis for advanced technology developments in fuel processor and fuel cell designs.

The reference power train design and commercialization study efforts will also continue. The follow-on effort will update the reference power train design based on developed capability to model transient operation of the fuel cell power system, plus additional considerations emerging in the course of vehicle analysis. The commercialization study will continue, examining a spectrum of candidate applications and affecting factors, while also focusing in depth on methanol fuel infrastructure requirements and economics, reflecting a methanol fuel specification developed during this program effort.

As presented in Figure 1.3-2, the 30-month follow-on effort proposed serves as a basis for additional effort beyond the Phase II brassboard system, leading to a power system of appropriate output and packaging characteristics integrated into a selected vehicle.

# II. PROGRAM TASK 1: SYSTEM CONCEPTUAL DESIGN STUDY

## 2.1 GENERAL INTRODUCTION

The primary task during Phase I involved the design, assembly, and test of a laboratory "breadboard system" that documented the performances of components, subsystems, and systems of an indirect methanol fuel cell engine. An important supporting activity involved analytical modeling of this system; a model was written that predicts steady-state performance for several possible system configurations. This section describes the formulation and use of that model. A description of the selected ECE is included, with discussion of key characteristics and design features. Detailed discussions of key analyses that influenced the overall design of the system, including sensitivity studies regarding the effects of system component variations, are fully described in Reference 2.1-1.

The ECE system model was developed based on an existing, earlier code, the Los Alamos Fuel Cell System (FCSYS) code. The FCSYS code includes mathematical descriptions of a fuel processor subsystem, a fuel cell subsystem, and supporting ancillaries. Details on these subsystem models and their mathematical limitations are described in the FCSYS code documentation (Ref. 2.1-2).

Any new power generating source must integrate into a corresponding vehicle meeting total system requirements. During Phase I, results of ECE system calculations were transferred to TASC, an engineering analysis group under contract to Allison. TASC and NAO R&D/Power Systems established the vehicle mission requirements and utilized the calculated performance as input to a vehicular simulation model used by GM to model several classes of candidate fuel cell powered electric vehicles. This established the required performance of ECE/battery power plants in vehicles, characterized ECE/battery systems, and resulted in the recommendation of a particular vehicular configuration to the DoE. Importantly, the calculations highlighted required technical issues, suggesting the focus of continued development work.

Complete descriptions of the fuel cell/battery powered vehicle propulsion model development and applications, the vehicle mission/performance requirements results, and the vehicle type recommendation are presented in the Initial Conceptual Design Report (Ref. 2.1-3). Only a very brief overview of these subjects is presented in this report. Powertrain component requirements, sizing, packaging, reference powertrain designs, and the identification and prioritization of future R&D needs, are described and discussed in the R&D Tradeoff Analysis (Ref. 2.1-4). Regulatory and fuel issues, and the competitive analysis of fuel cell powered vehicles are discussed in the Fuel Cell Infrastructure and Commercialization Study (Ref. 2.1-5).

## 2.2 POWER SOURCE MODEL DEVELOPMENT AND APPLICATIONS

### 2.2.1 Introduction and Summary

The ECE in this program (refer to Figure 2.2.2-1) is an electrical power producing machine formed by integration of components including: 1) a chemical converter, the "steam fuel processor," which converts liquid methanol and liquid water to a hy-

drogen-rich gas (so-called reformate); 2) a proton-exchange-membrane fuel cell power stack fueled by reformate with air as the oxidant for electrochemical energy conversion; 3) ancillary equipment (air compressor/expander, pumps and heat exchangers, etc.), and; 4) an ECE control system. Some fraction of the fuel consumed must be burned to provide the heat of reaction for the fuel processor. Overall, the ECE is projected to feature sharply lowered emissions, high thermodynamic efficiency with concurrent decreased carbon dioxide production, and convenient refueling. The ECESYS code solves the energy and mass flows in an ECE system.

The four (4) major system components can be described as follows:

- **Fuel Processing** - The fuel processing subsystem includes a vaporizer section where liquid water and liquid methanol are vaporized and preheated to the reaction temperature, and a catalytic section, the "steam reformer", where the two vapors react to generate hydrogen and carbon dioxide, plus residual amounts of methanol and carbon monoxide. These sections are followed with gas cleanup in two sequential operations: shift zone and PROX. As some of the processing steps are endothermic, thermal energy is supplied either by an electrical source or by a burner that uses either or both of system fuel (methanol) or the dilute hydrogen stream that exhausts from the fuel cell anode.

- **Power Production** - The fuel cell stack is the power producing component of the ECE. Pressurized air is fed to the cathode and pressurized fuel, from the fuel processing subsystem, to the anode. The model also considers details of flow quantities, as measured by the stack "stoichiometries" (the ratio of the actual reactant flow rate to the theoretical flow rate required to maintain the electrochemical reactions within the stack at a given power level). The fuel cell stack is modeled using performance data derived either from contemporary stack designs that utilize an integrated high-quality water stream for both gas humidification and stack cooling or projected fuel cell stack polarization curves believed to be achievable within the next three to five years.

- **Air Management** - Pressurized air supplies the cathode feed, the burner air, and the PROX air. Pressurization is accomplished by a compressor; the efficiencies of the air management components are important in determining overall system efficiency. Exhaust air is fed through an expander unit that recovers, in part, the work required for air pressurization.

- **Thermal Management-Water Management** - System components require thermal control for optimum performance. As with internal combustion engines, system efficiency losses result in waste heat. Because most heat loss occurs as part of the conversion processes in the fuel cell stack, the majority of system heat is rejected at the stack operating temperature. A number of heat exchangers are included to recuperate as much of the waste heat as possible to provide heat to drive the fuel processing components. System heat rejection occurs through a liquid-air heat exchanger, similar in concept to that in a contemporary automobile. The ECE produces water, and some product water recovered in this heat exchanger is recycled to be reused in the fuel processing stream and for gas humidification within the fuel cell stack. The remaining water is discharged.

The ECE model provides steady-state simulations for a variety of conditions. This code can be utilized to analyze various "performance cases," such as a system operating at a single design point (for example, a 50-kW system operating at 50,000 watts) or at an "off-design point," (such as a 50-kW system operating at part load, for example, 20,000 watts). The code also estimates heat flow through heat exchangers and includes a rudimentary solution that sizes those heat exchangers for operation at rated engine output.

Output parameters derived from the ECE system model include the following:

- **Conversion Efficiency** - Ratios of output electrical power to input chemical power are calculated. Computational results, using a *projected* fuel cell stack polarization curve equivalent to that already achieved in reference cells and verified effectiveness coefficients and efficiencies for all other operating components, indicate a potential thermal-conversion efficiency exceeding 50% at part load operating conditions.

- **Thermal Integration** - Energy flows to and from components (motors, fans, compressors, expanders, heat exchangers, chemical reactors) are determined. Computations indicate, for example, that stack waste heat is useful for methanol vaporization under conditions where the anode pressure is sufficiently low. This mode of operation increases system efficiency by several percentage points.

Results from the ECESYS model, integrated into the electric vehicle simulation code, were used in vehicle mission studies to determine required ECE/battery sizes. Various vehicle designs were evaluated using a subjective scoring system. When factors such as performance, system packaging, range, and consumer acceptance were considered, the all-purpose mini-van was recommended to the government for further study. An ECE/battery powered vehicle is projected to provide performance comparable to vehicles powered by existing internal combustion engines, and can also yield more than double the thermal efficiency in fuel usage. Very low projected emissions suggest such a vehicle can exceed future projected ultra-low-emission vehicle (ULEV) emission requirements.

### 2.2.2 System Description/Model Development and Results

A schematic of the system as currently modeled is presented in Figure 2.2.2-1. The code performs mass and energy balances, determining temperatures, input heat requirements, fluid flow rates, and parasitic losses. The efficiency of the fuel cell and the parasitic losses are used to determine system efficiency.

The fuel processor subsystem includes the fuel and process water preheaters and vaporizers, the reformer, shifter, PROX, process stream cooler, and the burner and various heat exchangers required to satisfy the reformer endothermic heat of reaction and heat transfer to the vaporizer. Not depicted are burner gas heat exchangers to at least a portion of the shift zone reaction and cooling water heat exchanges to the PROX units. The basic fuel processor layouts developed in previous work at Los Alamos are described in Refs. 2.2.2-1 to 2.2.2-3. The fuel cell subsystem is simply the fuel cell and the cooling system required to maintain the fuel cell at its operating temperature. A third subsystem, which might be called the intake/exhaust subsystem, includes the air compressor that compresses ambient air for the fuel cell

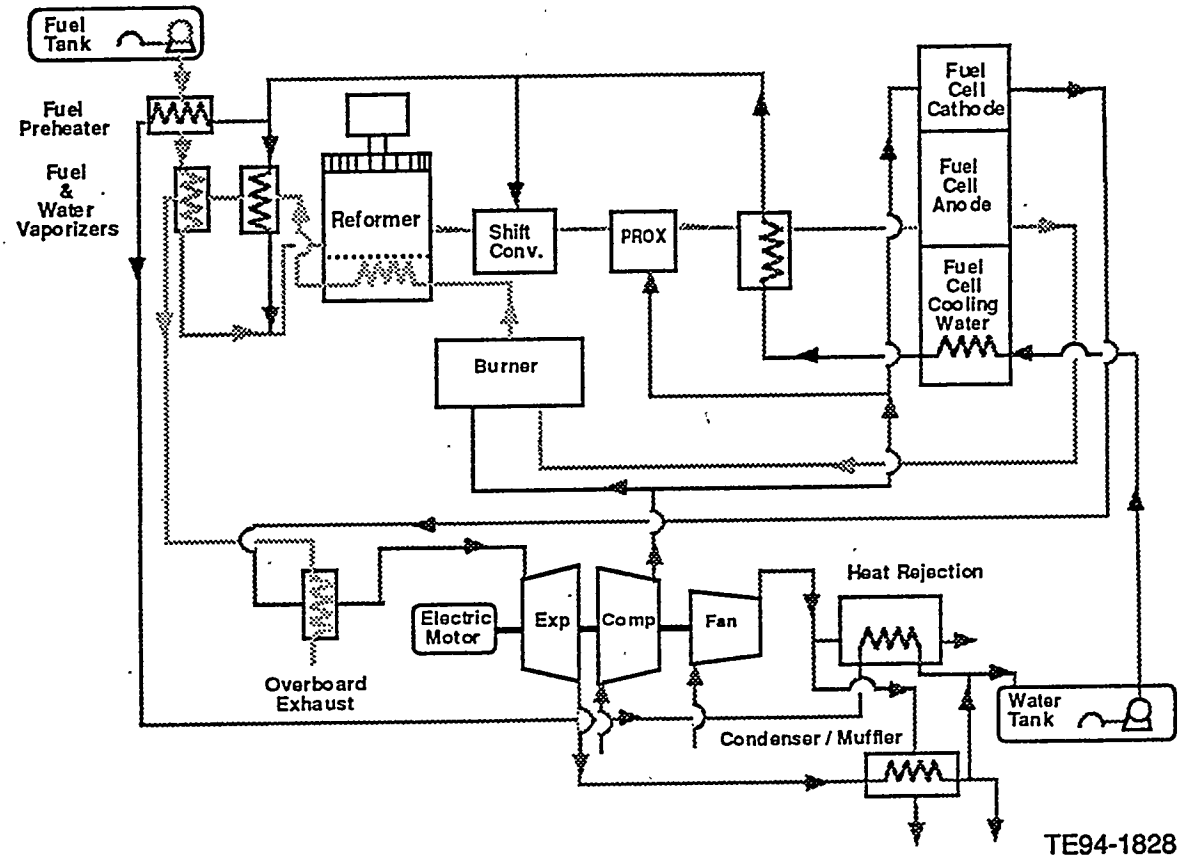


Figure 2.2.2-1. Simplified schematic of the conceptual design ECE. The vaporizer and reformer heat exchangers are actually calculated in parallel with the burner exhaust gases (rather than in series as depicted) in the current model.

cathode, burner, and PROX, an exhaust gas expander to drive the compressor, and a motor/generator (a motor only is depicted, but in reality this would be a motor-generator) for auxiliary shaft work, either to provide power to the compressor or to accept power (transferred to the batteries) from the expander. The third subsystem also includes a fan and heat exchanger for coolant water waste heat rejection and subsequent collection of the cooled water in a water tank. In the schematic presented, there is also a condenser to reclaim water from the expander exhaust stream using fan-supplied air as the coolant; this water is also partially returned to the water tank. This clean water collection in the water tank eliminates the requirement for carrying external clean water to supply water for stack humidification and the fuel processor. The fourth subsystem, which accomplishes control, is not depicted in Figure 2.2.2-1.

- **Water flow** - As depicted in Figure 2.2.2-1, fuel and water are fed to the system under pressure using small pumps that pressurize and meter these liquids. High-purity system water first cools and humidifies the fuel cell stack. After servicing the fuel cell, the cooling water exhausts at the fuel

cell operating temperature. This stream then passes through a heat exchanger where the process stream exiting the PROX is cooled to near fuel cell operating temperature. After cooling the fuel processor stream, a small amount of the total water flow is injected into the second stage portion of the shifter increasing the steam to hydrogen ratio of the gas stream, thereby lowering the CO mole fraction. Another fraction of the water stream is used for the reformer reaction process; this water is pumped through the water vaporizer and then into the reformer stream; the remainder (most) of the water is used to preheat the fuel, and is then routed to the heat rejection unit and water tank, along with condensate water recovered from the exhaust stream. The heat produced in the fuel cell is a result of the fuel cell inefficiency and is a significant fraction (~30-40%) of the total system energy. Since the fuel cell must operate at a relatively low temperature, the coolant (water, in this case) leaving the fuel cell is also at this relatively low temperature. It is difficult to use much of this heat in a profitable manner and most of it, except for that used in fuel preheating, is rejected to the atmosphere.

- **Fuel flow** - After passing through the preheater, the fuel is fed into the fuel vaporizer, where heat from the burner exhaust gas brings the methanol to the fuel processor operating temperature. If the fuel cell operating temperature is above the boiling temperature of the fuel at the anode operating pressure, the temperature of the water in the fuel preheater is hot enough to vaporize the fuel. This situation can increase overall system efficiency by several points. The reformer reactor, where fuel and water are converted to hydrogen, carbon dioxide, and carbon monoxide is endothermic. A third (parallel) burner exhaust heat exchanger is required to supply this thermal energy. The burner operates on air supplied by the compressor and either system fuel (methanol), unreacted hydrogen, from the anode exhaust, or a mixture of the two fuels. Methanol must supply the burner fuel during the brief system start-up period. During operation, hydrogen from the anode exhaust (usually mixed with some methanol) provides the burner fuel. Because there must be some hydrogen in the anode exhaust for efficient fuel cell operation, the use of hydrogen mixed with methanol in the burner results in the best system efficiency. The burner operates at the pressure set by the anode outlet.

Not all the methanol is converted in the steam reformer, and under usual conditions of steam to hydrogen ratio and temperature, appreciable mole fractions of (undesirable) carbon monoxide can occur as part of the reformer exhaust stream. Unreacted methanol is primarily converted in the first portion of the shift zone which operates at the reformer temperature and acts as a plug flow reactor. In the latter portion of the shift zone, additional water is injected to promote the forward shift reaction between water and carbon monoxide to decrease carbon monoxide and produce additional hydrogen. In the final gas cleanup step to remove the remaining carbon monoxide, air is injected into the process stream and the oxygen in that air serves to preferentially oxidize (PROX) any remaining traces of unreacted methanol and (primarily) carbon monoxide (a small amount of hydrogen is oxidized as well).

- **Air flow** - The hydrogen rich product from the fuel processing section supplies the anode side of the fuel cell stack, while the cathode fluid is air supplied by a compressor. This compressor is currently assumed to be an oilless, constant-displacement device such as a water-cooled scroll machine (Ref. 2.2.2-4). The electrochemical reactions consume hydrogen at the anode face of the membrane and electrode assembly and oxygen at the cathode side to produce electric power, heat, and product water.

To recover energy from the compressed gas streams, a heat exchanger transfers waste heat from the burner exhaust to the cathode exhaust, and the cathode exhaust is then directed to the expander. The burner exhaust leaving the heat exchanger is vented to the atmosphere. The expander, which may also be a scroll machine, is intended to supply at least part of the shaft work required by both the air compressor and a heat rejection system air fan. The schematic shows an electric motor to supply the shaft work that can not be supplied by the expander. In principle this could be a generator to charge batteries or fly wheels if the expander can supply excess power during down transients.

Finally, the exhaust stream from the expander passes through a condenser to reclaim the cathode water, part of which is routed back to the water tank while the rest is dumped overboard. The resulting exhaust stream is then vented to the atmosphere. Other possible sources of condensed water are the expander itself (condensation may occur within it) and the fuel cell. The main water stream is cooled in a water-to-air heat exchanger. The cooling air is supplied by the fan and is exhausted to the atmosphere.

***Overall System Efficiencies***

The overall system efficiencies reported in this section are the net electrical power (gross electric power output of the fuel cell minus motor power and other parasitic loads) divided by the chemical energy rate of combustion of the system fuel. The chemical energy of the fuel is based on its lower heating value (LHV). (The selection of the LHV parallels the way that internal combustion engine efficiency is calculated and thus permits simple comparisons between the two technologies.) "Motor power" is the required compressor power plus the fan power minus the power supplied by the expander. For simplicity, the overall system efficiency can be expressed as the product of two terms, the "fuel cell efficiency" and the "balance of plant (BOP) efficiency". The "fuel cell efficiency" is calculated by dividing the achieved voltage per cell by 1.18V cell voltage (the oxygen reduction potential). Because of the fact that all other system components that degrade efficiency must be included in some manner, the "BOP efficiency" includes these effects. Consequently, efficiency contributions of the entire system exclusive of the fuel cell are incorporated into the "BOP efficiency" term. This approach results in charging some of the parasitic losses, for example, the air compression work, to the "BOP efficiency".

The conceptual design system calculations are based on parameters now demonstrated or believed to be achievable during the near term, 3-5 years. The fuel cell polarization curve utilized in the system efficiency calculations is illustrated in Figure 2.2.2-2, and is simply a *linear* function running through 0.7 volts per cell at a current density of 1.0765 amps/cm$^2$ (1,000 amps/ft$^2$) and 0.5 V at 2.153 amps/cm$^2$ (2,000 amps/ft$^2$), which are project performance goals. (This type of linear function

through the Tafel region, the useful part of the polarization curve, is typical in fuel cell measurements). The nonlinear parts of the polarization curve, the activation region, the low current density region, and the very high current density region which includes the mass transport limitation region, are not normally suitable operational zones. Most of these calculations utilized pressures, temperatures, and flow stoichiometries at the low end of demonstrated technology, and present a challenging set of conditions. However, good voltage performance at these conditions has been demonstrated on reference cells. Assumed efficiencies of the other components are within demonstrated ranges. Heat exchanger effectiveness ranged between 50-90%. The trade-offs involved in heat exchanger design are between heat recovery, operating temperature differences ("availability" of recovered heat), and heat exchanger volume, weight, and cost. Sensitivity calculations demonstrating the impact on overall system efficiency of variations in these assumptions can be found in the Phase I ECE Performance Analysis Report (Ref. 2.1-1).

Some key operating parameters, including part load and full load power, temperatures, and flow rates of the Conceptual Design ECE at the full design output of 60-kW and at specific off-peak operating conditions are presented in Table 2.2.2-I. Complete computational output from the ECESYS code for the 60-kW full-power case, the example problem, is presented in Ref. 2.1-1. The full-power case operating conditions were computed using the ECESYS "design" option. In this case the heat exchangers are "designed" utilizing user-selected efficiencies and allowable pressure drops. The calculated efficiencies of the fuel cell, "reformer," and overall system as a function of load are displayed in Figure 2.2.2-3. The off-peak cases were run with

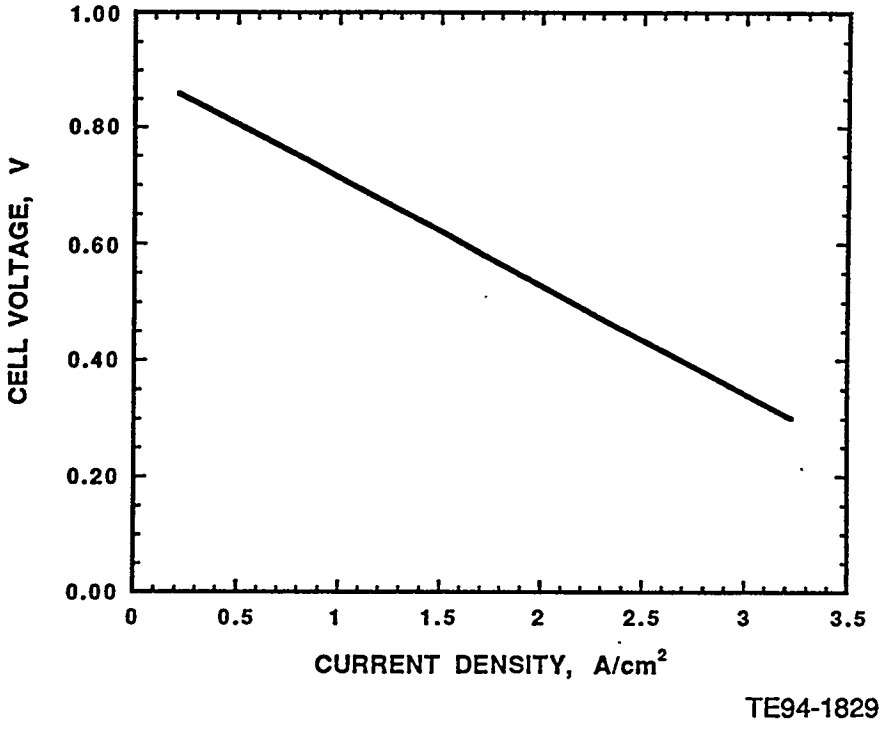


Figure 2.2.2-2. "Forecast" polarization curve used in most system-level studies. The values of 0.7V per cell at 1,000 amps/ft² (1.076 amps/cm²) and 0.5V at 2,000 amps/ft² (2.153 amps/cm²) are project performance goals.

the ECESYS "rating" option; in this option the only input parameter change was the fuel cell electrical power output, while the heat exchanger parameters were fixed at the full-power "design" values. Component efficiencies, such as those for the compressor and expander, were assumed to remain *constant* at .76 across this duty cycle. This assumption is not conservative, and will be addressed as components are designed and estimates of component efficiencies as a function of load become available. However, modern pressure-volume machines such as scroll compressors/expanders do show broad regions where efficiency is relatively constant as flow rates are changed, although of course efficiency for any fan design is normally low at the very lowest range of mass flows. If required, the pressure-volume machines will be staged and brought on-line as flow requirements increase to retain high operating efficiency.

### 2.2.3 Integration of Power Source Model Results into the Vehicle Propulsion Model

A vehicle simulation model, proprietary to GM and identified collectively as VSIM (Vehicle Simulation Model), was used to calculate vehicle energy usage and vehicle performance characteristics for a variety of vehicles. The ECE system model was used to generate projections of peak and off-peak power steady-state performance; a data integration process then transformed code outputs into compatible VSIM inputs using a hybrid powertrain model. Specific ECE system model data included the relationships between calculated electric power and voltage, current, fuel/air/water consumption, and estimated emissions. Code-generated estimates

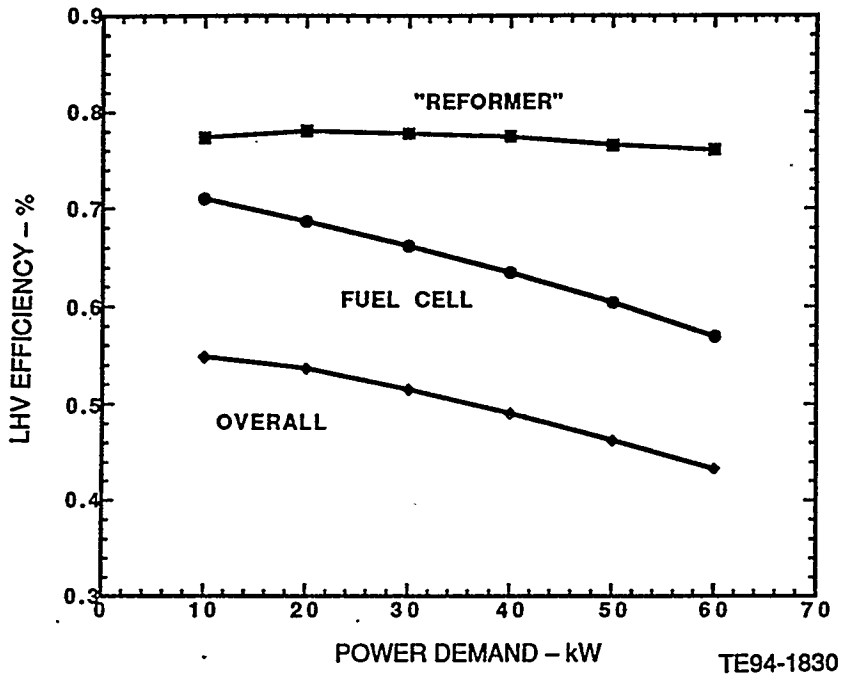


Figure 2.2.2-3. Projected efficiency of a 60-kW ECE as a function of load. Reformer efficiency represents the efficiency of the entire system exclusive of the fuel cell stack.

Table 2.2.2-I.
Projected system characteristics for a 60-kW ECE at full power and part load.

| Fuel Cell Power<br>Electrical (gross)<br>Electrical (net) | 10 kW<br>8.5 kW | 20 kW<br>17.3 kW | 30 kW<br>25.8 kW | 40 kW<br>33.3 kW | 50 kW<br>43.7 kW | 60 kW<br>51.0 kW |
|---|---|---|---|---|---|---|
| "Reformer" Efficiency | 0.7737 | 0.7809 | 0.7779 | 0.7746 | 0.7657 | 0.7605 |
| Fuel Cell Efficiency | 0.7100 | 0.6868 | 0.6618 | 0.6345 | 0.6040 | 0.5691 |
| Overall Efficiency | 0.5486 | 0.5363 | 0.5148 | 0.4905 | 0.4625 | 0.4328 |
| Fuel Cell Current Density ($A/cm^2$) | 0.1438 | 0.2974 | 0.4629 | 0.6438 | 0.8453 | 1.076 |
| Fuel Cell Voltage (V) | 0.8733 | 0.8448 | 0.8140 | 0.7804 | 0.7429 | 0.7000 |
| Fuel Cell Stack Active Area ($m^2$) | 7.962 | 7.962 | 7.962 | 7.962 | 7.962 | 7.962 |
| Cell Active Area ($cm^2$) | 465 | 465 | 465 | 465 | 465 | 465 |
| Current (Amps) | 66.79 | 138.1 | 215.0 | 299.1 | 392.7 | 500 |
| Total Volts (V) | 149.7 | 144.8 | 139.5 | 133.7 | 127.3 | 120 |
| Number of Cells | 171 | 171 | 171 | 171 | 171 | 171 |
| Fuel Cell Temperature (°C) | 90 | 90 | 90 | 90 | 90 | 90 |
| Reformer Temperature (°C) | 230 | 230 | 230 | 230 | 230 | 230 |
| Anode/Cathode Pressure (Bar) | 1.5/3.0 | 1.5/3.0 | 1.5/3.0 | 1.5/3.0 | 1.5/3.0 | 1.5/3.0 |
| Cathode Stoichiometry | 2.0 | 2.0 | 2.0 | 2.0 | 2.0 | 2.0 |
| Reformer Water Stoichiometry | 1.3 | 1.3 | 1.3 | 1.3 | 1.3 | 1.3 |
| Fuel (Methanol) Flow Rate (g/s) | 0.770 | 1.594 | 2.490 | 3.470 | 4.575 | 5.855 |
| Water Flow Rate(g/s) | 0.562 | 1.165 | 1.820 | 2.540 | 3.350 | 4.279 |
| Air Flow Rate (g/s) | 9.26 | 19.17 | 29.88 | 41.66 | 54.93 | 70.10 |
| Fuel LHV (kW) | 16.20 | 33.51 | 52.24 | 72.93 | 96.35 | 123.10 |
| Burner Heat Input (kW) | 3.27 | 6.83 | 10.73 | 15.23 | 20.93 | 26.68 |
| Fuel Preheat Recovery (kW) | 1.02 | 2.12 | 3.30 | 4.61 | 6.08 | 7.70 |
| Fuel Vaporization Heat Input (kW) | 0.18 | 0.38 | 0.59 | 0.83 | 1.10 | 1.48 |
| Water Vaporization Heat Input (kW) | 1.43 | 2.95 | 4.61 | 6.44 | 8.52 | 10.91 |
| Reformer Heat Input (kW) | 1.43 | 2.97 | 4.63 | 6.47 | 8.52 | 10.32 |
| Reformate Cooling (kW) | 0.41 | 0.84 | 1.30 | 1.78 | 2.26 | 2.73 |
| Reject Heat (kW) | 3.68 | 8.34 | 14.21 | 21.36 | 30.45 | 42.50 |
| Burner Exhaust Heat Recovery (kW) | 0.19 | 0.43 | 0.72 | 1.14 | 1.83 | 2.90 |
| Compressor Power (kW) | 1.36 | 2.81 | 4.38 | 6.11 | 8.60 | 10.28 |
| Expander Power Recovered (kW) | 0.61 | 1.54 | 2.42 | 3.39 | 4.53 | 5.71 |
| Fan Power (kW) | 0.38 | 0.75 | 1.13 | 1.51 | 1.89 | 2.28 |
| Motor Power Input (kW) | 1.12 | 2.02 | 3.10 | 4.23 | 5.42 | 6.69 |

of ECE component weights and heat-transfer rates were also utilized. In addition, ECE system model outputs were used with auxiliary calculations to estimate system start-up times and ECE response for both up-load and down-load transients. Major inputs to VSIM are listed below, with those provided from the ECE power source model highlighted with an asterisk:

ECE operating characteristics
- power*
- fuel usage*
- weight*

Driving profiles
- schedules
- grades

Vehicle parameters
- size, weight, drag coefficient

Powertrain system component characteristics
- battery
- power conditioner
- motor
- transmission
- energy management strategy

Outputs from the VSIM code include:

Energy usage
- fuel economy
- distribution of losses

Vehicle performance characteristics
- gradability
- acceleration
- vehicle range

Emissions
- water
- regulated emissions

### *Vehicle Mission/Performance Requirements Overview And Vehicle Type Recommendation*

A series hybrid vehicle configuration with regenerative braking was chosen for evaluation, incorporating modular subsystems as depicted in Figure 2.2.3-1. The fuel cell was sized to meet long-term vehicle gradeability requirements; the battery was sized separately to duplicate either *maximum performance* (matching conventionally powered vehicle 0 to 60 mph acceleration) or *similar performance* (meeting the relatively modest acceleration requirements of the Federal Urban Driving Schedule during warm-up). With vehicle mission requirements defined to be similar to conventional vehicles and a vehicle evaluation (scoring) procedure established, four passenger vehicle types in each of the two performance classes *(maximum and similar)* were evaluated. The four passenger vehicle types evaluated were three automobiles (large, mid-size and compact) and a mini-van, each having EPA "average" vehicle characteristics.

As a result of the evaluations a *similar performance* mini-van was recommended as the vehicle choice for further parametric tradeoff analysis and for the reference power train design (RPD). The analysis summary, average ranking, and additional details can be found in the Initial Conceptual Design Report (Ref. 2.1-3).

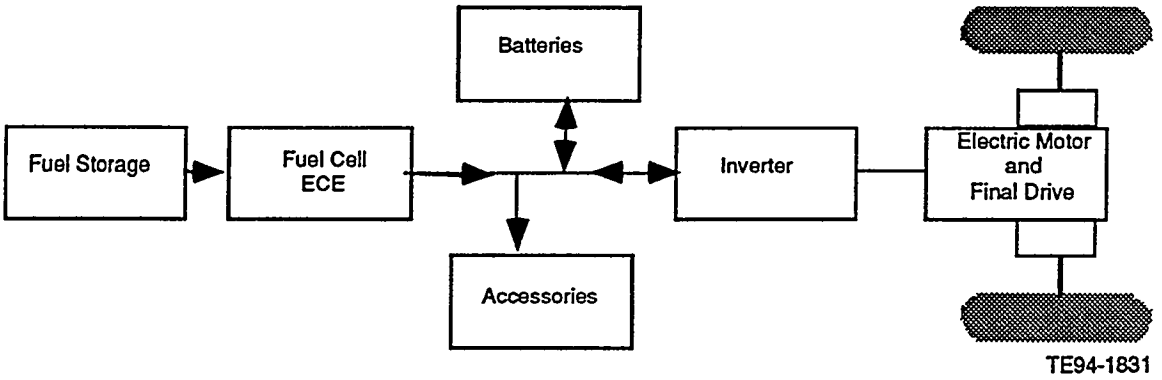


Figure 2.2.3-1. Series fuel cell/battery hybrid power train model. The two-way energy flows between the drive motor and electric bus indicates the potential for regenerative braking.

# III. PROGRAM TASK 2: COMPONENT RESEARCH AND DEVELOPMENT

## 3.1 GENERAL INTRODUCTION

Although the overall emphasis of this project is on system engineering, it is understood that in transportation applications, systems will require improvements in a number of components; excellent component performance is essential to achieve acceptable system performance. Special emphasis was placed on the research and development activities of this task as significant advances in membrane and electrode optimization and fuel cell stack and fuel processing components were expected at the beginning of the program. These component R&D efforts have resulted in advanced stack and fuel processor concepts considerably different from those presently in use.

Specifically, several key components required special developmental emphasis.

- ***Membrane and electrode development and reformate/air fuel cell research and development*** - One developmental focus was on improved MEA. These studies were performed by team members at Dow, who prepared advanced membrane and electrode materials, and team members at the GM NAO R&D Center who used expertise in custom surface treatments of carbon to form high-performance thin-film low Pt loaded electrodes. JDC personnel also conducted thin-film low Pt loaded electrode studies in coordination with the LANL core technology group and GM's NAO R&D Center. However, the JDC's primary task involved the reference cell testing portion of this effort. During this first phase, electrochemical reference cell testing of reformate-air reactants yielded performance exceeding 0.700V at 1000 amps/ft$^2$, the initial program design target. This research team also placed considerable emphasis on understanding causes and remedies for the adverse effects noted following the admission of carbon dioxide to PEM anodes. These adverse effects, while resolved, are still not totally understood and some technical issues remain. Further, additional effort is still required to ensure high performance and long-life stability on low Pt loaded electrodes in the presence of reformate gases. No work was accomplished on bipolar plate development; large active area advanced cells/stacks were designed but not fabricated, as primary emphasis was placed on understanding the effects of reformate reactant on Ballard stack operation. Bipolar plate development and low cost membrane and electrode assemblies still remain as critical technical and economic issues.

- ***Fuel processing catalyst development*** - Commercial methanol fuel processing is typically completed in large-scale, steady-state reactors. The focus for transportation applications is on compact, transient-capable designs, the design of unique heterogeneous catalyst reactors. These tasks were accomplished jointly between the JDC, which performed the analytical modeling design work and catalyst testing, and the AC Rochester Division of General Motors (AC Rochester), which developed new catalyst formulations and geometries. Two major catalyst types were explored: reforming catalysts prepared on monolithic supports for mechanical stability, reduced volume, and low flow resistance; and oxidation catalysts, prepared on similar monolithic

supports. The latter oxidation catalysts are used in the PROX operation, cleaning the product gas through preferential oxidation of CO in the presence of $H_2$. This involved identifying conditions that routinely permit removal of CO to levels <10-ppm, thus avoiding degradation of the fuel cell stack performance. Transient operation of these PROX devices is still a technical issue; further development work is required.

Details regarding these developmental efforts are described in the following subsections.

## 3.2 DOW MEMBRANE AND ELECTRODE DEVELOPMENT EFFORT

### 3.2.1 Introduction and Summary

High performance MEA are critical, common components of fuel cell systems based on PEM. High performance MEAs, with very similar if not identical structures, are required for each of the presently envisioned PEM based systems. Different integration problems exist for each envisioned fuel base.

MEAs and their use in a cell stack are illustrated in Figure 3.2.1-1. The MEA of today is a multi-layer structure composed of a proton conducting polymer membrane, thin electrocatalytic layers attached to each side of the membrane, and current collectors or supports "attached" to each catalyst layer. Attachment here means adhered to, but can also mean a simple compressive contact. The membrane layer is a perfluorocarbon ionomer such as Dow XU-13204.20, a sulfonic acid functionalized fluoropolymer (PFSA). The catalyst layers generally are thin microporous polymer bonded particulate materials. Platinum black bonded with polytetrafluoroethylene is a common example. The supports or current collectors are microporous carbon or graphite materials. Graphite paper made with chopped graphite fibers or woven graphite cloths are example materials. These supports generally are "coated" with polytetrafluoroethylene or polymer-conductive particulate mixtures to modify their structure and wettability. The other major repeating component of the stack is the bipolar plate. This component serves to separate oxidant and fuel gases, to define gas flow/distribution, and to conduct electron current from cathode to anode . In the stack assembly these two components, the MEA and the bipolar plate, are combined alternately along with appropriate sealing materials and cooling plates. The finished stack unit is leak free and supplies DC power at current densities up to approximately 2000 amps/ft$^2$ when supplied with hydrogen fuel, pressurized air, and cooling water.

Membrane-electrode structure, bipolar plate, and stack mechanical design must be integrated to provide optimum performance. For example, in the bipolar configuration shown in Figure 3.2.2-1, compressive forces are used to produce gas tight seals and electrical contact to the MEA supports. The quality of these electrical contacts is determined by the surface properties of both the support and the bipolar plate, by support thickness and porosity, and by the allowable thickness variation in the bipolar plate. Likewise, gasketing design to provide effective sealing depends upon the structure and materials of both the MEA and the bipolar plate. Improved MEA designs can enable the use of more conductive but "weaker" membrane materials, but also may allow simpler bipolar plate or gasketing designs which would reduce the cost of component manufacture.

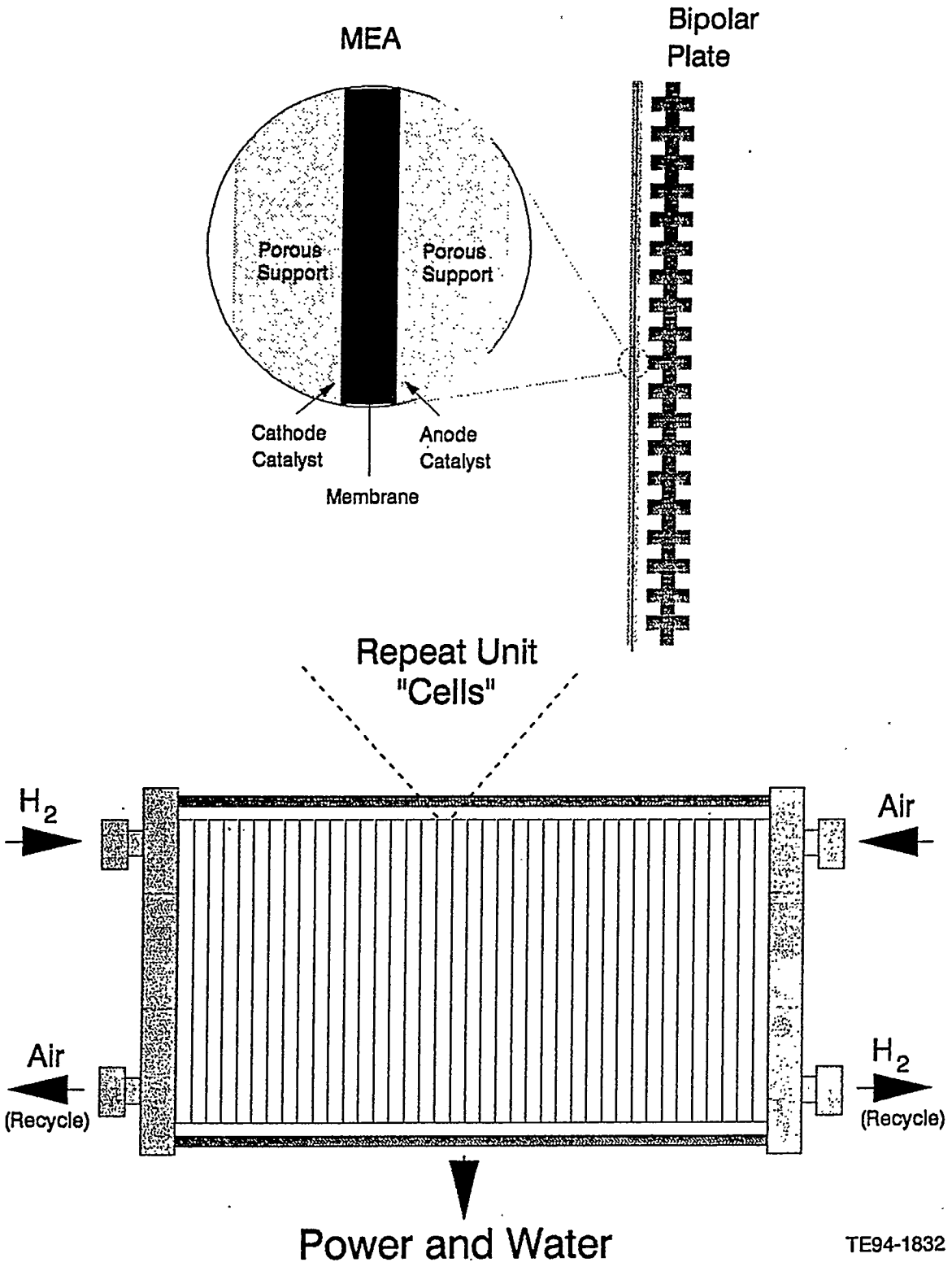


Figure 3.2.1-1. Stack/MEA structures.

Dow as a subcontractor to Allison undertook the task to deliver an improved MEA on a best effort basis and to provide membrane and membrane-electrode assemblies to Allison and Ballard Power systems in support of other contract tasks.

Contract work was conducted by membrane and fuel cell research groups at Dow's Texas Division in Freeport. The contract tasks are listed in Figure 3.2.1-2; the approaches used to accomplish the primary research tasks are also presented schematically in the same figure. The first task, improvement of the central MEA element, the PFSA membrane, was the major focus involving both property measurement and performance evaluations as MEAs in fuel cell operation. Dow sought a more quantitative knowledge of property trade-offs and improved correlation with fuel cell performance. This work spanned a range of skills which included Dow personnel involved in polymer synthesis, fabrication of membranes, measurements of membrane properties, and fabrication and testing of membrane-electrode assemblies. Internal "standard" fabrication and testing methods were utilized. The second major task was electrode structure improvement with technical goals targeting higher performance on air and low catalyst loadings. In this task variations of electrode composition and fabrication processes were followed by structural characterization and evaluation of actual fuel cell performance. The third task, the assessment of MEA assembly costs, was required to address the potential to attain the stringent cost targets required for motive application of fuel cells. The fourth task involved the supply of membranes for stack and electrode development efforts by others within the program, while the last planned task was simply a cooperative effort to use quality, standardized test equipment and procedures for MEA evaluations.

Significant Dow resources were applied to this project and a broad range of work was accomplished. Many of the personnel and most of the Dow facilities used to develop improved membranes and electrodes, conduct fuel cell development, etc., were supported by internal Dow funding. Results of this non-supported work contributed to the accomplishment of the program tasks. Fabrication efforts produced 58 different polymers, 38 different membranes, and some 270 membrane-electrode assemblies. Most of these MEAs were tested in fuel cells using standard screening procedures while a smaller group was tested more extensively, in either lifetime tests or in evaluation of the effects of various test conditions on performance.

Internal Dow standard methods were used for polymer/membrane characterization while several methods were extended or developed to measure polymer or membrane properties. For example, gel permeation chromatography in a perfluorocarbon solvent was investigated in an attempt to measure polymer molecular weight and molecular weight distribution. Several methods to measure mechanical properties of films were also adapted. Capabilities to measure tensile mode stress-strain, creep, and tear tests (crack propagation) in aqueous environments up to 90°C were developed. Membrane transport properties, particularly conductivity (resistivity) and gas permeability, are critical performance determinants in fuel cells. Measurement of membrane resistivity in aqueous electrolytes up to 90°C required the use of a precision conductivity cell; this cell was developed and used with standard AC impedance methods. Techniques were also developed to measure resistivity in humid atmospheres, again to 90°C. Appropriate equipment was acquired and a wide range of membrane materials were evaluated.

Contract efforts resulted in the following accomplishments by task.

## Characterize/Optimize Perfluorosulfonic Acid Membranes

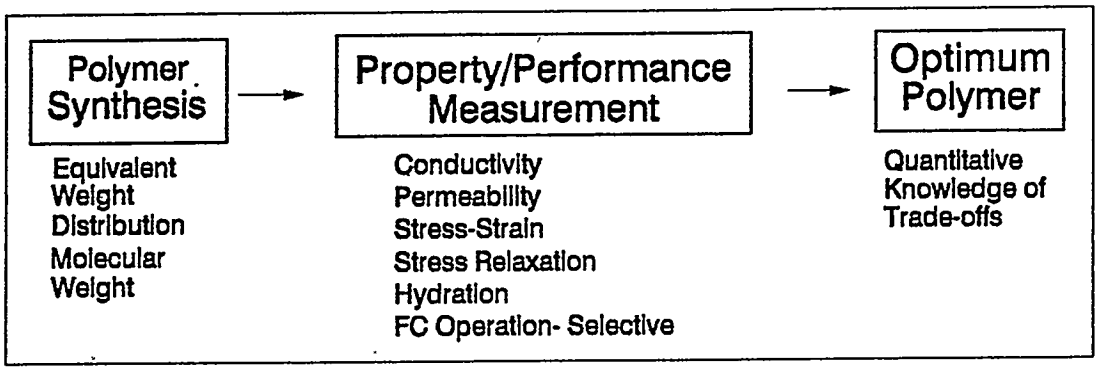


## Optimize Electrode Structure for PEMFC

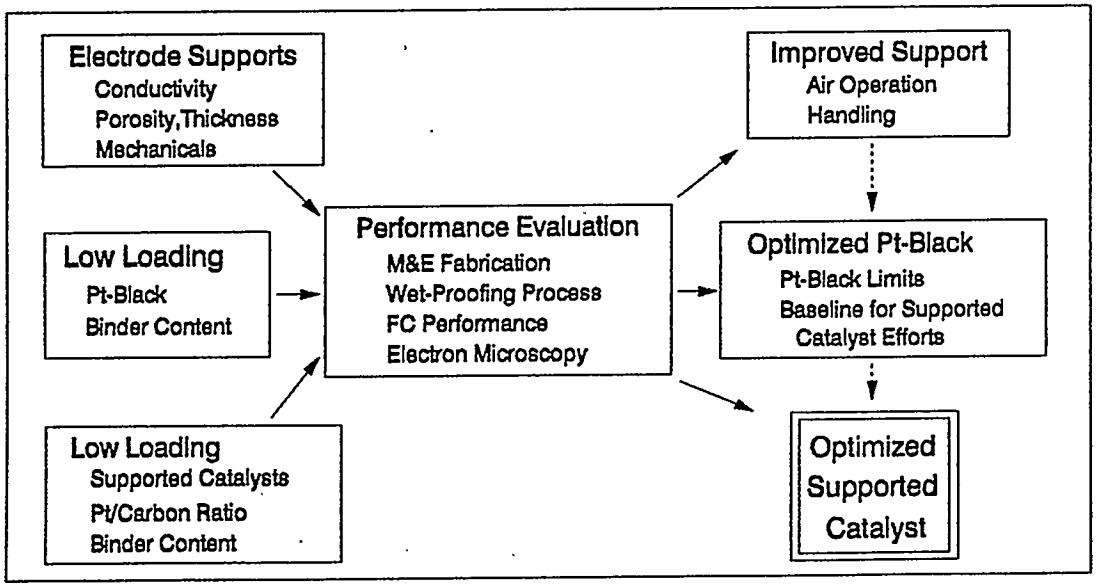


## Assess Costs of Membrane-Electrode Assemblies

## Deliver Membrane and Membrane-Electrode Assemblies to GM (Allison) and Ballard in Support of Other Contract Tasks

## Coordinate with GM (Allison), Ballard, and LANL to Develop and Test Optimized Membrane-Electrode Assemblies

TE94-1833

Figure 3.2.1-2. Dow contract tasks.

### *Membrane and MEA Supply*

Supply of membranes and membrane-electrode assemblies in support of other contract tasks was accomplished. Materials were supplied in response to requests from Allison personnel.

### *Characterize/Optimize Perfluorosulfonic Acid Membranes*

Membrane design is now more quantitative, and based on measurements of mechanical and transport properties over a range of polymer materials. The relationship between mechanical properties, particularly film modulus and film conductivity of Dow materials, is now quantitatively understood. Given the polymer equivalent weight and membrane thickness, both the strength, as determined by the film modulus, and the specific conductivity of the polymer film can be calculated. The primary determinants of measured properties are equivalent weight and post-fabrication processing conditions. Attempts to change equivalent weight distribution, the range in TFE units between functional side chains, and polymer molecular weight did not produce statistically significant impacts on film bulk properties.

Membrane resistivity during fuel cell operation was measured and shown to be nearly equivalent to the conductivity determined in a hot dilute acid environment. Film resistivity, as a function of polymer equivalent weight, was measured in dilute acid at 90°C and in humid air at 80°C using AC techniques. Membrane resistivity during fuel cell operation was determined by regression on both voltage and cell resistance data to be dependent on membrane thickness and current density.

Net water transport across the membrane was measured and found to be very near zero, less than 0.1 mole water per proton. Measurements, using standard MEAs and operating conditions, were conducted for membranes fabricated with polymers which spanned a range of equivalent weight (800 to 980 gm/eq). Over this range no difference in net water flux could be discerned.

High power performance with higher strength membranes was demonstrated through modifications to both the membrane polymer and the MEA fabrication process. Membrane-electrode assemblies, fabricated over the "full useful" range of polymer equivalent weight, performed comparably to XU-13204.20 with performance differences reduced to near those expected based on "bulk" conductivity differences. Thus, membrane materials with lower water content and two to three times higher film modulus provided fuel cell voltage at 1000 amps/ft$^2$ only 20 to 25 mV lower than those observed when XU-13204.20 was tested in a fuel cell.

### *Optimization of the Electrode Structure For PEM Fuel Cells*

MEAs based on improved processing of electrode support structures provided much higher current densities on air. Changes in composition and treatment process of both the support material composite (graphite fiber paper and PTFE) and the active electrode composite resulted in improved performance. In Dow test cells, current densities slightly above 1 amp/cm$^2$ were attained before the onset of significant transport limitations.

Platinum black loadings were reduced to approximately 1 mg/cm$^2$ using existing coating processes and further reduction is likely. Reduction of loading on the cath-

ode side did, however, lower air performance. Although no experimentally significant performance loss was observed on oxygen with lower cathode loadings, the best performance obtained on air was less than that observed using highly loaded electrodes. Fuel cell performance was unchanged by reduction in anode side Pt loadings in the range studied (4 to 1 mg/cm$^2$).

Lifetime testing was initiated but adequate performance stability on air was not demonstrated. Several lifetime tests were initiated and the longest operating time attained was 2000 hours (on-going test). Over this time frame, cell voltage at 500 amps/ft$^2$ decreased linearly with time from 0.74 to 0.65 volts, an average rate of -1.0 mV per day. Air injection in the anode, even under "pure" hydrogen operation has been shown by the LANL Core Technology Group to alleviate performance decay. The possibility exists that contaminants, such as $CO_2$, in $H_2$ over long periods of operation lead to the formation of intermediate species that can poison the anode.

***Assessment of Costs Of Membrane-Electrode Assemblies***

Based on Dow's understanding of potential system economics, and an internal analysis of membrane economics, membrane cost will not be a limiting factor. Presently, and through the early stages of commercialization, membrane prices will be high.

***Phase I Project Goals Requiring Further Effort***

Fuel cell power performance better than that provided by Dow XU-13204.20 was not achieved. Improved fuel cell power performance along with mechanical "integrity," can, however, be projected using thinner membranes combined with improved MEA fabrication processes.

High fuel cell power performance with ultra-low Pt loadings was not achieved. Efforts under the contract focused on low platinum black loading; reductions to as low as 0.75 mg/cm$^2$ of MEA are envisioned. Work by others has demonstrated that lower loadings can be achieved with carbon supported platinum. Cost effective processes and stable long-term performance need to be demonstrated.

Adequate performance stability on air was not demonstrated. It is, however, fully anticipated that performance stability, adequate for both motive and stationary applications, will be demonstrated. Continuing efforts will be required using both existing and newly developed MEA structures.

### 3.2.2 Discussion of Developments and Results

***Fuel Cell Test Operating Conditions***

Fuel cell performance data were obtained using standardized equipment and operating conditions.

All fuel cell polarization data were taken after overnight operation on air at an intermediate current density which maintains the cell voltage above 0.6 volts. The standard procedure to obtain a fuel cell polarization curve begins with data collection at the highest current density permitting operation above 0.3 volts; a maximum current density of 4.3 amps/cm$^2$ (4000 amps/ft$^2$ ) was allowed. After steady state operation is attained the voltage is recorded and the current and gas flows are reduced

to a lower setting; flow stoichiometry is maintained in the moderate to high current density regimes. Lowest system flows are 0.3 liters/min. hydrogen and 0.5 liters/min. air; stoichiometry is not maintained at low current density operation.

The net water flux across the membrane under operating conditions is "measured," this net water flux is actually a calculated number based on a mass balance on all the water entering and leaving the cell. The actual data required to compute this flux, in addition to the cell operating conditions are: the quantity of water entering the cell from the humidifiers, the quantity of water trapped in the "knock-out" vessels in the exit gas streams, and the relative humidity and temperature of the exit gas streams. Other necessary data, such as gas flows, current density, and gas pressures are part of the cell operating conditions. Formation of water at the cathode is assumed to be the only source of product water formed in the fuel cell. The computational procedure involves the following steps: the water introduced into the feed gas streams by the humidifiers is measured under the same temperature and flow conditions to be used during cell operation; the cell is then operated at constant current for several hours, usually overnight, and the dew points of the exit gas streams are measured; water in each knock-out vessel is then drained and weighed. This data constitutes a complete water balance on the cell. Total water entering the cell plus the cathode water formed should equal the total water recovered, i.e., the weighed liquid water and computed water vapor in the exit gases. The net water flux is then calculated from the difference between the entering and recovered water content of both the fuel and oxidant streams. The difference between these two values (which should be numerically identical) and a comparison of the total water recovered to the combined entering and produced water are measures of the quality of the experiment. Equipment permitting single cell testing at high temperature and pressure was also installed. The major difference of this test stand compared to the standard test stands involves the addition of a pressure vessel and external humidification capability. The pressure vessel maintains a constant pressure differential between internal and external pressures, as internal pressure is increased; cell gasketing and porting, consequently, did not have to be re-designed. The equipment was designed for operation up to 150 psig and 160°C. Pressure control provides for variation of the upper pressure set condition. Direct injection of water, rather than membrane humidifiers, was needed in order to control and maintain the desired water content in the feed gases at the planned high temperature range of operation.

### *Membrane Development*

#### Membrane Properties and Fuel Cell Performance

The objective of the membrane development effort was improved polymer performance in fuel cells. Higher power capability clearly remains the goal but this must be attained while retaining the mechanical strength required for M&E fabrication and handling. Further, gas permeation must be within acceptable limits to ensure safe fuel cell operation. The present Dow membrane, XU-13204.20, which has manageable mechanical properties, has been used in MEAs that have produced the highest power density observed in PEM fuel cells. The more quantitative definition of terms such as manageable or acceptable properties must be determined in the context of any down stream processing requirements and the specific mechanical and chemical environment within the fuel cell. MEA fabrication process detail, cell design, and stack operating conditions all introduce different property requirements which impact the choice of an optimum material. The present optimization effort is

targeted to increase strength properties while improving, or at least maintaining, the excellent power density performance observed when XU-13204.20 is used as the membrane.

As membrane development efforts often require the testing of membranes with different properties in a fuel cell test apparatus, a "standardized membrane and electrode assembly (MEA)" was utilized so that the effects of membrane property changes were clearly delineated. This standardized MEA is composed of a single catalyst layer type and composition, a standard graphite paper support, and utilizes the same fabrication process conditions. Both anode and cathode catalyst layers were platinum black bonded with polytetrafluoroethylene; platinum loadings during this membrane development effort were high, 4 mg/cm$^2$. The graphite paper supports were TPG-60 (Toray Industries, Inc.), a graphite fiber based material. Fabrication procedures and actual compositions of this standardized MEA are proprietary. In other MEA development efforts, as well as in some performance optimization efforts, both electrode composition and fabrication processes were modified.

One of the first efforts in the membrane development task involved measurements of film properties over a broad range of membrane equivalent weights to provide a more quantitative understanding of the effects of film property variations on membrane characteristics. Both transport and mechanical properties were measured. The relationship between the film modulus and conductivity at 90°C in aqueous environments is presented in Figure 3.2.2-1.

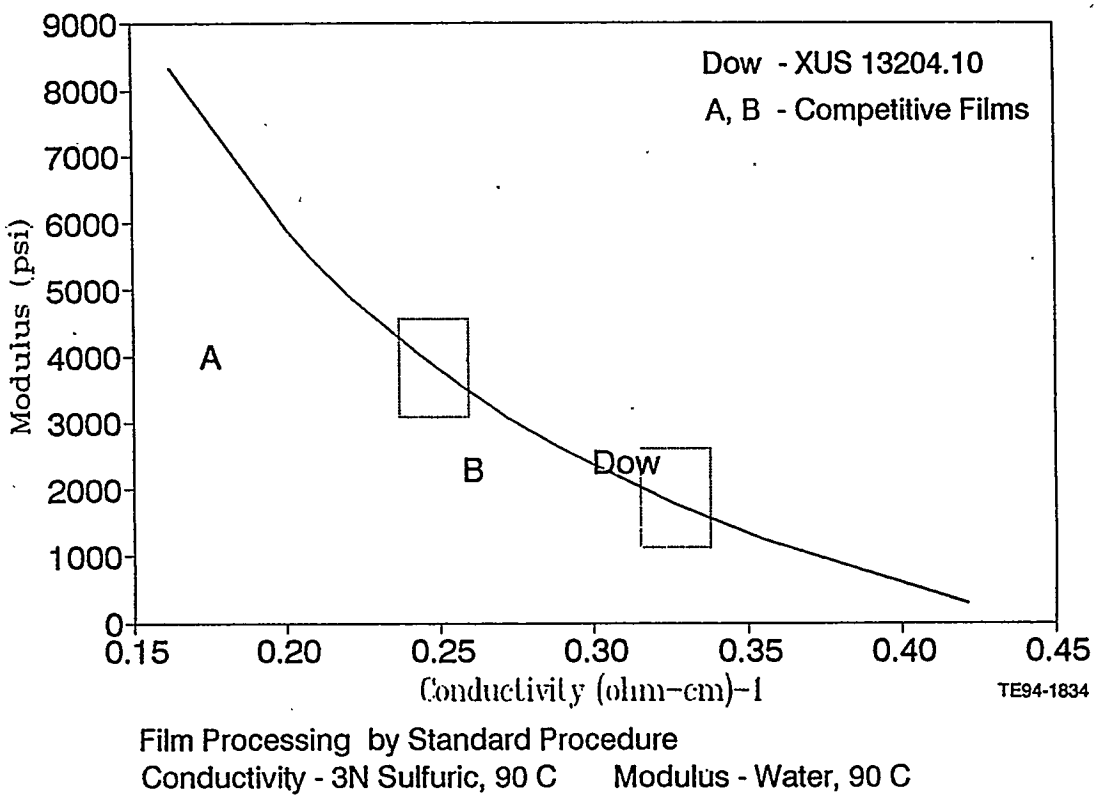


Figure 3.2.2-1. Film modulus as a function of film conductivity.

The rectangles on the curve indicate the location of the experimental designs described later in this report. Clearly, strength, as indicated by the film modulus, decreases as film conductivity increases. The film modulus can, however, be increased by a factor of eight while the film conductivity decreases by only a factor of two. Thus, membrane strength can be increased with only a minimal effect on conductivity. For example, in the modulus range of present commercial materials, roughly 2000 to 4000 psi in our test conditions, Dow membrane conductivity decreases 22% from 0.31 to 0.24 $(ohm\text{-}cm)^{-1}$ as the modulus increases. Assuming these conductivity values correlate to fuel cell operating conditions, this change in "bulk" conductivity will increase the resistive voltage loss by only 13 mV for a 5 mil thick membrane at 1000 $amps/ft^2$. However, the tear resistance nearly doubles with these same changes in film conductivity and modulus. Competitive films A and B are long side-chain polymers. The general observation is that competitive materials have lower conductivity at equivalent strength, i.e., film modulus.

The behavior of membrane polymer under stress is important to the long-term mechanical integrity of an MEA structure. In particular, the behavior of the membrane under compressive load is important for fuel cell applications. Although stress-strain measurements in the compressive mode have not as yet been performed, tensile mode stress-strain and creep of fully hydrated films have been measured. Examples of film stress-strain and creep compliance data are presented in the next three figures; measurements were performed in hot water, thus maximizing water content, so that "worst case" data were generated. Results such as those presented in Figure 3.2.2-2 are typical for hydrated ionomer films; elongation is less than 100% prior to rupture while the elastic range is typically restricted to low strain levels representing less than 10% of the elongation.

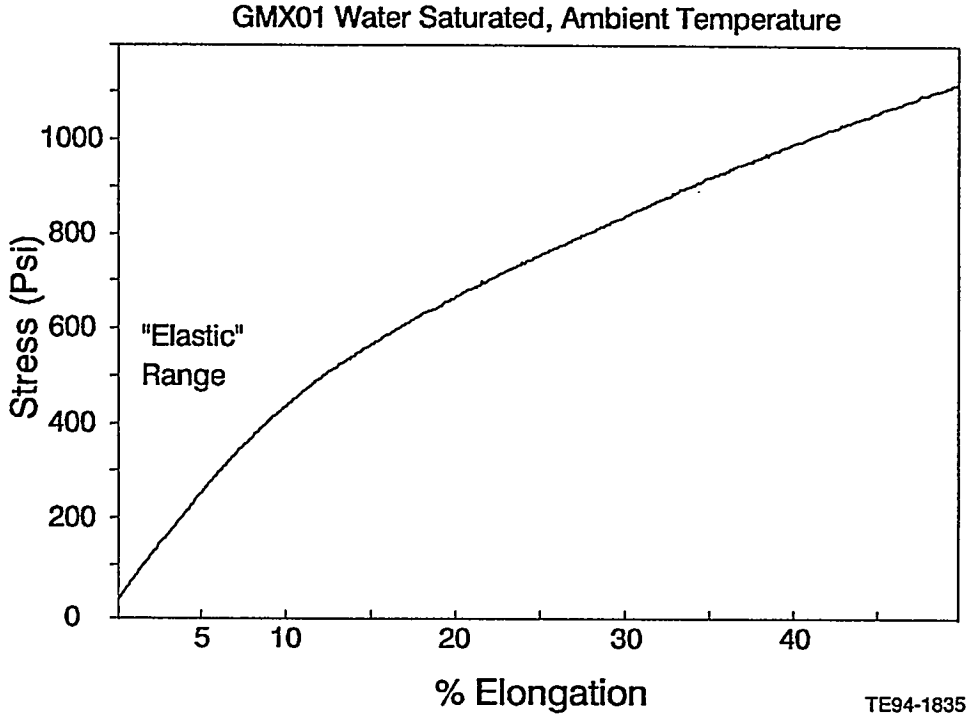


Figure 3.2.2-2. Membrane stress (psi) as a function of % elongation.

The creep compliance behavior for two experimental films with different equivalent weights, GMX07 and GMX01, both under low initial strain within and at the "edge" of their elastic range, respectively, is presented in Figure 3.2.2-3. No increase in strain is observed in the former while very slow compliance is observed for the latter.

Similar data for these two materials, with both at a higher strain well outside their elastic range, is presented in Figure 3.2.2-4. Both materials indicate they possess the same creep compliance in this regime of testing.

These data support two conclusions: first, a decrease in equivalent weight (GMX07 had a higher equivalent weight than GMX01) to improve conductivity did not change the creep compliance; second, if ionomer films are used at strain levels well within the elastic range, the condition expected in the compressive mode, significant material deformation, or creep, should not be observed.

Transport properties of the membrane are also critical to the performance of PEM fuel cells. Film (membrane) conductivity, a function of hydration of the film, is in turn a function of the operating conditions within the fuel cell. Film conductivity determines the resistive values of the membrane and can clearly affect the output voltage of the MEA within an operating fuel cell. Within the presently accepted conceptual framework, water transport properties, diffusivity, and permeability, are also fuel cell performance determinants. These basic transport properties, in combination with operating conditions, determine the water gradient in the membrane and thereby determine the performance of a particular membrane material. Gas permeability of the hydrated film is also important for safe fuel cell operation.

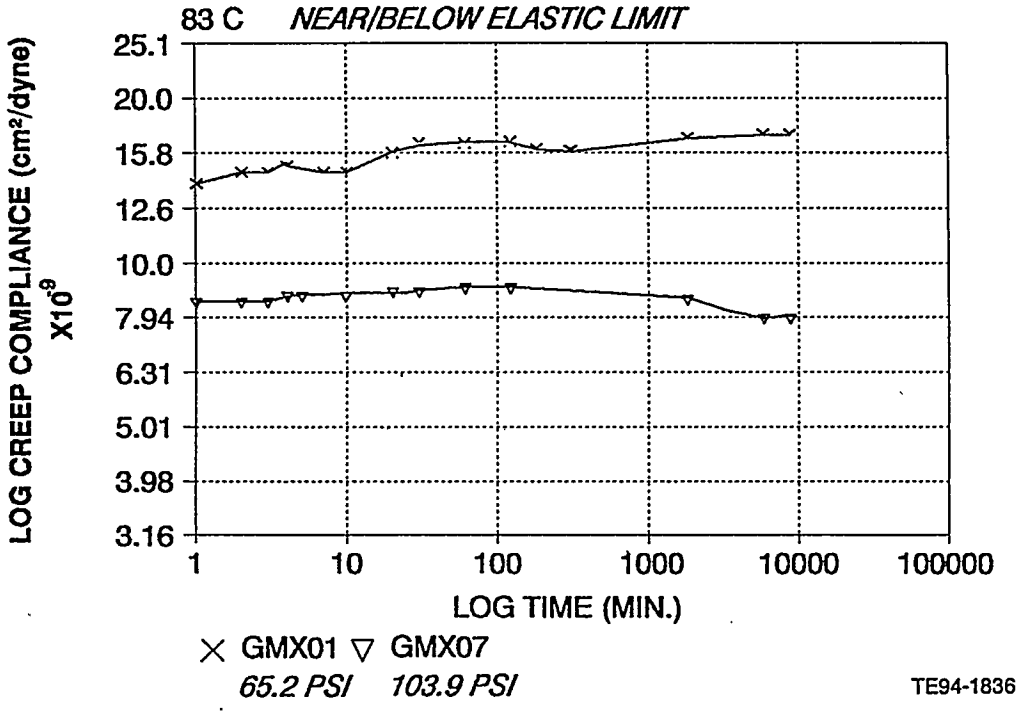


Figure 3.2.2-3. Film creep compliance as a function of time and low initial strain state.

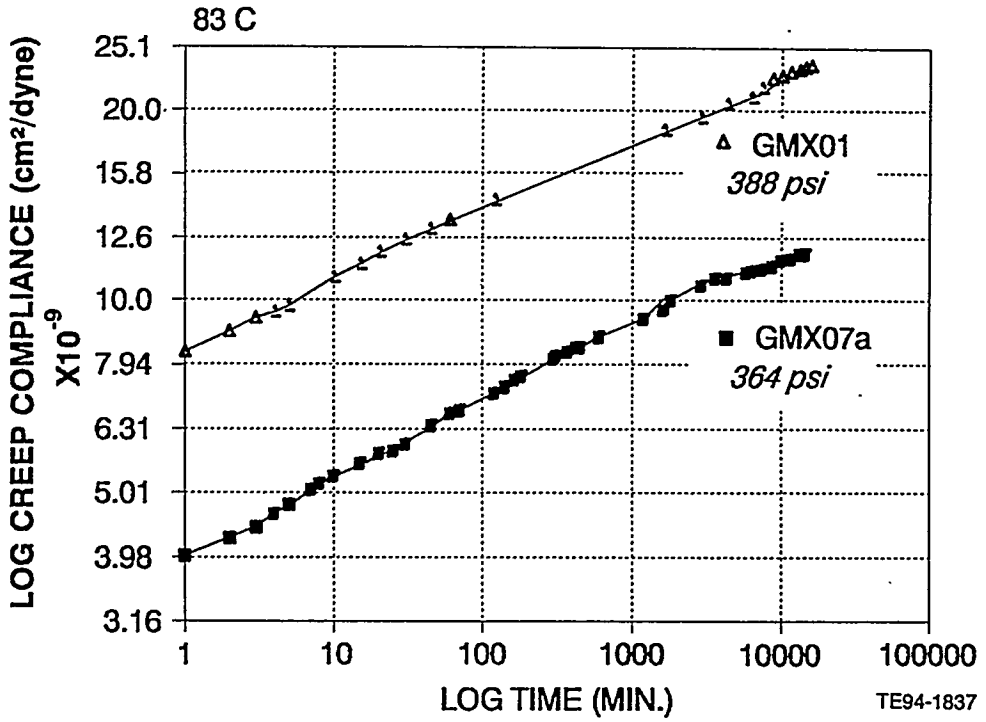


Figure 3.2.2-4. Film creep compliance as a function of time and high initial strain state.

Certain properties of the membrane polymer, principally equivalent weight and functional side-chain structure affect conductivity and gas permeability of the membrane. These transport properties, conductivity and gas permeability, were measured in this task.

Gas permeability of both hydrogen and oxygen through the membrane were determined at ambient temperature for polymers with equivalent weights between 790 and 920, the range in the experimental membrane designs described below. Permeability of the polymer film increased slightly as the equivalent weight was decreased, and as the water content of the membrane increased. In comparing gas permeability at the equivalent weight extremes of the experiment, 790 and 920 daltons, the hydrogen permeabilities were 52 and 37 barrers, respectively. Oxygen permeability varied even less and in the above film equivalent weight comparison, the values were 28 and 27 barrers, respectively. Permeability measurements on individual polymers were reproducible and flux was a very linear function of film thickness and pressure differential; permeability did not change with thickness. Permeability under fuel cell operating conditions was not measured during the contract effort, but, in other Dow funded work XU-13204.10 and Nafion 117™ were compared over a range of temperatures. Permeability of both membranes increased with temperature; the permeability of hydrogen, for example, was determined to be as high as 220 barrers at 90°C.

Resistivity, the inverse of conductivity, was determined over a broad range of equivalent weights for Dow short side-chain polymers in both aqueous acid water at 90°C and water saturated air at 80°C. In aqueous acid values ranged between 2.5

and 5 ohm-cm, while in humid gas values ranged from 8 to 17 ohm-cm. Assuming liquid water is present on the cathode (as it is formed there), 100% relative humidity gas exists at the anode, and that resistivity can be approximated by a linear gradient (the simplest assumption), the expected resistivity in the cell ranges from roughly 5 ohm-cm for the low equivalent weight end to 10 ohm-cm at the high equivalent weight. At 1 amp/cm$^2$ and a typical 0.01 centimeter thick film, these values would give rise to IR losses of 50 and 100 mV, respectively. For XU-13204.20, produced from an 800 equivalent weight polymer, the measured resistivity values are 3.5 and 9 ohm-cm, for aqueous and humid environments, respectively, yielding a gradient based value of 6.25 ohm-cm and an expected IR loss of 62 mV.

However, the membrane resistivity of XU-13204.20 in operating fuel cells is actually closer to the value measured in dilute acid. The $H_2/O_2$ polarization data for MEAs with different membrane thicknesses is depicted in Figure 3.2.2-5.

Based on this data, the membrane resistivity as a function of current density is presented in Figure 3.2.2-6.

The resistivity value of 4.5 ohm-cm (up to 1.5 amps/cm$^2$) is intermediate when compared to the dilute acid and humid gas values, but much closer to the liquid phase value. This may be the result of "back diffusion" of the cathode water toward the anode resulting in a stable, hydrated membrane even at the anode face. Net water transport data, measured to be near zero, tend to support this observation. This

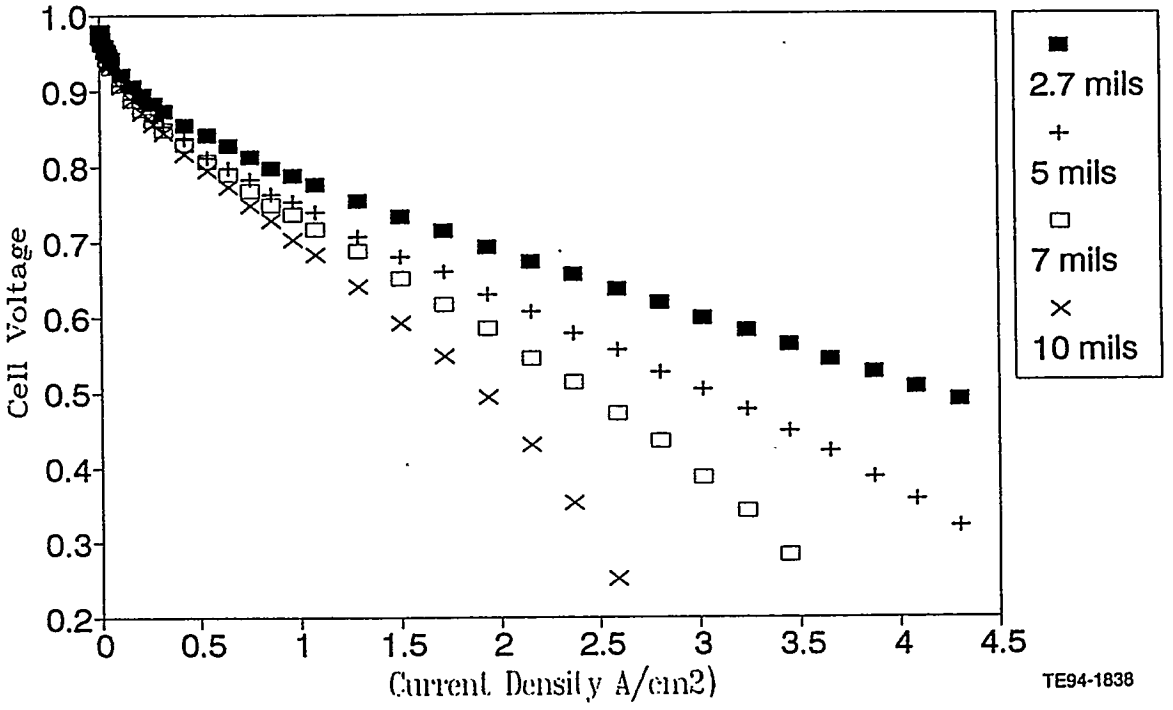


Figure 3.2.2-5. Cell voltage as a function of current density and membrane thickness.

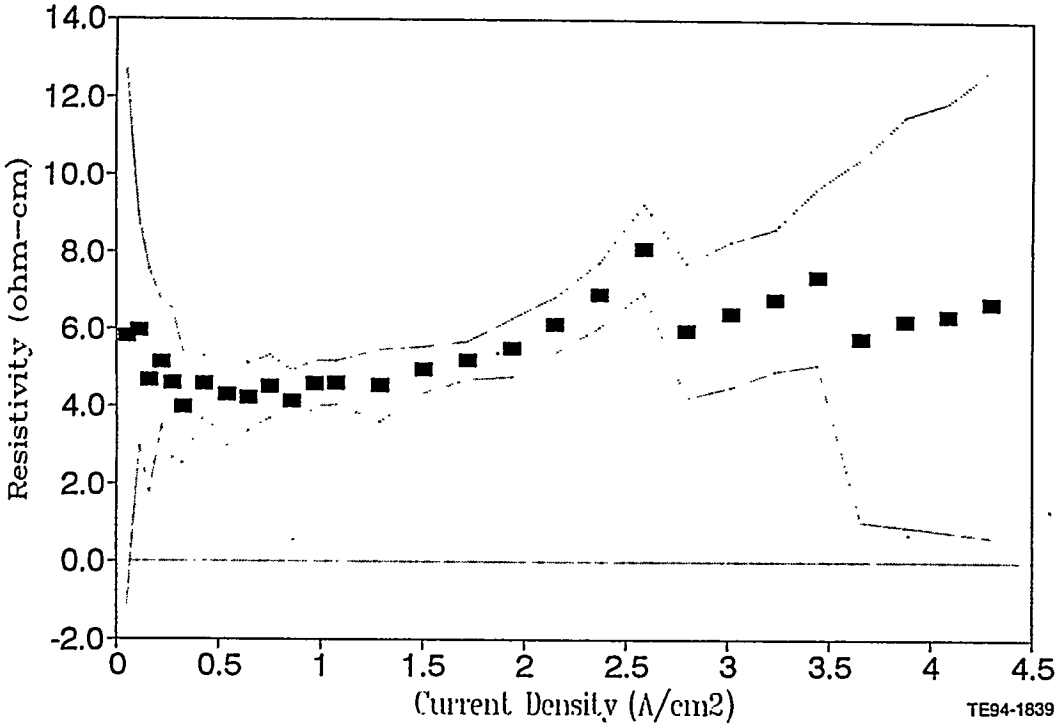


Figure 3.2.2-6. Membrane resistivity as a function of current density.

phenomenon is described in more detail below. The membrane resistivity values in Figure 3.2.2-6 were determined by linear regression of the voltage as functions of the membrane thickness and current density from the fuel cell performance data.

Cell resistance measurements (ohm-cm$^2$) as a function of current density provided equivalent, supporting results. See Figure 3.2.2-7.

Cell resistance of the thinner membranes remained nearly constant over the entire current density range while the cell resistance of the thicker membranes increased at high current densities; further, the onset of resistance increase moved to lower current densities with increasing thickness. These observations agree qualitatively with published transport models. Internal modeling efforts similar to published models are in progress.

Water transport across the XU-13204.20 membrane is essentially zero over a wide range of fuel cell operating conditions. Full fuel cell water balances were performed using Dow membrane XU-13204.20 over a range of current density, cell operating temperature, pressure, and pressure differential across the membrane. The high end current density employed in these tests was 1.94 amperes/cm$^2$ (1800 amperes/ft$^2$). A summary of these data, attained by plotting the calculated transport in moles of water per mole of protons as a function of fractional recovery, appears in Figure 3.2.2-8.

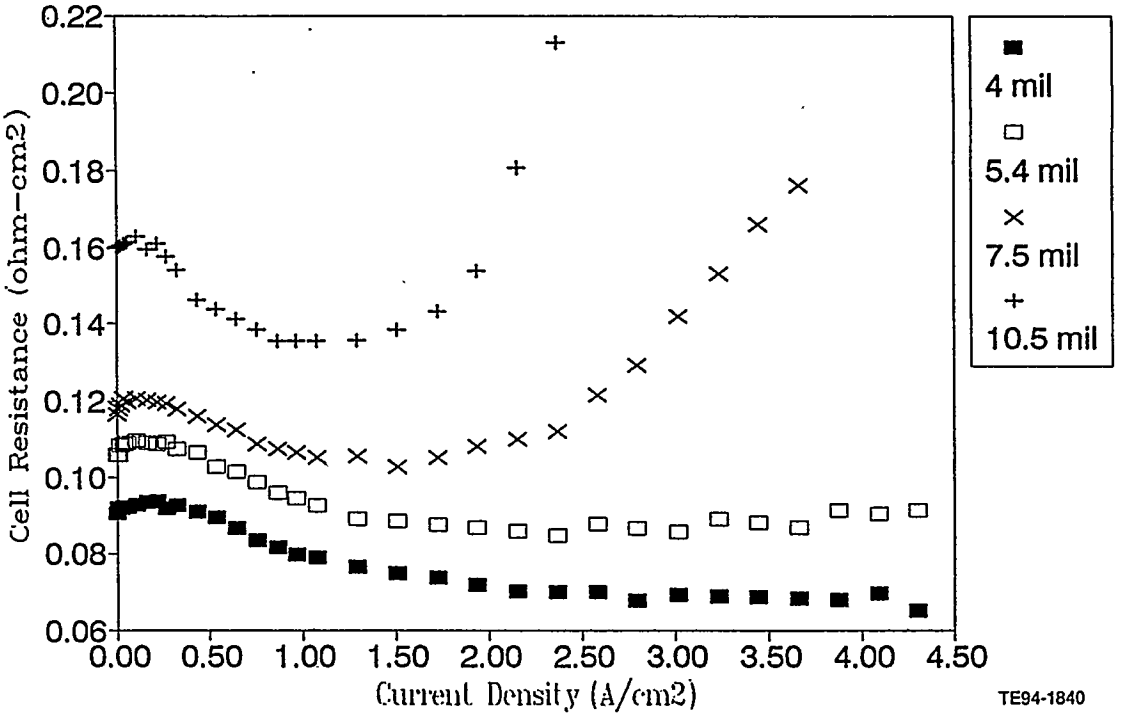


**Figure 3.2.2-7. Cell resistance as a function of current density and membrane thickness.**

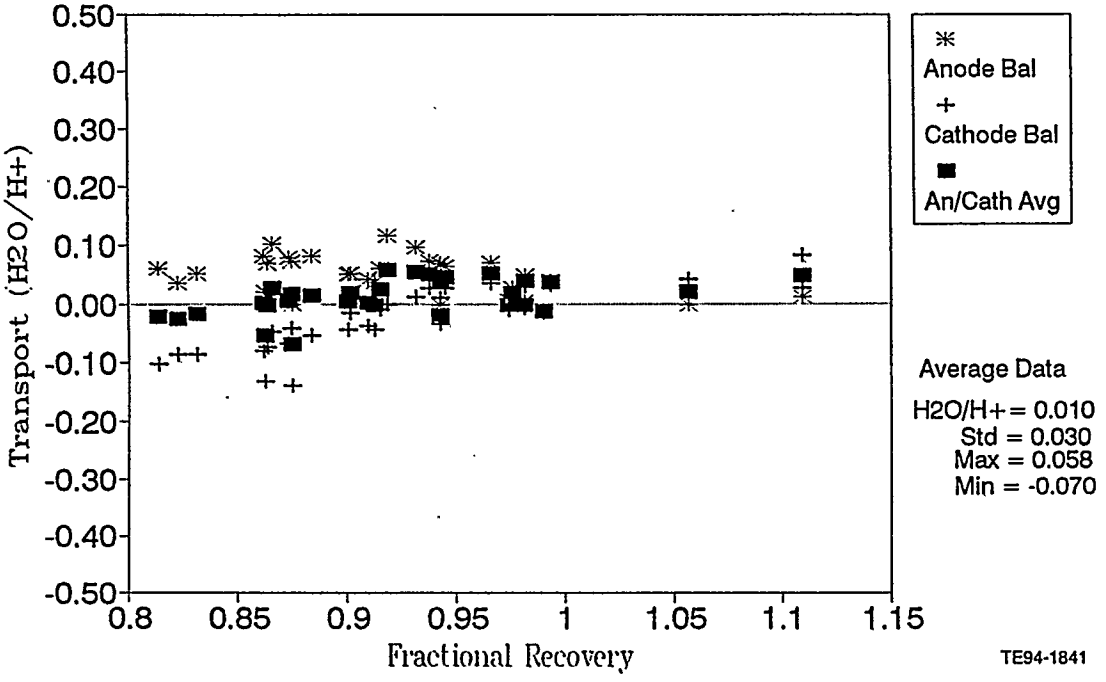


**Figure 3.2.2-8. Osmotic water transport data.**

Fractional recovery is a measure of the quality of the individual experiment. For all conditions, the water transport was small, less than 0.1 for nearly all measurements and very close to zero for the best experiments, i.e., fractional recovery near one. The overall statistics with recoveries between 0.9 and 1.1 are shown on the right side of Figure 3.2.2-8; the average transport was 0.01 with an error of 0.03.

### Membrane and MEA Process Improvements

Membrane polymer properties were varied in an attempt to gain strength without sacrificing conductivity, i.e., to move away from the "standard" relationship between mechanical and transport properties. As an example of a step change, Dow monomer chemistry provides a shorter (probably the shortest possible) side-chain to link sulfonic acid groups to the main polymer chain. This provides higher charge density in the polymer at any given comonomer ratio, side-chain monomer to tetrafluoroethylene, which translates into higher conductivity for a given tensile modulus. An experiment was conducted to evaluate two basic polymer properties and their possible interaction with the prime property determinant, equivalent weight, as demonstrated in Figure 3.2.2-9. The two additional basic design polymer properties were "molecular weight" and "equivalent weight distribution". These are placed in quotation marks because no adequate measurement methods for these properties exist despite significant development efforts.

Polymer synthesis conditions were adjusted to produce modified polymers at two points on the equivalent weight axis, near 800 and 900 daltons; these points were previously shown as boxes in Figure 3.2.2-1. Regarding the molecular weight, Dow is able to measure polymer melt rheology and intrinsic viscosity, which are both

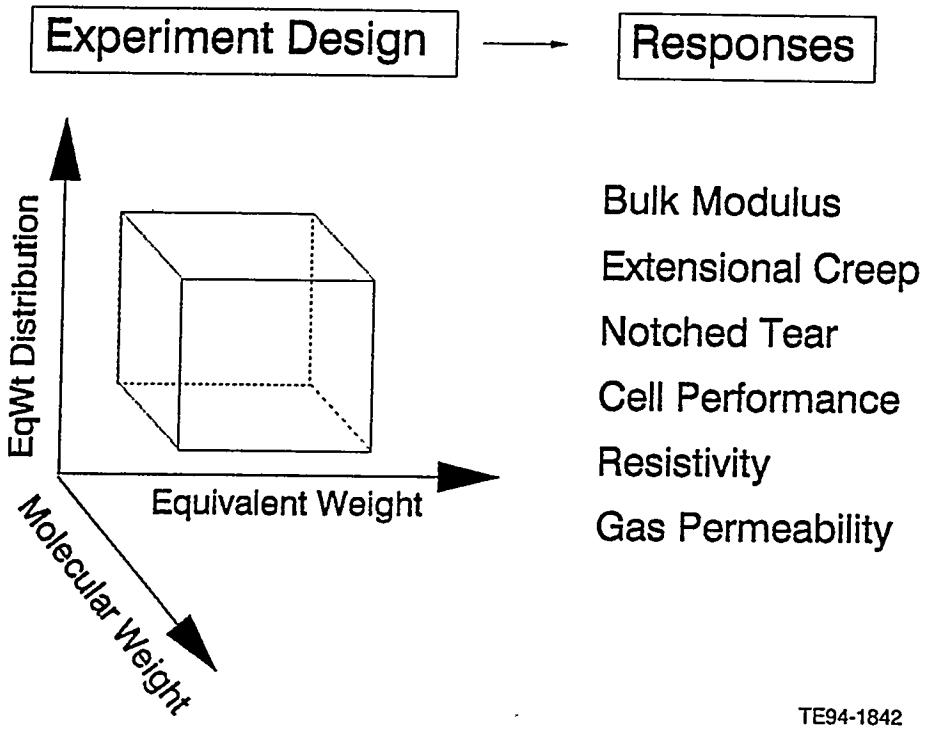


Figure 3.2.2-9. Effects of varying polymer properties.

proportional to, but are not direct measures of, molecular weight. In this experiment, high-end targets for melt rheology were selected so as to ensure the ability to fabricate films. The actual variable used to obtain different equivalent weight distributions is a process condition since no direct measure of equivalent weight distribution exists. Overall results were disappointing. Measured property values for membranes in this experiment indicate that equivalent weight is the only statistically significant factor. Follow up synthesis and evaluation of higher molecular weight polymers, polymers with extremely high melt viscosity, resulted in only a small increase in film modulus, roughly 10%.

Fuel cell performances of MEAs based on the polymers designed and fabricated in these experiments were measured. For these tests, MEA composition and processing conditions were held constant in order to precisely delineate polymer effects. Without any MEA process changes, fuel cell performance did not correlate with the primary performance related bulk property, conductivity. Concurrently, the fuel cell based membrane resistance data, including attempts to measure individual MEA component contributions to total cell resistance, suggested significant contributions other than that from the membrane. Cell related resistance and "quality" of the electrode-membrane interface within the MEA were found to be very important.

Follow-up from these results involved tailoring the MEA processing conditions, a more in depth study of polymer rheology, and attempts to improve the interface via surface modification. The impacts of MEA process change on oxygen and air performance of XU-13204.20 are presented in Figures 3.2.2-10 and 3.2.2-11, respectively.

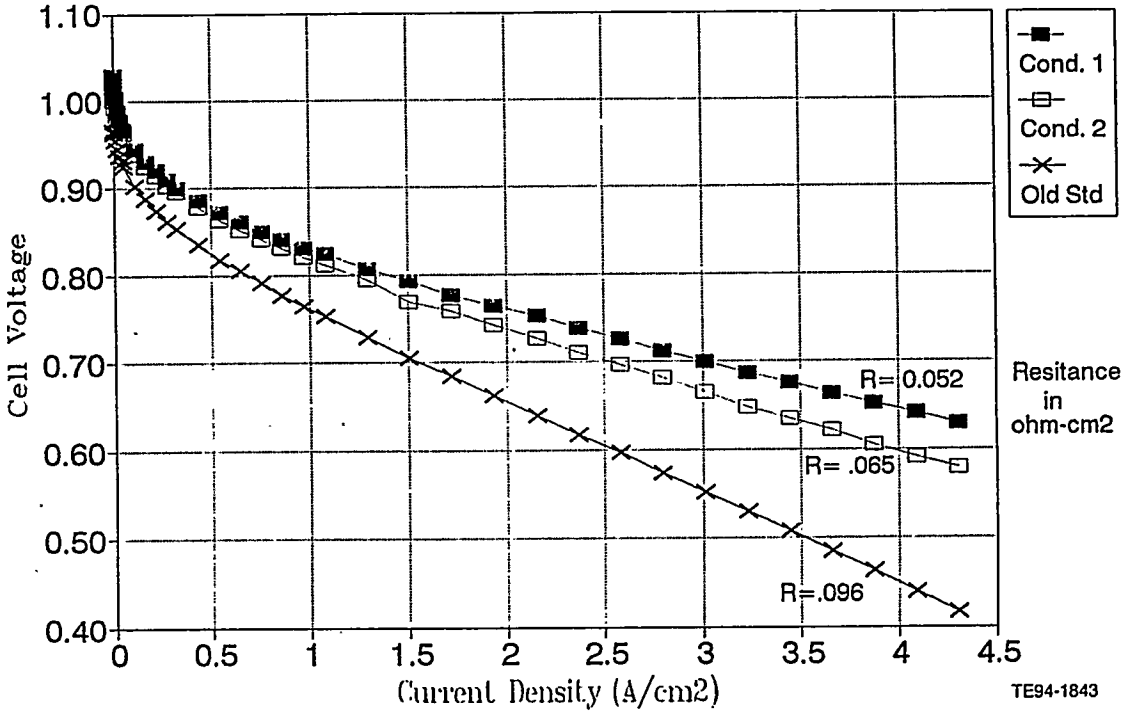


Figure 3.2.2-10. Impact of MEA process change, cell voltage as a function of current density, $H_2/O_2$ reactants.

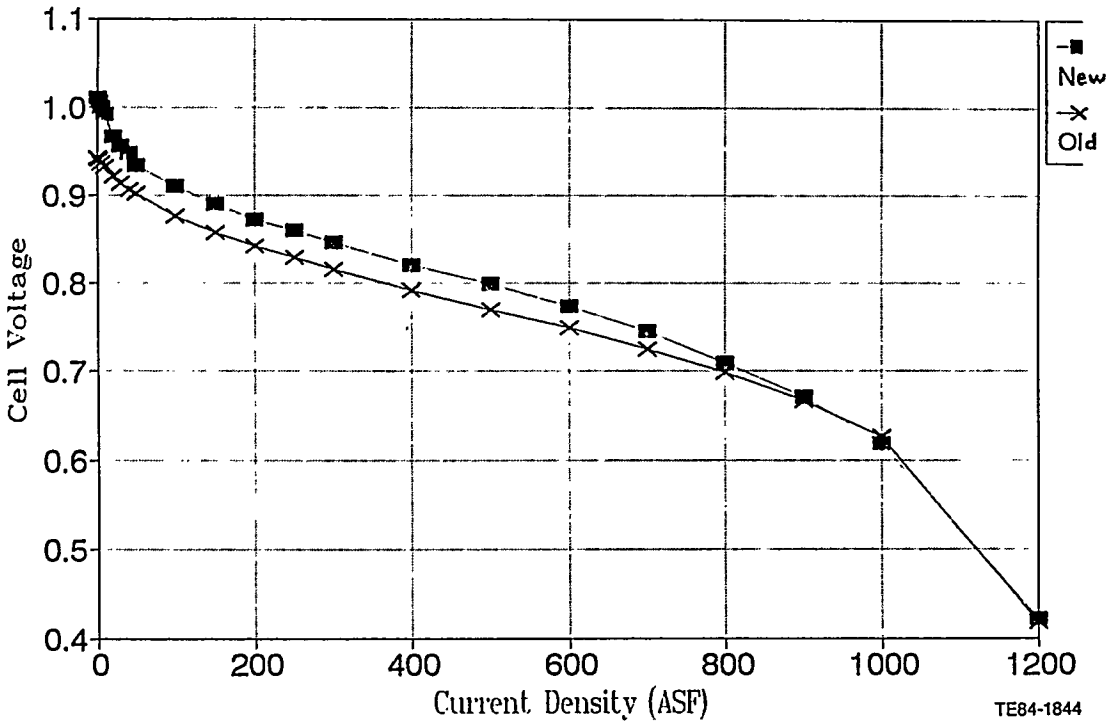


Figure 3.2.2-11. Impact of MEA process change, cell voltage as a function of current density, $H_2$/air reactants.

The lower curves in the figures demonstrate data for the standard process used in the experimental design work while the upper curves illustrate the impact of process changes. Oxygen performance was increased significantly, some 80 to 90 mV at 2 amperes/cm$^2$. The resistance values were obtained via regression of the voltage as a function of current density data using a combination of linear and logarithmic terms; resistance is closely approximated solely by the linear term when the fuel cell is operating with oxygen. With the "improved" process, the total resistance was very near the value expected for the hydrated membrane alone. As depicted in Figure 3.2.2-11, cell voltage on air was also increased by the process change. Voltage at low current density was increased by roughly 30 mV but the air (oxygen) transport limitations at higher current densities was unchanged. Performance comparisons of a standard process MEA with a modified MEA employed on a modified membrane made with a higher equivalent weight polymer are presented in Figures 3.2.2-12 and 3.2.2-13.

Both oxygen and air reactant curves are depicted. Performance of the high equivalent weight polymer nearly equals that of XU-13204.20. More results of the MEA process change on various films resulting from the experimental design work are presented in Figures 3.2.2-14 and 3.2.2-15. GMX09 and GMX13 are both films fabricated from 900 equivalent weight polymers while GMX11 was produced from a 980 equivalent weight polymer. Compared to XU-13204.20 (GMX01) using a MEA fabricated with the "old standard" process, each of the materials can be processed to provide near equivalent voltage performance, at least over the current density range of primary interest. Comparison of results on air, Figure 3.2.2-15, also support this conclusion.

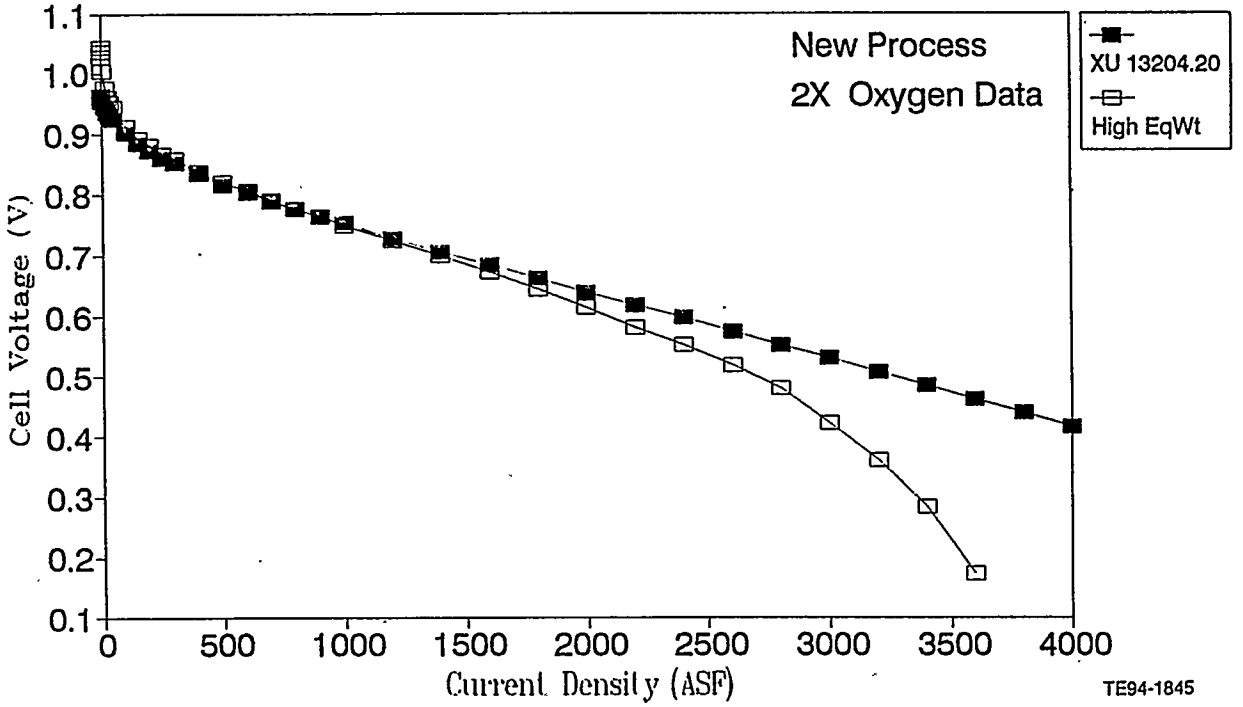


**Figure 3.2.2-12. Polymer comparisons - modified polymer, cell voltage as a function of current density, $H_2/O_2$ reactants.**

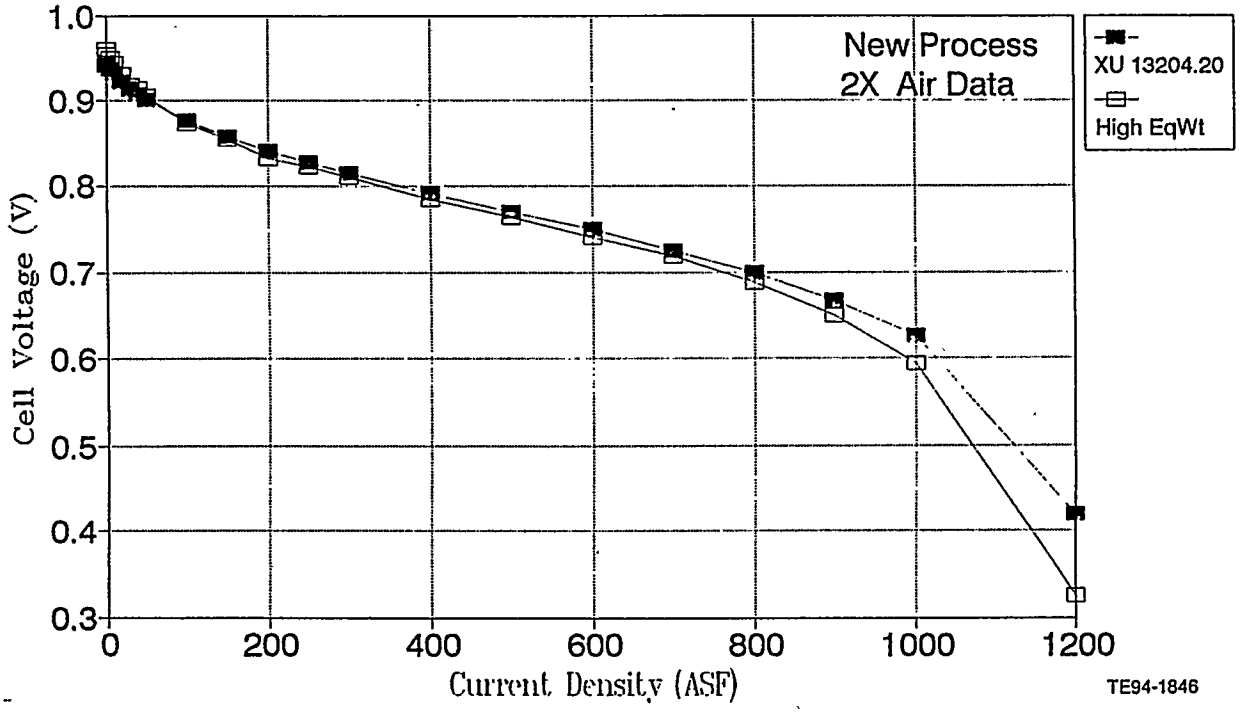


**Figure 3.2.2-13. polymer comparisons - modified polymer, cell voltage as a function of current density, $H_2$/air reactants.**

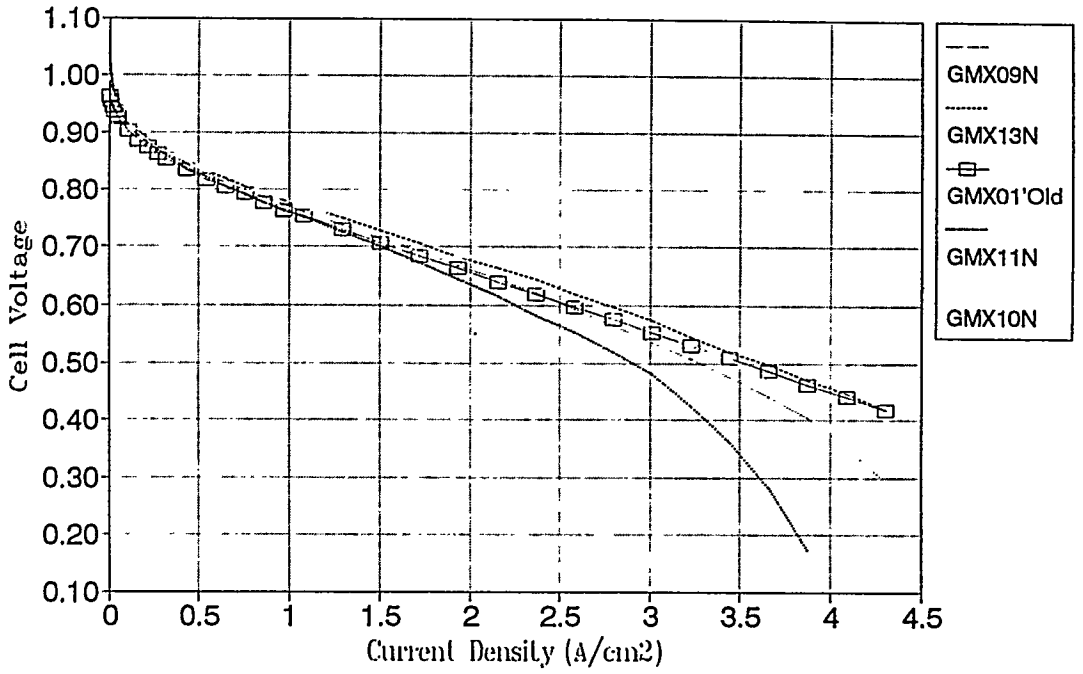


**Figure 3.2.2-14. Impact of MEA process/polymer change, cell voltage as a function of current density, $H_2/O_2$ reactants.**

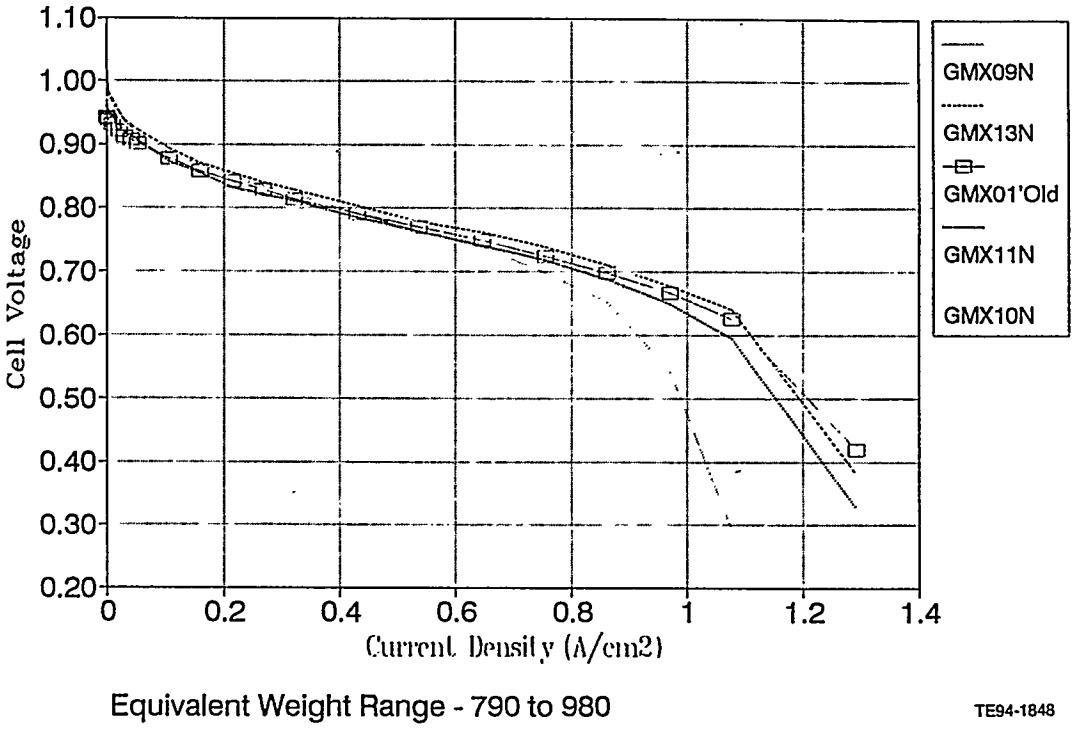


**Figure 3.2.2-15. Impact of MEA process/polymer change, cell voltage as a function of current density, $H_2$/air reactants.**

Surface modification of membranes was also evaluated as a means of improving performance. The performance improvements using one such modification on an intermediate equivalent weight (895) polymer film is illustrated, for oxygen and air reactants, respectively, in Figures 3.2.2-16 and 3.2.2-17.

In these figures the performance of an MEA using XU-13204.20 (equivalent weight of 800) is included for reference. The performance of the higher equivalent weight film was improved by the modification, but, clearly, modification of the surface did not compensate for the difference in "bulk" conductivity between the two films. Both equivalent weight and thickness are critical controls for membrane performance. Using surface modification, "acceptable performance" has been demonstrated with films made with polymer equivalent weights as high as 1260 daltons.

The primary conclusion of the membrane development section is that several approaches to improving the performance of MEAs based on stronger, higher equivalent weight polymer films were successful. Polymer modification combined with optimization of MEA fabrication process provided MEAs with nearly equal performance; the small voltage differences observed for different membrane polymers approached those expected based upon simple bulk resistivity differences.

***Electrode Development***

The second Dow Task under the contract was to improve electrode and MEA structure. Dow's effort in this area has been schematically described in Figure 3.2.1-2 in the Introduction and Summary to this section. Dow's objective was to produce membrane-electrode assemblies which provide high power performance on air with

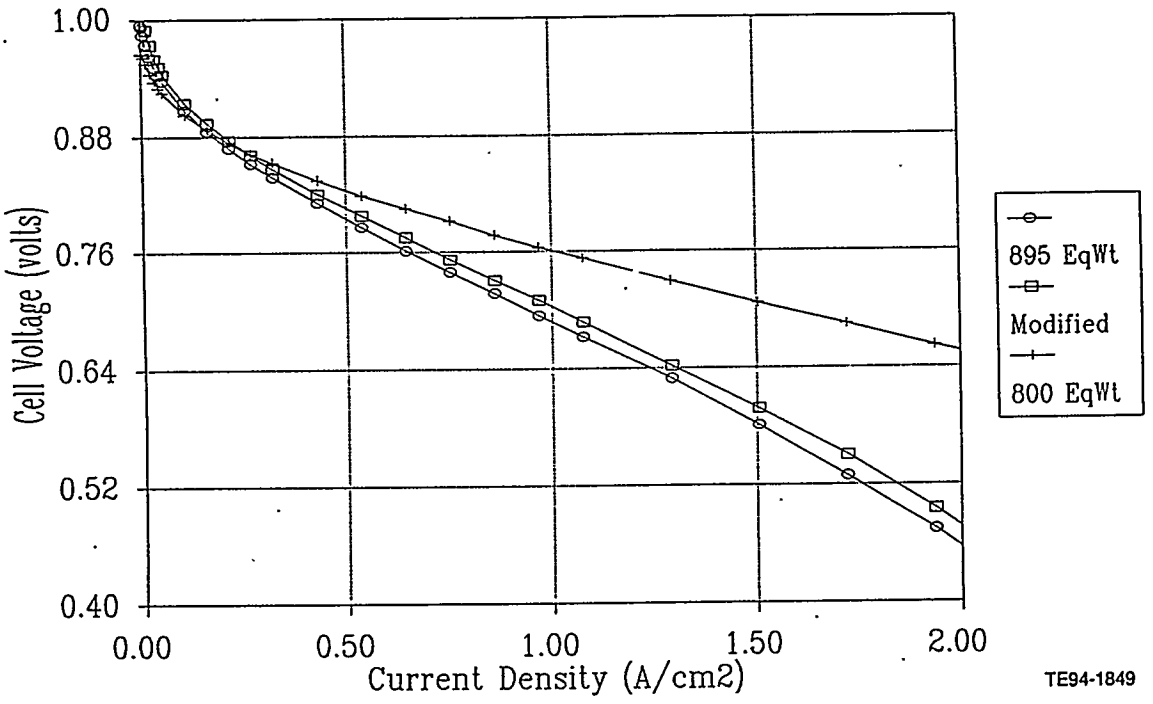


Figure 3.2.2-16. Impact of Membrane Surface Modification, Cell Voltage as a Function of Current Density, $H_2/O_2$ Reactants.

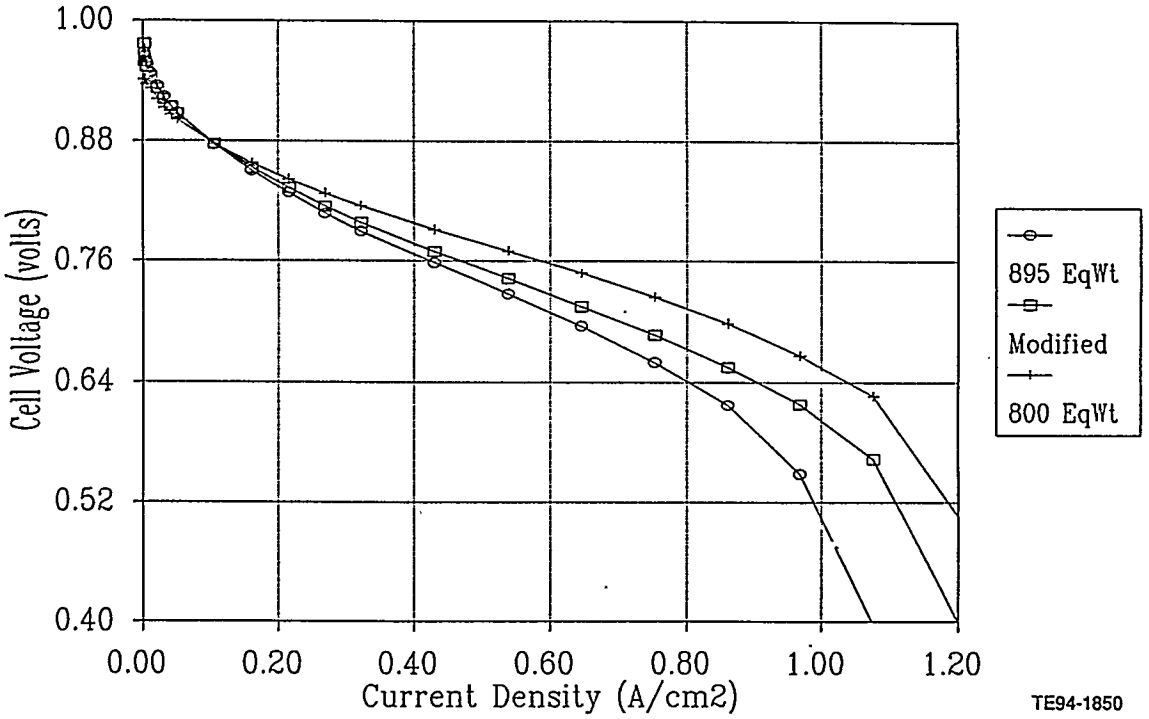


Figure 3.2.2-17. Impact of Membrane Surface Modification, Cell Voltage as a Function of Current Density, $H_2$/Air Reactants.

low platinum loadings. As is clear from the literature of electro-reduction of oxygen, platinum is the best catalyst available, but even with platinum the exchange current density is still quite small. The overvoltage for oxygen reduction, even at low current density, is by far the largest component of fuel cell efficiency loss. Dow's focus, however, was to develop new processes and improved compositions that create structures which provide higher platinum utilization and improved gas transport for operation on lower pressure and lower stoichiometry air. Both platinum black and carbon supported platinum catalysts were evaluated. Although the lowest catalyst loadings will require supported catalysts, low loadings with platinum black are attainable and most of Dow's work to date has involved platinum black catalysts. The electrode development effort is experimentally complex, involving electrode composition factors and variations in both electrode coating and MEA lamination processes. Work to date, focused entirely on the cathode, has comprised electrode and MEA fabrication, evaluation of fuel cell performance, and attempts to correlate performance with structure. Microscopies, optical, SEM, and TEM, were used extensively.

Performance on air was improved dramatically through change in both composition and processing of the graphite paper supports. Air performance of two MEAs, one fabricated with an earlier process and one with the improved process, is compared in Figure 3.2.2-18.

Although performance varied somewhat with the old process, limiting currents rarely exceeded 800 amps/ft$^2$. With the improved process, using an XU-13204.20 membrane, air performance is reproducibly between 0.62 and 0.66 volts at 1000 amps/ft$^2$ in Dow's test cells under standard conditions. Stoichiometry and flow

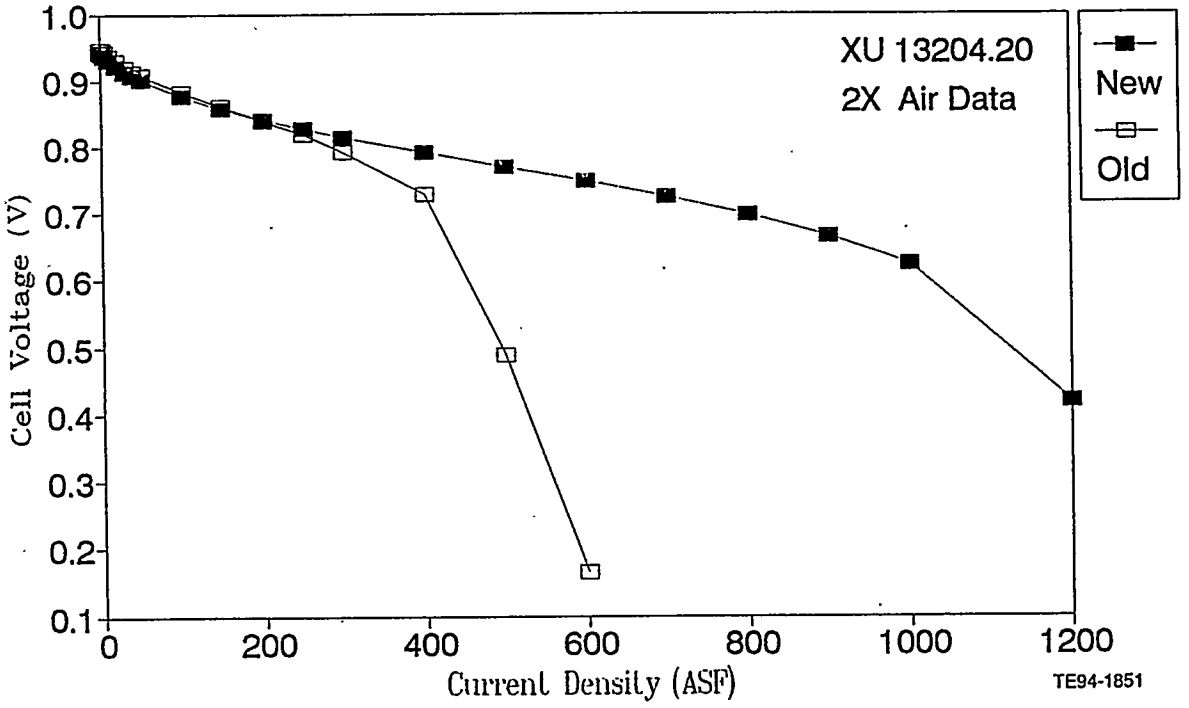


Figure 3.2.2-18. MEA process modification, cell voltage as a function of current density, $H_2$/air reactants.

field plate design also impact performance; the performance and the sensitivity to structure of the graphite support paper differ with test conditions.

Data comparing the performance on oxygen of platinum black electrodes at 1 mg/cm$^2$ loadings with that obtained using the standard loading of 4 mg/cm$^2$ is presented in Figure 3.2.2-19.

Clearly, no significant performance difference is observed down to 1 mg/cm$^2$ loadings on either the anode or cathode. Performance on air suffered far greater as the Pt loading was decreased. To improve air performance at reduced Pt-black loadings, only small modifications to "standard" fabrication process were required; these modifications focused on changes to the support structure and on alternative approaches to coat the catalyst layers. The hydrogen/air reactant performance of an MEA, representative of Dow's present capability with low platinum black electrodes, as compared to the performance of a control MEA with 4 mg/cm$^2$ loading is presented in Figure 3.2.2-20.

Intermediate loadings were evaluated but performance is presented only for the lowest, "successful" loadings attained. First, modifying the support structure improved the performance of MEAs with both high and low catalyst loadings. Without support structure modification, performance on air decreased significantly with decreased loading; however, with the support structure modification, performance still slightly decreased but was considerably improved, approaching that of the highly loaded cathode.

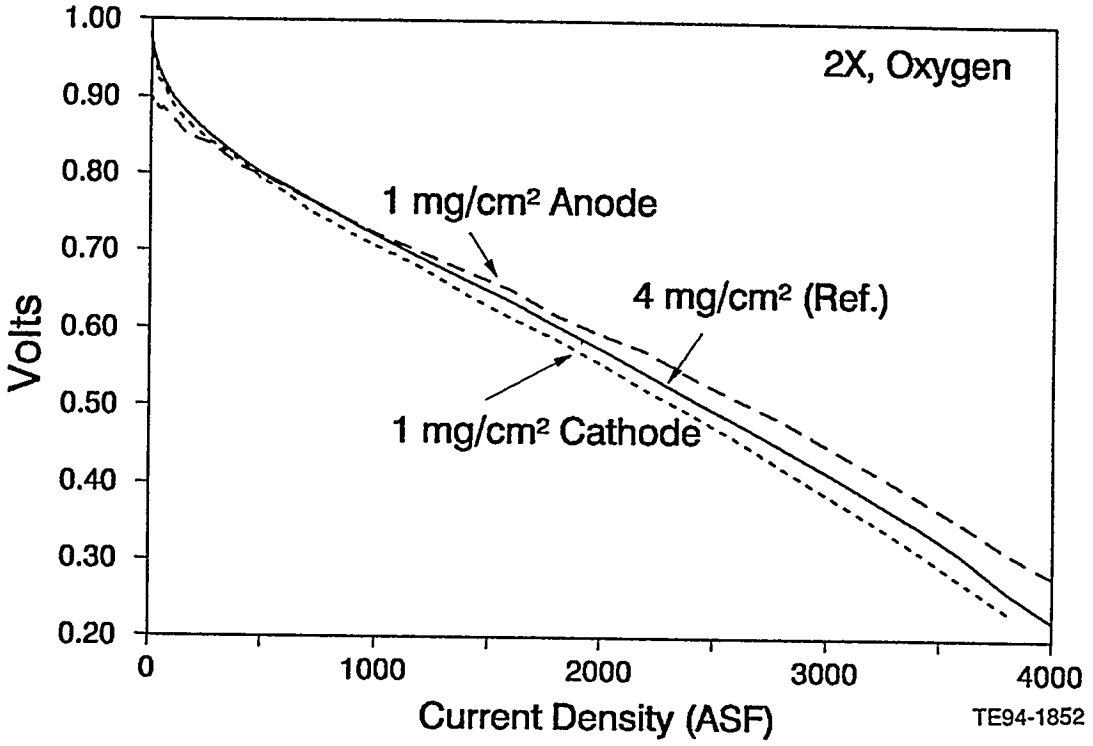


Figure 3.2.2-19. Effect of platinum loading, cell voltage as a function of current density, $H_2/O_2$ reactants.

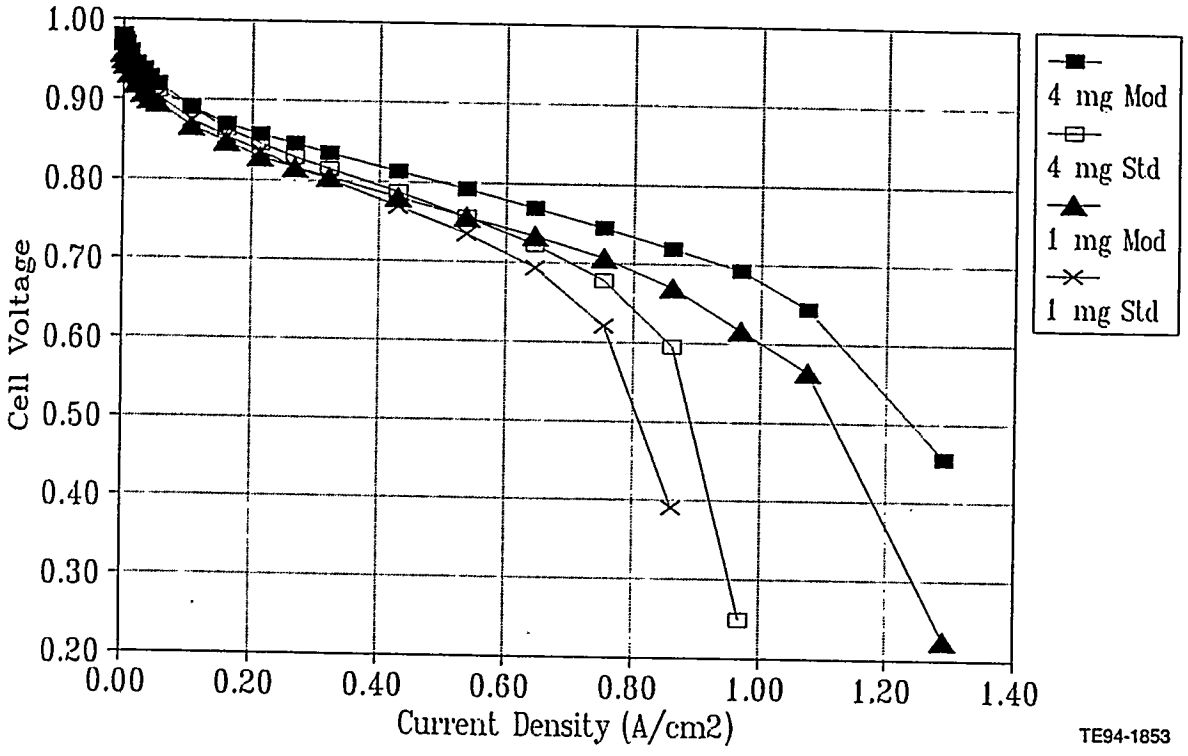


Figure 3.2.2-20. The effects of cathode loading and substrate changes on hydrogen/air fuel cell operation.

Performance loss with lower cathode loadings of platinum black is still too large; further work is planned. It is expected that electrodes with platinum black loadings down to 0.5 mg/cm² can be produced that have only a modest performance loss, but reduction in loadings much below 0.5 mg/cm² will require supported platinum. Work with supported catalysts was initiated during the first phase effort, but performance did not compare with the levels attained with platinum black.

### *Lifetime Demonstration*

Stable performance over long-term operation (years) is critical to the success of fuel cell systems. Clearly, stable MEA performance is at the heart of stable system performance. Attempts to demonstrate such stability were initiated and continue, but the desired stability has not yet been demonstrated. Early attempts suffered from instability of the test system as well as some loss in MEA voltage at constant current density. Results to date (10/93) are presented in Figure 3.2.2-21.

The MEA in this test had standard 4 mg Pt-black active electrodes but was fabricated with "improved" processing to give higher performance on air. The standard operating conditions described earlier were used with current maintained at 500 amps/ft² equivalent. Periodic upsets, such as tests to obtain full polarization curves, occurred and the cell was rebuilt once to replace a fouled humidifier membrane. Voltage decreased linearly with operating time at a rate of -1.0 mV/day. Further effort in this area is required; recent data by Los Alamos researchers indicate that air injection on the anode, even when $H_2$ is used as the reactant, restores cell voltage losses similar to those observed in Figure 3.2.2-21. This is believed to be due to $CO_2$ contamination; "pure" $H_2$ contains several ppm of $CO_2$ which appears to affect long term performance.

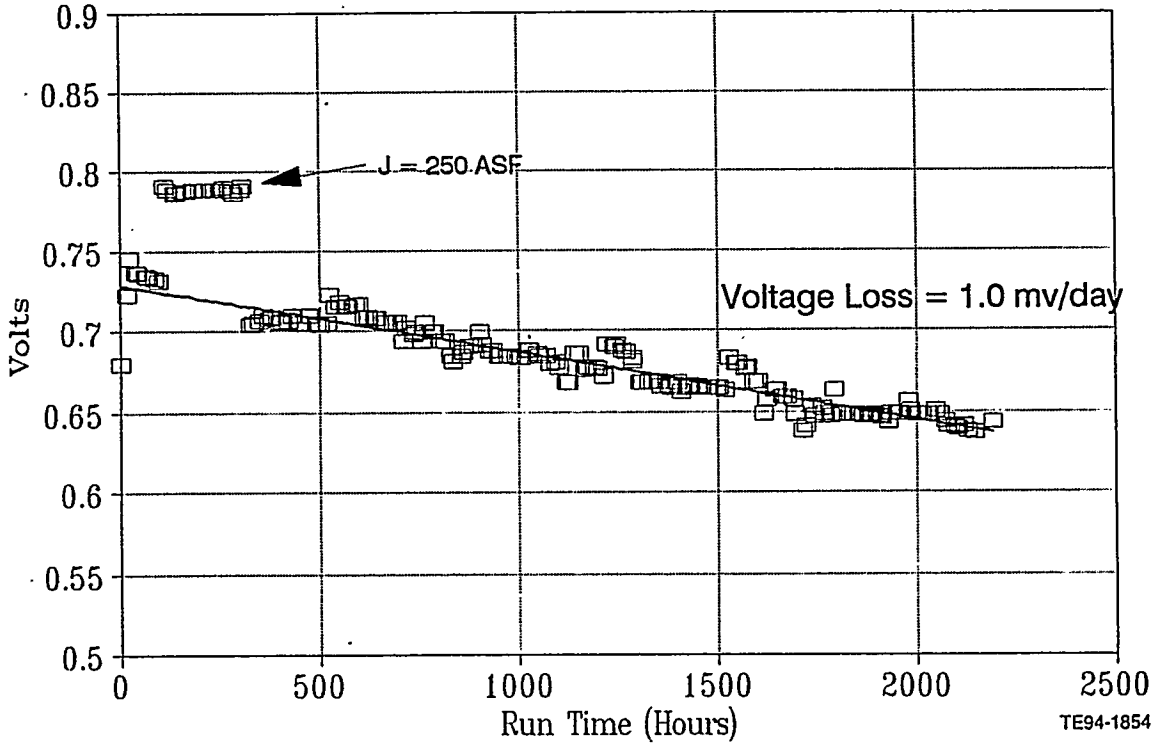


Figure 3.2.2-21. Lifetime test, cell voltage as a function of time.

### *High Temperature Operation*

For motive applications, high temperature operation could provide a means by which to manage carbon dioxide and/or carbon monoxide poisoning of the anode catalyst. This was the primary reason for work in this area. Testing capability was installed (non-contract funded) and initial testing was accomplished. Short-term performance on hydrogen and air to 150°C was demonstrated. Operation to 500 amps/ft$^2$ was tested; no "significant" change in cell voltage was observed when data from 80°C to 150°C is compared. Significant is qualified because small changes were observed, but both system conditions and MEA performance were variables; more systematic and extensive evaluation is needed.

### *Development Goals for Phase II*

Several goals of the first phase effort were not fully attained. Power performance better than that provided by Dow XU-13204.20 was not achieved. Improved power performance with acceptable MEA "integrity" likely can be achieved with thinner membranes combined with improved MEA fabrication process. High power performance with ultra-low Pt loadings was not achieved. Efforts under the contract focused on low platinum black loadings and reductions to as low as 0.50 mg/cm$^2$ of MEA are envisioned. Work by others demonstrates that higher platinum utilization can be achieved with carbon supported platinum. Better performance at lower flow pressures and stoichiometries is highly desirable; both cost effective processes and stable long-term performance need to be demonstrated. Adequate performance stability on air was not demonstrated. It is fully anticipated that air stability, adequate for both motive and stationary applications, will be demonstrated. Continuing effort will be required with both existing and newly developed MEA structures.

Two additional goals should be addressed. First, carbon dioxide and carbon monoxide resistant anode catalysts should be evaluated with emphasis on long-term performance demonstration. Second, MEA fabrication capability, based on processes consistent with volume production, should be demonstrated and used to support stack development efforts within the project. A minimum of three to four hundred MEAs will be needed for this effort, most in a size larger than those supplied in Phase I. Addressing this effort from a "production" view point will aid Dow's assessment of potential total costs of membrane-electrode assemblies.

## 3.3 ELECTRODE STRUCTURE AND CATALYST DEVELOPMENT EFFORTS AT GENERAL MOTORS NAO R&D CENTER

### 3.3.1 Introduction and Summary

GM NAO R&D research on PEM fuel cell electrode/membrane assemblies is directed towards attaining both low cost and high performance to aid in the commercialization of the fuel cell within the transportation sector. Factors determining cell performance are catalyst utilization, catalyst activity, ohmic voltage losses, and water management.

Commercially available E-Tek electrodes have an estimated catalyst utilization of only about 15%. Catalyst utilization has been increased dramatically by efforts at LANL and GMR&D on preparing thin catalyst layered electrodes with low Pt load-

ings (< 0.2 mg/cm$^2$). Thin layer electrodes do produce a lower voltage performance (and in some low current regions perhaps even a lower catalyst activity in terms of A/mg) compared to high Pt loaded electrodes at higher cell voltages, where the cell performance is controlled by oxidation reduction kinetics reactions. However, when the cell performance is dominated by ohmic polarization losses at higher current densities, thin layer electrodes, while still producing a slightly lower voltage at comparative current densities, do have a significant advantage in catalyst activity compared to Pt-black electrodes.

The problem of catalyst activity assumes increased importance when operating on methanol reformate and air. Deactivation of the Pt catalyst due to the presence of $CO_2$ and CO in the fuel stream can be partially overcome by modifying Pt with Ru and by mixing air with the reformate fuel. Ohmic polarization losses become important at operating current densities higher than 300 ma/cm$^2$, especially at lower operating temperatures and pressures. Ohmic losses at the membrane/ electrode contact zone may be reduced by optimizing the MEA preparation method, controlling the loadings of polymers, such as Teflon and Nafion, and by enhancing the conductivity of the carbon support used to disperse the catalyst. Finally, water management in the cell is a critical issue since it can lead to cell failures due to membrane drying and electrode flooding. The approach utilized in this R&D effort is to optimize the hydrophobicity of the carbon support to meet the differing needs of the electrode reactions and to optimize the properties of the current collector to facilitate transport of gases to the catalyst layer.

GM NAO R&D has developed a simple Nafion™ slurry coating technique for preparing ultralow Pt loaded thin film electrodes. The technique can be applied to any type of membrane and has led to nearly an order of magnitude improvement in catalyst utilization (activity). The method, subject of a U.S. patent December 1993 (Ref. 3.3), involves coating thin film electrodes ($\geq$ 0.2 mils thick) on a membrane or a carbon current collector using a Nafion™ slurry containing catalyzed carbon. The current collector method has been applied to membranes from various suppliers and with vastly differing physical properties and is easily adapted for mass production. On the other hand, the methods developed by Wilson and Gottesfeld at LANL require either the membrane to be in the sodium form or more laborious decal procedures. Thin film electrodes were employed for fuel cell evaluation involving various membranes, catalysts, catalyst preparation methods, carbon supports, and catalyst loadings. Catalyst utilization was a maximum of 6 amps/mg at a Pt loading as low as 0.1 mg/cm$^2$/cell and an assembly with a Pt loading of 0.14 mg/cm$^2$/cell performed better than an assembly with E-Tek electrodes with a total Pt loading of 1.0 mg/cm$^2$/cell. Carbon supports suitably pre-treated led to a 50% improvement in cell performance compared to the as received Vulcan XC-72R carbon. In catalyst studies, the Pt preparation method used at GMR&D helped achieve a higher fuel cell voltage, even with negligible carbon support pre-treatment, compared to the E-Tek electrodes that are prepared by a peroxide oxidation method. Also, Pt-Ru catalyst alloys helped reduce the $CO_2$ poisoning problem at the fuel electrode. A 3 mil experimental membrane from Asahi Glass delivered the best performance among the various membranes that were tested; the activity of the membranes tested increased in the following order: Asahi (3 mil) > Nafion 112™ > Dow XU-13204.2 (5 mil) > Nafion 115™ > Nafion 117™. These results should, however, be interpreted as qualitative in nature. Test results were obtained on hydrogen and oxygen reactants at temperatures $\leq$50°C and pressures not exceeding 4 psig. While the performance attained to date is extremely encouraging (given the operating

pressures and temperatures to which GMR&D has been restricted) individual membrane and electrode assemblies may exhibit different trends at elevated pressures and temperatures. Further, a comparison of 3 mil Asahi and 2 mil Nafion™ membrane performance to 5 mil Dow membrane performance is inconclusive considering the 50+% improvement in cell performance when the Dow membrane is thinned from 5 mil to 2.7 mil (refer to Figure 3.2.2-5). All of these MEA's will be tested at appropriate temperatures and pressures in Phase II.

### 3.3.2 Discussion of M&E Development and Results

The current-voltage performance of a thin film GMR&D assembly with a Pt loading of 0.14 mg/cm²/cell is compared in Figure 3.3.2-1 with the performance of a conventional assembly prepared from commercially available E-Tek electrodes (1.0 mg Pt/cm²/cell).

The catalyst utilization of the thin film assembly is nearly an order of magnitude higher than the assembly prepared from E-Tek electrodes. A consideration of the various factors that determine catalyst utilization showed that the thin film electrode structure localizes the catalyst within the dimensions of the reaction layer, while maintaining a high degree of electrolyte and catalyst dispersion and minimizing the fraction of catalyst atoms that are poisoned by polymers used to prepare the electrodes. On the other hand, the catalyst is dispersed over a thickness of nearly 4 mils in a conventional electrode such as the E-Tek electrode; only a fraction of the catalyst atoms are accessible to the Nafion™ electrolyte, thereby considerably reducing the catalyst utilization efficiency.

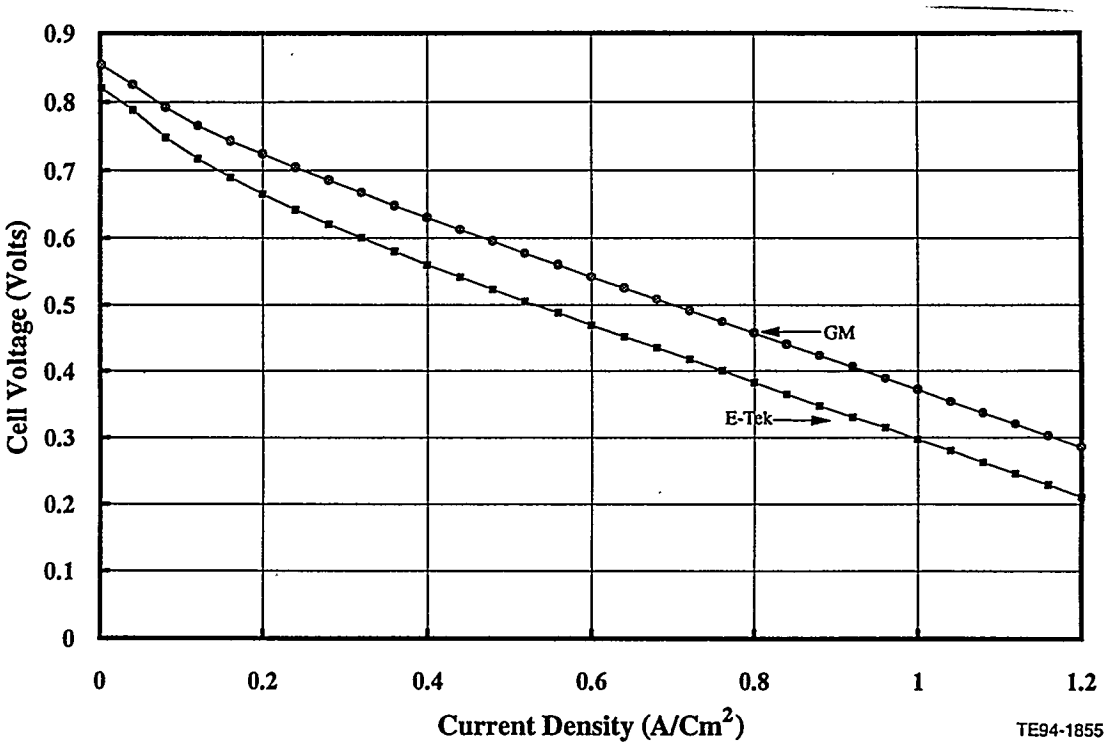


Figure 3.3.2-1. GMR&D thin film assembly performs better than a commercially available E-Tek electrode with a 7-fold excess of Pt. The fuel cells were operated on $H_2/O_2$ at 50°C and 4 psig $O_2$ backpressure.

Thin film electrodes are usually prepared without any Teflon binder, which is also the wet proofing agent in conventional electrodes. The addition of up to 15% Teflon did not have any appreciable effect on the performance of these thin film electrodes. However, it is desirable to eliminate Teflon in the slurry to assist electrode preparation. In the absence of Teflon, thin film electrodes depend on the physical properties of the carbon catalyst support to optimize hydrophobicity at the electrodes. Eight different carbon supports with a wide variation in their physico-chemical properties were evaluated at GM NAO R&D after suitable pre-treatment.. The performance of the thin film MEA within a fuel cell with this optimized carbon support demonstrated nearly a 40% voltage improvement over Vulcan XC-72R.

The low Pt loaded electrodes generally suffer from lower rate constants for oxygen reduction. In general, with an increase in the Pt loading, the exchange current density increases and the Tafel slope also becomes slightly lower due to a more uniform potential distribution in the catalyst layer pores. However, it is important to note, as demonstrated in Figure 3.3.2-2, that at low voltages (or high current densities) the performance of low Pt loaded electrodes increases remarkably and the catalyst utilization is nearly an order of magnitude higher than that for the high Pt loaded electrodes.

$CO_2$ poisoning of the Pt catalyst was investigated utilizing Pt and Pt-Ru electrodes. Hydrogen oxidation is a very fast surface reaction with an exchange current density as high as 8-20 ma/cm$^2$. Thus with an electrode roughness factor of 70, even at ultralow Pt loadings, the current-potential relation for hydrogen oxidation is quite linear and the anode voltage loss at an apparent current density of 0.5 amps/cm$^2$ is only about 25 mV. When pure hydrogen is replaced by a mixture of 75% $H_2$ and

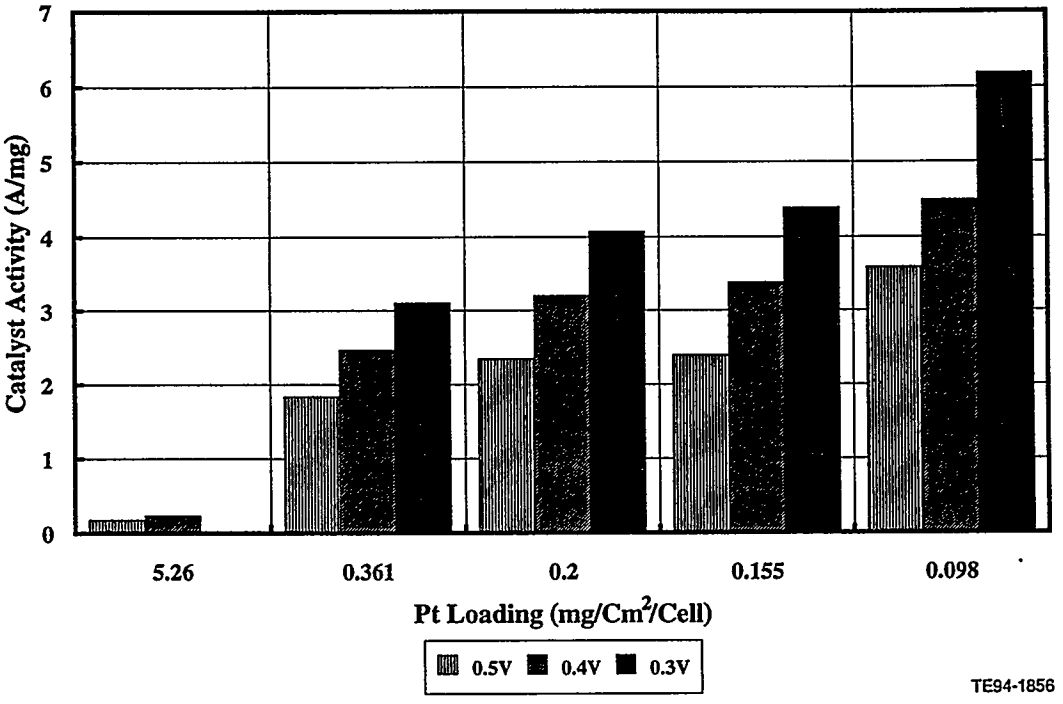


Figure 3.3.2-2. Catalyst utilization increases with a decrease in Pt loading for thin film electrodes on a Dow membrane. The fuel cell was operating on $H_2/O_2$ at 50 °C.

25% $CO_2$, the cell performance drops by about 35 mV at 0.1 amps/cm$^2$ and by as much as 200 mV at 0.56 amps/cm$^2$. This loss can only be explained by the formation of some type of adsorbed COH poison on the Pt sites. A model for the $CO_2$ effect on $H_2$ oxidation indicates a possible role for a slow charge transfer step involving a COOH type intermediate. However, when Pt-Ru is used as the anode catalyst, a negligible drop in small reference cell performance occurs up to a cell voltage of 0.5V. In the presence of Ru, two effects are possible; first, Ru, being in the partly oxidized state, may not adsorb hydrogen, thus preventing the adsorption or interaction of $CO_2$ with H to form COOH and, hence, the COH poison. Second, if COH is formed on Pt sites, Ru(OH) at an adjacent site may help oxidize the poison at lower voltages. Operation in large active area cells (increased flow residence time) or at high current densities (lower voltages) still appears to require air injection into the anode entrance to totally oxidize the COH poison. To date this appears to be true even if Pt-Ru alloy catalysts are utilized.

Three types of perfluorosulfonic acid membranes, which differ in their equivalent weights and structures of the side-chains, were investigated using GMR&D's thin film assembly preparation methods. The current-voltage performance of the membranes from DuPont, Dow, and Asahi Glass are presented in Figure 3.3.2-4.

The 3 mil Asahi membrane demonstrated the best over-all performance whereas Nafion 117™ performance deteriorates rapidly at higher current densities. The Asahi membrane demonstrated the least resistance and appears well optimized for fuel cell operation. The limiting current behavior observed for Nafion 117™ and 115™ probably indicates that these membrane and electrode assembly combinations are not very effective for water management at the cathode. The low porosity and

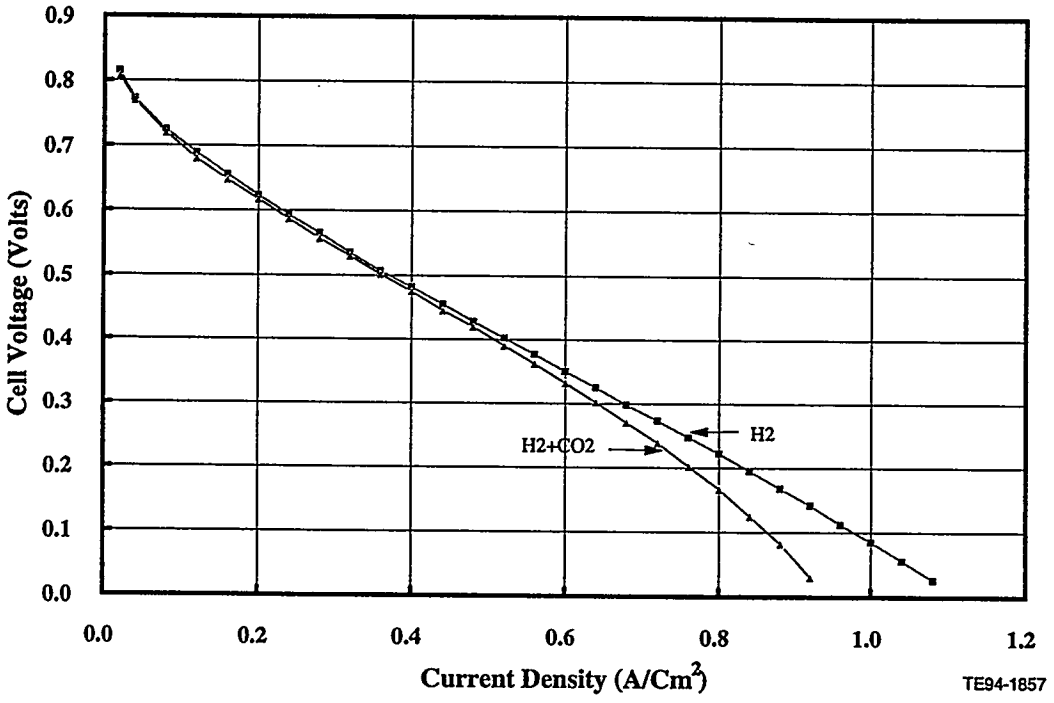


Figure 3.3.2-3. Pt-Ru catalyst at the fuel electrode demonstrates negligible deterioration in the presence of $CO_2$ in a reformate/oxygen cell at voltages > 0.5 V.

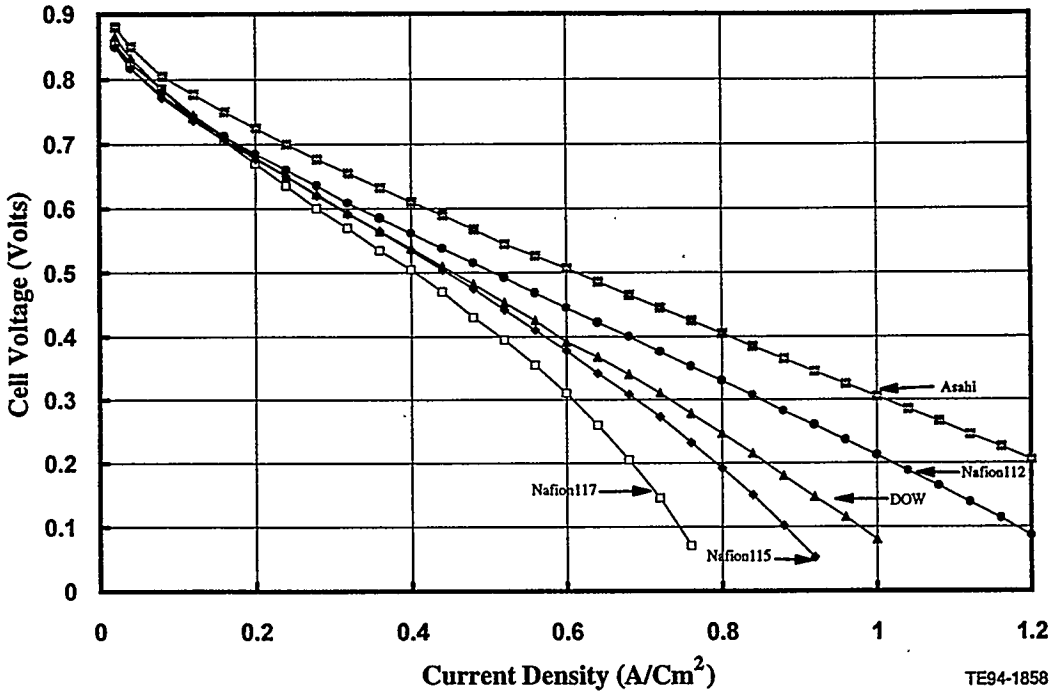


Figure 3.3.2-4. $H_2/O_2$ cell performances for various membranes at 50°C, 4 psig $O_2$ backpressure and a Pt loading of about 0.15 mg/cm²/cell.

the larger pore sizes in the Nafion™ membrane leads to decreased water transport through the membrane causing cathode electrode flooding and, hence, reduced mass transport of oxygen to the reaction sites. This phenomenon does not occur with thinner membranes, such as Nafion 112™, because the water transport increases as the membrane thickness decreases. Comparison of 3 mil Asahi and 2 mil Nafion™ membranes with 5 mil Dow membranes, etc., must be carefully interpreted, as noted earlier.

$H_2$/air or reformate/air data was not presented in this electrode structure and catalyst development effort because the data was not consistently stable at the operating temperatures (≤50°C) and pressures (≤4 psig) at which the tests were conducted. During Phase II, reformate/air testing will be conducted at elevated pressures and temperatures using JDC reference cell test stands.

## 3.4 JOINT DEVELOPMENT CENTER REFERENCE FUEL CELL RESEARCH AND DEVELOPMENT

### 3.4.1 Introduction and Summary

The PEM fuel cell utilizes a unique fuel cell geometry built on the two alternate faces of an ion exchange polymer sheet. This geometry developed as a result of the PEM fuel cell's significant capability to permit simpler water management. Unlike earlier low temperature fuel cells the polymer electrolyte rejects product water with no electrolyte dilution. However, it is still understood that total water management

in existing PEM cell devices remains a significant engineering challenge. Insufficient membrane moisture levels lead to decreased ionic conductivity and structural shrinkage, while excess water can result in flooding of the porous electrode layers. A significant part of the research and development focus, therefore, has been to evaluate new fuel cell devices designed to yield improved voltage performance.

Specifically, JDC personnel conducted studies of thin-film low Pt loaded electrodes in coordination with the LANL Core Technology Group and GM's NAO R&D Center. However, the JDC's primary task involved the "reference cell" testing portion of this effort to improve fuel cell performance. All fuel cell stacks are composed of individual cells; the operating characteristics of these cells, assuming that the stack provides fairly uniform flow to each cell, determines the operating characteristics of the stack. Consequently, a cost effective technique to improve fuel cell stack performance involves basic and applied research at the single cell and short stack level (3-5 cells) utilizing scaled reference cells. Advanced test stands were built to make detailed investigations utilizing these reference cells; areas of investigation include:

- membrane and electrode development emphasizing water removal characteristics of the assembly and improved performance
- gas flow-field distribution concepts and their effects on flow uniformity, cell water removal, and cell performance
- existing state-of-the-art (SOA) membrane and electrode evaluations including the effects of cell operating conditions such as temperature, pressure, flow stoichiometries, humidification, and anode gas composition on cell water removal and performance.

This section describes the approaches taken to accomplish these tasks and presents some significant results obtained during Phase I.

### 3.4.2 Reference Fuel Cell Fixture and Test Stand Development

Appropriate testing is necessary to achieve credible results on PEM devices. New hardware was designed, fabricated, and utilized to accomplish the testing program. New test stands were developed that permit controlled, highly reproducible conditions of temperature, pressure, gas feed composition and flow, and cell clamping forces. Moreover, the test stands were automated so that an appropriate safety envelope was maintained during the reference fuel cell test program. During the later part of these activities software was developed that now permits measurements to be performed under precise computer control; for example, flow stoichiometries now remain constant with current density changes This advance not only resulted in less operator time for specific tasks, but also yielded more reproducible test conditions.

The reference test stands were designed for maximum flexibility in testing both realistically-scaled single cells and short stacks consisting of up to 5 such cells in series. (This is referred to as a "semi- or short-stack" testing arrangement.) A flow schematic of the test stand is presented in Figure 3.4.2-1. Anode and cathode gaseous feeds are fed from the left-hand-side of the schematic through valves, filters, etc. into one of three mass flow controllers (MFCs). Three MFCs are required to achieve the desired flow accuracy throughout the full range of required flow rates. The flame arrester at the outlet of the MFC is a piece of sintered stainless

steel. This fixture is also fitted to include a small quantity of powdered Nafion™ that serves to absorb any foreign cations in the stainless steel tubing. The fuel (anode) gas stream is blended using hydrogen and carbon dioxide. Under emergency shutdown conditions nitrogen flooding occurs at high flow rates to quickly purge hydrogen from the anode feed tubing. (Hydrogen flow is also automatically interrupted during an emergency shutdown.) Liquid water is fed into the anode stream using a high-pressure liquid chromatograph pump. This positive displacement pump feeds small, controlled flows of distilled water into a heated vaporizer. Following steam introduction, heat tracing on all of the feed lines is required. Humidified anode gases then flow into the fuel cell test fixture and subsequently, after water condensation, vent through a back-flow pressure regulator. In these experiments the term flow stoichiometry refers to the actual flow divided by the theoretical flow required to just accomplish the electrochemical reactions. In gaseous mixtures of air and hydrogen/carbon dioxide, both mixed with steam, stoichiometries are calculated based on the actual reactant, oxygen or hydrogen.

The air (cathode) pneumatic flow scheme is similar in concept to the fuel side. Air and/or oxygen can be used as the cathode reactant during testing. (This permits the generation of any cathode feed between 100% $O_2$ to 20% $O_2$.) The cathode flow scheme also includes provision for a high flow nitrogen purge. This feature is useful for extinguishing potential fires that might occur between combustible test parts (for example, graphite flow plates) and oxygen. The cathode flow is also humidified using a positive water feed system similar to that on the anode. It is possible to set the water flow rates at elevated levels that result in a two-phase water mixture, i.e., produce a relative humidity in excess of 100%. This level of water flow is most often beneficial on the anode side of the fuel cell.

Both the cathode and anode streams are exhausted from the fuel cell test fixture and then fed to a gas-phase condenser (10°C) that removes essentially all water and steam from the stream. Liquid water is collected in a vessel on an analytical balance (± 0.1 mg). Water product levels are determined for both the anode and cathode streams permitting an accurate assessment of cell water balance during experiments.

The reference cell test fixture used for fuel cell experiments are depicted in Figure 3.4.2-2. The fixture is formed from a block of polycarbonate. The block includes fittings for gas flows and for drop-in flow fields. Gasketing is accomplished using O-rings set into milled grooves in the fixture. The fixture consists of two flat blocks, each of which is fitted with water flow channels used for temperature control. Under most conditions during single cell testing the experiment is heated by pumping hot water into these channels. (This occurs because heat losses in a single, small cell are significant compared to the heat generated from the electrochemical processes.)

Pressure, temperatures, and flows are continuously monitored during tests by a Hewlett Packard DACQ system. Current and voltage using a Hewlett Packard power supply, usually operating in the constant current mode. This supply imposes a fixed current load and the voltage across the cell (measured at the two output terminals on the test fixture) is read. Setting current rather than voltage is more convenient because tests are performed at controlled flow stoichiometry.

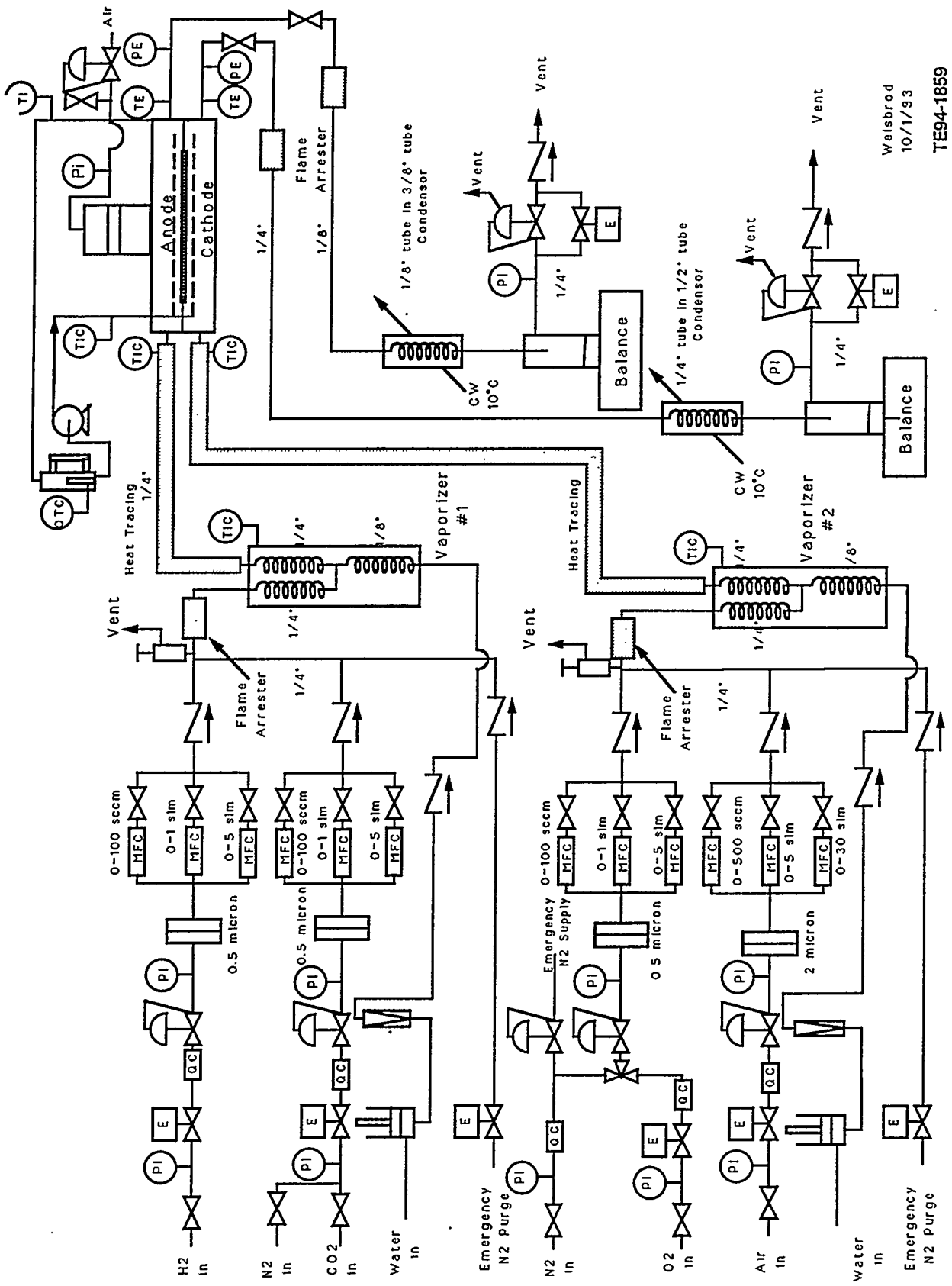


Figure 3.4.2-1. Reference fuel cell test stand flow schematic.

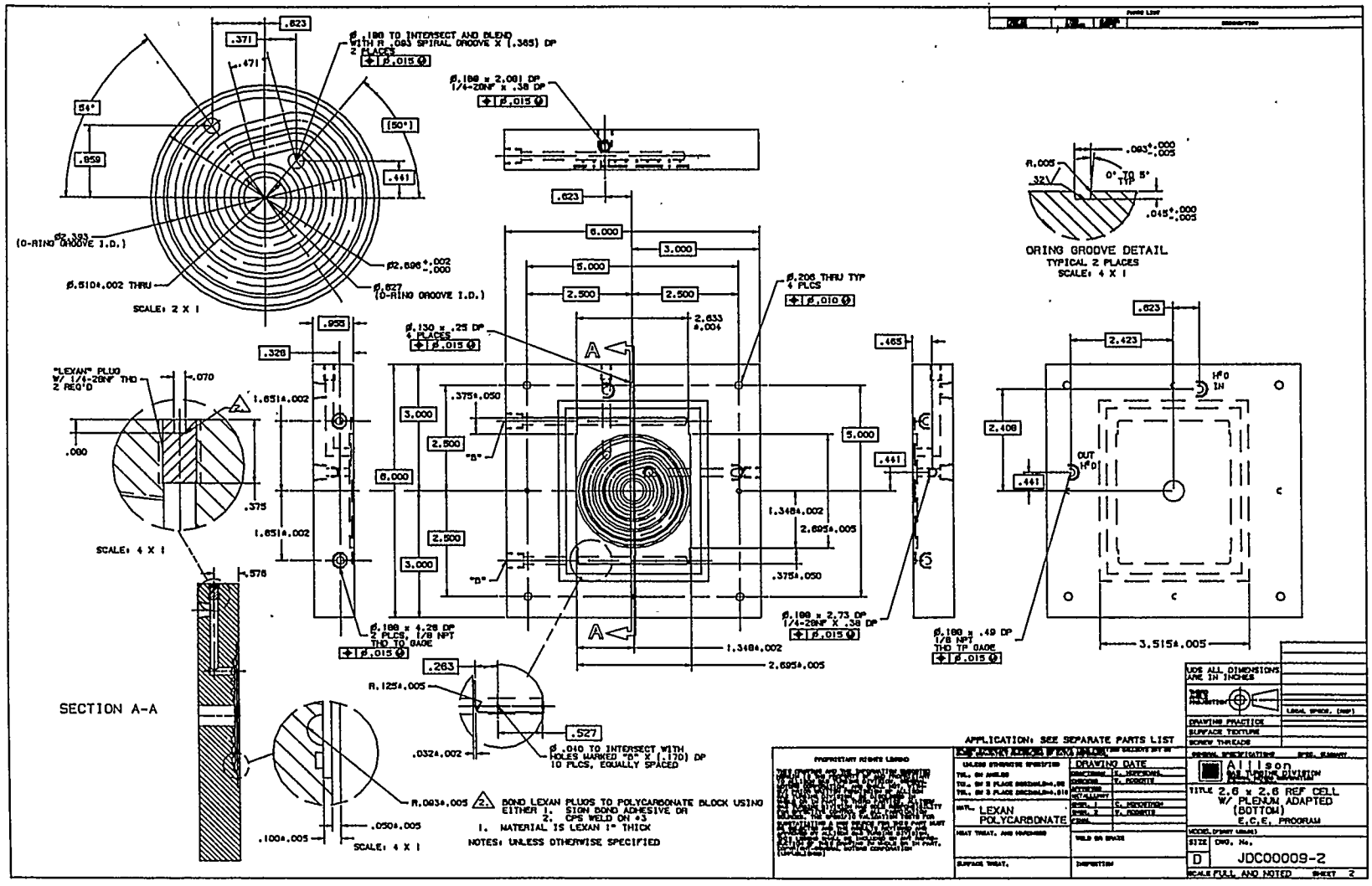


Figure 3.4.2-2. Reference cell test fixture.

Testing using hydrogen fuel requires suitable safety considerations. The primary control strategy is to limit flow into the test area, using the MFC, and then monitor the test environment using a sensitive hydrogen sensor. Hydrogen leaks cannot be excessive, due to the overall limited flow rates; however, if appreciable hydrogen concentrations are noted, hydrogen flow and the experiment are automatically terminated. Other controls utilize temperature sensors mounted in the cell fixture. Excess temperature within the test fixture, normally the result of a hydrogen-oxygen reaction, also sounds an alarm; further, if the temperature excursion is beyond set limits an automatic shutdown procedure is initiated. Preliminary leak testing is straightforward; the membrane and electrode assembly is mounted within the test fixture and pressurized, and the gas flow is turned off. Test pressure decay is then monitored.

Two test stands of the design described above have been completed during Phase I. Following improvements in controls and diagnostics, the stands were put to extensive use and became an integral component in the PEM development activities. In the following section some key results are identified that both summarize the types of experiments conducted and indicate the level of contemporary PEM performance.

### 3.4.3 Membrane and Electrode Development

Contemporary PEM M&E hardware utilizes so-called "zero gap" electrochemical designs, with the electrochemical layers bonded directly adjacent to the membrane electrolyte film. All films studied in these activities were polyperfluorosulfonic acids, ion exchange polymers typified by the Nafion™ class of polymers developed by the DuPont Company. These materials contain a "Teflon-like" polymer backbone containing periodic ether linkages connected to a perflouronated side chain. The side chains terminate in sulfonic anion groups; these are the active cation exchange sites for the ion exchange process. A newer class of these polyperfluorosulfonic acid materials has been developed by Dow and much of the technical thrust of the M&E activities during Phase I has been to demonstrate the performance of the Dow-derived polymer electrolyte films. However, other film materials have also been extensively studied.

Historically, M&Es have been fabricated by building layers on the membrane film directly, either by depositing a thin layer on that film or by building the active electrocatalytic layer on a graphite current collector, usually a graphite paper or cloth containing a controlled amount of a non-wetting agent such as polytetrafluoroethylene (PTFE). That treated graphite piece is then bonded to the membrane film. The first route, using the "decal" technique (forming the catalyst layer on a second surface and then transferring that thin "decal" to the film), is the principal historical method by which PEM hardware has been prepared. The current collector method is the principal historical route used to manufacture phosphoric acid fuel cell hardware and when applied to PEM M&E manufacture is often referred to as using "gas diffusion electrodes."

The overall technical objective is to form an electrode layer that has optimum features of electronic and ionic conductivity, electrocatalytic activity, and permeability to gaseous reactants and liquid water product. Because the fuel cell system for transportation applications utilizes gaseous reactant mixtures (hydrogen plus carbon dioxide and oxygen plus nitrogen) the fluid dynamics of the porous layers constitute an important design consideration. In contemporary PEM designs the

porous electrode is dead-ended against the membrane face. During operation one gaseous constituent is consumed (for example, oxygen from air) enriching the second (nitrogen). Electrodes with improper designs will flood with the diluent, reducing the diffusion rate of reactant. In a similar manner, product water, generated at the cathode interface, can fill porous electrode volumes, blocking access to active reactant molecules. With a dead-ended flow path, as in contemporary designs, successful electrode layers must be sufficiently thin so that the diluent, i.e., nitrogen, and the product, i.e., water, can easily exit the structure. Consequently, the thrust behind these initial development M&E efforts is to form thin layer electrodes.

The essential layer ingredients are: a supported electrocatalyst, such as small particles of platinum bound to porous carbon; ionic conductors, such as a stabilized polyperfluorosulfonic acid layer , and, perhaps, an adhesive, such as some quantity of porous PTFE. The solubilized polyperfluorosulfonic acid can serve both as the ionic conductor and adhesive.

The major technical challenge in forming such a thin layer electrode is to obtain coherent adhesion between the electrocatalytic layer and the polymer film. Techniques were developed that alter the polymer properties by the addition of either organic solvents, such as ethylene glycol, or by the incorporation of organic cations, such as the tetra butyl ammonium ion. These ionic additives tend to change the nature of the plasticity of the film and the ability to bond to that film. The goal is to form a melt-processable layer that adheres strongly both to the polymer film and to the electrocatalytic layer.

Although successful adhesion is apparent by good electrochemical performance of the resulting assembly, the exact reasons for lack of fabrication success are less certain, as even some strongly adhering layers sometimes give only marginal performance. Both successful adhesion and successful reactant and product transport are necessary. Further, there is always the requirement for fast proton transport from the thin electrocatalytic layer into and from the film. It is suspected that improper chemical and thermal processing may lead to an adhesion that alters the surface chemistry of the film, perhaps driving the surface pendant sulfonic acid groups (the sites for ionic transport) away from the surface and into the film. This improper processing may then result in a thin non-conductive performance-limiting polytetrafluoroethylene layer at the interfacial plane.

The general procedure utilized at the JDC, in contrast to GM NAO R&D's work, follows earlier "decal" procedures. A carbon black mixture, termed an "ink", is formed by mixing carbon-supported platinum, solubilized Nafion™, and the plasticizing agent, either an organic solvent or organic cation. This ink is then transferred to a decal backing , usually a treated plastic sheet. The ink and backing are heat treated to remove excess solvents. The decal is then pressed onto a cleaned polymer film and following hydration and subsequent ion-exchange processing, the completed assembly is rinsed in deionized water. Before use as a membrane/electrode assembly the decal backing layer is removed and the film and thin layer catalyst electrode is then bonded to a wet-proofed current collector. Normally a two-sided assembly is prepared; two separate decals are used, with one bonded to each of the two faces of the film to form the anode and cathode electrocatalytic layers. Obviously the two layers can be formed with differing catalysts, geometries, and processing conditions.

Fabrication procedures were systematically varied to determine conditions which yielded, reliable layer adhesion. The following data derived from these thin diffusional electrocatalytic layers built directly on polymer films represent the culmination of this development effort. These thin film electrode catalysts contain only small quantities of expensive, precious metals(~0.05 mg/cm$^2$) , unlike the more highly loaded (~4 mg/cm$^2$) electrodes used in the Ballard-supplied stacks. Performance results obtained with two membrane and electrode types, both formed using the Dow experimental polyperfluorosulfonic acid polymer and operated on hydrogen-air reactants, are compared in Figure 3.4.3-1. The Dow M&E was supplied by Dow for reference fuel cell evaluation using the fixtures and test stands described earlier. The Dow M&E assembly details are proprietary; however, it should be noted that the test specimen contains 4 mg of Pt/cm$^2$ of active area on each membrane face. As indicated, this particular test specimen yielded the "best hydrogen/air performance" observed during the Phase I testing program; however, most Dow M&E assemblies performed at about 0.6-0.7V at 1A/cm$^2$. The second curve represents the performance of a thin layer M&E assembly prepared at the JDC. This particular specimen contained only 1.3 mg/cm$^2$ on each surface of the electrolyte film. As indicated in Figure 3.4.3-1, test data were obtained under identical conditions of temperature (80°C), equal anode and cathode pressure of 3 atmospheres, and relatively high reactant flows. It should be noted that these high reactant flows, particularly on the cathode, can be achieved through recirculation of much lower stoichiometry flows. Under such conditions recirculation introduces relatively small parasitic losses. Data presented are for constant stoichiometry conditions. These test results are typical of well formed M&E assemblies. Further research on thin film assemblies should yield even better performance at lower Pt loadings. Long term, stable operation, as is evident from this test program, is possible with the ability to exceed 0.7V at 1,000 ma/cm$^2$ on reformate/air reactants, at least for highly platinum loaded electrodes.

### 3.4.4 Flow Field and Reactant Distribution Developments

Fuel cell stack hardware must incorporate systems that continuously deliver gaseous reactants and promptly remove water product, particularly from the cathode compartments. Channels within the bipolar plates, etc., that accomplish this are typically referred to as "flow fields". Within PEM cells a significant fraction of the total water inventory must be liquid due to the necessity to maintain liquid water conditions in the membrane. The result is that flow field and electrode/current collector design and manufacture must be capable of flowing a continuous two-phase gas and liquid mixture.

During this development effort considerable emphasis was placed on improving and characterizing the performance of advanced flow fields. Two different basic design approaches were explored:

- ***Screen packs*** - Metallic screen packs were formed from thin sheets of expanded niobium and zirconium metals, each of which were welded together to form a laminated flat package. Usually three to five sheets were used to form one pack; the welded assembly was then cut to size and platinum coated to minimize contact resistance and prevent the formation of surface oxides. Porous graphite felt or cloth, used as an electrode backing (current collector), is positioned between one face of the screen pack and that of the electrocatalytic layer on the membrane.

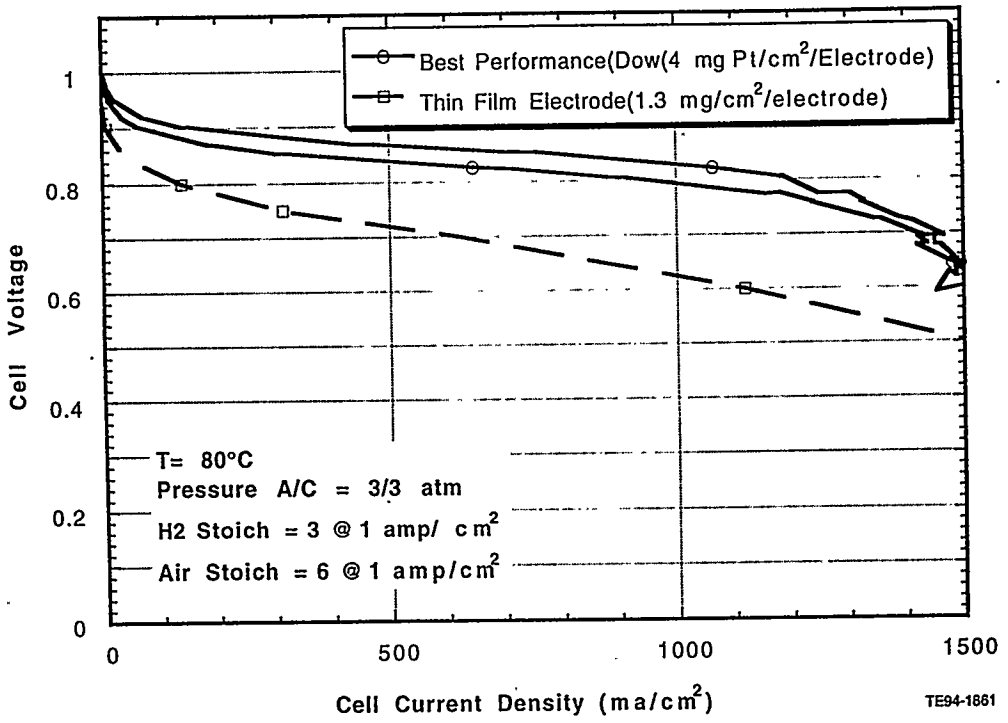


Figure 3.4.3-1. Reference fuel cell hydrogen/air reactant test results using Dow membranes and electrodes with high and low Pt loadings.

- ***Flat graphite plates*** - Customized graphite plates, surface ground to assure flatness, were mill machined to form a pattern of channels suitable to direct reactant or product flows. Many different geometries are possible for flow distribution control; moreover, the graphite itself can be permeable to some of the transported fluids and thus part of the transport may occur away from the milled channels.

Platinum coated metals and high purity graphite have both demonstrated adequate corrosion tolerance within the PEM fuel cell testing environment. Consequently, the present testing focus involved flow distribution dynamics. Two types of tests were performed to evaluate flow field design: first, gas reactant dispersion was determined to assure that the gas was uniformly delivered; second, pressure and water saturation measurements were used to determine both the required flow field geometry and graphite electrode backing characteristics for prompt water removal. Significant improvements in flow field design also required optimization of the manifolding and routing of gas inlets. Considerable improvements in flow distributions have been demonstrated using a series of inlets that admit gaseous reactants simultaneously at several locations.

The first technique used in evaluating flow fields involved the use of an absorbing dye as a tracer. Distilled water was continuously pumped through the channels into a spectrophotometric absorption cell. At a specified time, the clean, distilled water was replaced with water containing the dye. A UV-Visible spectrophotometer was used to provide a continuous readout of solution absorption in the effluent stream.

Flow results are presented in Figure 3.4.4-1 which indicates the change in dye fractional concentration as a function of time as measured by changes in the light absorption at a flow rate of 1 ml/minute. The "dead volume curve" represents results with the cell removed from the flow system; i.e., neglecting the volume upstream between the dye injection site and the cell entrance and the volume downstream between the cell exit and the UV instrument. In general, fluid dispersion is characterized by a calculated function that describes the flow volume (determined by time to 100% fractional concentration) required to reach full concentration in the output. These results can differentiate various port inlet arrangements and other strategies to achieve more uniform coverage of the entire active cell area.

The second technique, used to evaluate water removal characteristics, measures both the pressure drop and the extent of flow following water saturation as a function of water saturated gas flow rate. Pressure drop in a flow field must be sufficient to ensure uniform gas distributions; further, a sufficient pressure drop (gas momentum) is necessary to remove water. The pore level capillary number, defined as the microscopic ratio of viscous to gravity forces, describes conditions under which viscous forces overcome capillary forces thereby permitting liquid water flow. This number is particularly important in characterizing the graphite electrode backing paper's (cloth) capability to resist wetting, allow removal of water, and permit

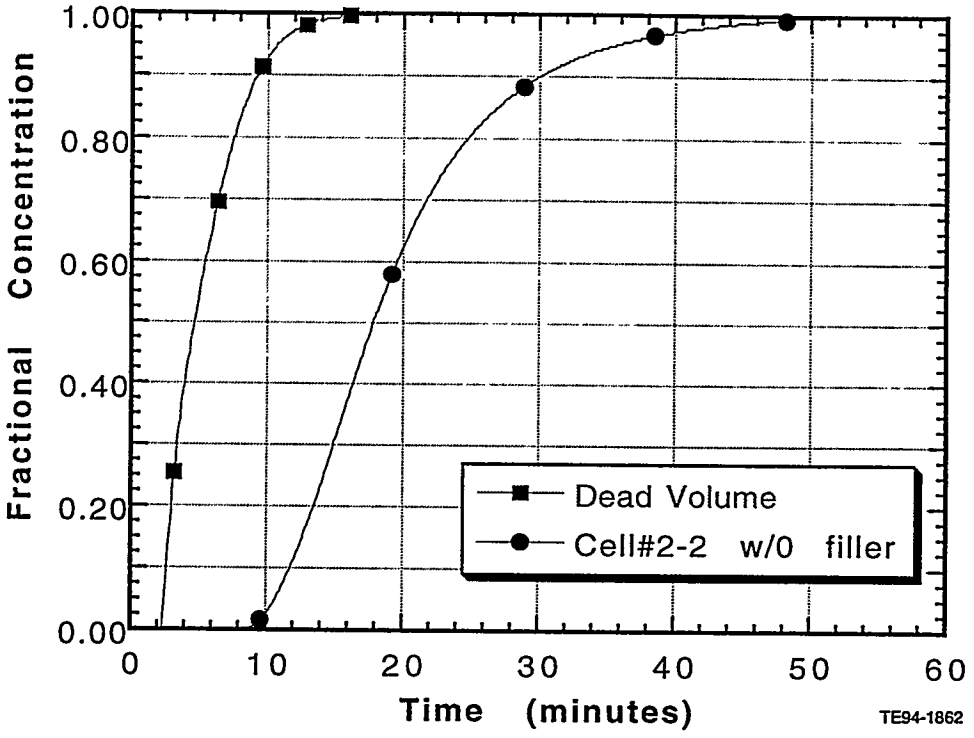


Figure 3.4.4-1. Example of the evaluation of candidate flow fields through use of an absorbing dye as a tracer and a UV-visible spectrophotometer.

gas flow to the membrane face, and is defined as:

$$N_C = \frac{U\mu}{\sigma} = \frac{K\Delta P}{L\sigma}$$

where

U = superficial velocity, cm/sec
$\mu$ = gas viscosity, poise
$\sigma$ = interfacial tension between air and water, (50 dynes/cm)
K = permeability (darcies)
$\Delta P$ = pressure drop across capillary
L = capillary length

When $N_c$ becomes greater than $10^{-3}$, capillary forces are no longer effective and water removal rates can be rapid.

Simultaneous measurements of pressure drop and liquid saturation levels required specially designed hardware. The extent of water saturation was determined gravimetrically; the cell with graphite paper or cloth electrode backing and graphite plate flow field was initially totally water saturated and the subsequent weight loss was recorded as a function of water-saturated gas flow rate into and out of the cell. At some point in time an equilibrium relative humidity is attained and as it is a measure of the "wettability" of the graphite paper (cloth) electrode backing and the blockage effects of the flow field channels. As expected, increases in gas flow lead to different relative humidity levels within the cell. Some relative humidity must always be present to provide water for diffusion through the membrane. Flow field and graphite electrode backing paper (cloth) design optimization occurs when low flow rates and, hence, low $\Delta P$'s result in adequate water removal so that cell flooding is prevented and reactant gas flow to the membrane face is uniform.

While more work is required to determine optimum flow field designs it is of interest to note that the excellent fuel cell performance presented in Figure 3.4.3-1 was achieved using JDC fabricated graphite plates with advanced flow fields determined by the techniques described. The advanced flow fields developed to date are not shown because their design is considered proprietary to GM.

### 3.4.5 Single Cell (Reference Cell) Results for PEM M&E Evaluation

Advances in sealing techniques were required for single cell testing that permit successful operations with membrane and electrode assemblies that may vary in thickness from 0.015 to 0.035 in (0.38 mm to 0.89 mm), depending upon design and vendor. Membrane materials extrude under high stress, so a flat gasket is generally preferred contrasted to an O-ring in which high point stress can be generated. To accommodate a wide range of graphite electrode paper or cloth thicknesses, gasket compression of the selected material to 75% of its original thickness is required. At 75% of the original gasket thickness the active area sealing force is only 30% of the total applied force. Good success was achieved working with commercial materials for sealing between the membrane faces and the polycarbonate surfaces.

The test hardware fixtures described earlier are designed to accept "drop-in" flow fields permitting rapid examination of the effects of various flow field designs on

single cell performance. Experimental flow fields are formed as thin rectangular sections, 0.050 in thick (1.3 mm), shaped to fit into the recess in the cell assembly. As described above, both metallic composites and graphite plates have been successfully used during M&E testing.

Graphite flow fields are machined at the JDC using a computer controlled milling machine. This machine was physically modified to establish ± 0.0001" (0.002 mm) tolerance on the depth control of the cutting tool. Various channel patterns have been machined. A series of experiments were also completed to evaluate different numbers of reactant inlet and exhaust points ("port control") and different channel geometries ("plate control"). In general, graphite flow fields demonstrate considerably improved performance compared to screen packs through most of the useful range of current densities. Only at the very highest current densities, those which also result in the highest rates of water formation, do screens demonstrate superior performance. Under very high water generation rates (corresponding to water production at current densities greater than 1,200 ma/cm$^2$), liquid water must exhaust continuously along a specific channel with the entire product flow "integrating" along that channel. Apparently, screen packs have flow "short cuts" for water drainage that are advantageous at these high generation rates. Graphite plate flow channels that can duplicate high current density "screen pack" performance are being actively investigated.

Because of the extensive nature of this test program only a few key experiments, selected to summarize the direction and progress of the work performed at the JDC, are reported here.

### *Influence of Temperature and Pressure*

A series of experimental results were performed using Dow-supplied M&E assemblies. These were formed using the Dow XUS-13204.20 experimental membrane and equipped with Dow proprietary platinum-based electrodes. Typical results obtained with sample MEA 1-2 are presented in Figure 3.4.5-1. Test conditions as indicated on the figure are isobaric (same anode and cathode pressures) at 3 atmospheres with hydrogen flow set for a stoichiometry of 3 and air flow set for a stoichiometry of 6 at the current density level of 1 amp/cm$^2$. (These specific tests used constant flow conditions, rather than constant stoichiometry; they occurred prior to the test stand automation procedures.) Temperatures on single cell experiments are set by controlling the temperature of the flowing water bath that enters both halves of the test fixture. For these tests, reference cell performance results were obtained at temperatures between 70 and 90°C.

These tests, utilizing fixtures equipped with screen pack flow fields, demonstrate the expected performance improvement with temperature increase. High current density performance is compromised at the lowest temperature, 70°C, probably due to the result of low water removal rates under such conditions. Causes of water retention at this low temperature are not fully understood, however, the decreased gas momentum and increased water viscosity at lower temperature may play roles. The increased water vapor pressure with increasing temperature may also be significant, assuming that steam transport is faster than liquid water transport.

Studies of the effects of temperature on cell performance studies were continued using another Dow membrane and electrode assembly. Higher temperature data, un-

der slightly different flow conditions, are presented in Figure 3.4.5-2. These data were obtained using a Series 2 assembly, a sample with a different carbon paper electrode backing, also supplied by Dow; this assembly produced poorer overall performance than that produced by MEA 1-2 as indicated by a comparison of the data to Figure 3.4.4-1. Test results for this MEA indicate similar polarization curves at 80 and 100°C. At elevated temperatures, performance at higher current density is deficient. At 120°C, the data depicted in Figure 3.4.5-2 demonstrate a characteristic limiting current behavior, probably an indication that oxygen transport rates are no longer sufficient to sustain high performance levels. It is suspected that the high steam vapor pressure resulted in dilution of the cathode oxygen concentration. At an increased pressure, 4 atm, however, the oxygen pressure increases proportionally and the performance of the cell begins to recover. For example, at 120°C and 4 atm, the oxygen mole fraction rises to 7.6%. Stable and useful results can be obtained at 120°C with the Dow assemblies, but either lower current densities or higher pressures are required. There may be some advantages of higher temperature operation, such as decreased sensitivity to contamination of certain gaseous constituents, CO, $CO_2$, etc, that degrade electrochemical kinetics at the reacting layers or better thermal integration with the fuel processor. However, higher temperature operation also requires increased pressure which in turn increases system complexity.

There can be certain system advantages when operating with low pressure air. Consequently, tests were also conducted to assess operation at near ambient pressures. Performance of a Dow Series 2 assembly at ambient pressure conditions and different operating temperatures is presented in Figure 3.4.5-3. Stable performance

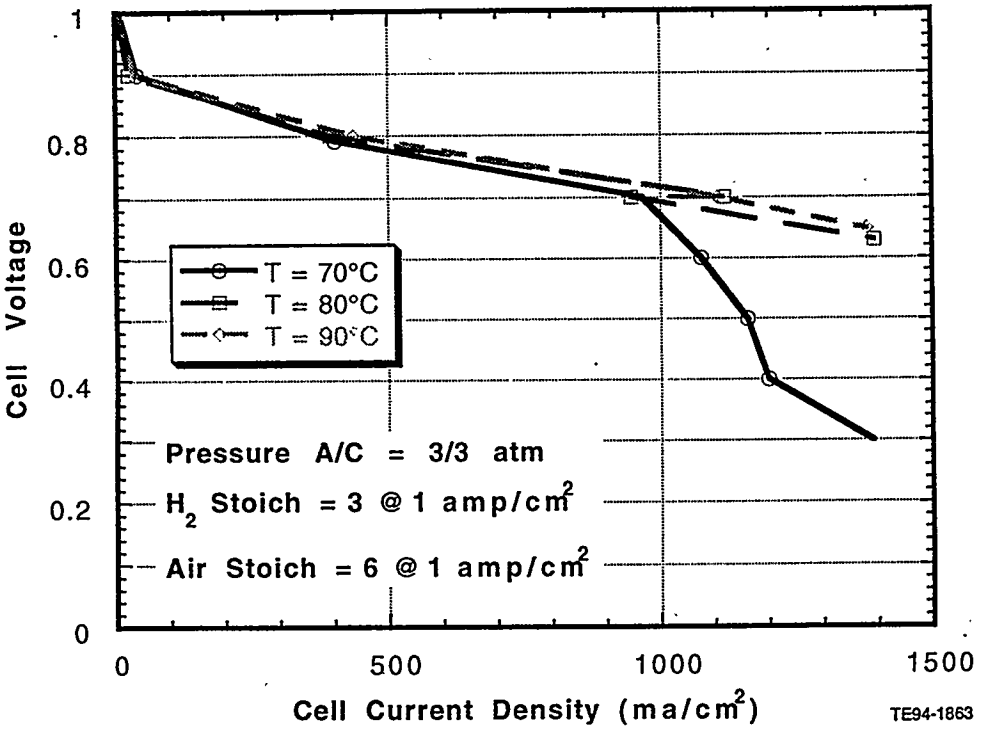


Figure 3.4.5-1. Reference cell Dow MEA, hydrogen/air reactant voltage as a function of current density and cell temperature at 3 atm pressures.

(> 0.5 V at 1,000 ma/cm²) was attained at both 70 and 80°C. This is between 60-70% of the performance attained at 3 atm pressure. However, this reduction in voltage performance has an adverse effect on system thermal efficiency. At increased temperatures, such as 90°C, voltage performance plummets; most likely this decrease is the result of membrane dehydration. It is well known that the electrolyte films dry at elevated temperatures and low pressures. These test data confirm the conventional wisdom that near optimum voltage performance is obtained at about 20°C below the boiling temperature of water at the operating cathode pressure.

### *Influence of Flow Stoichiometry*

Product water removal is a critical element in fuel cell "reactors". In the filter-plate design (flat plate with internal flow channels) explored in these studies, momentum within the cathode air stream is the principal driving force to remove product water from the test piece. The majority of water, at least in the regions thermally removed from the actual electrochemical conversion sites, is in the liquid state. Only at higher flow stoichiometries (greater gas mass) may this condition be altered and then probably only at zones which actually experience very high flow mass and velocities, such as within the flow channels.

Experiments were conducted using a 100% saturated hydrogen anode stream maintained at a constant stoichiometry of 1.43 (at 1,400 ma/cm²), which is the equivalent of an anode stoichiometry of 2 at 1,000 ma/cm² when the flow is kept constant. Cathode stoichiometry, which influences the oxygen concentration gradient in the cathode compartment, however, was varied in these tests. For example, at a stoi

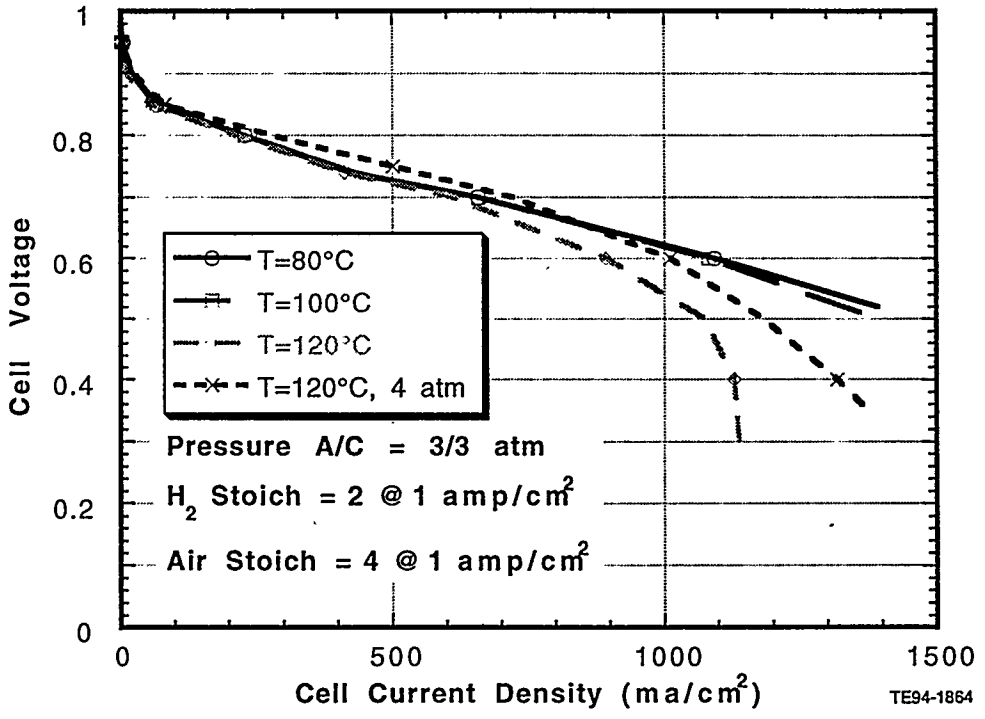


Figure 3.4.5-2. Reference cell Dow MEA, hydrogen/air reactant voltage as a function of current density and cell temperature at 3 atm pressures.

chiometry of 1, oxygen concentration varies from 0.20 to 0.00 from inlet to outlet, a far less-than-ideal condition. At a stoichiometry of 6, however, operation approaches differential reactor conditions, with essentially no appreciable oxygen depletion. There is no reason to expect any improvement at stoichiometries greater than 6. High flow rates, however, can result in conditions where steam saturation is less than 100%, and under such conditions water vaporization processes can be influential in thermal management. For example, with water generated at a current equivalent to 1,000 ma/cm$^2$, and an inlet relative humidity of 75%, the outlet relative humidity situation under these conditions is only 95%; therefore, additional liquid evaporation can occur. Cell performance as a function of various air stoichiometries, again using a Dow-derived M&E assembly, are presented in Figure 3.4.5-4. As demonstrated, high air flows are more important at high current densities; significant voltage loss can occur using lower flow stoichiometries under these conditions. Operation below 500 ma/cm$^2$ indicates no real advantage in utilizing high cathode flow stoichiometry. These test results suggest that proper system operation may dictate a variation in cathode flow operating conditions so as to maximize efficiency. For example, if high momentum (high cathode stoichiometry) conditions are only necessary for product water removal at peak power operation, such high flow conditions may be relaxed by lowering pressure and flow under "cruise" conditions. This could influence air compressor system design considerations.

### *Effects of Anode Gas-phase Contaminants*

Reformed fuels consist of a mixture of hydrogen, carbon dioxide, and other diverse chemical constituents. Although technologies exist for separation of hydrogen from

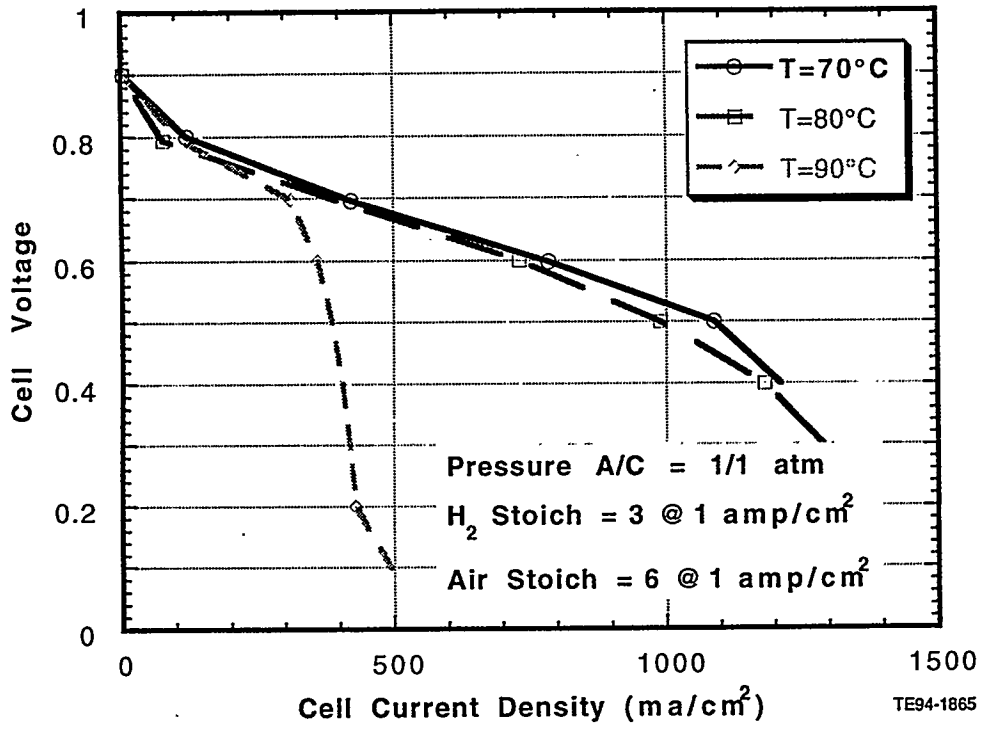


Figure 3.4.5-3. Reference cell Dow MEA, hydrogen/air reactant voltage as a function of current density and temperature at ambient pressure conditions.

the rest of the gaseous mixture, at present such processes are technically difficult and not feasible for application to automotive systems. Moreover, because of the extremely low tolerance of PEM anodes to CO (less than 10 ppm of CO appears necessary to avoid catalyst poisoning), most likely a PROX device would be required even if a "gas separator" concept were in place.

The fuel mixture is derived from a "steam reforming" process and is commonly referred to as a "reformate" stream. Because CO control is mandatory, reformate flow entering the fuel cell must contain a lower concentration of CO, by about a factor of $10^5$, than is generated during the initial "steam reforming" process.

Carbon monoxide is one anticipated contaminant with known adverse consequences. Methane, methanol, other lower molecular weight alcohols, aldehydes, ketones, etc., can also be expected to be present as low level constituents in the fuel feed stream. Studies were performed using the test stand and advanced PEM hardware to examine the influences of various low level constituents

- ***Carbon monoxide*** - Carbon monoxide, at temperatures of interest for PEM stack operation adsorbs onto platinum surfaces blocking access to hydrogen molecules, thus poisoning the catalyst. Because of the fast kinetics of hydrogen oxidation, performance degradation is not evident until a majority of platinum electrocatalytic sites are CO-covered. Conversely, if the exchange between CO in the gas phase and the adsorbed state remained rapid, then hydrogen oxidation rates could remain fast. Clearly such rates do slow dramatically and, thus, long-lived CO adsorbates are suspected. Approaches for CO management in PEM anodes must consider mechanisms that diminish the bonding strength between CO and Pt. Operating at higher temperature is one approach. Another such approach involves oxidation of the adsorbed CO species, either through pulsing the anodic potential or through the addition of reactants such as molecular oxygen or water. The third is to modify the electrocatalytic sites, usually through the use of a binary or ternary alloy, to reduce the adsorption residence time. The use of molecular oxygen (air) and/or alloys proved to be effective.

  Adding air (oxygen) to a hydrogen-containing mixture avoid explosive gaseous mixtures. The lower flammability limit of hydrogen corresponds to 25.8 mole per cent air; therefore the formation of a mixture with a maximum oxygen content of 5 mole per cent was considered to be a safe procedure. Although normal hydrogen safety procedures are described at atmospheric pressure, the flammability limit is essentially the same up to 3 atmospheres.

  Tests were performed in the reference cells using platinum black electrodes, similar in loading to those used in Ballard PEM stacks, to determine the equilibrium and kinetic response to CO contamination. Carbon monoxide concentrations from 20 to 500 ppm were studied; tests were conducted using hydrogen-carbon dioxide mixtures. Cell current densities were measured while the cell was maintained at a constant potential, 0.6 V; upon CO addition, a current transient was observed. When the lower current level stabilized, air was injected in stepwise increasing concentrations until full current density recovery was obtained.

These tests were performed using a reference cell that permitted gas composition measurements on the inlet and outlet sides of the anode stream. Data demonstrated, as expected, successful conversion of CO to $CO_2$ following air injection. As reported by others, this "in situ" CO processing is successful, with highly loaded Pt electrodes, up to concentrations of CO as high as 200 ppm. At 200 ppm, the required oxygen concentration for successful CO conversion in these type of electrodes was 5%, resulting in a combustion process that can consume 10% of the fuel. Significantly, 5% is also the upper safe limit for oxygen injection into a hydrogen mixture. Highly loaded catalyst alloy mixtures used in the Ballard stack electrodes were much less sensitive to CO; concentrations of 220 ppm CO were successfully converted to $CO_2$ by 1 to 2% air injection. These results are described in more detail in Section IV. In any event, low catalyst loadings, regardless of alloy type, are poisoned by much lower concentrations of CO and require a higher percentage of air injection to destroy the long-lived CO adsorbates. These tests clearly indicate the requirement for adequate CO removal (<10-ppm) in the post reformer fuel processing stream.

- ***Carbon dioxide*** - Ballard stack testing, as described in Section IV, using hydrogen-carbon dioxide anode mixtures demonstrated excessive voltage performance loss, the result of carbon dioxide intermediate species poisoning. This effect has previously been reported. A series of experiments were completed to document $CO_2$ effects, and to identify conditions that permit successful PEM operation even when an appreciable carbon dioxide concentration (~25%) exists in the fuel stream. Reference cell tests were performed to determine the $CO_2$ poisoning mechanism. A gas chromatograph, equipped with a sensitive flame ionization detector, was connected to monitor the composition of both the inlet and exhaust stream to and from the anode. These tests utilized a standard Dow M&E, fabricated with 4 mg/cm$^2$ Pt. (This electrode type appears to demonstrate the most drastic voltage losses with carbon dioxide.) Anode gas feed was set at a water saturated 100 ml/minute hydrogen and 33 ml/minute carbon dioxide flow mixture at 80°C. Cathode feed was nitrogen, to eliminate any possible reaction with "cross over oxygen" flowing at 1,000 ml/minute. Under conditions of 3 atmosphere pressure on both the anode and cathode components 2,000 ppm $N_2$, i.e. "cross over nitrogen", but no detectable CO, was measured in the anode exhaust. Confirming analyses indicated that the rate of the reverse shift reaction between carbon dioxide and hydrogen is extremely slow at 80°C; consequently, it appears that low levels of CO generated in the anode <u>are not</u> the cause of the voltage loss due to carbon dioxide concentrations in the anode inlet flow.

  While many spectroscopic studies tend to support the view that the same chemical species is formed from adsorption of $CO_2$ or CO, that apparently <u>is not</u> the case. The adsorbed $CO_2$ related species is believed to be a COH-type species that adsorbs on platinum sites. This compound is readily removed by the addition of air to the anode feed. Also, there is clear evidence that certain metallic alloys demonstrate little or no adverse effects with carbon dioxide in the anode feed. Thus several technical solutions are apparent that result in successful operation of PEM hardware with reformate feeds.

  Actual reference fuel cell test data, demonstrating one of these solutions, is presented in Figure 3.4.5-5. The upper curve indicates pure hydrogen per-

formance; the performance loss with 25% carbon dioxide is depicted by the lower curve. (This M&E was not a high performance assembly; however, trends were similar to the other test specimens.) A small voltage loss due to hydrogen dilution effect is anticipated; 25% nitrogen mixed with pure hydrogen was used to demonstrate this effect Clearly, the voltage loss due to the presence of $CO_2$ exceeds that due to dilution effects. However, the addition of 0.5% $O_2$ or 2+% air (by volume) to the anode feed completely eliminates any adverse $CO_2$ effect. One-half percent of oxygen concentration within the anode feed is well within acceptable safety limits but does result in combustion of twice that fuel volume. Moreover, all of the combustion heat is deposited into the cell hardware and this excess heat must be removed by the stack coolant flow.

These adverse effects of carbon dioxide removal can be accommodated through simple operational strategies. However, work on improved anode catalysts, which may result in the elimination of any necessity for air injection into the anode compartment, remains of interest.

- ***Methanol*** - Another contaminant studied was methanol, a possible "break through" compound in the fuel stream that may exist due to incomplete conversion under certain off-design fuel processing conditions. Reference fuel cell experiments were conducted by adding methanol to the anode feed up to concentrations as high as 10% by gaseous volume. Test results demonstrated a wide range of methanol contamination tolerance. Even with a methanol volume concentration as high as 1%, only a 10% loss in voltage performance

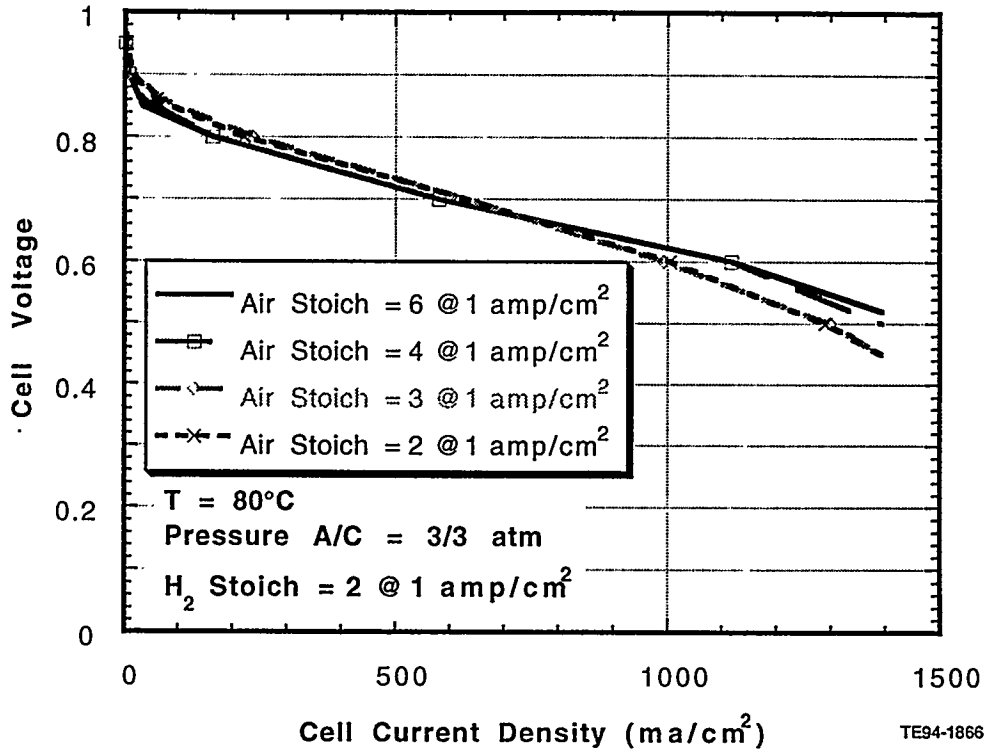


Figure 3.4.5-4. Reference cell Dow MEA, hydrogen/air reactant voltage as a function of current density and cathode stoichiometry.

was observed. In actual system operating conditions excess methanol is processed in the first shift stage; consequently, there is little chance that anode feeds to the fuel cell would ever contain more than a few ppm of methanol.

## 3.5 FUEL PROCESSOR RESEARCH AND DEVELOPMENT

### 3.5.1 Introduction and Summary

The ECE includes components for generating hydrogen using on-board chemical processing (steam-reforming) followed by a series of sequential chemical steps required to purify the hydrogen fuel gas steam. Vaporized methanol and water are reacted on surfaces of heterogeneous catalysts to form a hydrogen-rich stream for the anode (fuel) input. As in an IC engine fuel flow must track power production demand. This hydrogen-rich fuel stream is contaminated with unreacted methanol, CO, and other constituents that may possibly degrade fuel cell performance, through poisoning of either the fuel cell (hydrogen) anode catalyst or the (air) cathode catalyst. Contaminants such as methanol can also dissolve in the aqueous membrane phase and may cause a decrease in physical strength of the polymer. Removal of these fuel contaminants occurs within fuel processor gas cleanup sections, which include shifters (catalytic reactors similar to the reformer but plug flow in nature) and preferential oxidation catalysts to remove the remaining CO and (trace amounts of) methanol.

Methanol is rapidly converted to hydrogen by chemical reactions on heterogeneous catalyst surfaces at relatively low temperatures (~250°C). As a consequence this molecule serves as a unique "hydrogen storage" reactant. Methanol steam reforming has been historically depicted as the combination of the methanol decomposition reaction and the water-gas shift reaction:

$$CH_3OH = 2H_2 + CO \quad (1)$$

$$CO + H_2O = CO_2 + H_2 \quad (2)$$

These reactions, when summed, represent the conventional methanol steam reforming reaction:

$$CH_3OH + H_2O = 3\,H_2 + CO_2 \quad (3)$$

Mixed metal oxide catalysts such as CuO-ZnO, and a variety of elements used as dopant agents, have been the most frequently used heterogeneous catalysts for hydrogen production from methanol. These low-cost materials operate with hydrogen-dosed surfaces, dominated by metal-hydrogen (Zn-H) and oxygen-hydrogen (-OH) bonding. Several possible mechanistic routes have been suggested for the steam reforming process, all more complex than those simply suggested by Reactions 1 and 2. Moreover the forward shift reaction, (2), is conducted under excess water conditions, so the hydrogen product is accompanied by excess water (steam) and CO. Because the entire set of reactions occur under conditions where stream reforming kinetics are measured to be rapid, shift kinetics approach equilibrium. As a consequence, resulting CO concentrations are close to equilibrium. The steam to carbon

ratio in useful systems can vary from 1 to 3. Shift reaction temperatures, within the second stage shifter, near 200°C can lead to CO concentrations of 0.5 to 4% depending on the water concentration. These high CO concentrations are still totally unacceptable in the anode feed for low-temperature (80-100°C) PEM stacks and would result in a severe fuel cell performance loss; the cell performance loss is dependent on temperature, catalyst formulation and loading, and other factors. A PEM fuel cell system requires CO control for good performance. CO removal has been emphasized in this effort as unreacted methanol was easily converted in the first portion of the shift zone which was operated at the reformer temperature and acted as a plug flow reactor. If any trace amount of methanol escaped through the shift zone it was always totally removed in the PROX unit. PROX processes are described in more detail below.

Several technical approaches have been proposed for CO removal from hydrogen-rich streams. Reduction to methane is technically feasible, though the presence of significant quantities of $CO_2$ in the mixture complicates processing. Separation of CO using membranes is possible, but low temperatures and large pressures and excessive membrane areas would be required and adequate separation to low concentration levels would be difficult. CO can also be oxidized with oxygen to $CO_2$ on appropriate catalysts. This approach requires reaction control to force CO oxidation to occur preferentially to hydrogen oxidation. This latter approach, PROX, has been pursued. Studies were specifically designed to determine the dynamics of oxidation of this approach. The process intent is to add oxygen to the gaseous mixture and then react the resulting mixture on the surface of oxidation catalysts. Measured effectiveness represents the result of the preferential oxidation rate of CO over that of hydrogen during reactions on catalyst surfaces.

Other catalyst development work also occurred during Phase I. Steam reforming processes require large energy inputs (~50 kJ/mole) to supply heats of reactions. As a consequence, much of the technical modeling development, an important adjunct of this catalyst work, considered heat flow during simulated processing conditions.

The emphasis of this R&D Task involved modeling, and the design and development of unique, bench scale heterogeneous catalyst reactors. These tasks were accomplished jointly between the JDC, which performed the analytical modeling design work and catalyst testing, and AC Rochester, which developed new catalyst formulations and geometries. Two major catalyst types were explored: reforming and shift catalysts initially in the form of pellets and later prepared on monolithic supports for mechanical stability, reduced volume, and low flow resistance; and oxidation catalysts, prepared on similar monolithic supports for CO and (trace) methanol removal. The primary emphasis of this R&D task was to understand the kinetics of the reactions occurring on the various catalysts: results from this work were used to create more efficient full scale fuel processing components. Advanced test benches were built to make detailed investigations of the catalyst reactions; areas of investigation included:

- oxidation of both CO and methanol within the PROX unit
- initial modeling of CO and methanol oxidation kinetics
- detailed modeling of CO and methanol oxidation kinetics including heat and mass transport

- reformer/shifter process kinetics using both pellet and monolithic catalyst geometries

Because the reformer/shifter process was working well on pellets, the majority of this R&D effort concentrated on understanding the CO and methanol oxidation kinetics within the PROX bench unit. Further, the study of the reforming/shifting process kinetics was hampered by the initial use of plug flow conditions to evaluate steam reforming catalysts. A "gradientless, stirred reactor," designed for monolith use, was procured late in the Phase I effort. This stirred apparatus will be useful in Phase II to accurately determine reforming/shifting kinetic processes. This section describes approaches to the above tasks and presents some significant results attained during Phase I.

### 3.5.2 Description of Reformer/Shifter/PROX Test Benches

This test apparatus (Figure 3.5.2-1) blends reactant streams to form a gaseous mixture (called synthetic reformate) of $H_2$, $CO_2$, CO, $H_2O$, and $CH_3OH$ that simulates the gaseous mixture produced during methanol fuel processing. Individual gas flow rates are metered with MFCs, while liquid (water, methanol) flow rates are metered using precise liquid metering pumps that transfer water into a vaporization section and then into the flowing gas. A typical simulated reformate mixture contains 69.5% $H_2$, 23.2% $CO_2$, and 6.4% $H_2O$ to approximate a reformer injection feed ratio of 1.3 moles of water per mole of methanol. Low level concentrations of CO, $CH_3OH$,

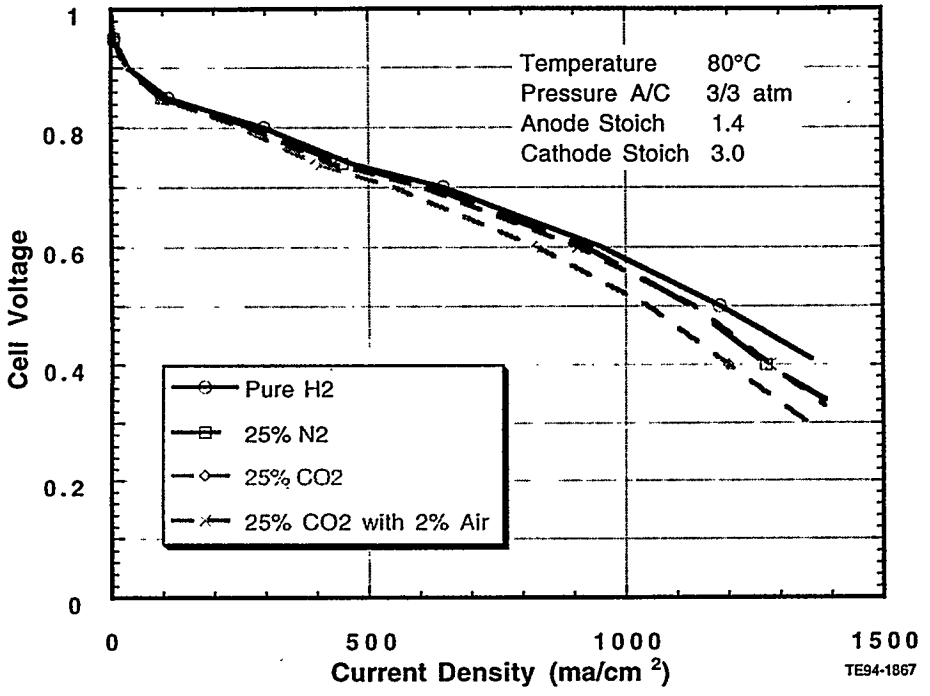


Figure 3.4.5-5. The effect of reformate and reformate with 2% air anode feed on the voltage - current characteristics of a Dow MEA in the reference cell.

and injected oxygen (air) were varied over the experimental ranges of interest. The addition of oxygen (air) into a hydrogen-containing gas can lead to explosive conditions; strict procedures are necessary to avoid dangerous gas mixtures.

Gas-stream inlet temperatures are controlled using a tubular heat exchanger that sets gas-phase temperatures prior to the reactor inlet. The experimental pressure can be set by a pressure controller to maintain isobaric conditions. The reactant streams are monitored for CO, $CH_3OH$, and $O_2$ concentrations with a gas chromatograph (GC) equipped with a thermal conductivity detector. Periodic GC calibration demonstrated sensitivities of ±5 ppm CO, ±10 ppm $CH_3OH$, and ±5 ppm $O_2$. Safety features, not depicted, include hydrogen sensors that immediately issue a warning when hydrogen is detected in the external (laboratory) atmosphere and subsequently, terminate hydrogen flow should laboratory concentrations achieve a potentially dangerous level. The test bench also has sensors that continuously measure laboratory carbon monoxide to assure that potentially dangerous CO levels do not occur.

The initial test bench used to determine methanol reforming and shifting catalyst and reaction dynamics is similar to that used for PROX studies and is also depicted by the schematic presented in Figure 3.5.2-1 This "methanol test bench" utilizes a premixed solution of methanol and water, blended to achieve the correct feed ratio. This solution is passed through a small volume vaporization unit that vaporizes the entire flow and then flows through a plug flow reactor that can be filled with catalyst pellets or a monolith coated with catalyst. Because of heat transfer limitations, this test bench was later converted to utilize a stirred "gradientless" reactor.

### 3.5.3 Development of Initial PROX Catalysis Model and PROX Test Bench Results

The PROX process involves a complicated competition between CO and $H_2$ oxidation. The nature of the preferential oxidation process is determined by the variation of reactant adsorption as a function of temperature. All three reactants, hydrogen, carbon monoxide, and oxygen are involved. Carbon monoxide adsorbs most strongly to platinum surfaces at low temperature, so strongly, in fact, that the sorbed molecule can effectively cover such surfaces and eliminate successful oxygen adsorption. This phenomenon can lead to a self-quench condition in which the sorbed CO effectively retards carbon monoxide oxidation to the point that the oxidation process ceases. At higher temperatures, hydrogen and oxygen can successfully compete for catalytic sites. Consequently, the process conditions require a temperature and catalyst formulation where carbon monoxide adsorbs preferentially, but not completely, leaving sites for oxygen reactivity. There are a wide range of conditions where successful CO removal may occur and, therefore, prediction of the optimum PROX condition is not possible. Considerable analytical modeling was required to determine the appropriate experimental studies. This section discusses models developed to describe the chemical kinetics occurring within the PROX reactor. Appropriate comparisons to experimental data are presented.

Two mathematical models of PROX reactors were developed. The earlier model assumes that no heat or mass transfer exists between the gas phase and the catalytic surfaces of the reactor. The chemical model predicts the outlet gas-phase composi-

tion based on reactor inlet conditions for the preferential oxidation of CO and $CH_3OH$ in a gas stream containing approximately 66% $H_2$. Methanol was included to cover those unlikely, but possible, operating conditions when some small concentration of methanol might appear in the gaseous mixture. The one-dimensional model assumes plug flow within an adiabatic, steady-state tubular reactor. The oxidation reactions of CO, methanol, hydrogen, and the *reverse* shift reaction are treated as irreversible, global catalytic reactions. The forward-shift reaction is not included because the conditions of interest are far removed from equilibrium and, therefore, reaction does not have significant kinetics.

The reaction rate expressions were written in forms of the Langmuir-Hinshelwood equation which show CO adsorption-related kinetic inhibition:

$$R_{CO} = -k_{CO} \frac{C_{CO} C_{O_2}}{\left(1 + K_{ad} C_{CO}\right)^2} \tag{4}$$

$$R_{H_2} = -k_{H_2} \frac{C_{O_2}}{\left(1 + K_{ad} C_{CO}\right)^3} \tag{5}$$

$$R_M = -k_M \frac{C_{CH_3OH} C_{O_2}}{\left(1 + K_{ad} C_{CO}\right)^2} \tag{6}$$

$$R_{RS} = -k_{RS} \frac{C_{CO_2} C_{H_2}}{\left(1 + K_{ad} C_{CO}\right)^2} \tag{7}$$

where the reaction rate coefficients

$$k_i = A_i \cdot \exp\left(\frac{-E_i}{RT}\right) \tag{8}$$

are written in the Arrhenius form. Note that the surface coverage of CO, shown here as an adsorption coefficient,

$$K_{ad} = A_{ad} \cdot \exp\left(\frac{E_{ad}}{RT}\right) \tag{9}$$

is assumed to preferentially dominate other species at the partial pressures and temperatures used during this conversion. The mass balance for each species is given by

$$\frac{d(uC_i)}{dz} = R_i \tag{10}$$

where $u$ is the bulk-gas velocity, and $R_i$ is the net molar production rate of each species determined by summing the formation and destruction rates. The mass balance equations for the species are:

$$\frac{d(uC_{CO})}{dz} = R_{CO} - R_{RS} \tag{11}$$

$$\frac{d(uC_{CO_2})}{dz} = R_{RS} - R_M - R_{CO} \tag{12}$$

$$\frac{d(uC_{O_2})}{dz} = \frac{1}{2}R_{CO} + \frac{1}{2}R_{H_2} + \frac{1}{2}R_M \tag{13}$$

$$\frac{d(uC_{H_2O})}{dz} = -R_{H_2} - R_{RS} \tag{14}$$

$$\frac{d(uC_M)}{dz} = R_M \tag{15}$$

The energy balance for the reactor simulation is written as:

$$c_p C_t \frac{d(uT)}{dz} + \sum_i \Delta H_i R_i = 0 \tag{16}$$

Changes in $u$ are determined from the ideal gas law and $c_p$ is the specific heat of the gas mixture determined from:

$$c_p = \sum_i \frac{C_i}{C_t} c_{p,i}(T) \tag{17}$$

where $c_{p,i}(T)$ is the specific heat of species $i$ evaluated at the local temperature.

This system of ordinary differential equations is integrated along the length of the reactor using a fourth-order Runge-Kutta method. The boundary conditions include the inlet reactor temperature, pressure, flow rate, and molar composition of the gas-phase mixture. Integration generates profiles of the temperature, velocity, and molar composition along the flow path.

In order to evaluate the reaction rates shown above, four pre-exponential factors, four activation energies, and the energetics for CO adsorption are necessary. Activation energies are assumed to be catalyst dependent, and literature values previously determined for platinum were used for the initial calculations. Literature values for required pre-exponential factors served as starting inputs to the model, but these were later adjusted to match measured data. The Arrhenius

parameters shown in Table 3.5.3-1 are those determined to correlate with those values in Figure 3.5.3-1.

Comparisons of the modeling and experimental results for specific, but separate, CO and $CH_3OH$ preferential oxidation cases are presented in Figure 3.5.3-1. The experiments were conducted using a 1 in. diameter, 1 in long ceramic monolith (400 channels/in$^2$) wash coated with 0.5% platinum; inlet concentrations were: 2,500 ppm for both CO and methanol, 170°C, a flow rate of 4.32 slpm, and a pressure of 2.14 atm. (For purposes of comparison, hydrogen flow of ~ 6 slpm is normally sufficient for about 1-kW power production.) Data depict outlet concentrations of the 1-in. monolith as a function of a variety of oxygen/fuel inlet conditions. These computations were calculated for "adiabatic" conditions in which all of the oxygen was consumed; good agreement with experimental results is evident. During the traverse along the catalyst sample, most of the oxygen is consumed either by the carbon monoxide oxidation or the hydrogen oxidation reactions. In either case, heat is generated; increasing the oxygen concentration results in hotter reactor conditions.

CO is efficiently removed using an oxygen/CO feed ratio of ~ 2; effective methanol removal requires an oxygen/$CH_3OH$ ratio of ~ 4. (On a molar basis, three times more oxygen is required to burn methanol stoichiometrically than the same number of moles of carbon monoxide, so this result is not unexpected.) In the CO preferential oxidation experiment higher oxygen feed concentrations result in higher catalyst temperatures and produce conditions in which reverse shift kinetics were accelerated. Under high temperature conditions, carbon dioxide is reduced by hydrogen to produce additional, undesired carbon monoxide. In these calculations and experiments, reaction heat was primarily delivered to the product gaseous mixtures and the temperature increases continuously along each flow channel until oxygen is totally consumed. Methanol conversion, as depicted however, was accelerated by higher reaction temperatures. Figure 3.5.3-1 demonstrates conditions where both CO and $CH_3OH$, when considered separately, can be effectively eliminated from the gaseous mixture. Fortunately this level of $CH_3OH$ never enters the PROX, otherwise removal of this concentration of $CH_3OH$ would increase the CO concentration required to be removed. Nevertheless, the model and experimental results demonstrate that the PROX unit could be designed to cope with such an event.

Analytical results depicting the only CO concentration along a specific monolith channel are presented in Figure 3.5.3-2. Reactor conditions are the same as those

Table 3.5.3-I.
$A_i$ and $E_i/R(K)$ for the arrhenius rate coefficient expressions.

| Reaction | $A_i$ | $E_i/R$ |
|---|---|---|
| CO oxidation | $2.15 \times 10^{14}$ | 12,600 |
| CO equilibrium | 0.655 | 961 |
| $H_2$ oxidation | $2.20 \times 10^{3}$ | 1,708 |
| Reverse shift | $1.30 \times 10^{17}$ | 18,100 |
| Methanol oxidation | $5.00 \times 10^{11}$ | 3,970 |

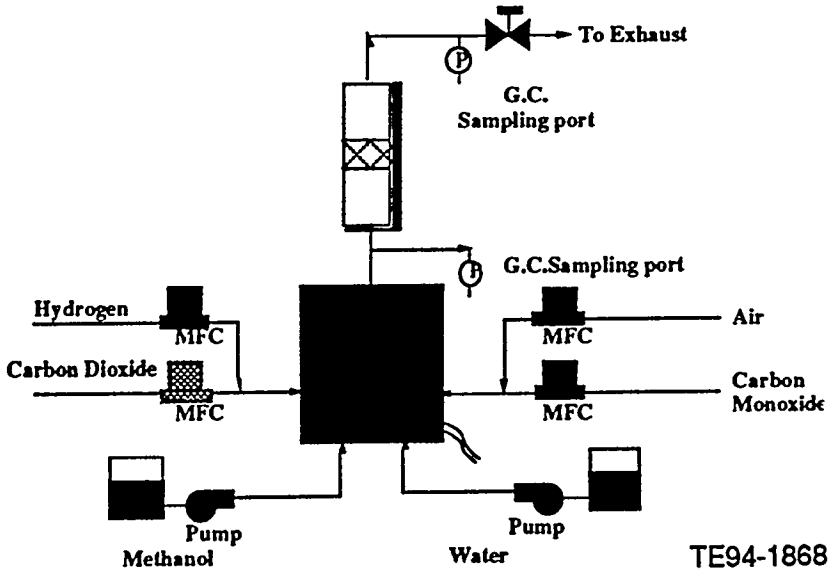


Figure 3.5.2-1. Preferential oxidation and reformer/shifter test bench experiment.

stated in Figure 3.5.3-1 except the inlet temperature has been increased to 200°C, the oxygen injection concentration is now 0.92%, and methanol is absent from the mixture. The CO is quickly reacted to $CO_2$ in the first part of the catalyst channels; CO oxidation is complete within a short reaction zone. The remainder of the oxygen continues to react, however, burning hydrogen. Heat is released continuously, and the temperature along the channel increases. These conditions lead to the formation of additional CO, which results from the reverse shift reaction. In this example the exit CO concentration is actually double that of the entrance concentration.

Controlling the inlet temperature, the monolith catalyst length, the oxygen concentration, or the catalyst type and loading enables increased effectiveness in removing CO.

The present analytical model, tuned using experimentally-derived parameters, was also used to interpret data from the test benches. A comparison of modeling (dotted line) and experimental results for CO and $O_2$ outlet concentrations as a function of the inlet CO concentration are presented in Figures 3.5.3-3 and 3.5.3-4, respectively. A synthetic reformate mixture at 2.14 atm (absolute) was injected, along with a constant 0.92% $O_2$ flow, into a 1 in., 2.0% platinum monolith; total flow was 4.32 slpm. At high inlet CO concentrations, depending on inlet temperature, platinum surfaces can be totally CO covered. The extent of the self-poisoning effect (CO adsorption poisons CO oxidation) is expressed in the model by the CO adsorption terms in the denominators of the reaction rate expressions. Both the model and experimental results are evident in the figures in that no CO conversion occurs and yet significant concentrations of $O_2$ are present.

At inlet concentrations slightly below the self-poisoning level, the outlet CO concentration approaches zero. As the inlet CO concentration is further decreased the outlet CO concentration begins to increase. This is the result of altering reaction rates

for the CO oxidation and the onset of the reverse-shift processes. With sufficient, but not excess CO present, the CO oxidation occurs fast enough, but temperatures remain relatively low along the latter portion of the monolith channel to restrict reverse-shift conditions. An increase in the inlet CO concentration beyond this point results in CO poisoning of all reaction sites on the platinum surface. Under these conditions neither hydrogen nor CO react and the majority of the injected oxygen

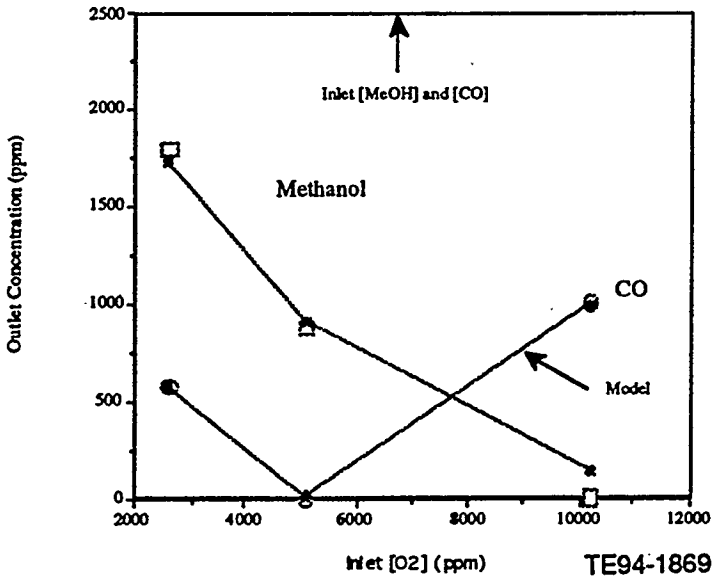


Figure 3.5.3-1. Comparison of modeling and experimental results for CO and CH3OH preferential oxidation.

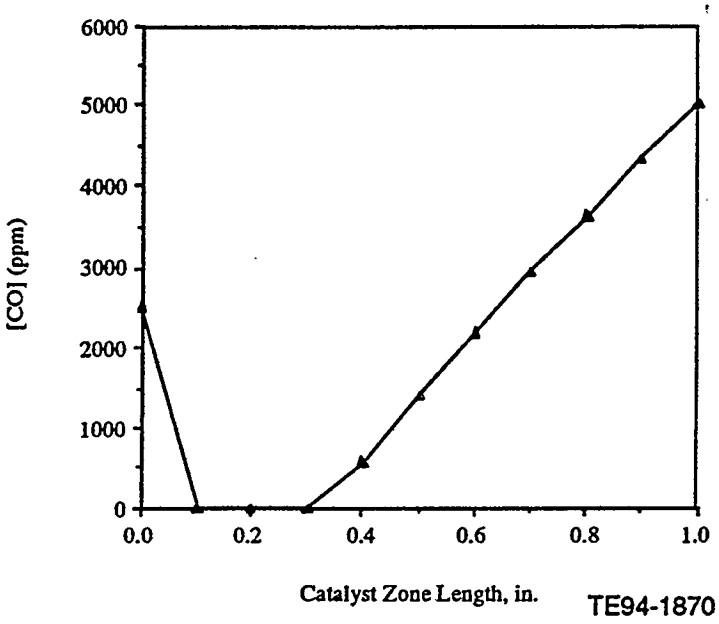


Figure 3.5.3-2. Model results of CO concentration removal and formation in short reaction catalyst geometries.

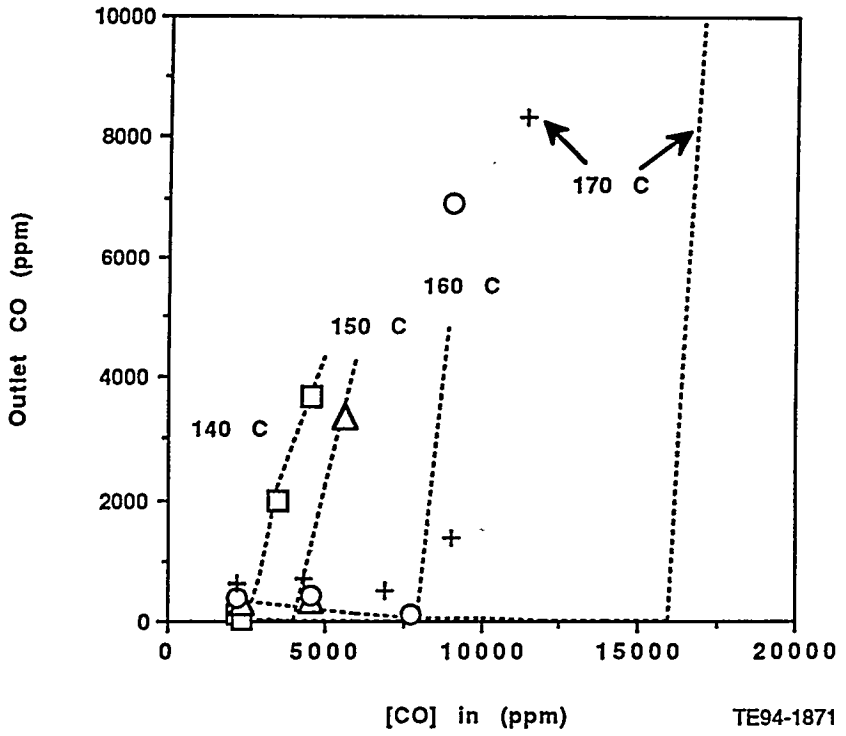


Figure 3.5.3-3. Comparison of modeling (dotted line) and experimental results for CO preferential oxidation in which outlet CO concentrations as a function of inlet CO concentrations and temperatures are presented. Data depict outlet CO concentration as a function of inlet CO concentration for 20 psig synthetic reformate mixture in a 1.0 in monolith with 2.0% Pt loading and constant (0.92%) oxygen injection.

emerges unreacted. However, a CO concentration decrease below this self poisoning level can result in full $O_2$ utilization within the monolith at properly controlled temperatures. With other parameters held constant, oxygen consumption generates more heat and the catalyst temperature becomes elevated. Under these higher temperatures, CO can then be regenerated via the reverse shift reaction after the initial CO has been converted to $CO_2$. In fact, an inlet CO concentration of zero can still produce excessive CO outlet concentrations due to the reverse shift reaction.

The combination of residence time and temperature is critically important in the successful operation of a PROX device; success is a function of obtaining sufficiently fast oxidation rates while restricting reverse shift rates. Pressure, temperature, flow rate, monolith length, and reaction stoichiometry all affect the residence time. The theoretical and experimental effects of monolith length and flow rate on the outlet CO concentration, again as a function of CO inlet concentration, are presented in Figures 3.5.3-5 and 3.5.3-6. The case depicted in Figure 3.5.3-6, short monolith with high flow (1/4" and 8.8 slpm, respectively), indicates that insufficient response time is allowed for CO oxidation to light off except at the low inlet CO concentration of ~ 2500 ppm.

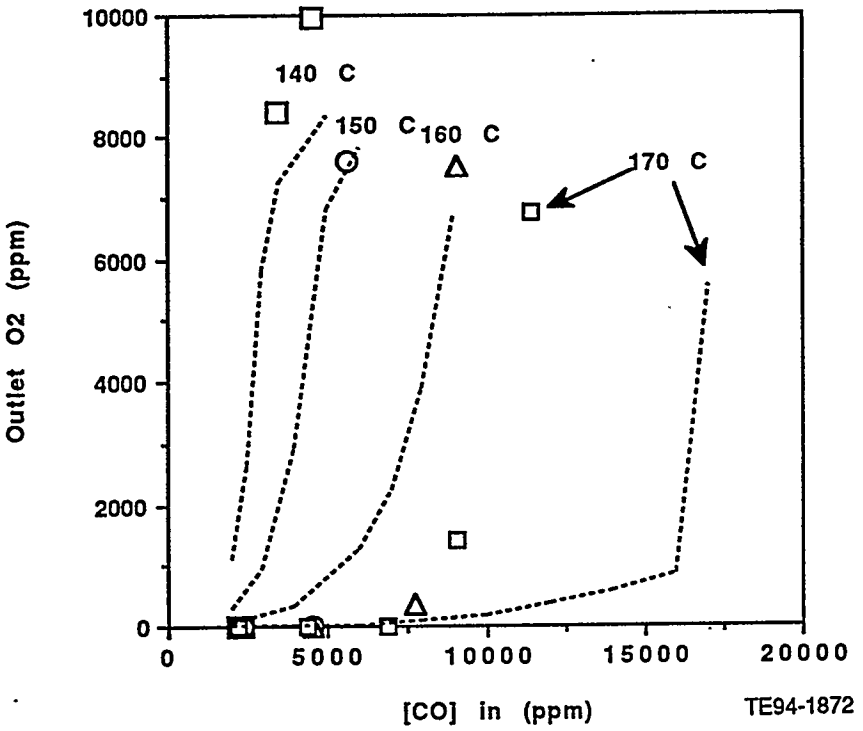


Figure 3.5.3-4. Comparison of modeling (dotted line) and experimental results for CO preferential oxidation in which outlet $O_2$ concentration as a function of inlet CO concentrations and temperatures are presented. Data depict outlet $O_2$ concentration as a function of inlet CO concentration for 20 psig synthetic reformate mixture in a 1.0 in monolith with 2.0% Pt loading and constant (0.92%) oxygen injection.

The results described above assume (and appear to indicate) constant catalyst reactivity and a surface that is influenced only by CO and $H_2$ concentrations. Unfortunately, platinum catalysts can adsorb other molecules, including water, and it is understood that surface catalytic reactivity is a strong function of such absorbed species, especially oxygen. The detailed preconditioning treatment used for these experiments involved injection of 2% $O_2$ into synthetic reformate flowing through the monoliths to elevate the monolith temperature, under autothermal conditions, to the 400-450°C range for approximately 10 minutes. The monolith was then cooled under flowing conditions and used for the PROX experiments. This conditioning tends to establish reproducible surface conditions and must be conducted frequently with the catalysts studied to promote good reaction control.

### 3.5.4 Development of More Detailed Transient PROX Catalysis Modeling, Including Heat and Mass Transport and Further PROX Test Bench Results

The first, simplified model assumed an isothermal condition between the reacting gas stream and the solid catalyst surface. Although such an approach is straightforward computationally, this type of model is not always chemically correct. Rather, because of gas-phase heat transfer limitations, the catalyst sites and the

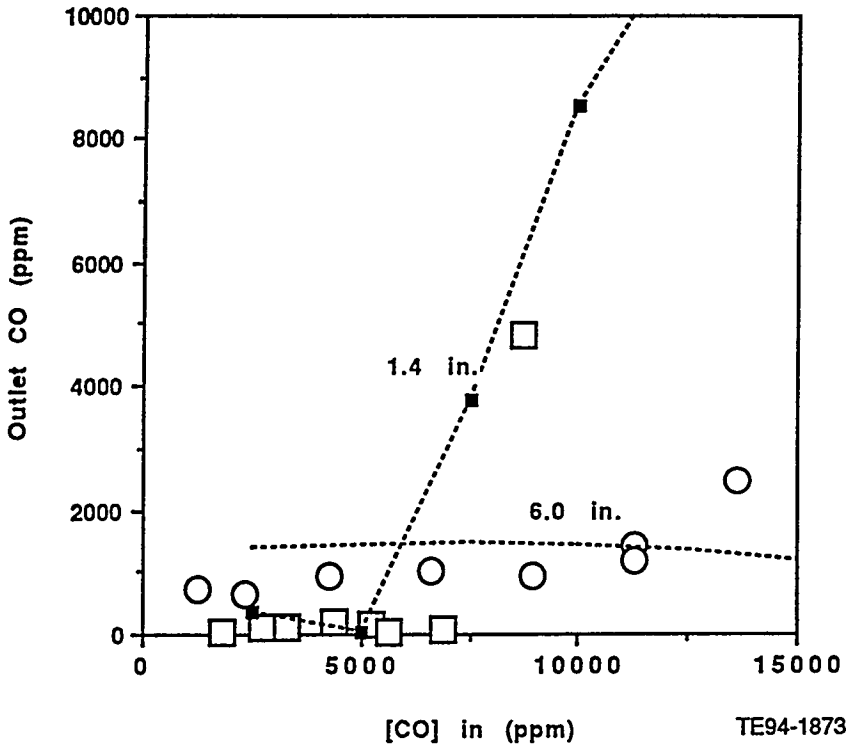


Figure 3.5.3-5. Comparison of modeling (dotted line) and experimental results for CO preferential oxidation in which outlet CO concentrations are presented as functions of inlet CO concentrations, monolith lengths and moderate flow rate. Data depict outlet CO concentration as a function of inlet CO concentration and monolith length for a 30 psig, 140°C, 8.8 slpm synthetic reformate mixture in monoliths with 2% Pt loading and constant (0.92%) oxygen injection.

bulk gas phase reach different temperatures thereby affecting chemical reaction rates. The second model, described in this section, accounts for transient conditions and heat and mass transport between the reacting gaseous mixture and the solid catalyst support. Terms for methanol oxidation are included in this model, but are not discussed here, because the actual gas-phase mixture used to refine kinetic parameters had virtually non-detectable concentrations of methanol. Other than that change, the reaction rate expressions are those previously described. However, the mass balance for each species $i$ is now given by

$$\frac{\partial C_{gi}}{\partial t} = -u\frac{\partial C_{gi}}{\partial z} - \frac{k_{mi}S}{\varepsilon}\left(C_{wi} - C_{gi}\right) \tag{9}$$

for the gas phase and

$$k_{mi}S\left(C_{wi} - C_{gi}\right) = R_i \tag{10}$$

for the solid phase, where $R_i$ is the summation of all reactions involving the $i$th species, $k_{mi}$ is the mass transfer coefficient for species $i$, e is the void fraction, $S$ is the surface to volume ratio, and $h$ (below) is the heat transfer coefficient. Mass

transfer calculations are required only for the species CO and $O_2$. (Changes in hydrogen, carbon dioxide, and water concentration are minimal under these conditions.) The heat balance for the gas phase is

$$\frac{\partial T_g}{\partial t} = -u\frac{\partial T_g}{\partial z} + \frac{hS}{\varepsilon C_{pg}\rho_g}\left(T_w - T_g\right) \tag{11}$$

and for the solid phase is

$$\frac{\partial T_w}{\partial t} = \frac{hS\left(T_g - T_w\right) - S\sum_j R_j \Delta H_j}{\rho_w C_{pw}(1-\varepsilon)} \tag{12}$$

where the j reactions include the 3 exothermic hydrogen, carbon monoxide, and methanol oxidation reactions and the endothermic *reverse* shift reaction.

The above system of equations was integrated, again using a finite difference method for the transient solution and a fourth-order Runge-Kutta method for the steady-state solution. Boundary conditions are required at the reactor inlet for temperature, pressure, flow rate, and gas-phase chemical compositions. Initial conditions throughout the entire reactor are also required. Integration over the length of the reactor generates profiles of the temperature, velocity, and molar composition as a function of time and/or distance along the reactor.

The experimental data used to assess kinetic parameters in the transport model are presented in Figures 3.5.4-1 and 3.5.4-2. The resulting Arrhenius parameters used in the model are listed in Table 3.5.4-1 below. These data sets are the results of kinetic performance derived from the Mark II system experiments and have varying injection velocities, injection CO concentrations, and similar injection temperatures. Although the injection temperatures, as presented, are constant for any one data set, the experiments themselves are far from isothermal. For example, during the 5.2% air injection experiment, the temperature across the PROX ranged from an inlet of approximately 180°C to an outlet of 338°C.

Table 3.5.4-1.
$A_j$ and $E_j/R$(K) for the arrhenius rate coefficient expressions (data based on Mark II PROX experiments).

| Reaction | $A_j$ | $E_j/R$ |
|---|---|---|
| CO oxidation | $1.30\times10^{13}$ | 12,600 |
| CO equilibrium | 0.655 | 961 |
| $H_2$ oxidation | $2.20\times10^{3}$ | 1,708 |
| Reverse shift | $1.80\times10^{17}$ | 18,100 |

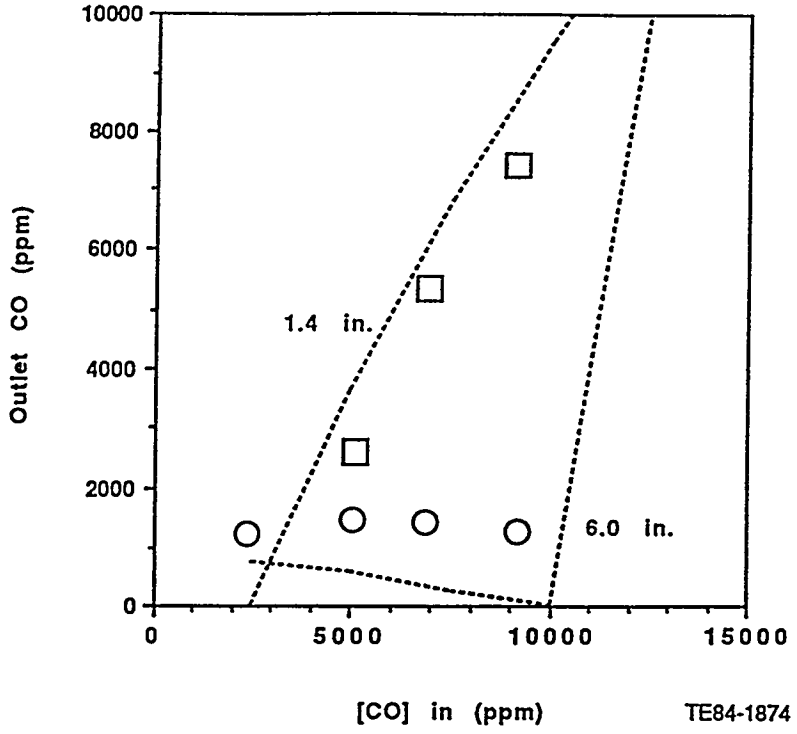


Figure 3.5.3-6. Comparison of modeling (dotted line) and experimental results for CO preferential oxidation in which outlet CO concentration are presented as functions of inlet CO concentrations, monolith lengths, and high flow rate. Data depict outlet CO concentration as a function of inlet CO concentration and monolith length for a 30 psig, 140°C, 8.8 slpm synthetic reformate mixture in monoliths with 2.0% Pt loading and constant (0.92%) oxygen injection.

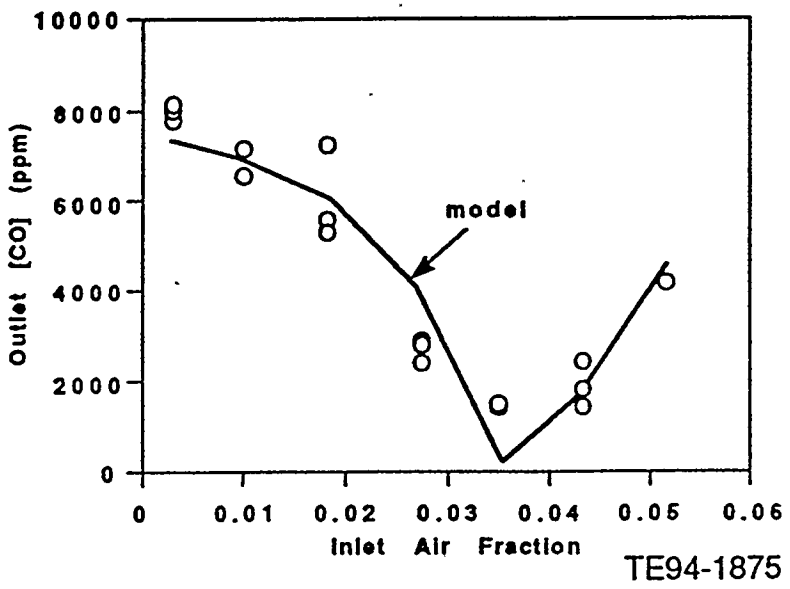


Figure 3.5.4-1. Steady-state enhanced PROX model results compared to data; outlet CO concentration is presented as a function of inlet air fraction for moderate flow rate and CO inlet concentrations. Data conditions were $u_{in}$ = 0.538 m/s (STP), $T_{in}$ = 180°C, and $[CO]_{in}$ = 7,500 ppm.

The model-calculated steady-state reaction conditions along one of the monolith channels are presented in Figure 3.5.4-3. The gas phase temperature increases slowly until that point where CO concentrations fall sufficiently to establish fast oxidation kinetics. These results indicate that CO oxidation occurs rapidly once the self-poisoning conditions are eliminated. Once CO is not present, however, oxygen depletion occurs quickly, the result of hydrogen oxidation. The consumption of oxygen, through either CO or $H_2$ oxidation, raises the temperature, resulting in conditions where reverse-shift kinetics are now sufficiently fast to generate additional CO.

The gas-wall temperature gradients within the PROX unit, although small, still have an effect. Computational sensitivity studies indicate that gas-wall temperature differences as small as about 10°C can alter reactivities, a result of the fact that both hydrogen and carbon monoxide oxidation rates are strong positive functions of temperature. Also, temperature differences between the gas-phase and catalytic surfaces within the PROX unit can increase under certain operating conditions where PROX units have large hydraulic diameters, high operating temperatures, gas mixtures without appreciable hydrogen concentration, and long monoliths (short monoliths have significant heat transfer enhancement because of entrance effects).

Bulk gas and wall species predicted concentrations for the "light off region" where CO kinetics rapidly increase are presented in Figure 3.5.4-4; data is based on the conditions for which the results presented in Figure 3.5.4-2 are based. Mass transfer effects follow similar trends as heat transfer within PROX units. Diffusivities are sharply increased during PROX processing, the result of the $H_2$ environment,

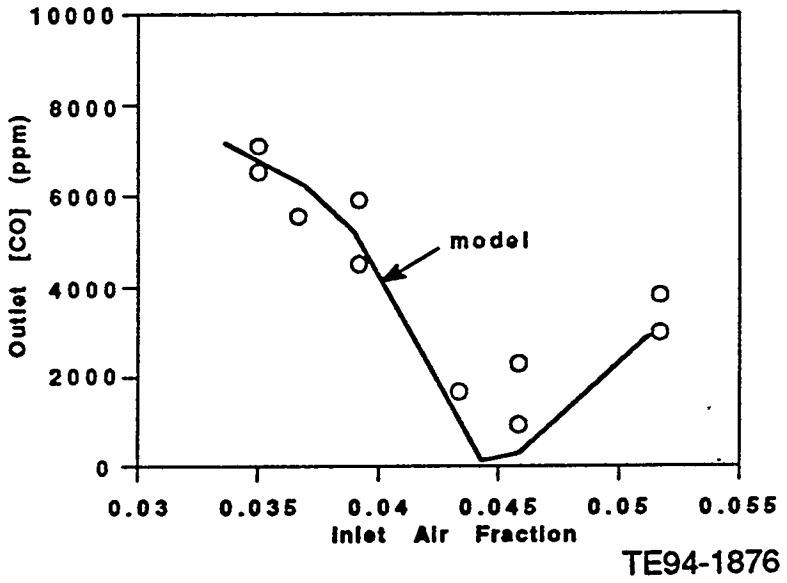


Figure 3.5.4-2. Steady-state enhanced PROX model results compared to data; outlet CO concentration is presented as a function of inlet air fraction for higher flow rates and CO inlet concentrations. Data conditions were uin = 0.673 m/s (STP), $T_{in}$ = 183°C, and $[CO]_{in}$ = 10,000 ppm.

while reaction rates, compared to a "catalytic converter," are lower because of the lower operating temperatures. Lower reaction rates tend to diminish concentration differences. It is interesting to note, as demonstrated in Figure 3.5.4-4, that during CO removal the CO concentration decreases in the direction of the wall; during CO generation (reverse shift) CO has the highest concentration at the catalyst surface.

The predicted CO concentration at the outlet of the monolith as a function of the inlet air fraction is presented in Figure 3.5.4-5. Inlet conditions are similar to those of Figure 3.5.4-2. However, several inlet velocities, corresponding to different hydrogen flow rates are depicted. Complete conversion of CO must be restricted to air fractions above approximately 0.025, or the stoichiometric oxygen quantity required for this inlet CO concentration conversion. At the two lower velocities and, hence, longer residence time cases (0.16 and 0.34 m/s), the model indicates that competition between CO oxidation, $H_2$ oxidation, and the *reverse* shift reactions set up reactivity conditions that preclude low CO output concentrations. As flow velocities increase, 0.67 m/s, CO conversion is far more complete at an injection $O_2$:CO ratio of about 1.0. When such low oxygen ratios are injected, only about 0.5% $O_2$ is left for $H_2$ oxidation. As flow velocities further increase, decreasing the residence time, CO removal can be achieved, but up to 8.2% air is required to accomplish this step at the 1.35 m/s case. Such a large quantity of excess oxygen results in appreciable hydrogen consumption and heat generation.

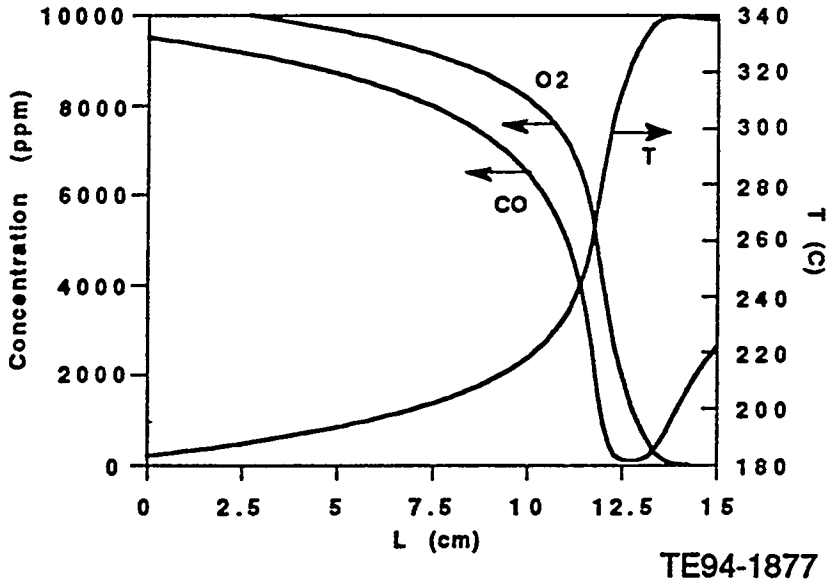


Figure 3.5.4-3. Predicted steady-state T, CO, and $O_2$ profiles for the 5.2% air injection case of Figure 3.5.4-2.

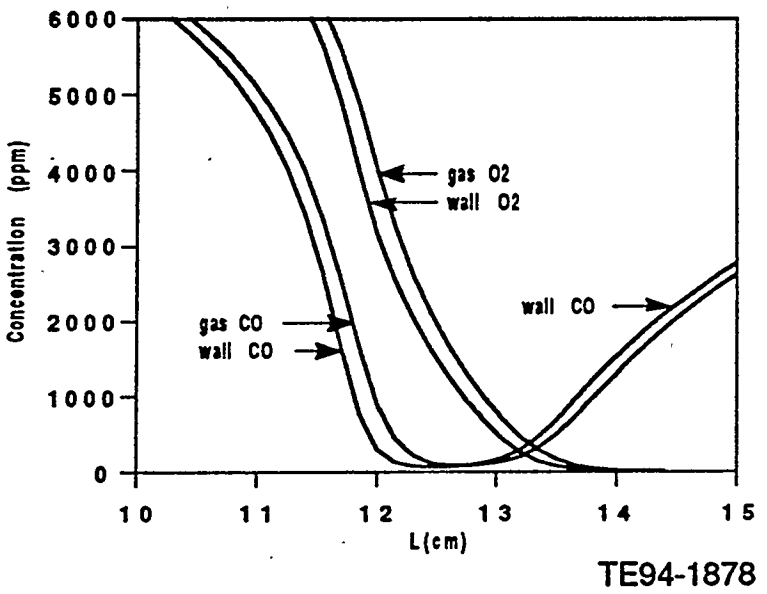


Figure 3.5.4-4. Predicted bulk gas and wall concentration profiles for the 5.2% air injection case of Figure 3.5.4-2. Data depicted emphasize the so-called "light off region", where CO kinetics rapidly increase.

Another important consideration of PROX operation is the start-up transient, the time necessary for the monolith section to reach useful temperatures from a cold-start. Computational results of start-up transients using a variety of different air injection compositions is presented in Figure 3.5.4-6. In this case the initial monolith temperature was 20°C and the gas-phase inlet temperature was 183°C. The results of varying the inlet air fraction are demonstrated. This modeling approach is an example of an "autothermal" start-up transient. Almost 200 s are required to reach the steady state, near-complete conversion point demonstrated in Figure 3.5.4-2 using the optimum air injection feed ratio of 4.48% . When larger air mole fractions are injected, start-up times are reduced; for example, injection of 16.7% air results in a start-up time of about 40 s. But, at this high air feed rate, heat is deposited at high rates and overheating leads to additional CO production as a result of the reverse shift reaction. The necessary strategy is to achieve rapid start-up without a consequent large evolution of CO. As an example, transients were analytically examined between the minima of Figure 3.5.4-5. Approximately 25 s were required to reach steady-state, assuming step changes in velocity and air injection at t=0, between the 0.67 m/s case at 4.4% air injection to the 1.35 m/s case at 8.2% air injection. Although 25 s were required to reach steady-state, the outlet CO concentration remained nearly constant during the transient as the inlet air fraction was adjusted with time.

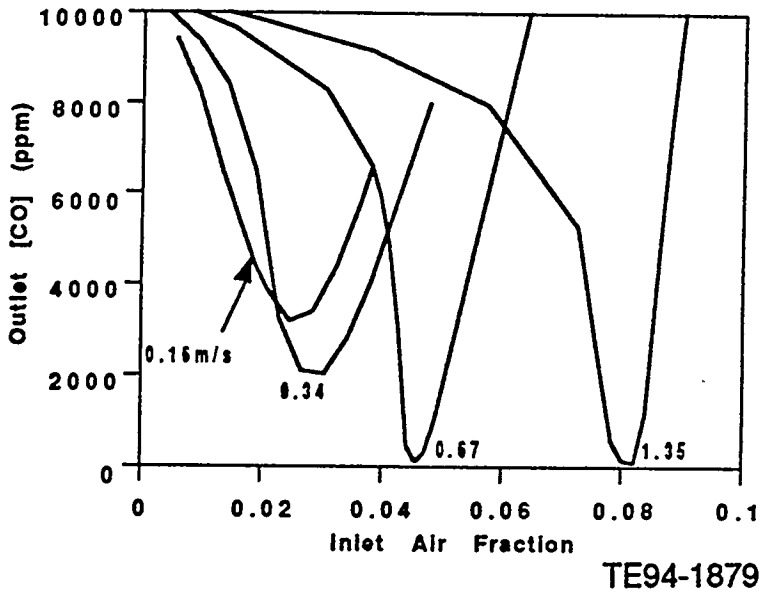


Figure 3.5.4-5. Steady-state CO monolith outlet concentrations as a function of inlet air fraction and velocity. Inlet conditions are the same as for Figure 3.5.4-2.

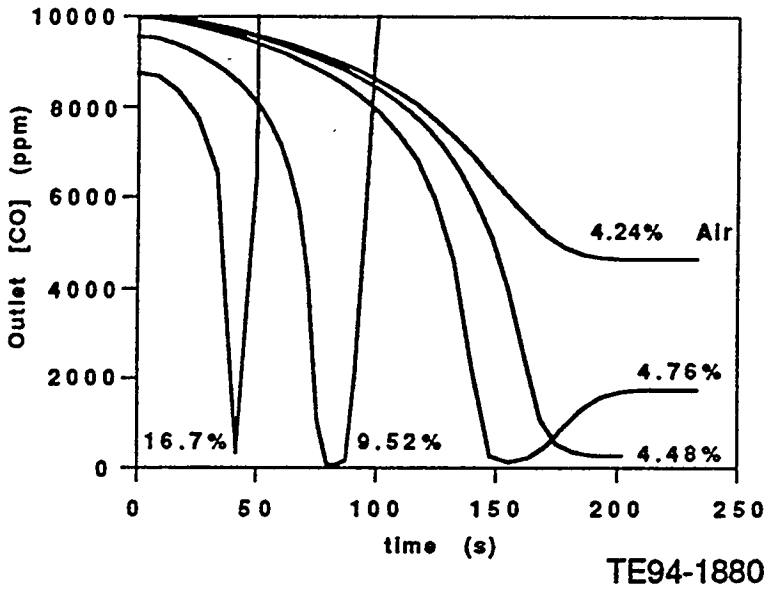


Figure 3.5.4-6. Outlet CO concentrations for a variety of start-up conditions. Inlet conditions are for a 183°C inlet gas stream and a 20°C monolith temperature. Initial monolith heating occurs due to a heat transfer from the hot inlet gas; subsequent heating occurs due to the conversion reactions. Curves indicate various air injection rates using identical PROX flow rates.

### 3.5.5 Reformer Test Bench Modeling and Results

The initial reformer test bench fabricated during this program is similar in design to the plug flow PROX test bench described earlier in this section; however, the apparatus was designed to investigate the methanol steam reforming reaction rather than the PROX gas cleanup reactions. The reforming studies require introduction of a methanol-water mixture into a vaporizer; that gas stream is then reacted on surfaces of heterogeneous catalyses.

Although many different metal oxide mixtures can serve as reforming catalysts, studies concentrated only on conventional catalyst types. Two types of CuO/ZnO reforming catalysts were investigated. First, C18HC ($CuO/ZnO/Al_2O_3$), a commercially available (United Catalysts), low temperature shift catalyst, was investigated. This catalyst, as supplied, comes in the form of small right cylinders (pellets) and was used for the majority of the ECE system work conducted during the first phase effort. The second catalyst was again formed as a CuO/ZnO mixture, but, was then coated by AC Rochester on a 400 channel/in$^2$ cordierite monolith.

Steam reforming catalysts only demonstrate useful kinetics following a reductive activation step. This process is usually accomplished by reaction with a dilute hydrogen gas mixture. The reduction process started with 6% $H_2$ in Ar at 150°C; the hydrogen concentration was then slowly increased, until, after 2 hours, pure $H_2$ at 250°C was introduced. It is understood that the oxygen concentration of the surface quickly follows the steam/hydrogen ratio of the gas phase mixture, so the final state of activation is set by the chemical feed stream, not by the activation step.
Preliminary results of a comparison of these two catalyst types were not definitive.

A thorough evaluation of reforming kinetics was completed, focusing on heat transfer dynamics. For the same reasons that advanced heat transfer, via heated recirculating reformate, is used in the Mark II steam reforming section, a stirred reactor was selected for reformer/shift catalyst evaluation. Several different so-called "gradientless reactors" were evaluated and one specifically designed for monolith operation was procured. This stirred apparatus will be useful both to control thermal excursions during activation and to determine reforming kinetics.

# IV. PROGRAM TASK 3: 10-kW FUEL CELL STACK DEVELOPMENT

## 4.1 GENERAL INTRODUCTION

An essential component of the ECE system is the fuel cell stack, the electrochemical device that produces electrical power from reformate and air feed streams. In the low-temperature stacks utilized for these studies, the cell zone of ionic conductivity is formed using a sheet of an ion-exchange polymer. These fuel cell stack designs follow the pioneering work done at General Electric, under NASA support, where oxygen-hydrogen fuel cells using Solid Polymer Electrolyte™ membranes were deployed (the Gemini program). Because the ion transfer process of interest is *proton* transport, the devices are designated PEM fuel cells. The majority of the fabrication effort of this task was accomplished at Ballard. Six stacks were delivered for utilization in Phase I activities. Four Stacks, SN-108, 109, 110, and 111, were early delivered prototypes, while Stacks SN-161 and SN-212, representing an improved, modified design, were delivered during the final months of Phase I. These were all supplied with membrane materials synthesized by Dow; electrodes were designed by Ballard.

Task 3 activities at the JDC concentrated on performance and reliability testing of these stacks. The intent of these tests was to determine optimum operational conditions using synthetic reformate (a mixture consisting of 75% $H_2$ - 25% $CO_2$) and air. Parameters including pressure, temperature, water coolant flow rate, humidification section design, flow stoichiometry, current, and voltage were varied during these tests. Tests involved each stack, on separate test, up to power levels exceeding 5-kW.

- ***Ballard stack performance*** - Detailed stack tests revealed optimum conditions for operation of contemporary stacks. During this program phase, work at Ballard also resulted in improved manufacturing operations, evidenced by more consistent results in cell-to-cell repeatability. The best reformate-air performance was evident in the last stack delivered, SN-212; average cell voltage of 0.60V at 1000 amps/ft$^2$ on reformate/air reactants was achieved. Approximately 500 hours of operational experience was obtained during tests of various stacks at the JDC.

- ***Carbon dioxide poisoning*** - Similar to the reference cell tests, control tests indicated performance degradation following $CO_2$ feed to the anode compartment. Unlike the rapid performance loss resulting from CO poisoning, $CO_2$ poisoning results in slow voltage degradation over an hour or more. It was concluded that this is the result of a COH-type intermediate species adsorbate that tends to block access of hydrogen to active anode sites. The addition of a small quantity of air to the anode stream was one successful method of removing this performance degradation, particularly when anode alloy catalyst mixtures were utilized. The optimum alloy and anode air addition contents are still being investigated.

Details regarding these development efforts are described in the following sections.

## 4.2 DESCRIPTION AND USE OF BALLARD PEM STACKS

There are many possible polymer chemistries to utilize for membrane syntheses. However, ion exchange polymers used in these experiments were routinely manufactured from polyperfluorosulfonic acid materials. These thermally and chemically stable membranes can be considered as electrolyte solutions with extremely low anionic mobility. (Anions are grafted to the polymer backbone.) It is recognized that finite quantities of liquid water are required for high conductivity; if the membrane is in a dry state, even though protons are present, the materials are not conductive. Because of this necessity for liquid water content, membrane operating conditions are limited to those temperatures and pressures where such conditions are realized. Consequently, as indicated below, the focus of the stack development program at the JDC has been to identify suitable regimes for achieving long term, stable and efficient stack performance.

Fuel cell membranes were supplied by the Dow company. At Ballard, proprietary electrode technology was used in conjunction with the Dow membrane in MEA; these MEAs were then incorporated into power stacks of a nominal power level of 5-kW. These membrane materials utilize polyperfluorosulfonic acid polymers, similar in overall chemistry to earlier Nafion™ materials prepared by DuPont, but formed using different polymer precursors that result in membranes with higher ionic conductivity. Although Ballard did not report the proprietary electrode composition, it was understood that electrodes used for this project were made of finely divided metal particles, "platinum black" and, possibly, alloys of this material, using a loading of 4 mg Pt/cm$^2$, a high catalyst loading by contemporary standards. However, there was no emphasis during Phase I of this project to develop a lower cost fuel cell stack for Phase I of this project. Rather, the intent was to focus on initial system integration issues that were not sensitive to catalyst loading.

During the course of the program, six Ballard PEM stacks were delivered for testing. Considerable technical evolution in the form of improved performance occurred during the program duration. Stacks were composed of standard Mark V (Ballard) 0.25 ft$^2$ active area cells using 35 cells/stack. Ballard hardware includes interlaced cooling plates positioned so that one cooling plate cools two cells. The stack includes a series of membrane humidifiers, positioned between one of the end plates and the active electrochemical cells. The active stack section includes two metallic current take off plates. One end plate is fitted with an hydraulic ram that works to exert forces to minimize intercell resistance. The other end plate serves as the fluid connection manifold. The manifold has six connections, fuel (hydrogen or reformate) inlet and exhaust, oxidant (air) inlet and exhaust, and cooling water in and out. The single water feed provides water both to the humidification section and the active cooling plates. The stacks are formed using a so-called "filter press" configuration.

## 4.3 FUEL CELL STACK DEVELOPMENT AND TESTING

### 4.3.1 Introduction and Summary

In earlier DoE Electric Vehicle Programs, extensive work has been conducted to develop suitable, reliable protocols for battery testing. These testing procedures were thoroughly reviewed and some elements were adapted during the development of

stack testing protocols. Fuel cell stack testing, however, involves test parameters in addition to voltage and current measurements. Basically, these added parameters include mass and thermal transport, such as the mass flow of reactant and product chemical species and heat flow within the stack. Because of the operating conditions, water, a product of the electrochemical process, is both in the gaseous (steam) and liquid state. Prompt water removal is a function of fluid dynamics within the stack envelope. Moreover, Ballard hardware utilizes liquid water for both humidification and cooling. Special test features are required to distinguish the proportion of the flow used for each function.

Task 3 activities at the JDC concentrated on performance and reliability testing of the Ballard fuel cell stack. Detailed stack testing was designed to determine the optimum conditions for operation of contemporary stacks utilizing both hydrogen/air and reformate/air reactants. As might be expected, performance as a function of operating conditions was somewhat different for the four early stacks as compared to the later two improved stacks. A considerable amount of effort, similar to the reference cell tests, was devoted to reformate/air operation to overcome performance degradation following $CO_2$ feed to the anode compartment. The addition of a small quantity of air to the anode stream was one successful method of removing this degradation, particularly when anode alloy catalyst mixtures were utilized. However, as air injection into the anode under inappropriate operating conditions can be detrimental, work on even more improved anode catalysts, which may result in the elimination of any necessity for air injection into the anode compartment, remains of interest. Successful catalyst-only operation with reformate-air has been reported on small reference cells; to date, operation without anode air injection on stacks has not been successful.

An advanced test stand was constructed to perform the detailed stack testing; areas of investigation included:

- stack repeatability determinations – hydrogen/air reactants
- effect of test conditions – hydrogen/air reactants
- effect of flow rate on cell-to-cell reproducibility – hydrogen/air reactants
- effect of stack temperature on performance – hydrogen/air reactants
- effect of cathode conditions on performance – hydrogen/air reactants
- the use of synthetic reformate and its subsequent effect on performance, stack repeatability measurements, test conditions, cell-to-cell reproducibility, and anode conditions on performance
- consideration of stack start-up transients

This section describes the test results measured under the above conditions and presents some significant results attained during Phase I.

### 4.3.2 Stack Test Stand Description

A unique test stand was fabricated to facilitate PEM stack tests. The schematic of this device is presented as Figure 4.3.2-1. This test stand meters gases, shown on the upper right hand figure, from on-site supplies. Hydrogen is supplied from 50,000 scf tube trailers at 99.9% purity. Carbon dioxide (99.9%) is stored as a liquid; vaporized $CO_2$ is fed to the test stand. Oxygen (99.9%) is also available from a 50,000 scf tube trailer as is air ("breathing air" grade) or nitrogen (99.9%). (Custom blending oxygen with nitrogen can prepare a synthetic air mixture with different

oxygen content, a technique useful for specific stack performance tests.) Alternatively, air is generally supplied from an on-site oil-free air compressor. The test bench includes MFCs (used as mass flow meters (MFMs) for hydrogen and air) for each of the four feed streams. Gases are fed into the fuel cell stack at rates controlled by the electrochemical current and by the setting of valves in the anode and cathode vent streams. The (air) cathode exhaust exits through the wall of the laboratory while the (hydrogen) anode exhaust stream exhausts through a tall, hydrogen-venting pipe. Test pressures are separately controlled for the anode and cathode sides.

The water flow path is depicted in the lower left hand side of the figure. Water is transferred through the stack using a vaned pump that drives water through a stainless-steel cross flow heat exchanger and then through the stack. This circuit also includes a set of ion exchange filters that continuously "polish" the water to maintain high resistivity (> $10^6$ ohm). In the Ballard stacks, cooling water is lost during stack circulation because of the feed to the membrane humidification section; as a consequence the water inventory must be continuously replenished. This is accomplished by controlling the water level in a "make up tank". Total "make up" water is recorded; this corresponds on average to the amount of water added to humidify the incoming reactant gases.

The stack exhausts water from both the anode and cathode compartments. Water is primarily produced in the cathode portion of the stack; some excess water can be detected in the anode compartments due to back diffusion from the cathode. Under such conditions the osmotic water transport appears to be negligible and a considerable portion of the anode humidification can pass through the anode. Water production or accumulation rates are determined using the same measurement strategy. The anode and cathode exhausts are individually cooled to 10°C, a temperature at which essentially all of the water exists in the liquid form. The water then collects in "condensers," which, when full, automatically empty. Each dump cycle involves a specific water quantity; total water quantities are that quantity times the number of cycles.

Electrical output from the stack, typically as high as 250 amps at 20 volts (5-kW) is fed directly to a Curtis pulse width modulator (PWM) , a unit designed for electric vehicle use. The load current is controlled by the pulse width, a parameter which is easily set through computer control. Electrical output from the PWM is released directly into a section of water-cooled stainless steel tubing. Measurement of the flow through the tubing and the temperature increase permits an independent assessment of the power level. Power is, however, primarily measured through use of an integrating power meter along the transfer line from the stack to the PWM. Refer to Section 7.2.2 for a detailed discussion of the PWM and true power output measurements.

This test stand, detailing PEM stack evaluation, has performed well for several years. Hydrogen testing requires certain safety concerns. Both internal "leaks" within the fuel cell stack and external "leaks" require continual management. The test computer is utilized as the locus of the safety controls for all of the experiments. Prior to any test procedure start-up careful flow measurements are performed between the various flow paths (anode-to-cathode, anode-to-water, etc.); experimental tests are then initiated only if internal leak rates are at safe, low levels. Once testing is initiated, the most critical leakage path is anode-to-cathode, through an un

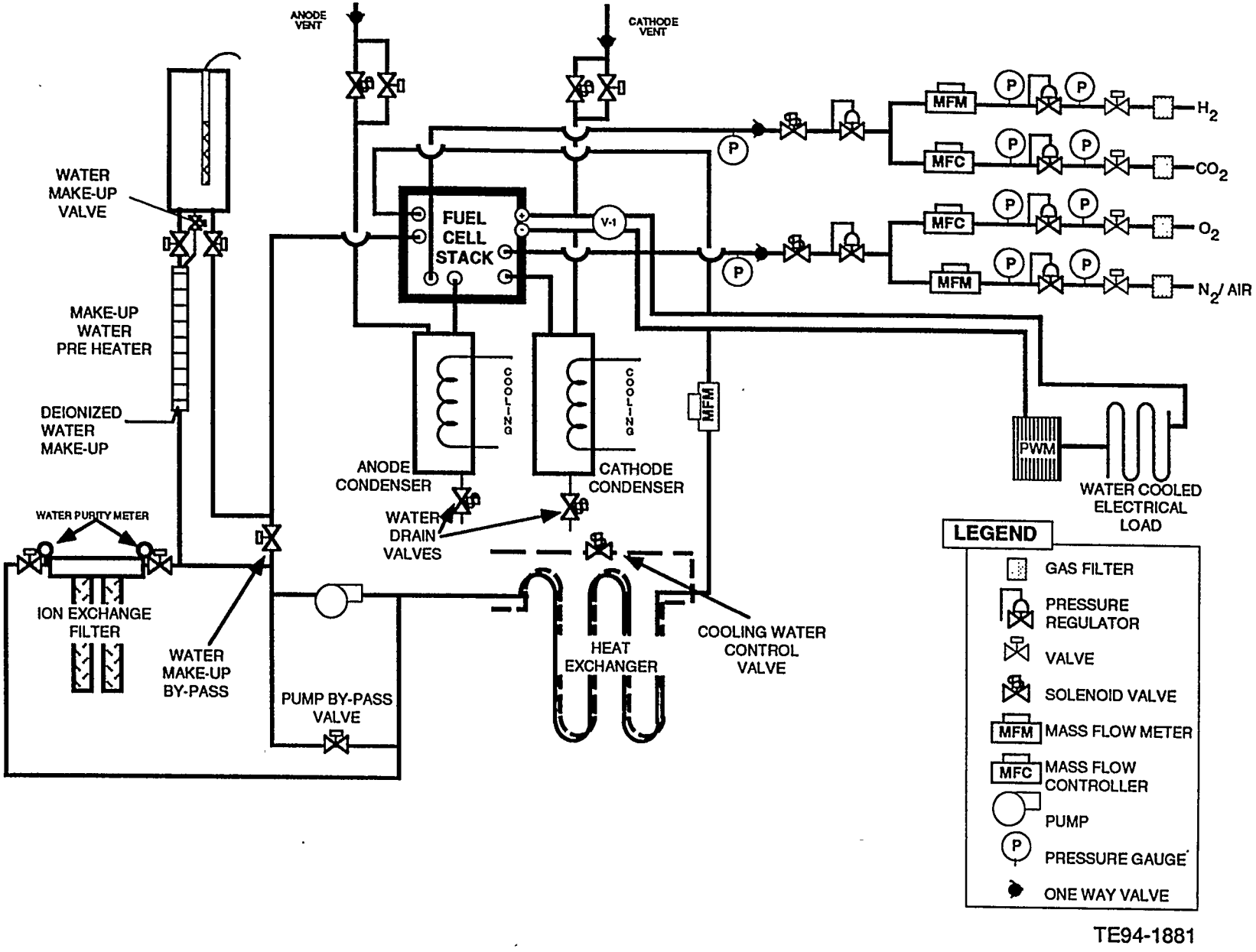


Figure 4.3.2-1. Simplified schematic of the fuel cell stack test stand. The functions of the various components are discussed in some detail in the text.

planned leak in any one of the many membrane sheets. Such a leak is detectable by a low single cell voltage, a condition that is readily monitored. (If such a condition occurs hydrogen is chemically combusted, rather than electrochemically consumed and the bad cell produces a low voltage output.) The computer continuously measures each single cell and notifies the operator of any specific cell voltage loss performance. (A severe voltage loss results in automatic test shutdown.) The test stand is fitted with hydrogen sensors to detect any overboard leak. Again, the data system continuously monitors hydrogen concentration levels, gives a warning when hydrogen is first detected at serious concentration levels, and terminates the hydrogen flow to the test laboratory if a dangerous level of hydrogen is measured. The termination level has been set at 25% of the LEL value for hydrogen/air mixtures.

The following parameters are controlled during all stack tests:

- ***Stack temperature*** - The cooling water flow in the "cold" heat exchanger flow is automatically controlled to sustain a set temperature in the cooling loop and, hence, in the stack. Stack temperature is normally measured as the temperature of the cathode exhaust; this temperature has been found to be numerically similar to the temperature of the cooling water exhaust. Under most energetic conditions, the stack coolant picks up about 10°C during traverse through the system. Consequently that type of temperature gradient exists within the stack.

- ***Current level*** - Most electrical power control tests are completed by setting the current through variation of the PWM. Voltage levels are then recorded at that current. Because stack cooling is limited by design, sustained high current operation can result in some expected stress on the stack. Ballard recommended that sustained upper current levels of 1,000 amps/ft$^2$ not be exceeded during program tests. Because the stack is 0.25 ft$^2$ in active area, sustained currents were, therefore, always approximately ≤250 amps. The Ballard stacks can clearly operate at higher currents than this, i.e., up to 1300-1500 amps/ft$^2$ at 0.5 V, depending on the reactants utilized; but Ballard places a ten to fifteen minute test duration on the stacks at these higher power levels.

- ***Gas composition*** - As described above, both the anode and cathode feeds can be varied. Hydrogen or hydrogen-carbon dioxide mixtures compose the anode feed mixtures. Binary mixtures of nitrogen and oxygen or pure air serve as the cathode feed. During these tests there was no provision to assess internal humidification levels. In general, it was assumed that the multi-membrane type humidification system should reach nearly 100% relative humidity, therefore providing that level of humidification to the active membranes in each cell through the manifolding system.

- ***Gas dynamics*** - As described above, both the feed flow rate and the feed pressures are set independently. Fuel cell test results are dependent on flow rates (refer to discussions later in this section), in part by the effect of higher flow rates on liquid water removal. Flow rates in these studies are stated, as is the case in most fuel cell literature, in terms of stoichiometry. Because of the gaseous mixtures, the stoichiometry levels are calculated only on the quantity of reactant. For example, an air "cathode stoichiometry of 2.0 in. delivers twice the quantity of oxygen needed for the specified current level.

Likewise an anode synthetic reformate stoichiometry of 1.5 delivers a gas stream with 1.5 times the quantity of hydrogen and 25% of that flow volume of carbon dioxide. However, even a small quantity of carbon dioxide can drastically alter the fluid dynamics of the anode feed compartment; for example, 25% mole fraction of carbon dioxide (having a molecular weight of 44) alters the gas density significantly compared to a 100% mole fraction hydrogen flow (hydrogen having a molecular weight of only 2). The standard test procedure used in the measurements described in the following sections measured performance under "constant stoichiometry" conditions rather than "constant flow" conditions. Constant stoichiometry at each point on the polarization curve requires continuous adjustment of gas flows as current levels are varied. Pressure is controlled by simultaneous adjustment of the pressure regulators and valves.

### 4.3.3 Stack Test Results

The intent of the stack tests conducted during the program were to confirm modeling parameters and to determine appropriate operational parameters and conditions for stack integration into the ECE. Duration testing was not a goal, nor was there any emphasis to achieve higher power levels than those attained at 1000 amps/ft$^2$. Working with Ballard personnel, the following "ground rules" were established: stack temperature should always be less than 95°C; maximum stack pressure should be 50 psig; and differential pressure, between anode and cathode, should not exceed 30 psig. In addition, cooling water flow was controlled so that a $\Delta$T across the stack of 10°C was not exceeded. Individual cell voltages were carefully monitored and the stack was never to operate with any single cell below 0 volts; cell reversal can result in early cell failure.

Many hundreds of hours of test data were attained during the program, and only a small fraction of that total test data is presented here. The results below are presented as a representative summary.

#### *Stack Repeatability*

Some of the first stack tests explored the voltage stability in Ballard fuel cell stack hardware. Tests were performed using hydrogen/air reactants under a series of test conditions. Test results for both Stack SN-110 and SN-111, two of the initial stacks delivered early in the program, are presented in Figure 4.3.3-1. These polarization performance tests were repeated over a month's time during March, 1992. The initial experiments were conducted at 30 psig, repeating test data attained at Ballard. However, subsequent tests were conducted at pressures elevated to 33 psig to correct the high-altitude Los Alamos test conditions to the sea level conditions of Vancouver. As depicted, test data were reproducible and stable, a typical condition present throughout the nearly two years of testing.

#### *Test Condition Effects*

The initial tests were conducted using stack operating conditions specified by Ballard. With Ballard's concurrence, these conditions were varied systematically to determine the best performance for Stack SN-111; the resulting polarization performances (average cell voltage as a function of current density) are presented, for

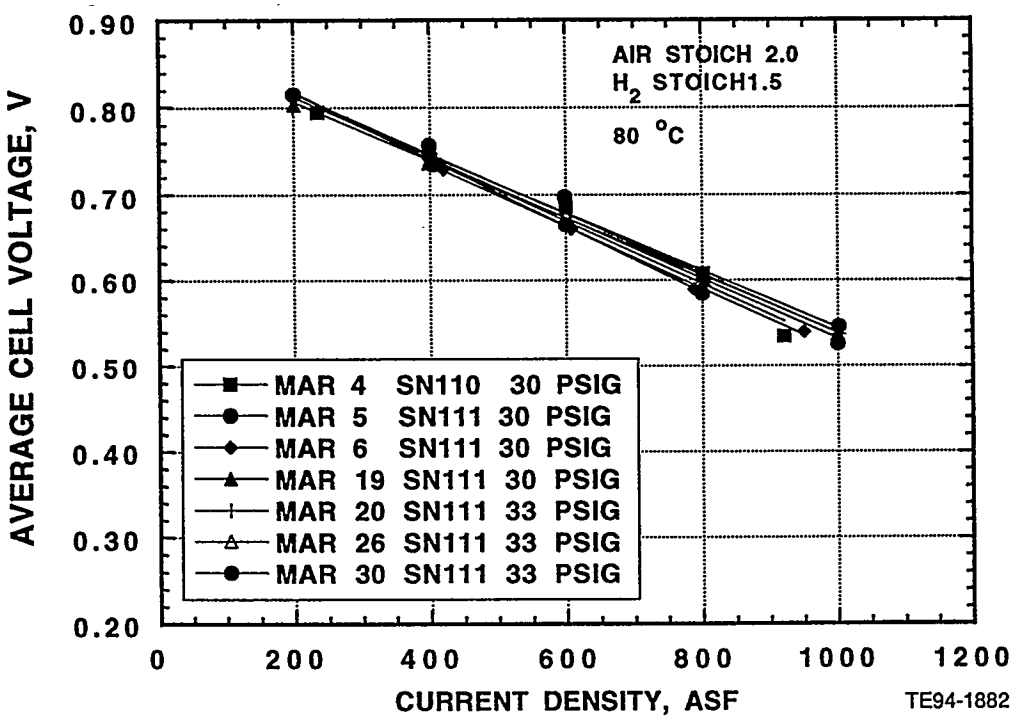


Figure 4.3.3-1. Performance polarization curves using hydrogen/air reactants for 2 Ballard prototype stacks, demonstrating reproducible, stable performance over a month of testing. The increase in cathode pressure from 30 to 33 psig compensated for the high-altitude Los Alamos test conditions to allow reproduction of the sea-level test conditions at Ballard.

two different operating conditions, in Figure 4.3.3-2. The lower curve depicts results for the test conditions suggested by Ballard while the upper curve, the JDC operating point, depicts results when temperature, cathode pressure and stoichiometry are elevated. Both of these polarization curves represent stable, reproducible conditions. All of these initial tests were conducted using hydrogen/air reactants to establish baseline data prior to reformate/air testing. All of the Ballard stacks were first subjected to hydrogen/air testing; polarization performance results attained in 1993 for an improved Ballard Stack, SN-212, are presented in Figure 4.3.3-3. This stack incorporates improved flow fields, manifolding, and thermal management, combined with improved electrode designs (Pt-alloy anode catalysts for CO and $CO_2$ tolerance) and other strategies for water removal. Operating conditions used to attain the polarization curve presented in Figure 4.3.3-3 are essentially the same as those used to attain the upper polarization curve of Ballard Stack SN-111 (an early prototype) in Figure 4.3.3-2. These operating conditions are designated as the JDC operating point; the hydrogen pressure utilized to obtain the data presented in Figure 4.3.3-3 is slightly greater (33 psig) than that utilized (20 psig) to generate the polarization curve presented in Figure 4.3.3-2. This slight increase in hydrogen pressure did not affect the polarization curve for Stack SN-212; a $H_2$ pressure of 33 psig was used to permit a direct comparison with reformate/air data on this stack as the fuel processor used to generate reformate normally is set to operate at 33 psig. Comparison of the polarization curve of Stack SN-212 with the best polarization curve attained using Stack SN-111 indicates that SN-212's performance in-

cludes a 40-50 mV increase in voltage at the 1000 amps/ft² level. Stack 212's level of performance on hydrogen-air reactants is exceptional; it is only about 50-60 mV below most of the better reference cell data at the same current density. The performance of this and other improved stacks have been remarkably stable over more than a year of operation.

### *Effect of Flow Rate on Cell-to-Cell Reproducibility*

Stack performance maps represent considerable data and the exact format to best depict that data, indeed the criteria for "best" performance, is still poorly defined. Stack voltage, either as the bus bar voltage or as an "average cell voltage" (bus bar voltage divided by cell count) can also be misleading because only a few single cells with diminished performance can quickly lower such an average. The data system developed to help determine stack performance measures all cells during a stack test; typical data for Ballard SN-111, for example, are presented in Figures 4.3.3-4 and 4.3.3-5. All of the average cell voltages and the standard deviation around the stack "average cell voltage" attained at an air stoichiometry of 2 (all data was taken under "constant stoichiometry" conditions) are presented in Figure 4.3.3-4. Cell number describes location in the stack, with cell 1 adjacent to the humidification section, farthest from the "front" manifold end plate. As depicted in the figure, cell 1 is producing only about 95 mV. Cells 29 and 35 are also significantly poor performers. All of these data were measured at the maximum current level, a con

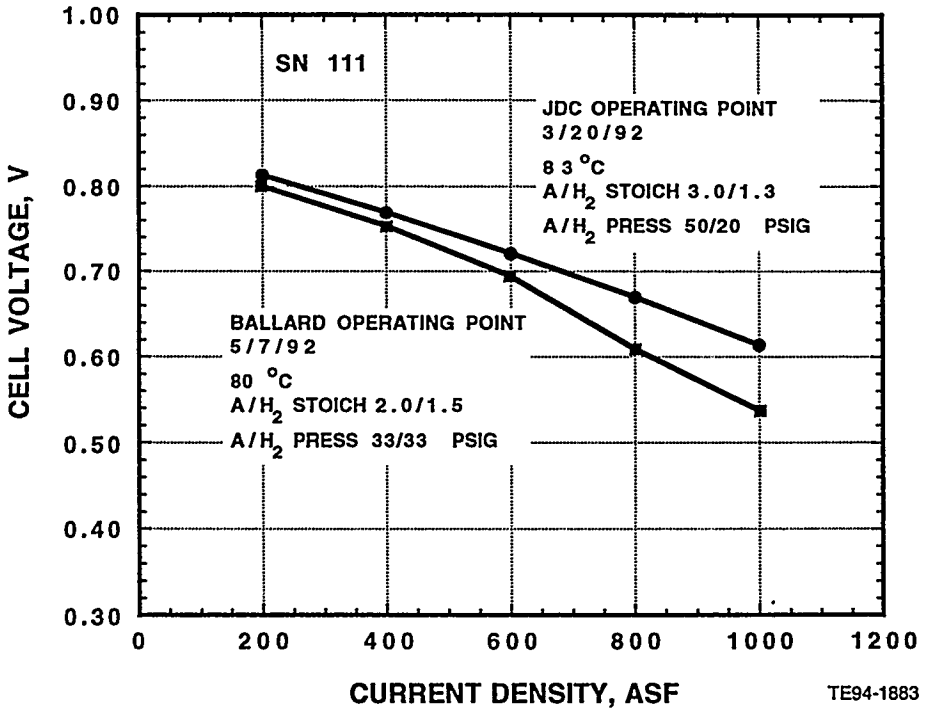


Figure 4.3.3-2. Performance polarization curves using hydrogen/air reactants for a Ballard prototype stack at two test conditions. The lower curve corresponds to test conditions used by Ballard, while the upper curve represents the JDC conditions derived from systematic testing of the stack with stoichiometry and pressure varied to achieve optimum stack performance.

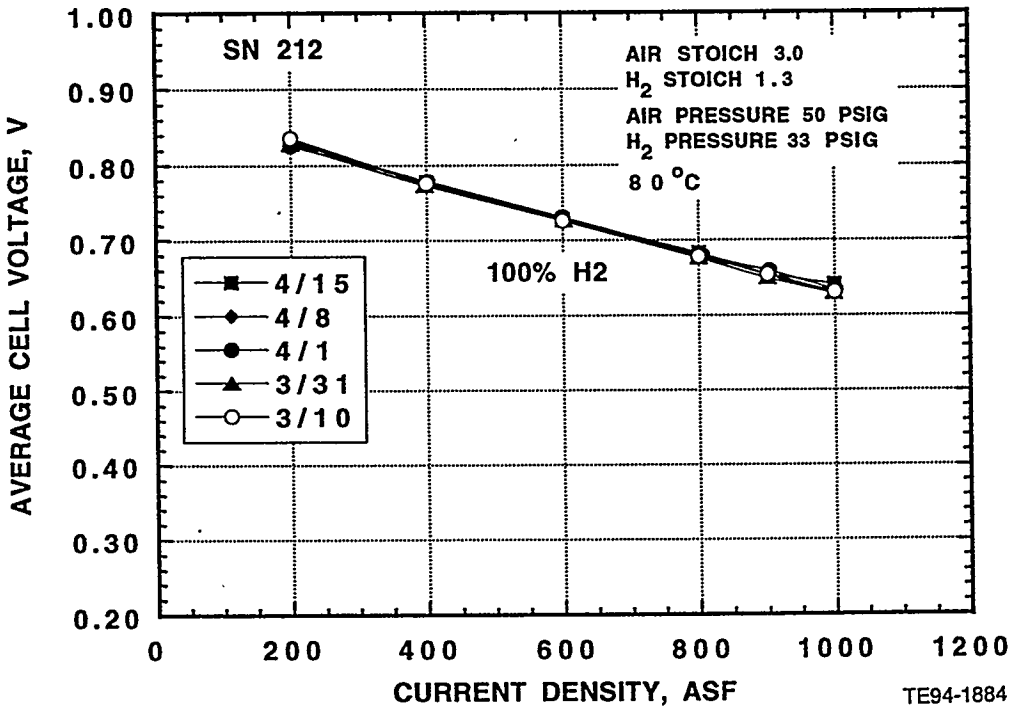


Figure 4.3.3-3. Performance polarization using hydrogen/air reactants for a Ballard improved stack. Tests were conducted at the JDC operating conditions (with slightly elevated anode pressure) to achieve optimum stack performance.

dition that emphasizes such single cell variation. Identical type data, attained using a cathode flow rate increased to a stoichiometry of three is presented in Figure 4.2.3-4. Cell 1 now has increased voltage performance (to 440 mV) while the other previously poorly performing cells deliver voltage levels indistinguishable from their neighbors. The power output level from the stack also increased from 4.57-kW to 5.37-kW with increased cathode flow being the only change in operating condition. These data are typical for a cathode flooding condition and suggest that wet proofing in this early Ballard stack was not optimized. These data also suggest that flow variations, keeping all other parameters constant, can be useful to determine parameters that have major effects on performance.

### *Effect of Stack Temperature on Hydrogen/Air Performance*

A series of average cell voltages at several different current density levels, all as a function of cathode outlet temperature, is presented in Figure 4.3.3-6. These data were attained under constant hydrogen and air stoichiometry. The highest current density set is truncated because the stack is inoperable, under the test boundary conditions, at high current and low temperature; almost all of the cells tend to flood and enter regimes of voltage reversal under such operating conditions. Voltage performance, as depicted on the figure, is surprisingly insensitive to temperature. At lower current densities, there is a small voltage gain. However, at 250 amps (1,000 amps/ft$^2$) the data actually depict a slight voltage sag as cell temperature is increased past 85°C. The 200 amp (800 amps/ft$^2$) data, however, does demonstrate a sharp increase with temperature. These temperature data cannot be very definitive;

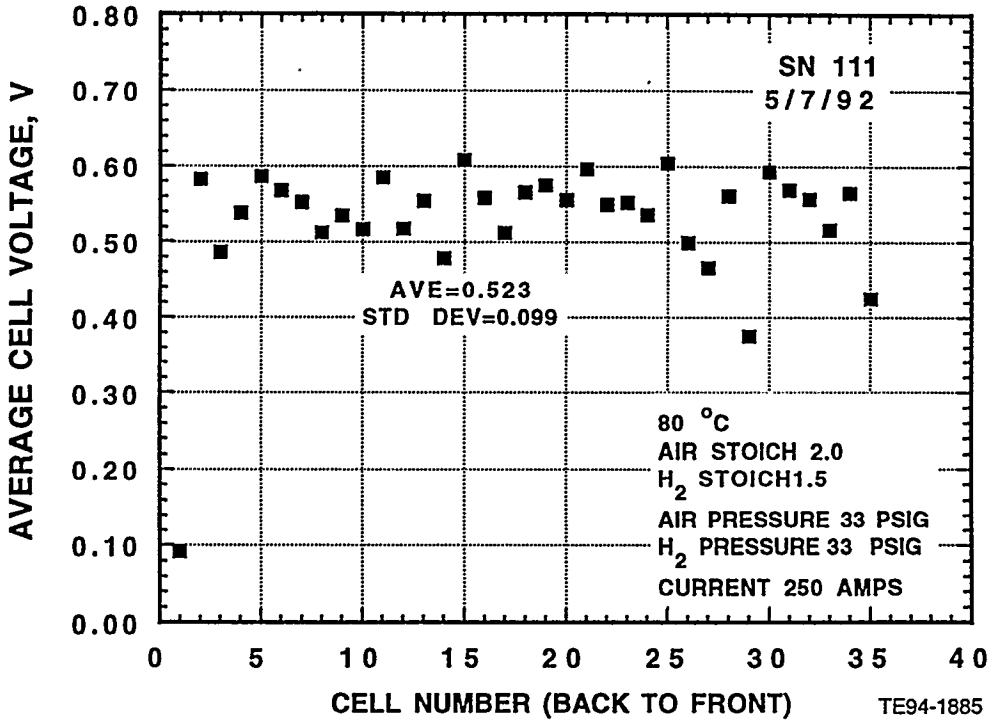


Figure 4.3.3-4. Average Cell Voltage Data and Voltage Standard Deviation About the Average Demonstrate the Variation in Cell-To-Cell Voltages Measured in a Ballard Power System Prototype Stack as a Function of the Ballard Operating Point Conditions Presented Earlier in Figure 4.3.3-2. Cell 1, the poorest performer, is adjacent to the humidifier section and may be experiencing cathode "flooding."

increasing the cathode flow, for example, can produce some trend effects since water dynamics, the process of product removal, changes with both cathode flow and stack temperature. Water removal alone most likely dominates "electrochemical" variations. In any event cell temperatures above 83°C, regardless of current density level or reactant type, produced negligible increases in cell voltage output.

### *Effect of Cathode Conditions on Hydrogen/Air Performance*

A series of test data attained under identical conditions of temperature (80°C) at the highest current density (250 amp) presenting average cell voltage as a function of cathode pressure variation appears in Figure 4.2.3-7. These data indicate very poor performance with air pressures below 25 psig; above that pressure the voltage increases nearly linearly (50 mV) to 40 psig. Above 40-45 psig the cell voltage is not a significant function of pressure. These data were determined with an early Ballard Stack, version SN-111. The increase in voltage as a function of increasing the cathode flow stoichiometry is presented in Figure 4.3.3-8; results are for the same stack. Although the results show continuous cell voltage improvement, with increasing cathode flow stoichiometry, most of the improvement is apparent well before a cathode stoichiometry of 2.0. The principal effect of increasing the cathode stoichiometry is to increase the performance of poorly performing cells, thus raising the overall stack average cell voltage. Cells performing well are only slightly affected by increasing the cathode stoichiometry above 2.0.

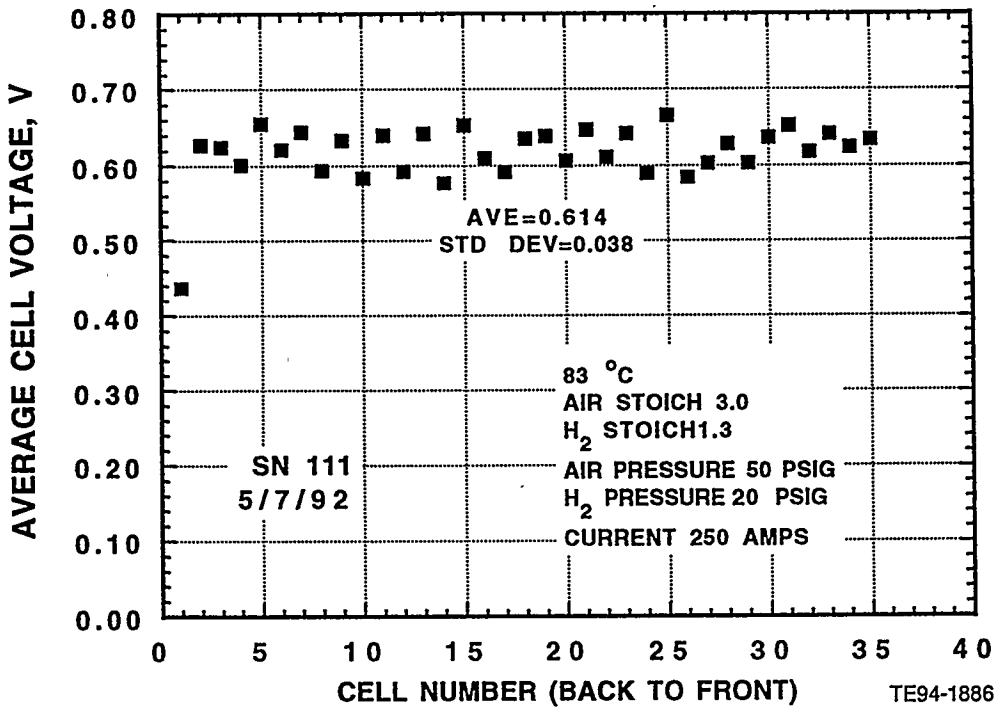


Figure 4.3.3-5. Average Cell Voltage Data and Voltage Standard Deviation about the Average Demonstrate the Variation in Cell-to-Cell Voltages Measured in a Ballard Power System Prototype Stack as a Function of the JDC Operating Point Conditions Presented Earlier in Figure 4.3.3-2. Note that the higher performance at the JDC Operating Point" (50 psig cathode) is due to both a higher average cell voltage and a smaller cell-to-cell deviation. Cell 1, the poorest performer, is adjacent to the humidifier section and may still be experiencing cathode "flooding" at the higher cathode stoichiometry.

Ballard's improved stacks such as SN-212 demonstrated far less voltage dependence on pressure and air flow variations. For example, cathode air pressure was varied from 21 to 50 psig at several different air flow conditions while the average cell voltage of Stack SN-212 was being measured, Figure 4.3.3-9. While the cell voltage does increase up to about a cathode air pressure of 40-45 psig, the lower pressures do not produce drastic reductions in average cell voltage. In fact, there is probably no increase in system efficiency if this stack is operated above 35 psig cathode pressure. In general, increasing cathode air flow leads to a stack performance increase; again, however, there is little cell voltage increase at cathode stoichiometry flows in excess of 2.5.

### *Effect of Anode Conditions on Hydrogen/Air Performance*

Similar stack anode flow and pressure variations were conducted to determine optimum anode feed conditions to both the prototype and improved Ballard stacks. Average cell voltage as a function of anode pressure variation is presented in Figure 4.3.3-10. Results for two different stacks, SN-111 and SN-212 are depicted. Both stacks demonstrate an initial increase with increasing anode pressure, although both stacks operate surprisingly well at low pressures.

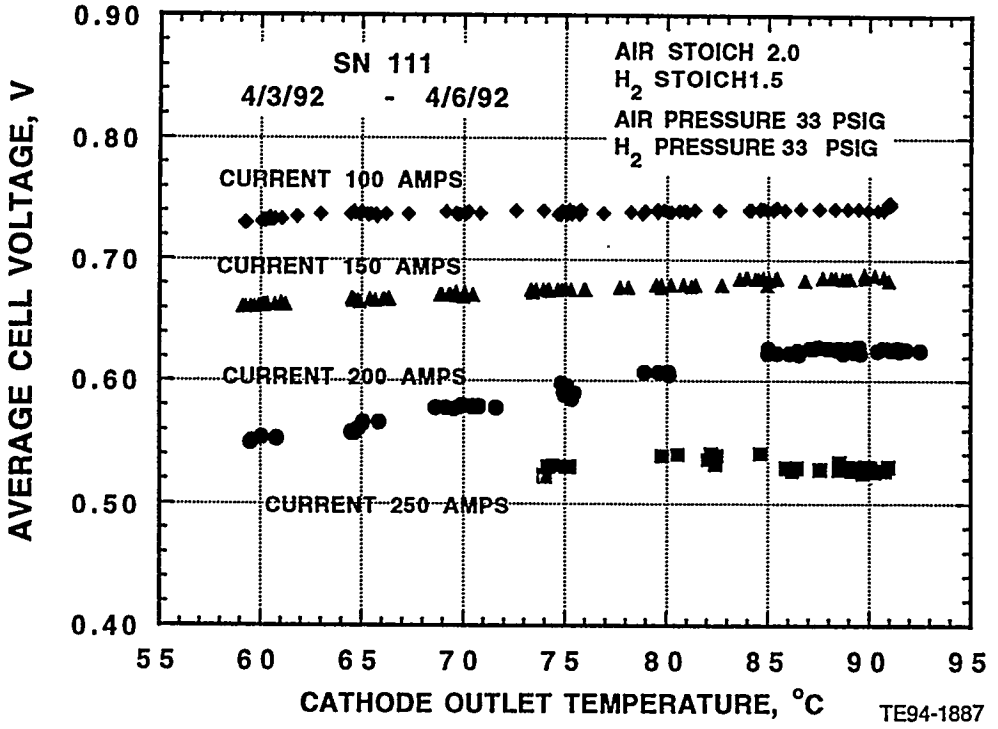


Figure 4.3.3-6. Test data for a Ballard prototype stack demonstrating the effect of stack temperature on hydrogen/air performance. Here, stack temperature is represented by the measured cathode outlet temperature. Voltage performance is surprisingly insensitive to temperature.

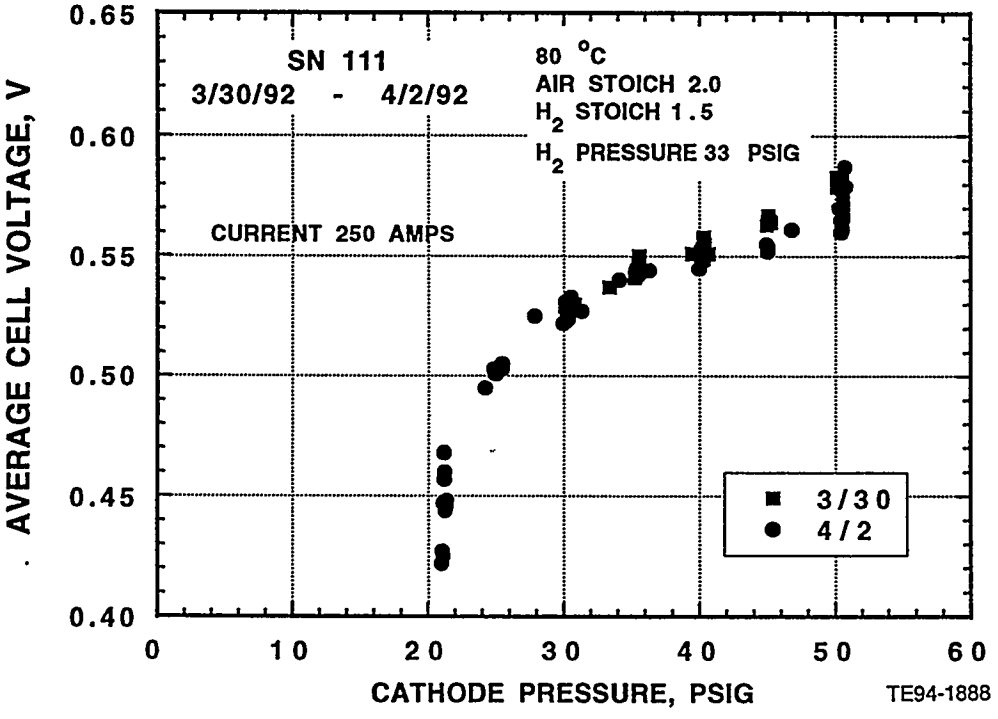


Figure 4.3.3-7. Test data for a Ballard prototype stack demonstrating the effect of cathode pressure on hydrogen/air performance. Average cell voltage is very dependent on cathode pressure up to about 40 psig.

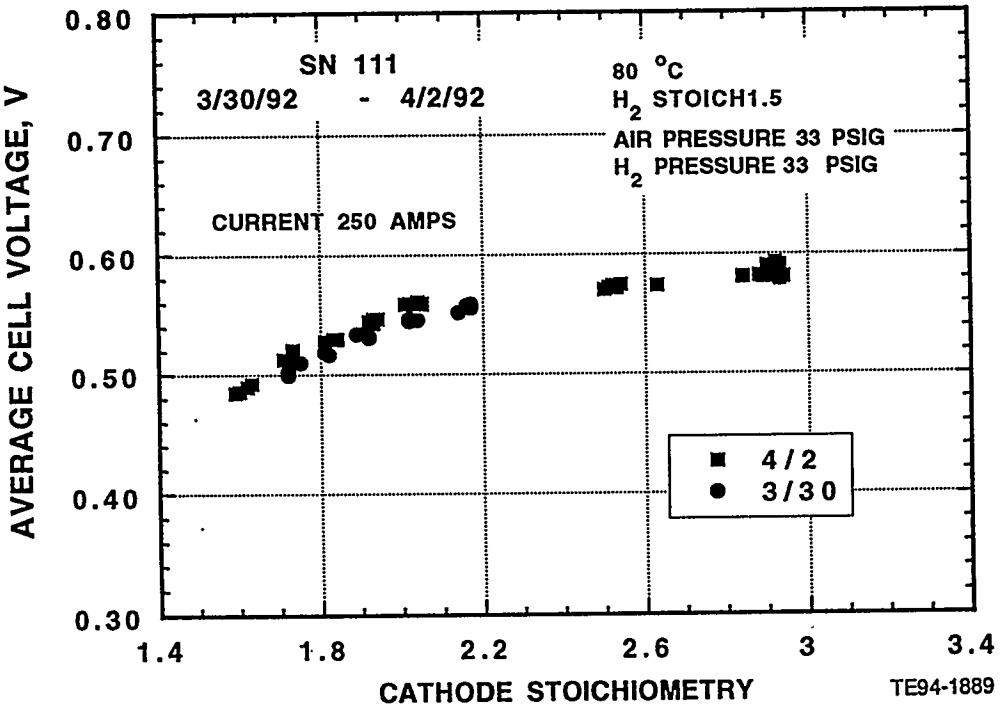


Figure 4.3.3-8. Test data for a Ballard prototype stack demonstrating the effect of cathode stoichiometry on hydrogen/air performance. Most of the cell voltage performance improvement occurs before cathode stoichiometry attains a value of 2.0.

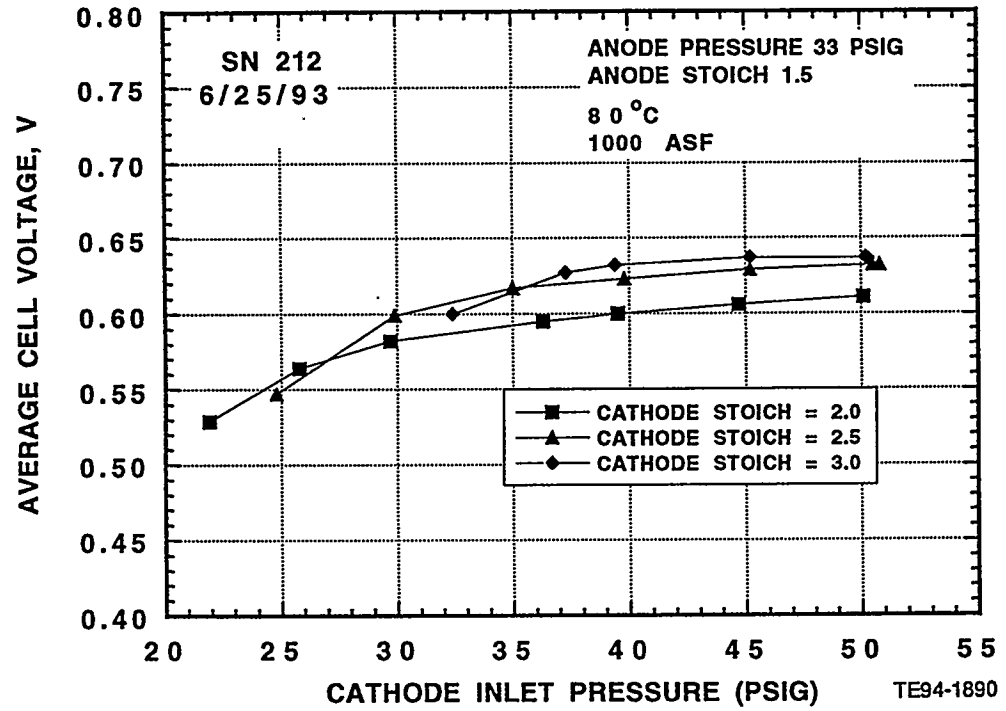


Figure 4.3.3-9. Test data for a Ballard improved stack demonstrating the effects of cathode pressure and stoichiometry on hydrogen/air performance. Note the effects, particularly of cathode pressure, on average cell voltage are much less than those measured on the early "prototype" stack (see Figures 4.3.3-7 and 4.3.3-8).

SN-111 results indicate only modest initial anode voltage improvement with increasing anode pressure and actually appears to develop a voltage sag above 25 psig. The more advanced test hardware, SN-212, demonstrated only a modest cell voltage gain above 15 psig; this data suggests that this PEM stack can operate successfully over a wide range of anode pressures. Further, increasing the cathode air stoichiometry, while increasing the overall stack performance, had no effect on the observed stack voltage trend with increasing anode pressure.

Average cell voltage as a function of anode flow stoichiometry is presented in Figure 4.3.3-11. Again, results for both Stack SN-111 and SN-212 are depicted. Stack 111 test results indicated an increase in cell voltage with increasing anode flow up to an anode stoichiometry of about 1.18. Above that stoichiometry cell voltage, within Stack 111, is relatively independent of anode flow. Stack 212 results are nearly completely independent of anode stoichiometry.

### *Effects of Synthetic Reformate on Stack Performance*

Following the hydrogen-air experiments these stacks were evaluated under ECE conditions by substituting a mixture of 75% hydrogen and 25% carbon dioxide in place of pure hydrogen for the anode flow. This gas mixture, chosen to replicate that coming from a methanol reformer, is known as "reformate." Literature values on reformate-air usage as fuel cell reactants are inconclusive, but there is some information that carbon dioxide, at least on some anode electrode systems, causes appreciable cell voltage loss. This was the observed result when the first experiments were conducted on Ballard Stack SN-110.

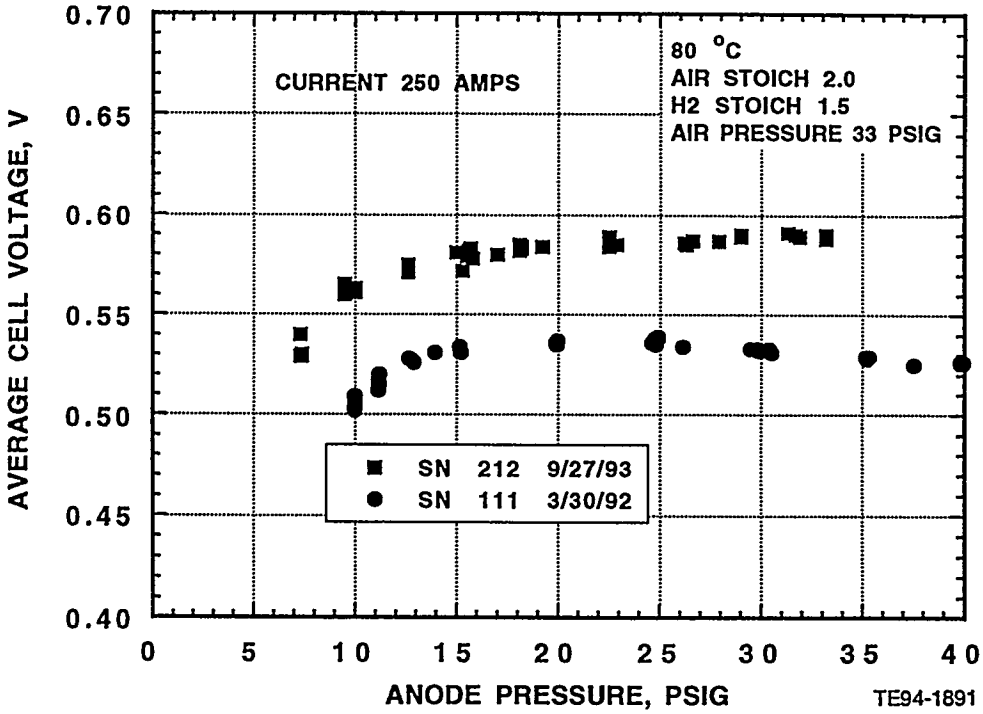


Figure 4.3.3-10. Test data for a Ballard prototype stack (SN-111) and an improved stack (SN-212) demonstrating the effect of anode pressure on hydrogen/air performance.

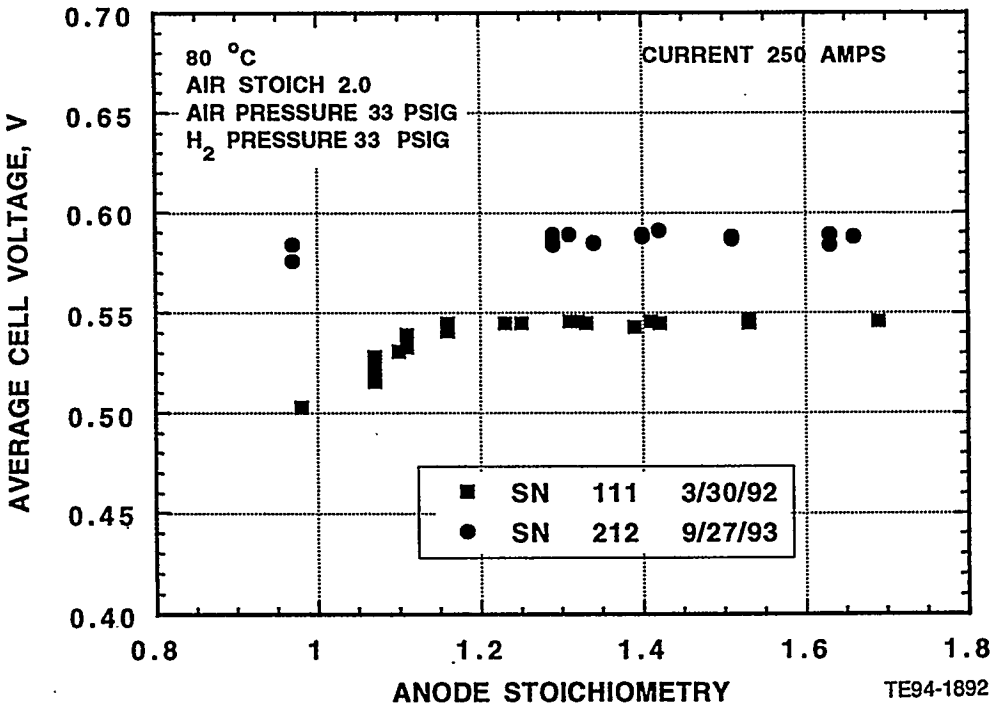


Figure 4.3.3-11. Test data for a Ballard prototype stack (SN-111) and an improved stack (SN-212) demonstrating the effect of anode stoichiometry on hydrogen/air performance. Average cell voltage of the improved stack is nearly independent of anode stoichiometry.

Test data, average cell voltage as a function of current density, for this stack are summarized in Figure 4.3.3-12. The 100% hydrogen trace is typical performance for this prototype stack. However, when 25% $CO_2$ was added to the anode feed severe voltage loss resulted at the higher current densities. Average cell voltage fell 300 mV at the highest current density, a 50% power loss.

One early explanation for this performance loss was the possibility of CO in the anode feed. Certainly, small quantities of CO are a common contaminant in commercial carbon dioxide. However, when the $CO_2$ was mixed with hydrogen to form reformate, the inlet CO concentration of this reformate was generally less than 1 ppm. Moreover these experimental results did not correlate with the known results of CO contamination. Carbon monoxide is an effective, rapid anode poison. The "$CO_2$ derived" performance loss was not visible at first, and unless considerable time was taken to complete a polarization curve, the performance loss was easily missed. Acceptable voltage levels were first observed, then the entire stack voltage decreased during the next 10-30 minutes. In fact, the results presented in Figure 4.3.3-12 are for $CO_2$ "stabilized data," that is, the voltage measurements were attained 20 minutes after any parameter change. Moreover, a CO-poisoned stack rapidly recovers when pure hydrogen is introduced. Recovery in pure hydrogen following $CO_2$ usage was far less rapid.

Basically there are three, somewhat parallel mechanisms proposed to explain the $CO_2$ performance degradation.

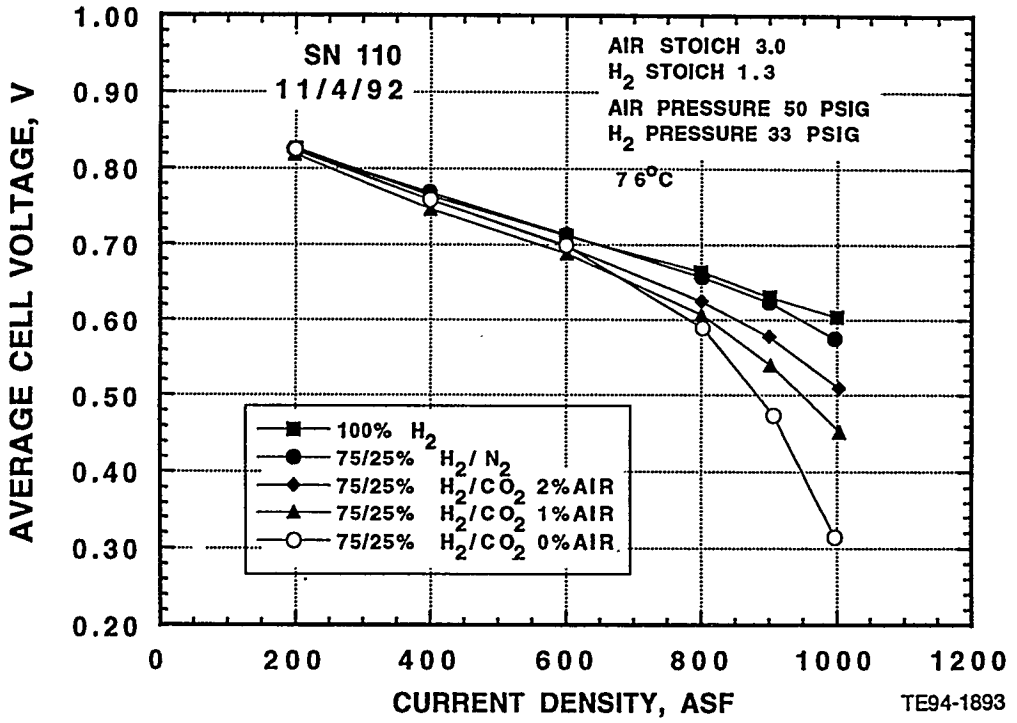


Figure 4.3.3-12. Test data for a prototype stack demonstrating the effect of anode gas composition on stack performance. The mixture of 75% hydrogen and 25% carbon dioxide represents synthetic reformate, ("reformate" is the term given to the gas stream exiting the methanol fuel processor). The 75% $H_2$/25% $N_2$ test separates the diluent effect using an inert gas. See the accompanying text for a discussion of anode air injection.

- ***Fluid dynamics that result from $CO_2$ addition and $CO_2$ chemical effects that influence transport:*** Carbon dioxide blocks access through the porous electrocatalytic layer, limiting access of hydrogen to the catalyst sites. This "pore blocking" may not be well predicted by nitrogen results because of higher water content (a saturated reformate flow carries more water than a saturated hydrogen flow with the same stoichiometry) and carbon dioxide-water solubility in the layer network. Other mass transfer factors may be important as well. For example, carbon dioxide may react with ion exchange sites, especially those in the anode catalytic structure, to decrease protonic mobility. Conversely, when carbon dioxide is in the gas stream, the higher gas momentum may remove liquid water at higher rates, resulting in dehydration and lesser ionic conductivity. Alternatively, carbon dioxide may cross the membrane and cause flooding on the cathode.

- ***Carbon dioxide adsorption*** - Carbon dioxide is thought to interact with H on platinum in the potential region of interest. This adsorption is not quantitative; probably due to fast turnover rates hydrogen still has access to sites. However, after some time, the adsorbed $CO_2$, reacting on the hydrogen-covered platinum surface, is converted to another reduced species:

$$Pt + CO_2 = Pt{\cdot}CO\ OH$$

$$Pt{\cdot}CO\ OH + H_{ad} = PtCOH + H_2O$$

The COH species is formed slowly but desorption is also slow. A steady but thorough titration of platinum sites occurs, removing some fraction from participation in hydrogen oxidation. However, not all sites are blocked, even after some equilibrium is attained the fuel cell continues to perform.

- ***Carbon monoxide contamination*** - Carbon monoxide, even though it is effectively not present in the anode feed, could be slowly synthesized through the reverse shift reaction, the result of a chemical reduction of $CO_2$, and eventually reach sufficient concentration to poison the platinum sites. Obviously none of these performance loss mechanisms are mutually exclusive and several could be operative.

  Stack performance data indicate carbon dioxide in the anode feed compromises fuel cell stack performance, especially at high current densities. The slow degradation kinetics are quite dissimilar to what is found with carbon monoxide on platinum electrodes. Therefore, explanations other than carbon monoxide effects are more plausible, especially since repeated attempts to discern CO in the anode exhaust were unsuccessful. At these low temperatures the rate of the reverse shift reaction is apparently too slow to produce significant carbon monoxide to exit in the exhaust stream. However, the presence of high current density hydrogen oxidation could alter such rates, and sufficient CO may be formed to aid in the formation of the COH species absorbed on the Pt. The presence of $CO_2$ might also alter the chemistry of small quantities of CO so that the effects of the species are indistinguishable. In any event, no CO was ever detected in the anode exhaust.

The exact cause of the $CO_2$ derived performance loss is still unclear, although the data indicates the presence of a slow surface buildup of an adsorbed species. The challenge, then, was to identify a technical approach that permitted successful PEM stack operation on reformate. Three technical approaches became evident: 1) carbon dioxide separation from the anode feed; 2) an improved anode catalyst formulation, one not susceptible to the poisoning reaction; and 3) an alteration of the lifetime of the adsorbed species to make the platinum sites fully available for hydrogen oxidation. Hydrogen-carbon dioxide separation systems are too cumbersome and energy intensive, and thus not practical. The second two remedies, however, both had merit and were actively pursued.

- ***Effects of anode air injection on reformate/air performance*** - An operation to remove the adsorbed species involves air injection into PEM anode feeds. A small quantity of oxygen (air) is added to react selectively with the adsorbed species, forming $CO_2$. Although formally similar to a so-called *in situ* PROX approach, there are distinctly different operating scenarios. When CO is present as part of a contaminated feed stream, CO and oxygen are added simultaneously and react on a section of platinum at the entrance side of the anode compartment. Dynamics are then similar to the PROX process described earlier. The dynamics of the adsorbed species removal are quite different. In this case the active poisoning species is synthesized uniformly along the anode membrane face. Therefore the "fuel" is widely distributed and heat generated during the oxidation step is distributed as well. Moreover, since surface contamination is a very slow process there is no need

to add oxygen continuously; oxygen could be added in pulsed quantities, as needed. Improved safety (less chance for producing thermal "hot spots") and less fuel wastage would be the result.

The voltage improvement in Stack SN-110 that occurred as the result of air anode injection is also presented in Figure 4.3.3-12. Voltage improvement data are presented for both 1 and 2% air injection fraction. Considerable operational experience was achieved using anode air injection. With later, improved stacks, those fitted with advanced anode Pt-alloy catalysts, the voltage recovery with 2% air injection attained a level equivalent to that observed with a hydrogen-nitrogen dilutent mixture; this voltage was just a few mV less than that observed for 100% hydrogen. This voltage recovery is presented in both Figures 4.3.3-13 and 4.3.3-14 for Stack SN-212. The former figure is discussed in more detail later in this section; the recovered voltage is only 40 mV below that using pure hydrogen as the anode feed (Figure 4.3.3-13), or what would be expected from pure dilution effects. The second Figure, 4.3.3-14, represents results from a separate test of the same stack. The first portion of the test was performed using hydrogen and air and a polarization curve, the stepped trace of current and voltage was obtained. Then the anode feed was changed to a reformate containing 2% air. Again a polarization curve was attained. Very little voltage sag was evident; there was no evidence of any slow poisoning process. Moreover, the reformate data at the higher current density is 600 mV compared to the value of 640 mV under hydrogen-air conditions. A 40 mV loss is similar to that measured by adding a similar quantity of nitrogen to the anode feed and represents the expected "dilution" loss. Consequently, with the advanced Ballard stack design, including an improved anode electrocatalyst, the "$CO_2$ problem" appears to be well managed with air injection.

Although anode air injection provides a reproducible remedy for carbon dioxide poisoning, there is evidence that such injection must be controlled, at least with some alloy catalysts. Data presented in Figure 4.3.3-13 support this observation. Test data were obtained over five separate test days. Four of these test days demonstrate useful, reproducible performance with a polarization curve delivering 0.6 V at 1,000 amps/ft$^2$ as previously discussed. The fifth curve, however, is different. That particular polarization performance data was attained after a significant charge of air was injected into the anode, as part of a procedure to assure the crossover rate was low. At first it was thought that perhaps the resulting poor polarization performance data was due to the poor voltage production of one or more bad cells, but further examination of all of the cell data indicated a performance degradation in the entire stack. This performance loss was, fortunately, only temporary and was reversed by suitable, long term operation on hydrogen. If large air volumes, however, are allowed into the anode compartment in the absence of reformate the cell performance is compromised. Air is believed to cause complete oxidation of the anode alloy catalysts, thereby lowering the $CO_2$ tolerance and decreasing the rate of the hydrogen oxidation process during fuel cell operation. This observed loss is recoverable, at least if the injected air is terminated after only a limited flow quantity.

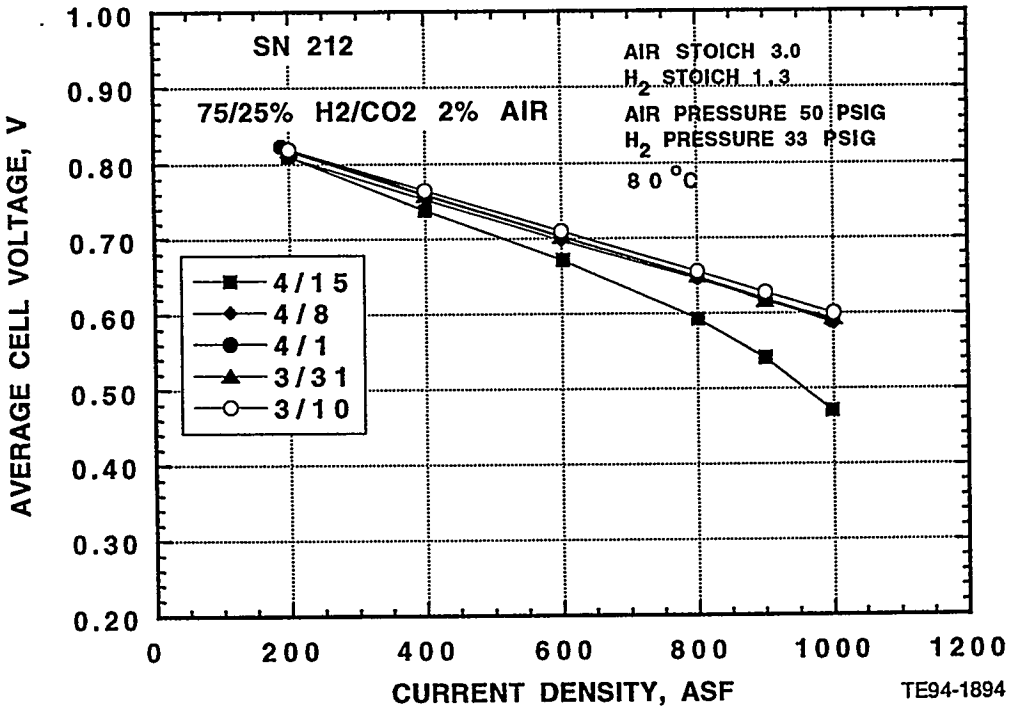


Figure 4.3.3-13. Performance polarization curves for a Ballard improved stack depicting reproducible reformate/air results followed by a one-time significant degradation in performance. The poor performance was exhibited following introduction of a significant amount of air (in the absence of reformate) into the anode during a procedure used to assure the membrane gas crossover rate was low. It is thought that air by itself may completely oxidize the anode alloy catalysts, thereby degrading the hydrogen oxidation process during operation. Stack performance recovered after operation on pure hydrogen.

- ***Effect of cathode conditions on reformate/air performance*** - The effect of cathode conditions on reformate/air performance were also investigated. Tests similar to those conducted using hydrogen/air reactants were performed on the improved stack, SN-212. The data were repeated using synthetic reformate (with 2% anode air injection) as the anode flow and air as the cathode flow. The results of these tests are presented in Figure 4.3.3-15. In general the reformate/air data are quite similar to the hydrogen/air data of Figure 4.3.3-9; there is little system advantage in operating the stack above 40-45 psig cathode air pressure or in increasing the cathode stoichiometry flow above 2.5. The overall voltages measured during the reformate tests are lower than those observed using hydrogen, the result, in part, of the dilution effects of the carbon dioxide.

- ***Effect of anode conditions on reformate/air performance*** - The effects of anode conditions on reformate/air performance were also investigated. As with the cathode investigations described above, tests similar to those conducted using hydrogen/air reactants were performed on the improved stack, SN-212. The data were repeated using synthetic reformate (with 2% anode air injection) as the anode flow and air as the cathode flow. The results

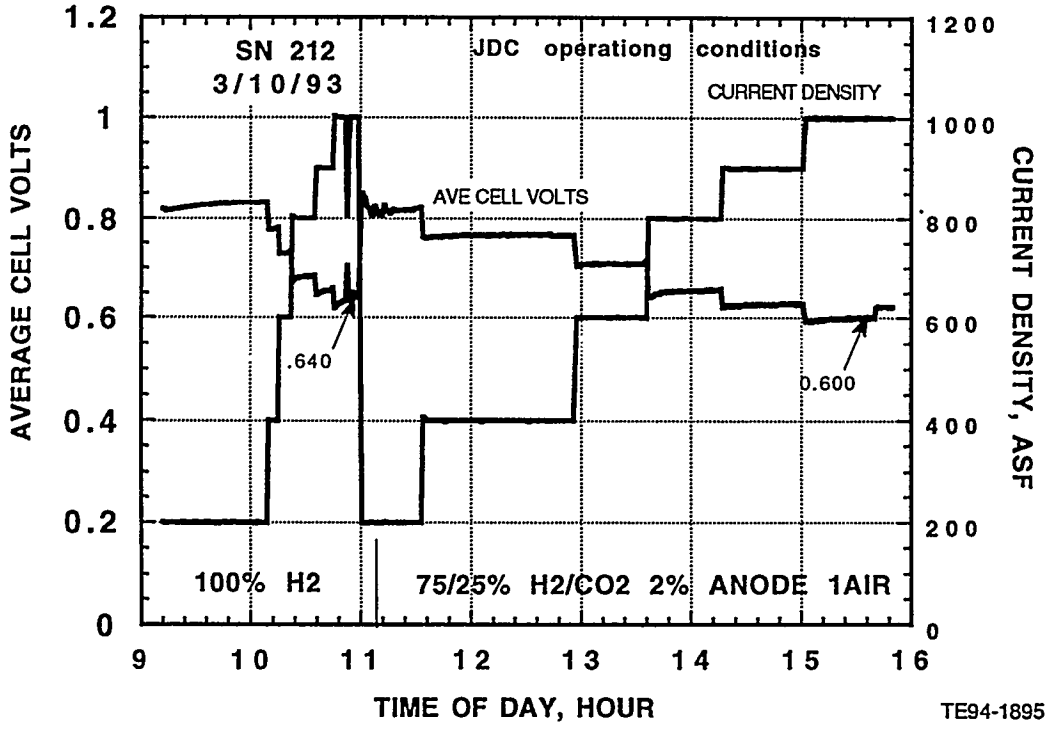


Figure 4.3.3-14. Test data for a Ballard improved stack incorporating advanced anode catalysts. This stack shows performance on reformate-air comparable to performance on 75% $H_2$/25% $N_2$, indicating that the advanced anode catalysts coupled with anode air injection adequately manages the "$CO_2$ problem."

of these tests are presented in Figures 4.3.3-16 and 4.3.3-17. Performance for both pure hydrogen and reformate (with air injection) are depicted in the figures. Similar to the cathode tests, all of these data were measured at the highest current density where differences between hydrogen and reformate performance tend to be maximized. Reformate performance is somewhat more dependent, as demonstrated in Figure 4.3.3-16, on anode pressure than is the performance when pure hydrogen is used as the anode reactant. There is a significant voltage gain between 10 and 20 psig when reformate is the anode reactant. Above 20 psig some reformate voltage increase does occur as pressure is increased, but the increase is insignificant compared to that observed between 10 and 20 psig. Optimal anode reformate operation with respect to system efficiency occurs between 20 and 30 psig compared to 15 psig when pure hydrogen is used. The effects of performance change with anode stoichiometry variation are presented in Figure 4.3.3-17. As was the case for pure hydrogen anode flow, Stack 212 average cell voltage on reformate is nearly independent of anode stoichiometries above 1.2. This is advantageous as system efficiency slightly improves with low anode flow and use of a mixed flow (anode vent gas and methanol) burner. More importantly, the size of the fuel processor, for given power levels, decreases with decreasing anode flow requirements.

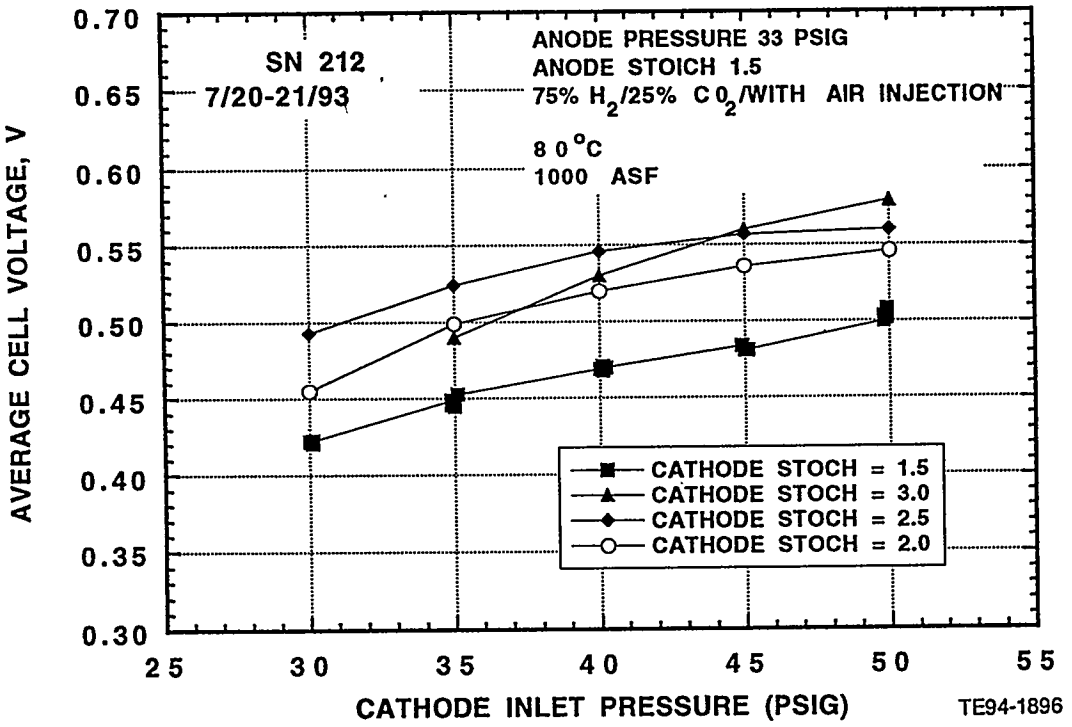


Figure 4.3.3-15. Test data for a Ballard improved stack operating on synthetic reformate with air injection as the anode feed. The effects of cathode pressure and stoichiometry on performance are presented. These effects are similar to those measured on $H_2$ (see Figure 4.3.3-9), but the voltage is lower, due in part to the diluent effect of the $CO_2$.

### *Stack Startup Transients*

The last data sets presented in Figure 4.3.3-18 demonstrate the results of tests where Stack SN-212 was started from a cold condition (laboratory temperature, approximately 20°C) and brought, under power, to the desired operating temperature of 80°C. Tests were repeated at three different current densities, 200, 400 and 600 amps/ft². At the higher current densities temperature increase due to power production inefficiencies had the largest effect in raising the stack voltage. Lower current densities did not produce sufficient heat production within the stack to warm it above 60°C. However, each data set indicated PEM hardware can easily be brought on line from a cold start, initially producing more than 50% of the maximum continuous power measured at the normal stack operating temperature. Following an experiment to repeat the 150 amp (600 amps/ft²) data, a routine crossover test discovered an intolerable leak rate and the stack was returned to Ballard for maintenance. It was not determined if these startup transients contributed to the stack failure.

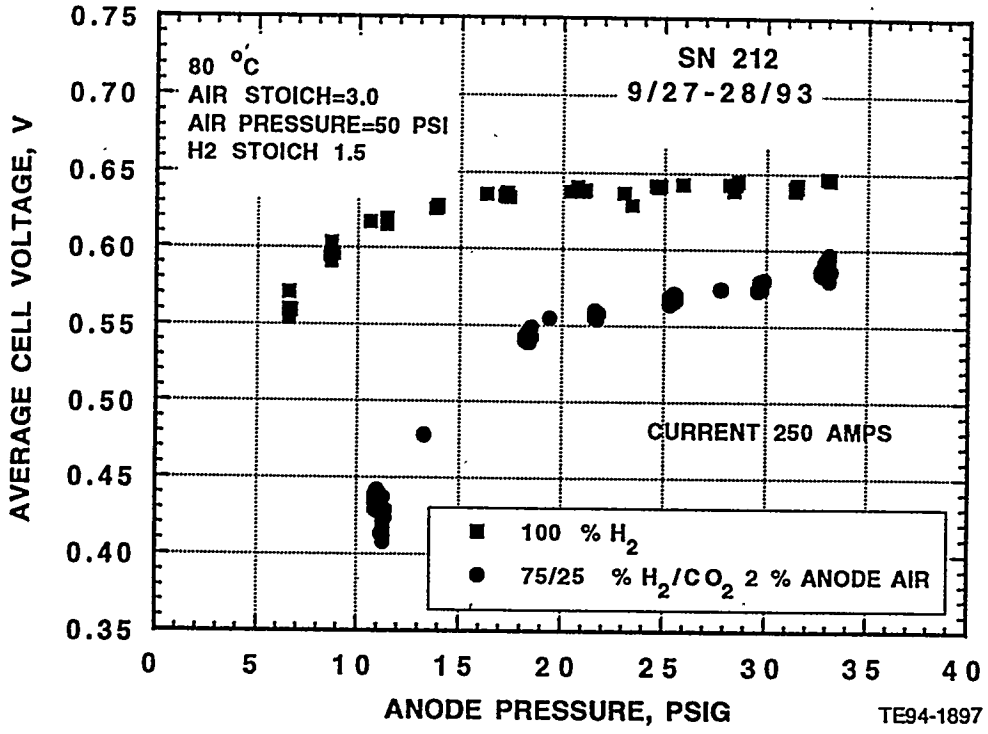


Figure 4.3.3-16. Test data for a Ballard improved stack demonstrating the effect of anode pressure on performance for both pure $H_2$ and synthetic reformate with air injection. Note the effect is more pronounced on reformate than with pure hydrogen.

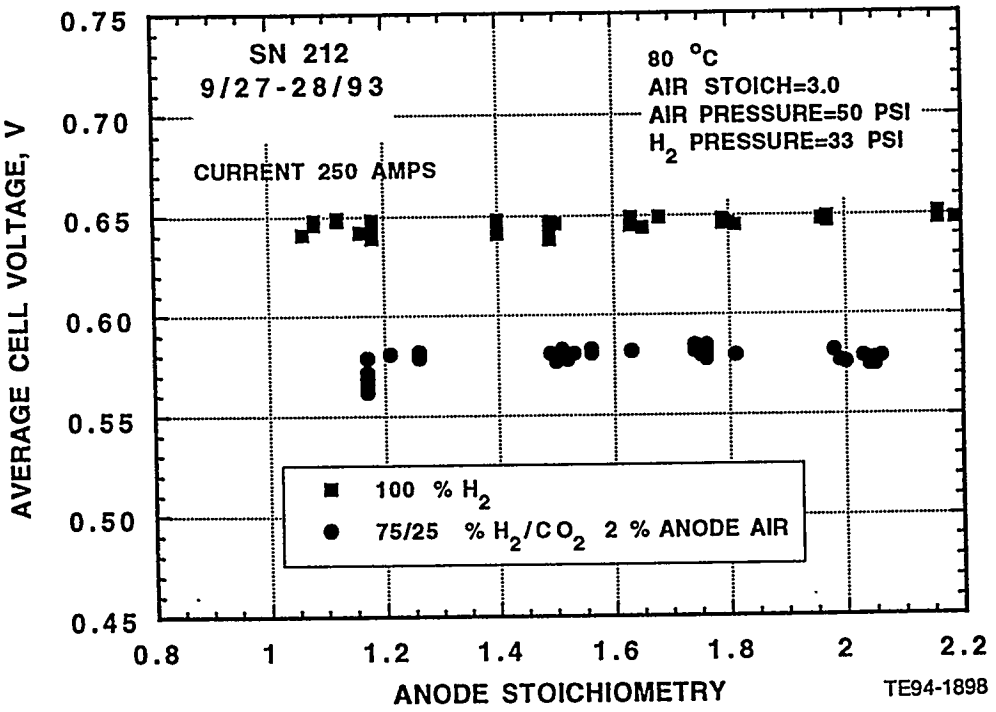


Figure 4.3.3-17. Test data for a Ballard improved stack demonstrating the effect of anode stoichiometry on performance for both pure $H_2$ and synthetic reformate with air injection. Little influence of anode stoichiometry on average cell voltage within the stack is evident for either reactant.

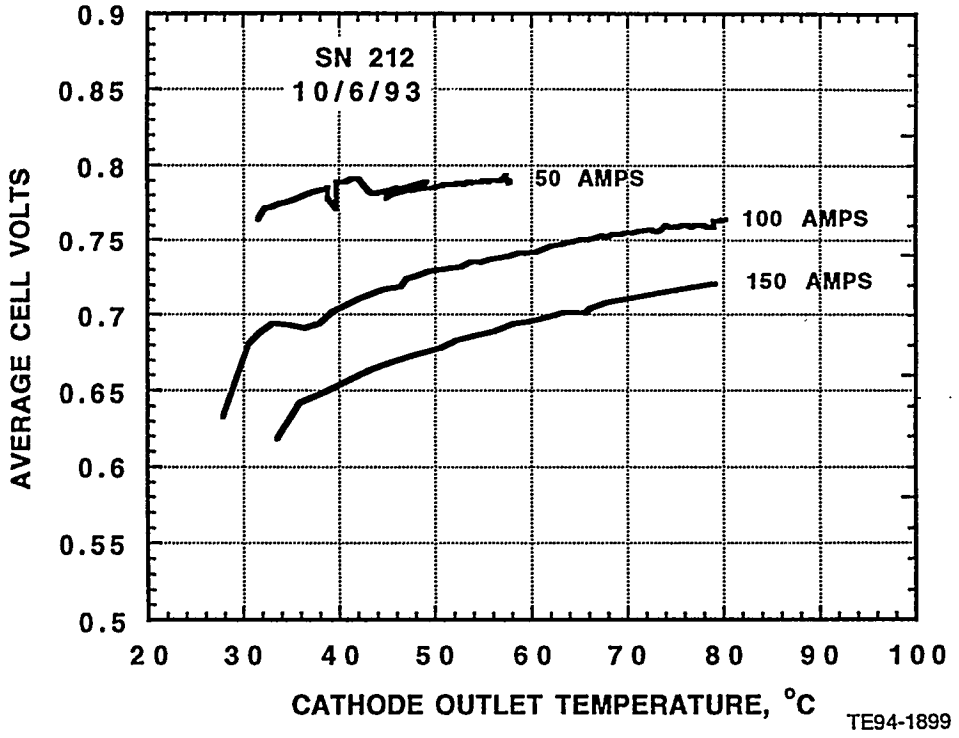


Figure 4.3.3-18. Test data for a Ballard improved stack measured during cold start-up transients. Each test began with the stack at ambient laboratory temperature (approximately 20°C) and was initiated by drawing a fixed current. The largest voltage effect from the self-heating temperature increase occurred at the highest current densities.

# V. PROGRAM TASK 4: 10-kW FUEL PROCESSOR DEVELOPMENT

## 5.1 GENERAL INTRODUCTION

Liquid methanol, derived from large, worldwide deposits of natural gas is increasingly being used for transportation applications. Predictions touting a "natural gas future" project that methanol, because of the ease of handling and storing a liquid fuel, compared to gaseous methane, could be the next large energy source for the planet. This program is based on the assumption that this liquid fuel can be readily available in the future and that the resource base is sufficient to expand methanol usage to provide a significant fraction of the fuel required for the transportation sector.

Methanol can be used directly in fuel cells, supplying the liquid or vapor fuel mixed with $H_2O$ to the anode compartment and reacting that with air on the cathode side to generate electrical energy for future transportation technologies. However, after decades of intense technical development, only modest power densities, ~0.1 W/cm$^2$, have been demonstrated using direct methanol fuel cells. The other technical approach for a methanol-powered fuel cell is to convert liquid methanol to hydrogen and then consume that hydrogen in a fuel cell device, generating electricity for traction purposes. This "indirect methanol fuel cell" requires an onboard chemical processing plant. However, the indirect approach leads to fuel cell stack operation with a hydrogen rich fuel known as "reformate"; and reformate-air fuel cells have demonstrated stable performance at ~ 1W/cm$^2$, about a factor of 10 larger than the alternative direct methanol approach. This suggests a clear advantage for the "indirect methanol fuel cell". This project has been developed around the concept that fuel processing can be achieved in a compact, affordable, reliable component.

Methanol, $CH_3OH$, is a compound with very flexible chemistry and is readily converted to a hydrogen-rich stream through one of many similar and interrelated chemical processes. Over the course of fuel processor development it has become apparent that, for the applications and efficiencies stressed in this project, steam reforming of methanol has process advantages.

Methanol processing requires intensive thermal energy for hydrogen generation. If methanol energy content is based on the heat of oxidation of that fuel, then approximately 25% of the total fuel enthalpy is required for hydrogen generation. This energy is distributed into three endothermic (heat requiring) steps:

1. Water evaporation and steam preheat: 50%
2. Methanol evaporation and fuel preheat: 25%
3. Endothermic requirement for the hydrogen generation reaction: 25%

Much of the engineering challenge for methanol-to-hydrogen technology is dictated by the requirements for this energy flow. The fuel processing hardware developed during this program was termed the Mark II system, a fuel processing design that was a direct outgrowth of earlier work completed at LANL. Separate unit operations were designed to derive the necessary fuel stream; activities focused on the design, fabrication, assembly, and testing of a fuel processor that could be used to

conduct preliminary system tests. This major program emphasis resulted in several key breakthroughs which are summarized below.

- **Fuel metering hardware** - Injection of water vapor and steam into the catalytic reformer was accomplished using newly-developed fuel injection hardware specially designed for methanol and deionized water operation. These components, and the required 12-volt automotive drive and control circuits, were provided by AC Rochester. The fuel metering hardware also consists of a JDC designed pool boiler in which liquid water and methanol are sprayed into the boiler resulting in rapid vaporization. The result is careful control of fuel flow with a minimum methanol inventory. This results in both safe reformer operation and high transient capability. Idle-to-full-power hot reformer operational transients were accomplished in less than 3 seconds.

- **Steam reforming hardware** - The compact vaporizer generates a custom-blended gaseous mixture of methanol and steam, typically in a steam to methanol molar ratio of 1.0 to 2.0. This gaseous mixture then flows to a "reformer" that includes the unique features of both fast gas phase heating and a heterogeneous catalyst. All studies reported here utilized a $CuO\text{-}ZnO/Al_2O_3$ catalyst material (United Catalyst C18HC) that is supplied as a pelletized material. The Mark II reformer can accept a catalyst charge of up to 10 kg, although most studies were conducted with less than this "complete" charge. In general this first unit operation works to convert approximately 98.5% of the feed methanol following the reaction:

$$CH_3OH + H_2O = 3H_2 + CO_2$$

This is the primary hydrogen generation step used in this indirect methanol fuel processing approach. Processing is done using a stirred reactor that fans the product stream through the catalyst bed and then through an interior electrically heated resistance heater. This heater supplies the required energy to drive the hydrogen generation process. Because of the relatively long residence time and the repeated exposure of the reactants and products to the heterogeneous catalysis surfaces, the reacting mixtures are converted to major chemical species whose concentrations are not far removed from equilibrium conditions. As most experiments utilize a steam to methanol ratio in excess of the 1:1 depicted in the above equation, excess steam is in the product gas. Because of this, a second significant reaction occurs that controls the concentration of CO in the product mixture:

$$CO + H_2O = H_2 + CO_2$$

This "shift reaction" equilibrium sets the CO concentration as:

$$[CO] = K_S \{ [CO_2] [ H_2]\}/[H_2O]$$

The numerical value of $K_S$, the equilibrium constant for the shift reaction, increases with temperature. The low temperature shift catalyst used in these studies can theoretically operate at temperatures as low as 180°C; however, that temperature has proven to be too cold for optimum conversion. If the reformer, or a portion of it, operates at too low a temperature, even if lower CO concentrations would result, far less methanol conversion would occur. This

condition would defeat the intent of fast hydrogen generation. Steam concentration could also be increased to lower CO concentrations, but steam generation is an energy intensive step, so such an increase results in decreased system efficiency. In general, the carbon monoxide concentration exiting from the first reforming step is about 12%, a high value, and certainly one that would cause immediate anode poisoning. The remainder of the fuel processing section concentrates on hydrogen purity issues.

- **Shift zone hardware** - Two major constituents that are considered to be contaminants are present in the reformer efflux; these constituents are breakthrough methanol and carbon monoxide. The shift zone acts to remove nearly all of the breakthrough methanol and significantly reduce the carbon monoxide level. The shift zone hardware consists of two catalyst beds that operate in series. The first shifter, operating at reformer temperatures, converts breakthrough methanol; under successful conditions, residual, unreacted methanol can be nearly undetectable, <5 ppm. The second shifter accepts additional steam, operates at lower temperatures, and results in significant CO control. The CO contaminant is reduced by the water-gas shift reaction, forming additional $H_2$ fuel and $CO_2$. Approximately 40 to 60% of the CO is removed in this second-stage shift operation. Changes to the reformer outlet path, described in Section 5.2, reduced the reformer methanol breakthrough to levels that could be eliminated within the shift zone.

- **PROX hardware** - The last section of the fuel processing hardware is a nonequilibrium process that operates to essentially remove all of the remaining (trace) methanol and CO, through the PROX of these constituents in the presence of a large molar excess of hydrogen. The process described here has already been discussed in a previous section of this report. Air is mixed into the process stream and then that air-containing mixture passes through an oxidation catalyst section that works to remove essentially all (trace) methanol and CO. In particular, CO removal is intractable in a single stage device; the oxidation process successfully utilizes a staged approach that adds air (oxygen) sequentially along two or more short catalyst chambers. CO (and/or methanol) removal using staged PROX devices that add air (oxygen) sequentially along two or more short catalyst chambers, arranged either in parallel or series configurations, or a combination thereof, is the subject of a GM/Allison assigned patent, Reference 5.1-1. Residual methanol, if it exists, is always entirely removed in the first stage.

The purpose of these development efforts, which are described in the following sections, was to demonstrate operation at a series of power levels (chemical flow rates) with sufficient fuel purity to drive a PEM stack.

## 5.2 MARK II FUEL PROCESSOR DEVELOPMENT

### 5.2.1 Introduction and Summary

This section describes in detail the hardware developed during this program for hydrogen generation. A series of evolutionary advances were achieved on each of the several components in this processing scheme. Major advances were accomplished regarding: the safety and reliability generation of the feed mixture, incorporation of plug flow reactor outlets within the reformer itself to help reduce methanol break-

through, resizing of the shifter units, and geometric optimization and control of the PROX units. These advances are described below, along with some of the significant results attained during the Phase I testing program of the fuel processing components.

### 5.2.2 Description of Components

The ECE demonstrator system under development utilizes a fuel processor apparatus denoted as Mark II. This apparatus is a laboratory tool, driven by electrical heating, which is impractical in any vehicular situation; however, in the present experimental phase this approach is both convenient and safe. The Mark II fuel processor is conceptually depicted in Figure 5.2.2-1. Four separate components are illustrated in the figure.

The fuel processor vaporizer section vaporizes liquid water and liquid methanol feed streams at the required pressure and flow rates. In the reformer component, the two vapors are continuously circulated through a catalyst section and react, with

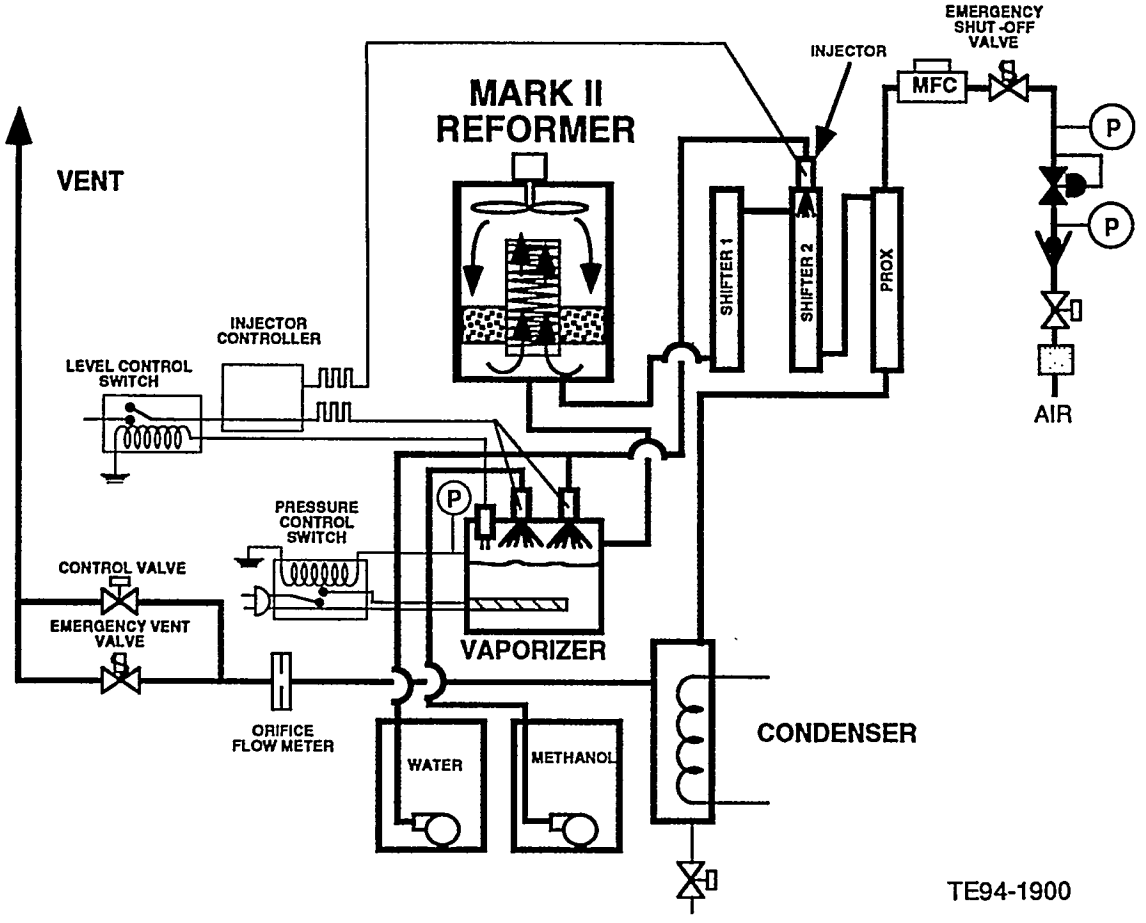


Figure 5.2.2-1. Simplified schematic of the Mark II fuel processor. The functions of the various components are discussed in some detail in the text.

the addition of heat, to generate hydrogen and carbon dioxide, plus residual amounts of methanol and carbon monoxide. These sections are followed with gas cleanup in two sequential operations: shift zone and PROX.

### *Vaporizer*

The vaporizer component generates a custom-blended steam-methanol mixture at rates corresponding to the required power level. Generally, the steam to methanol ratio ranges between 1.3 and 2.0 with flow rates sufficient to power 10-kW of fuel cell stack electrical output. The system utilizes recently developed automotive compatible fuel pump and injection hardware, specifically engineered for water and methanol service by AC Rochester. The injectors are fueled from a custom rail and controlled by an ECM. Flow to the injectors is supplied by pumps immersed in separate stainless steel tanks containing liquid water and methanol, respectively. These tanks are positioned on electronic scales that provide flow calibration, help determine liquid level, and aid in monitoring the performance of the injector hardware. The injector pulse width is set by an AC Rochester computer prom (programmable read only memory chip). Methanol and water are fed into the electrically heated vaporizer section corresponding to the required power level. The vaporizer heater is controlled by vaporizer pressure. Decreased pressure results in higher heater power, etc.; this strategy results in a nearly constant feed pressure, quite independent of fluid flow. Liquid level in the pool boiler remains essentially constant; float valves remain in the hardware, but now serve as safety markers to sense an adverse condition such as having too high or too low a liquid inventory.

The design of this pool boiler avoids a system that operates using a large volume of pressured, gaseous methanol, clearly a possible hazard. Rather, the two liquids are metered into a two-phase steam boiler. Because of the large difference in boiling temperatures between methanol and water, methanol traverses through the vaporizer with a short residence time; there is very little methanol inventory. Temperatures within the device are sufficiently hot that the equilibrium methanol concentration in the liquid water phase is only approximately 1%. Consequently, even in the unlikely event of a pool boiler rupture, the inventory is essentially hot water.

### *Reformer*

The primary hydrogen generation occurs within the catalyst volume of this component. As depicted in Figures 5.2.2-1 and 5.2.2-2, the reformer contains an integral fan that uses the circulating product gas flow to transfer heat between an internal electrical resistance heater and the catalyst sites. Control of fan speed and heater input control the rate of heat introduction; this heat transfer control technique is convenient and limits possible overheating during down-power transients. Reforming is best accomplished at temperatures between 230 and 260°C. In ordinary tube-in-shell devices, the heat flux cannot be rapidly reduced; as a consequence some overheating and subsequent catalyst deactivation could occur during load changes in conventionally heated reformers.

As described, heat is supplied to the reformer with a nominal 5-kW, 220 volt electrical heater. Components for this heater were originally designed as a gas phase heater for industrial purposes. A series of these commercial heater elements were

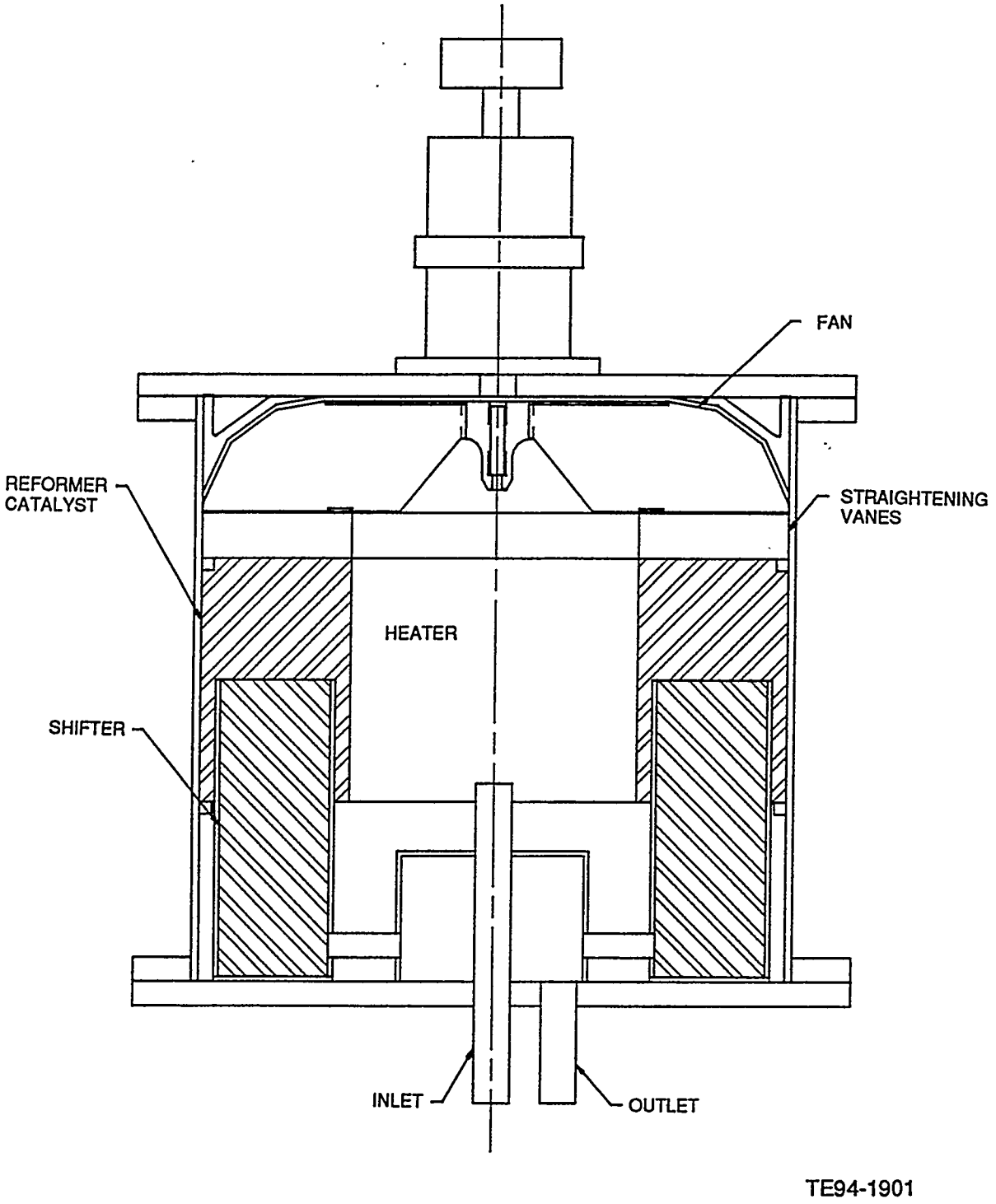


Figure 5.2.2-2. Modified Mark II reformer. Both the redesigned, aerodynamic fan and the new outlet flow path incorporating four in situ plug flow reactors are depicted. The redesigned fan improves the gaseous product recirculation flow to heat the catalyst bed while the plug flow reactors on the outlet flow path substantially reduce methanol "breakthrough."

mounted in a geometry suitable for the reforming application. The heater power input is controlled by a temperature controller receiving input from a thermocouple at the top of the catalyst bed. The heat supply in an automotive design fuel processor will, of course, be provided by a combustion process. The burner to provide this combustion process is not specifically complex, but the heat must transfer into a hydrogen-rich gas, therefore, considerable safety concerns must be addressed during the burner design. Because these design issues, although technically tractable, would certainly have slowed evolution of the Phase I ECE system, it was decided to proceed through this phase of the program using electrically heated components. The fan on the reformer is a straight-bladed design driven by a magnetically coupled, motor driven system. The mass rates of recirculating product gas to incoming reactant mass flow may exceed a factor of 1020 depending on fan speed. The reforming process is an endothermic step and the reacting portion of the gas stream (the quantity of incoming methanol and water vapor) cools both the catalyst and the recirculatory stream during the traverse because of this heat removal; the recirculating gas stream is subsequently reheated by passage over the internal electric heater so that the temperature differential across the catalyst bed does not exceed 10°C.

Early versions of the full-scale reformer had both an inefficient fan design and a flow path that permitted a small fraction of the incoming methanol and water vapor to bypass the catalyst and flow directly to the outlet. The first of these deficiencies was rectified by a new lightweight, aerodynamically designed fan. The second deficiency, methanol breakthrough, was substantially reduced by connecting the outlet to four plug flow catalytic reactors that extend up into the catalyst bed. As a consequence no fraction of the methanol can flow to the outlet without at least passing through these high temperature plug flow catalytic reactors. Both the redesigned fan and the new outlet path are depicted in Figure 5.2.2-2. The in situ plug flow reactors within the reformer act in concert with the first stage, high temperature plug flow reactor of the shift zone. With the installation of the new outlet flow path within the reformer "breakthrough methanol" been eliminated.

Since this new reformer outlet flow path was installed late in Phase I, some of the data presented in this section and in Section VII regarding the system development and test effort reflect results attained prior to this installation. In those cases, methanol "breakthrough" survived through the shift zone and was subsequently reacted in the PROX.

### *Shift Zone*

Although the reformer developed for this program is very compact and accomplishes the design task of rapid hydrogen production, contaminants still exit the device. These include unreacted methanol in the range of 0 to 1.5% and carbon monoxide in the range of 0 to 2%. The shift zone is designed to react methanol and reduce CO content. Two packed beds, utilizing the same catalyst as that in the reformer, are operated in series as depicted in Figure 5.2.2-1. The first shifter operates at the reformer temperature and acts as an additional plug flow reactor converting any remaining unreacted methanol. Then, using a second water injector, additional quantities of steam are added to the process stream prior to the second stage shift reactor to promote the water-gas forward shift reaction. Depending upon conditions of temperature (usually 220°C) and steam to fuel ratios in this second stage, the CO concentration emanating from this zone is between 0.25% and 0.75%.

Shift temperatures are controlled by varying the electrical power fed to heaters on the inlet lines to each unit. As described, the shift unit, at least in several configurations explored during these studies, consists of two series plug flow reactors with water injection between "Shift 1" and "Shift 2." The water injection rate into Shift 2 is controlled by an ECM supplied by AC Rochester. This injection rate can be varied so that as flow through the system is changed a constant steam to fuel ratio can be maintained. Obviously, additional water could also be injected in the vaporizer. However, there are advantages in utilizing a second water injection site. Water in the "shift zone" need only be heated to approximately 150°C, the temperature of that entrance point, compared to the approximately 250°C injection temperature of the steam reformer. Moreover, the excess steam does lower the methanol concentration, and this, in turn, could reduce the rate of hydrogen generation; although, at present, analyses continue to indicate that methanol conversion rates are limited by heat transfer rather than any inherent chemical reactivity.

***PROX***

CO control must be accomplished in the PROX component as PEM anodes are poisoned by even low CO levels. A controlled flow of air is inserted into the PROX units and the gaseous mixture is exposed to oxidation (Pt on alumina) monolithic catalysts. Under proper design conditions, oxygen within the air is injected at a ratio of approximately 2 moles of oxygen to 1 mole of carbon monoxide. Removal of CO down to <5 ppm has been accomplished in these adiabatic units. Following the PROX zone the reformate feed concentration approximates 65% $H_2$, 22% $CO_2$, 12% $H_2O$ and extremely low level impurities of CO, $CH_3OH$, and $CH_4$.

The gas phase temperatures of the PROX sections are primarily controlled by interstage heat exchangers. The quantities of air injected into the PROX sections are controlled through use of MFCs; the injected air flow rates in each unit are proportional to the volume percentage of the total fuel processor flow and the CO concentration entering each unit. Total fuel flow exhausting from the fuel processor, following cooling to remove water, is determined by measuring the pressure drop across an orifice plate. This delta pressure signal is fed to a controller and an output flow calculated. As the chemical flow from the device varies, the controller proportionately adjusts the air flows into the PROX units.

### 5.2.3 Mark II Fuel Processor Test Results

During the early portion of the Phase I project extensive testing was conducted on separate components of the Mark II fuel processing system. Although the overall fuel processing concept, steam reforming with subsequent gas cleanup, did not change during Phase I, continuous evolution occurred in component design and placement, and sensor and control strategies. Simultaneously with this hardware evolution, software activity was proceeding to develop control loops connecting the Hewlett Packard VEE DACQ computer, Omega controllers, and the RTOS control unit. Additionally, installation, calibration, and programming of the gas chromatography and other instrumentation required considerable optimization to achieve the rapid and accurate measurement of gas species, etc., to determine reaction processes occurring with the fuel processing components.

### *Shift Zone Test Results*

The Mark II fuel processing hardware was assembled as a complete subsystem in the new systems laboratory in February, 1993. Tests were initiated using the vaporizer section only, and then, as each additional component was checked out, the fuel processor subsystem was brought to full operational status. The results of one of these initial experiments are presented in Figure 5.2.3-1 in which the temperatures of various components are presented as functions of operating conditions and time. The purpose of the experiment was to determine suitable temperatures within Shift 1 and Shift 2 under the given water to methanol operating conditions for both effective removal of the residual methanol and optional reduction of the output CO level from the second stage shift reactor. Tests were initiated at about hour 8.5 and the fuel processor was operated at a steady-state condition for about five hours. The overall water to methanol ratio in the system was 1.85; 1.55 stoichiometry was injected into the reformer and the remaining .3 into the second stage shifter. The temperature of Shift 2 was then stepwise increased during the latter part of the test. The reformer thermocouples sample temperature in three locations, above, below, and within the catalyst bed. The vaporizer liquid temperature remained essentially constant at the boiling point of the methanol-water azeotrope. The residual methanol was effectively converted within the Shift 1 plug flow reactor when its temperature was held between 255 and 260°C, virtually the same temperature used for methanol conversion in the stirred-flow reformer. The variation of the Shift 2 temperatures revealed that outlet CO concentrations pass through a minimum and do not continuously increase as suggested by simple equilibrium predictions. These outlet CO concentrations as a function of Shift 2 catalyst temperature data are presented in Figure 5.2.3-2. The minimum CO outlet concentration appears at approximately 225°C. This result has been observed to be relatively independent of the chemical feed rate. At higher Shift 2 catalyst temperatures, CO increases as expected, moving toward the predicted equilibrium values for the increased temperatures. Kinetic complications occur as Shift 2 catalyst temperatures are lowered, slowing the shift kinetic rates, which result in outlet CO concentrations increasing at lower temperatures contrary to theoretical equilibrium predictions.

In a second experiment, using the operating conditions for the shifters as determined from the first experiment (Figure 5.2.3-2), concentrations of both Shift 2 outlet CO and methanol concentrations are presented as a function of fuel flow rate, Figure 5.2.3-3. The methanol data represents results attained prior to the reformer outlet flow path modifications incorporating four in situ plug flow reactors to reduce methanol breakthrough. The CO and methanol outlet concentrations are presented as functions of flow rate in terms of fuel cell stack amps equivalent, based on the Ballard stack design. The "amps equivalent," up to 250 amps, is the quantity of reformate necessary to maintain a stoichiometry of 1.3 in a single fuel cell stack with 35 cells operating at that equivalent current. For calibration purposes, 250 "amp equ" corresponds to a flow of 106 slpm. During most of this program, when a two fuel cell stack configuration was utilized to increase power output above 250 amps, the stacks were connected in a parallel configuration. Thus, when flow rates, in terms of equivalent amps, are quoted for a two stack configuration, particularly above 250 amps, approximately half of the flow was passing through each individual stack. For purposes of relating this back to the fuel processor the "total amps equivalent" still directly relates to the total quantity of reformate produced by the fuel processor. Problems arise only when the stacks are connected in a series configuration. Such a series connection was accomplished very late in the program

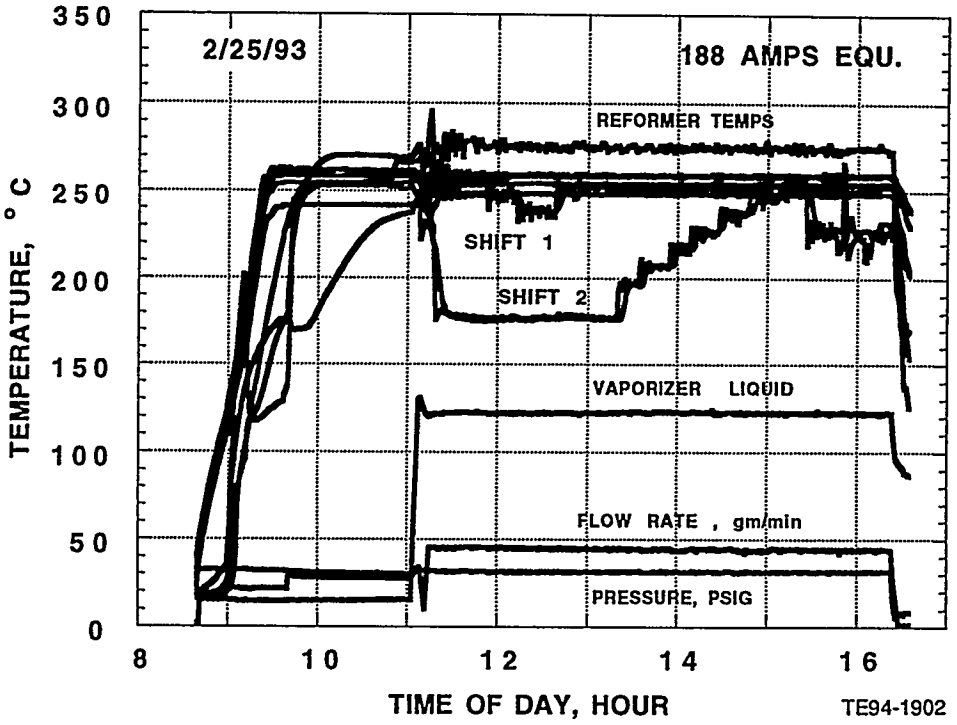


Figure 5.2.3-1. Operating data from an early test of the Mark II fuel processor. Parametric variation of Shift 2 catalyst bed temperature was performed from about 13:20 to 14:30 hours. The effect on CO concentration at the Shift 2 reactor exit resulting from this temperature variation is presented in the following figure.

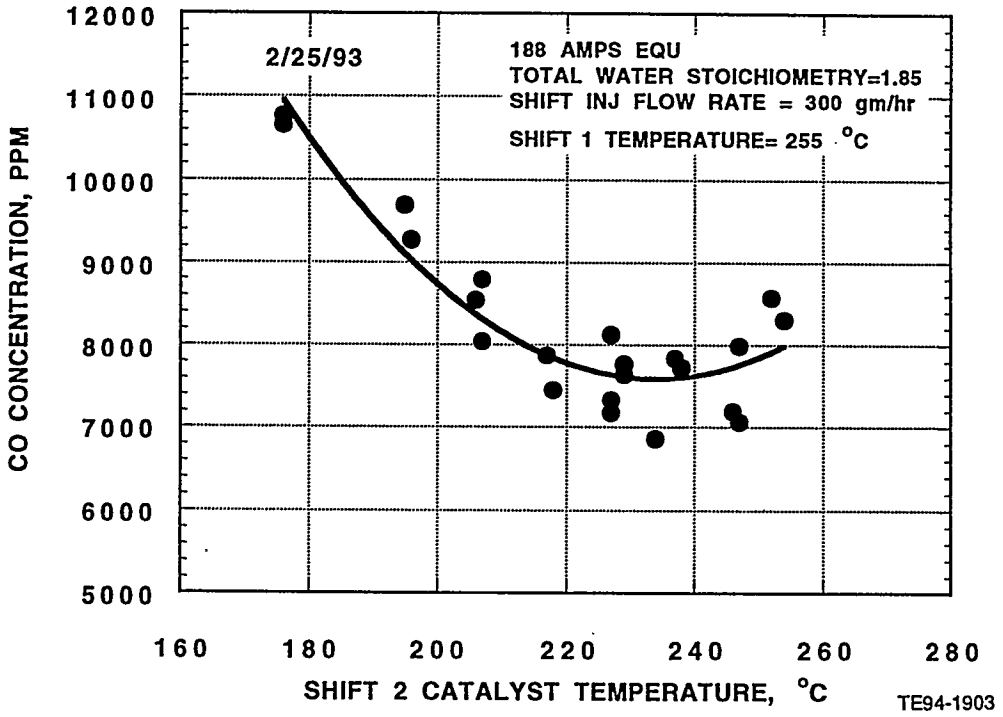


Figure 5.2.3-2. The effect on CO concentration measured at the shift 2 reactor exit resulting from a parametric variation of shift 2 catalyst bed temperature during early Mark II fuel processor testing.

and is now the standard two stack configuration. In this latter configuration the same amperage passes through both stacks while the total output voltage is nearly doubled. Equivalent amps now no longer directly corresponds to the total quantity of reformate required by the fuel processor unless the "value for the equivalent amps" is doubled. A more accurate method to express fuel processor output in terms of total stack output is through the use of the term "equivalent power produced." The total quantity of reformate produced by the fuel processor is directly proportional to the equivalent or total power produced.

No Shift 2 outlet methanol concentration was detected using the parallel stack configuration until the flow exceeded 250 amp equ; above this flow, as depicted in Figure 5.2.3-3, some "breakthrough" methanol was evident. However, after the reformer outlet flow path modifications, incorporating four in situ plug reactors, was installed, this "breakthrough" methanol was reduced to zero even at high flow rates. Carbon monoxide Shift 2 outlet concentration is flow dependent, as depicted in Figure 5.2.3-3. This is not an expected result and probably reflects some early nonoptimum vaporizer injector control strategies, additional CO generation through methanol decomposition, or some calibration difficulties with the gas chromatographic measurement. In any event, the CO concentration only varied between 0.4 to 0.7%, both values being well within the suitable feed range for subsequent PROX processing.

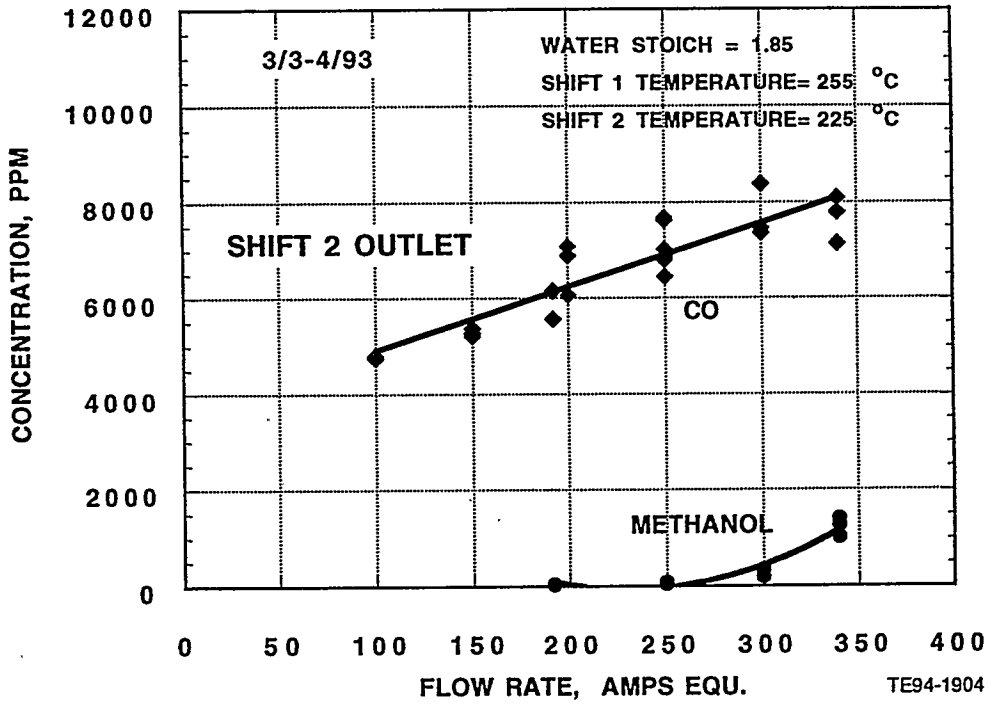


Figure 5.2.3-3. Measured carbon monoxide and methanol concentrations at the shift 2 reactor exit resulting from a parametric variation of flow rate during early Mark II fuel processor testing. A discussion of the "amps equivalent" unit can be found in the text (for calibration, 250 amps equivalent corresponds to 106 standard liters per minute). The appearance of methanol at the reactor exit has been referred to as "breakthrough."

Additional testing was conducted to determine the Shift 2 outlet CO concentration as a function of varying the overall input steam to methanol ratio in the feed stream. In this particular experiment all of the water was added in the reformer. Shift 2 outlet CO concentration as a function of the steam to methanol ratio is presented in Figure 5.2.3-4. The predicted CO concentration, if equilibrium levels were achieved, are also depicted in the figure. As is evident, the equilibrium predicted CO values are considerably lower than the actual outlet CO concentrations measured, although the shape of the experimental curve closely parallels equilibrium theory. It is suspected that the difference results from kinetic limitations; the 224°C temperature in Shift 2 may not be able to sustain kinetic rates that can attain equilibrium. Alternatively, carbon monoxide absorption may alter the localized concentrations at the active catalyst sites so that gas phase and surface concentrations are dissimilar, a well known phenomenon that can occur in these types of catalytic reactions. However, these data do demonstrate that, if the target concentration for CO in the Shift 2 exit gas is to be below 1%, then the overall steam to methanol ratio must be greater than 1.6. These tests did establish conditions that generated stable, reproducible conditions for the vaporizer, reformer, and shift sections.

The final shift zone investigations were performed to determine if CO and methanol Shift 2 outlet concentrations were partially independent of the location at which the steam was added, as long as the "overall steam to methanol ratio" in the flow was greater than 1.6 prior to exiting the second stage shifter. The results of two separate experiments involving the now modified reformer and shifters are presented in Figure 5.2.3-5. The data presented in this figure indicate that regardless of the op

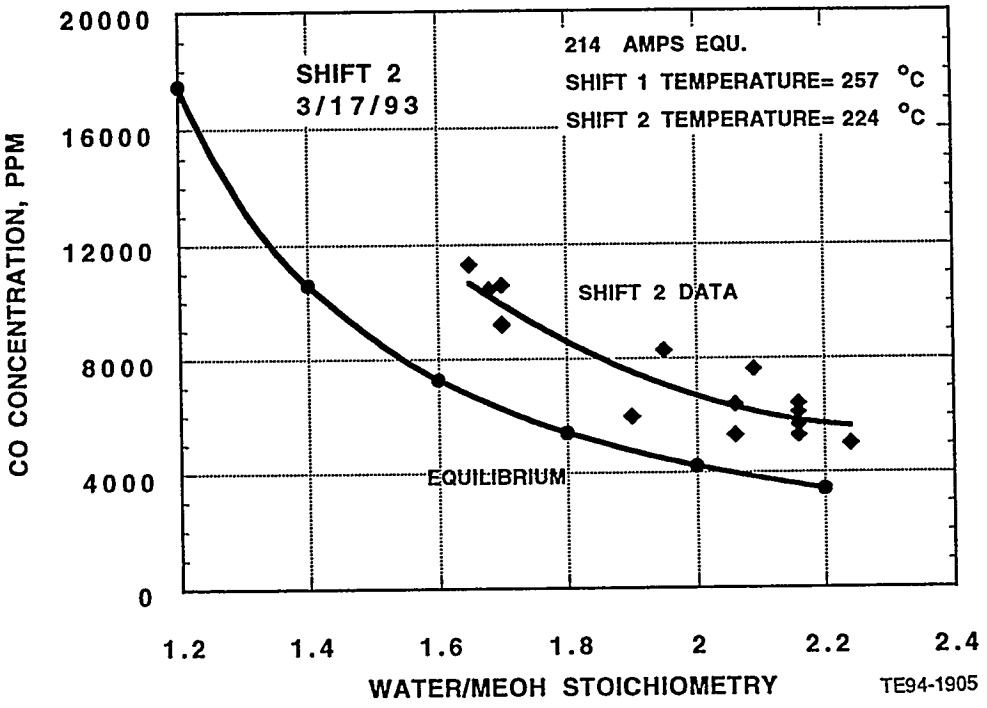


Figure 5.2.3-4. Measured carbon monoxide concentration at the shift 2 reactor exit resulting from a parametric variation of reformer steam-to-methanol ratio. The lower curve displays values expected if equilibrium levels were achieved.

erating conditions of the reformer the resulting CO and methanol concentration exiting the second stage shifter are, at least, slightly more related to equilibrium than process kinetics. In each case the overall steam to entering methanol ratio (called water stoich on the figure) exiting the second stage shifter is controlled at 1.85 moles $H_2O$ : 1 mole methanol. In one of the experiments the reformer was operated at a 1.55 steam to methanol molar ratio with 0.3 steam to methanol molar rates added in the second stage shifter; in the second experiment the reformer operated at a 1.35 steam to methanol molar ratio while 0.5 steam to methanol molar ratio was added in the second stage shifter. Operation of the reformer at higher initial steam to methanol ratios results in less CO and methanol exiting the reformer. In both cases flow through the first stage shifter removes nearly all of the methanol with a concurrent increase in CO. Flow through the second stage shifter results in a CO reduction to approximately the same level regardless of the process conditions as long as the same steam to methanol ratio is attained by the second stage shifter exit. Clearly, the CO concentrations are primarily controlled by the equilibrium of the water gas reaction. Reformer operation at lower steam to methanol molar ratios is, however, less energy intensive.

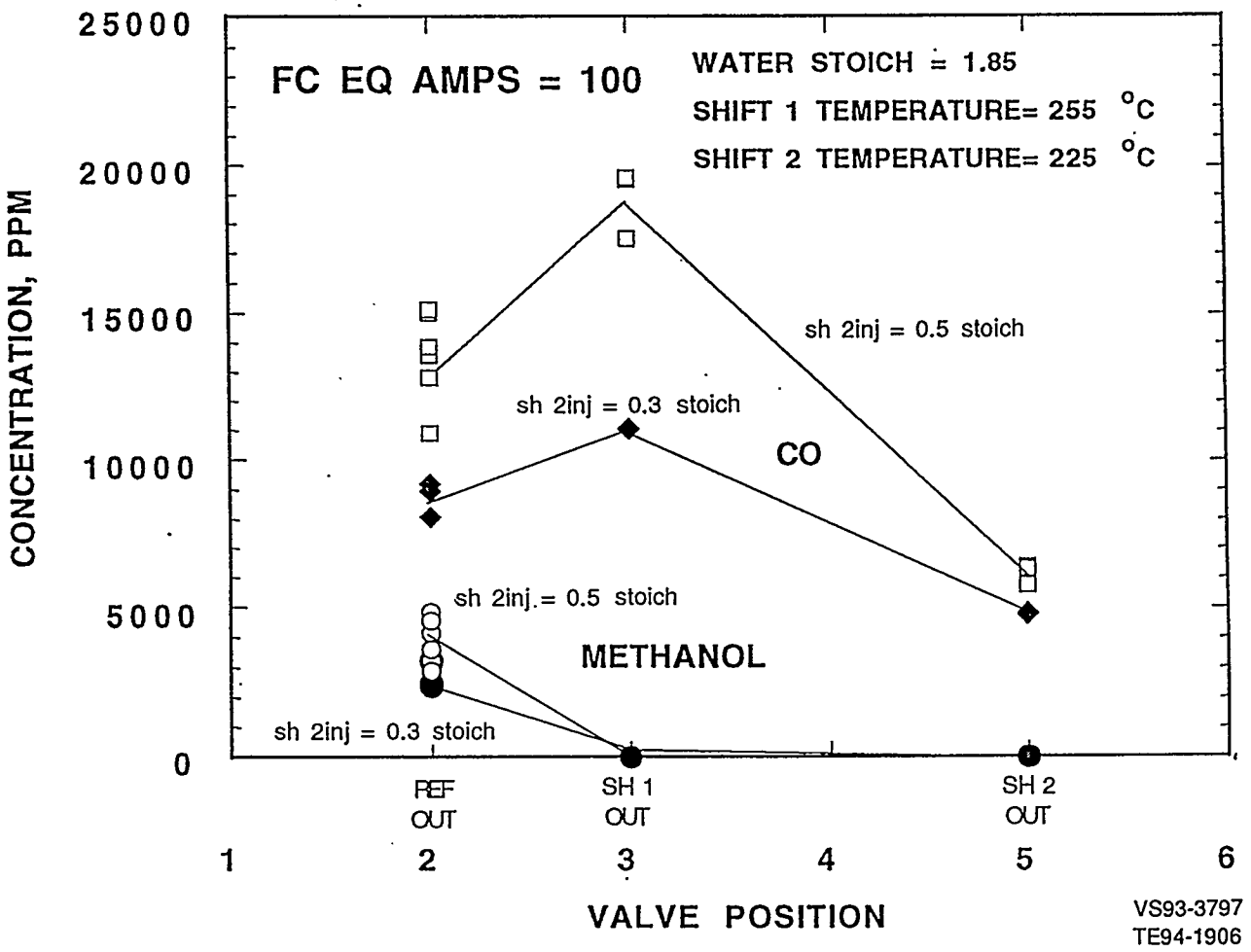


Figure 5.2.3-5. Concentration of methanol and carbon monoxide from reformer outlet to shifter stage two outlet as a function of water to methanol molar ratios in various parts of the fuel processing stream.

### *PROX Zone Test Results*

Following the completion of the reformer-shifter experiments, attention was directed toward the PROX sections. Those CO-removal units consumed the majority of the fuel processing engineering development effort. The intent of this effort was to establish controlled reactivity by independent control of temperature and residence time within full scale devices. There are two general approaches to control this type of short residence time oxidation process. First, the temperature of the incoming gaseous mixture can be controlled and then the subsequent heat of the combustion reaction increases the inlet temperature, heating both the solid catalyst and gas stream. This is the so-called "adiabatic" (constant heat) approach. Second, the temperature of the reactor catalyst and gases can be controlled, by utilizing a reactor that includes heat exchange features permitting heat removal. Such an approach, with sufficient heat removal, approximates an "isothermal" reaction condition. The experimental full scale PROX efforts described in this report were all "adiabatic." During the early bench scale tests PROX work was conducted on monolithic samples cut into 1 in diameter samples. High flow volumes required fabrication of suitable holders for full scale 3-in diameter samples (400 flow channel/in$^2$).

The fluid dynamics of these short residence time reactors are complicated, in part, due to the very low pressure drop through the devices. Even under high flow regimes the flow is very laminar and nonuniform flow distributions are to be expected. Extensive design and experimental effort resulted in suitable techniques that spread the flow over the entire active monolith area. Full scale PROX hardware was fabricated that permitted experiments with different flow geometries. One set of experiments was conducted using two inseries monoliths. PROX 1 was fitted with a 4% platinum loading (percentage catalyst loading describes the platinum concentration in the very thin wash coat, not the total weight, which is mainly the mass of the cordierite substrate) in a 1 in long section, while PROX 2 contained a 2% Pt loaded, 1-in long section. This arrangement worked well, but only with low flow rates up to about 100 amps equivalent. Longer sections of monolith were then installed in the two (2) PROX units, increasing the residence time of the oxidation step. Each PROX unit had its own unique length of monolith section. Although this technical solution was not totally effective for all flow rates, CO removal was effective for PEM stack operation over a wide range of operating conditions. CO removal is primarily accomplished in the first stage PROX. Typically that device lowers the CO concentration from approximately 0.75% (7,500 ppm) to about 1000 ppm (87% removal). Then the second PROX stage, working with much smaller total carbon monoxide and oxygen flows, but a far larger [$O_2$]/[CO] ratio, reduces the CO level to less than 5 ppm. Obviously, the thermal excursion in PROX 2 is far less severe and that device tends to operate closer to isothermal conditions.

Some representative data that demonstrate the effectiveness of PROX staging are presented in Figure 5.2.3-6. In this particular test, a third PROX section was added as a final cleanup section. Although it may appear that three separate air injection steps will result in ever increasing hydrogen consumption and limited efficiency, that is not the case. Each successive PROX converts far less CO, so the air requirements quickly decrease with series sequential staged devices. Gas chromatographic data for CO samples attained at various locations in the fuel processing system are presented in the figure. Again, the data was obtained at the highest stack operating condition. The abscissa in the figure labeled "time" is a reference to the

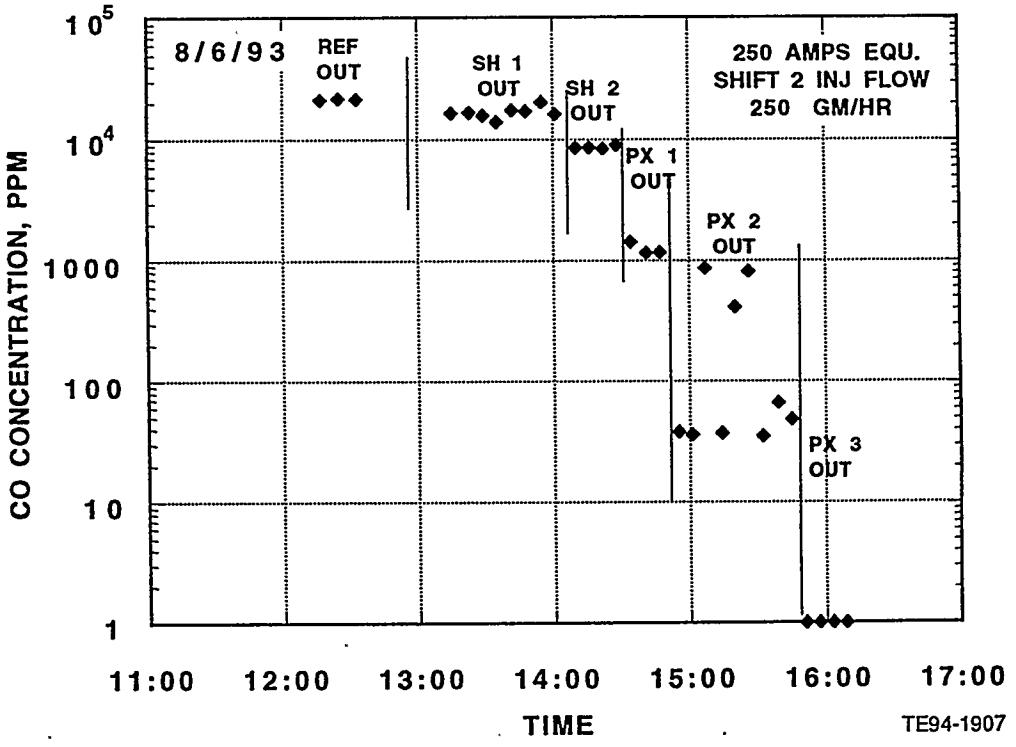


Figure 5.2.3-6. Representative data demonstrating Effectiveness of PROX processing for one configuration tested during Mark II fuel processor testing. Carbon monoxide concentrations were measured with a gas chromatograph at the outlet of each component. ("Time" on the x-axis in the plot is the time of the gas chromatograph sample collection during steady operation; the locations noted on the plot indicate the sampling location).

actual time of the GC sampling event. As expected, CO concentration leaving the reforming section is in excess of 2% (20,000 ppm). The shift zone successfully reduces the CO concentration down to about 8,000 ppm. PROX 1 further reduces the CO concentration to near 1,000 ppm. The PROX 2 CO outlet concentration initially indicated some scatter, but most of the CO outlet concentration was reduced to the vicinity of 50 ppm. PROX 3 was very effective with an inlet of only 50 ppm CO and reduced the output concentration to below detectable limits, <1 ppm. Such excellent gas cleanup was consistently possible, although the determination of the correct operational conditions for temperature, air concentration, and monolith length is most challenging as flow rates increase.

Emphasis during the later months of the project focused on very high system flow rates, especially the increased flow rates required to sustain operation of two Ballard 5-kW stacks. Successful operation of the Mark II fuel processor at 400 amps equivalent flow rate was achieved on 22 September 1993. This was equivalent to running each of the two (2) Ballard Mark V stacks at 200 amps (800 amps/ft$^2$). Very low PROX outlet CO concentrations were established at this level. Typical test results are presented in Figure 5.2.3-7, in which temperatures for the vaporizer, the reformer, the two (2) shift units, and various sections of the PROX zone are depicted. These tests were conducted to explore optimal PROX 3 temperatures to reduce CO outlet concentrations as the flow rate (hence, power) was varied. Tests were first conducted at 250 amps equ. and then, at close to

Hour 13, the flow was increased to 400 amps equ. Conditions were determined to produce in near zero (0) CO outlet concentrations over the entire flow rate variation. During this time the first experiment using two (2) fuel cell stacks in parallel configuration was successfully completed. This test produced approximately 8-kW electrical power.

The entire fuel processor must provide sufficient pressure in the exhaust stream to maintain proper fuel cell anode compartment inlet conditions. The Mark II fuel processor was unable to do this at the higher flow rates because of limitations in flow geometries producing excessive pressure drops between the vaporizer and fuel cell stack anode inlets. (It is, in principle, possible to substantially increase the pressure in the front part of the processor (the vaporizer) and then deliver the proper pressure to the fuel cell stack anode compartments. However, this approach proved to be impractical as the fuel pumps were not capable of sustained high pressure delivery). Three (3) other basic hardware limitations occurred when the system attempted to operate at 450 and 500 amps equivalent flow (nominally 9 to 10-kW electric output). First, excessive methanol breakthrough from the shift zone occurred due to insufficient heat transfer into this reactor to maintain the catalyst temperature. Straight forward modifications to this unit and to the reformer (incorporation of the plug flow reactors in the outlet path) have corrected these problems. The second limitation was the excessive pressure drops within the system at these higher power levels as described above. A pressure scan of the system is presented in Figure 5.2.3-8 for system flow rates of 200, 300 and 400 amps equivalent. At high flow rates the system pressure drop is greater than 15 psi. Most of

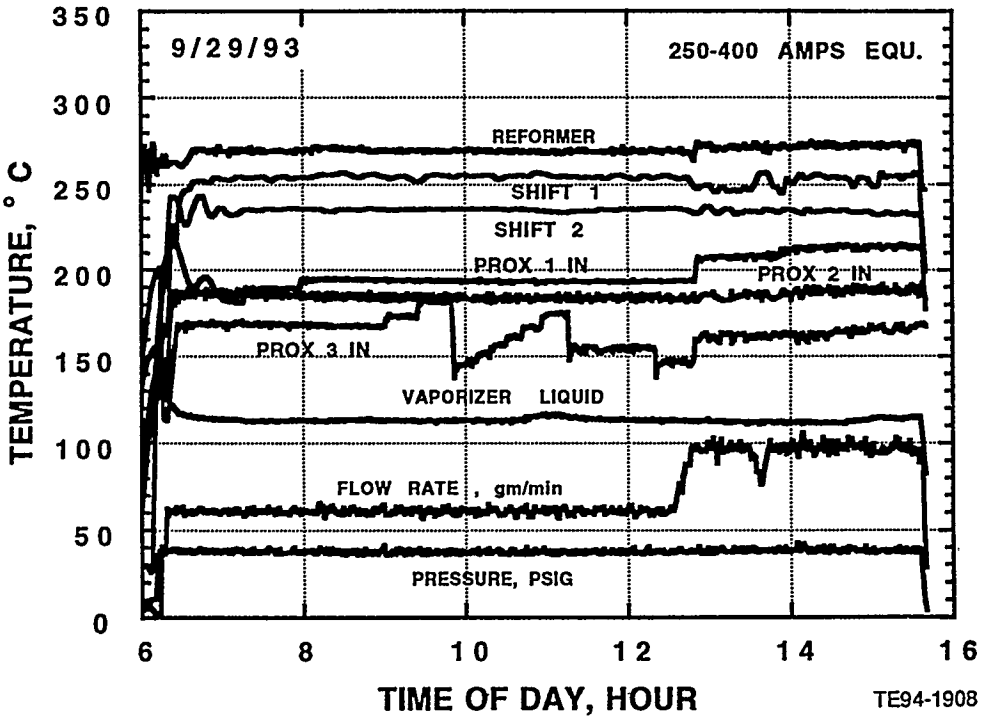


Figure 5.2.3-7. Operating data for a Mark II fuel processor test exploring the effect of temperature variation in a staged PROX configuration. This experiment also corresponds to the first operation of two (2) Ballard fuel cell stacks on Mark II reformate.

the pressure losses are in the 0.5-in tubing connection between the components and not the components themselves. Modifications to larger diameter tubing and fittings in Phase II will extend the device to higher flow levels. Finally, the present pump and injection system does not appear to be capable of delivering the required methanol and water flow to sustain 10-kW electrical output production. Improved pumps and injectors are being supplied by AC Rochester.

## 5.3 MARK III FUEL PROCESSOR

### 5.3.1 Introduction

While much of the actual development work to produce advanced fuel processing components will occur in the next program phase, concept designs for both an advanced integrated vaporizer and reformer component with combustion driven heat exchangers and the burner(s) to produce the combustion gases have already been initiated. Mark II reformer results have led to a series of design exercises that are exploring new concepts for this methanol-to-hydrogen generator. This new generation of fuel processor will comprise the Mark III 30-kW design and this short section primarily describes combustor/reformer concepts that may be useful in this evolution.

The design of an automotive applicable ECE system must, by necessity, include a combustor within the fuel processing section. The function of this combustor is to

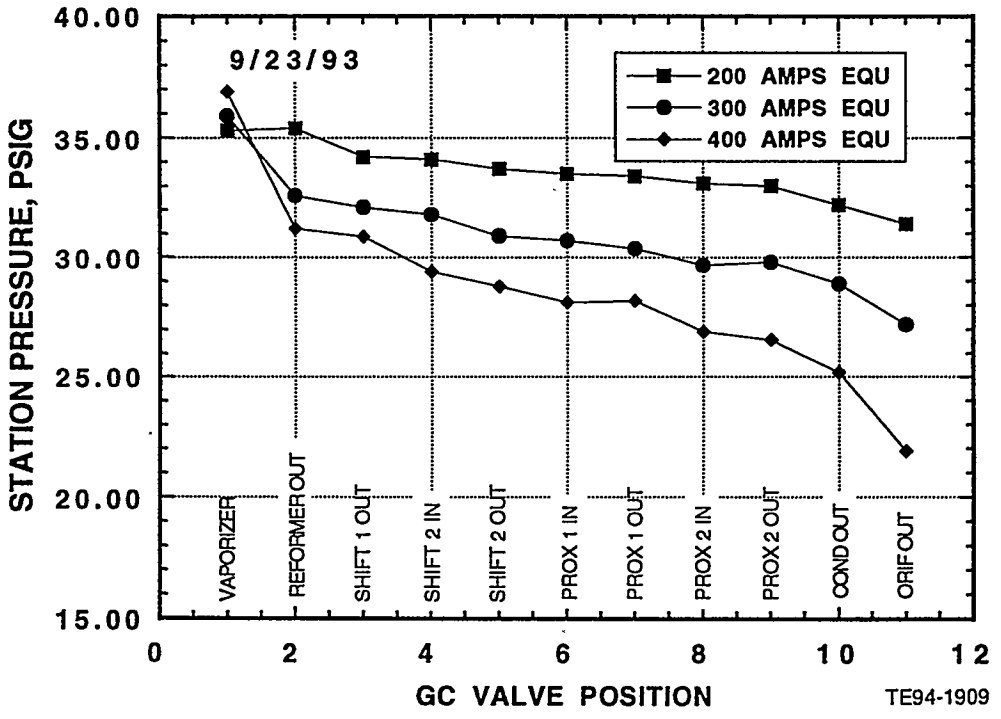


Figure 5.2.3-8. Pressure scans of the Mark II fuel processor as a function of flow rate as the hardware existed at the end of Phase I of the program. Excessive pressure drops precluded stack operation at high flow rates. Modifications are under way to alleviate this limitation.

supply the heat required to: vaporize and superheat the water and methanol inlet streams to the reformer, vaporize the water to the second stage shifter, startup the reformer and shifters, and resupply heat to the reformer and first stage shifter catalysts which have been cooled by endothermic catalytic reactions occurring within them.

In an automotive ECE configuration the combustor also functions to recover the energy available in the excess hydrogen exhausting from the fuel cell stacks. This energy recovery step increases the overall ECE system efficiency. Combustion of the hydrogen also ensures that only products of complete combustion are released from the ECE, an important consideration for restricting engine emissions. At sufficiently high anode stoichiometries, approximately 1.4, the anode vent hydrogen is sufficient to supply the entire heat input to the fuel processor. The system fuel, methanol, can also be supplied to the combustor to increase its heat output when the anode exhaust hydrogen is not sufficient, e.g., if the anode stoichiometry is purposely lowered. At startup of the ECE the combustor operates on pure methanol to provide heat for the vaporizers and chemical reactors.

### 5.3.2 Combustor/Reformer Conceptual Designs

ECESYS model calculations predict that the full power anode exhaust (burner feed) can range from a gaseous mixture with composition of 0.36 $H_2$, 0.42 $CO_2$, and 0.22 $H_2O$ at an anode stoichiometry of 1.4 to one with a composition of 0.17 $H_2$, 0.61 $CO_2$, and 0.22 $H_2O$ at an anode stoichiometry of 1.1. If the system operates at, or near, the lower anode stoichiometry methanol must be added to the combustor to provide the required heat for fuel processing. Operation at the lower anode stoichiometry actually presents some slight benefits in overall system efficiency and the fuel processor is smaller because less methanol must be chemically processed.

Full power anode exhaust only inlet feed for the combustor (at an anode stoichiometry of 1.3) is a gaseous mixture composition of 0.185 $H_2$, 0.205 $CO_2$, 0.077 $H_2O$, 0.111 $O_2$, and 0.422 $N_2$; the outlet gas temperature following combustion is 1612°K (2442°F) which is below the temperature at which significant $NO_X$ is formed. Full power combustor operation at a lower anode stoichiometry, 1.15, requires a methanol/anode exhaust feed mixture with an inlet composition of 0.011 $CH_3OH$, 0.133 $H_2$, 0.295 $CO_2$, 0.084 $H_2O$, 0.099 $O_2$, and 0.378 $N_2$; in this case the outlet gas temperature is 1412°K (2082°F). Although the burner gas temperature is lower in this case, the increased mass flow provides the same thermal energy to the heat exchangers. Pure methanol is the only fuel available for the combustor at startup; the inlet feed mixture composition at full power is composed of 0.103 $CH_3OH$, 0.011 $H_2O$, 0.185 $O_2$, and 0.701 $N_2$; this produces an outlet temperature of 2100°K or 3320°F which is well above the temperature at which significant $NO_X$ will be formed. The inlet composition for pure methanol was chosen so that the combustion products of this reactant would have the same total heat content as the two previous cases in which hydrogen composed a portion of the inlet fuel. In order to achieve the same heat content, the combustion temperature of the methanol/air combustion products must be greatly increased to compensate for the decreased mass of the combustion products compared to those of the first two inlet feed compositions. One method to increase the gaseous product heat content while simultaneously lowering the flame temperature is to inject a methanol/water mixture. This technique has been successfully utilized in gas turbine combustors.

As all of the calculations are for the full power condition (assuming this condition would also be utilized for quick startup) and represent three different fuel inlet compositions, it is apparent that the combustor will be expected to successfully operate over a wide range of operating conditions, including, at part load operation. As an example, if the estimated system idle is at 6-kW for a 30-kW ECE, the combustor turndown ratio would be 5:1, an ambitious value for contemporary burner designs.

# VI. PROGRAM TASK 5: 10-kW POWER SOURCE ANCILLARIES AND SYSTEM SENSORS/CONTROL DEVELOPMENT

## 6.1 GENERAL INTRODUCTION

Both steady-state and transient operation of the ECE system requires adequate ancillaries, sensors, and controls. For system operation, many functions must be controlled, among which are thermal management, air, water, and methanol feed rates, and water and energy reclamation. The core components of the fuel cell system also depend on a collection of devices that help provide these functions, called ancillaries.

The ancillaries built or selected during Phase I include those devices necessary to operate the breadboard 10-kW ECE system. These include: heat exchangers, condensers, cooling water circulation pumps, pumps and injectors for methanol and water delivery to the vaporizer, and injection metering valves to the second stage shifter and various PROX stages. Some of these have been described in previous sections when various components have been discussed. The following section presents an overview of these ancillaries, discusses future adaptations of some of them for the Phase II Mark III system, and, in particular, describes the air turbocompression system for the cathode side of the 10-kW system.

The major ancillary development to date involves the acquisition of oil-free scroll compressor and expander units applicable to provide air pressurization for the 10-kW integrated system. These units are of commercial design (Powerex Corporation) and require some modification to provide adequate air flow at the pressures required by the cathode portion of the fuel cell stacks. These units are presently undergoing bench testing prior to modification.

Steady-state and transient operation of the ECE system requires adequate sensors and controls. As with other engine designs, varying the load point requires provision for changing both fuel and cooling flows. This task involves a broadly based activity on both sensor development and on the integration of those sensors into a working control environment. Both computer software and rack mounted hardware development are included in this task. Sensor development has been a continuing activity during Phase I. Some sensors, such as thermocouples, are off-the-shelf; selection, calibration, and measurement are essential even for these existing devices. Some equipment has required special design and fabrication, the controllers that maintain vaporizer conditions are an example. Other items, especially chemical sensors that would replicate and eventually replace gas chromatographic measurements of specific gaseous constituents, are still in very early design phases.

The initial system DACQ and control computer software was based on a commercial instrument, the Hewlett Packard VXI hardware. This reliable system initially controlled most of the laboratory measurements and accomplished both experimental DACQ and some low level of experimental control. Importantly, safety features are also controlled using this equipment. Development of an automotive-oriented control environment has been proceeding throughout Phase I; an off-the-shelf real-time operating system that has the required speed and capacity is now being used. The system has been designed to parallel and surpass the control functions now pro-

vided by the Hewlett Packard VXI hardware. Successful operation of this system has been demonstrated; this new, fast electronic control system can to replace most of the functions of the present limited control systems composed of the HP-VXI hardware and various independent controllers.

## 6.2 POWER SOURCE SYSTEM ANCILLARIES

### 6.2.1 Introduction

The Mark II ECE is a complex system of components operating together to produce electrical power. To ensure proper system operation, many functions must be controlled, including; thermal management, compressed and injected air, injected water and methanol processes, and water and energy reclamation. The core components of the fuel cell system depend on component and system ancillaries to provide these functions.

The ancillaries designed during Phase I include those devices necessary to operate the breadboard 10-kW fuel cell system. In general, these devices can be classified according to function. The heat exchange (thermal management) ancillaries include heat exchangers for the reformer, shifters, and intercoolers between PROX stages, a condenser between the fuel processor and the fuel cell stack, and two condensers for the fuel cell stack anode and cathode exhausts. The fuel cell stack also has a water circulation pump that serves to cool the stack during operation, and provide heated water during startup when the stack is cold. Cathode air, currently supplied by the facility air supply compressor, will eventually be supplied by an integrated oil-free compressors, such as the high efficiency scroll compressor presently being tested at the JDC.

The JDC has taken a developmental approach to the fuel cell system design and implementation. Specific system tests were conducted to identify ancillary hardware requirements.

### 6.2.2 Description/Discussion of Ancillaries

The fuel cell system, excluding control functions, can be separated into three broad functions: fuel processing, electrochemical conversion, and air and thermal management. All three require ancillary support to properly function.

The Mark II system fuel vaporizer utilizes two injectors for fuel and water metering; established the fuel/water stoichiometry for the system. The injectors are supplied by pumps mounted in fuel and methanol tanks. The injectors meter fuel and water by pulse modulation. Each pulse injects a prescribed amount of liquid depending on the duration of the pulse, and total flow rate is determined by pulse frequency. Water is also injected into the second stage of the shift process, using the same approach. The characteristics of injector operation and control have been previously described in Sections 5.2.2 and 5.2.3. Proportioned amounts of air are metered and injected into the separate PROX units and also into the anode stream of the fuel cell stacks. This air is metered by MFCs to provide the precise amounts required for the PROX units and for $CO/CO_2$ control in the anode portion of the stack.

Cathode air is currently supplied to the 10-kW system by either air tanks or a facility oil-free air compressor. During Phase II, the air will be supplied by a dedicated

high efficiency compressor, mounted directly to the brassboard system. The compressor efficiency is an important parameter, since it directly affects overall system efficiency. Tests performed to date at the JDC using commercially available scroll compressors manufactured by Iwata have demonstrated compressor efficiencies of between 75-80%. A scroll compressor flow path is depicted in Figure 6.2.2-1. As depicted, there are two spiral flow paths; one each in the upper and lower portions of the compressor. While operating, one portion of the compressor remains stationary while the other orbits (does not rotate) in a circular motion. The orbiting motion moves air from the inlet on the outside of the spiral to the center exhaust of the spiral by a process similar to peristalsis. The volume of the air decreases as the radius decreases in this compression process.

The compressor will be mated to an expander when used on the 10-kW system during Phase II. The expander will utilize heated excess cathode (fuel cell air) exhaust reclaiming some of the energy (~40%) added during the inlet air compression process. The expander will be connected to the compressor via a clutch; during transients and off-design operation the devices will not necessarily rotate at the same speed. The expander will also be required to handle two-phase flow due to the cathode exhaust conditions. Expander devices are currently under consideration, but, to date, no testing has been performed on-site.

Another essential process that takes place within a fuel cell system is water management. As described earlier, excess water is injected into the fuel processor and second stage shifter to aid in the production of hydrogen, which in combination with other constituents exits the fuel processor portion of the system as a hot, humid gas.

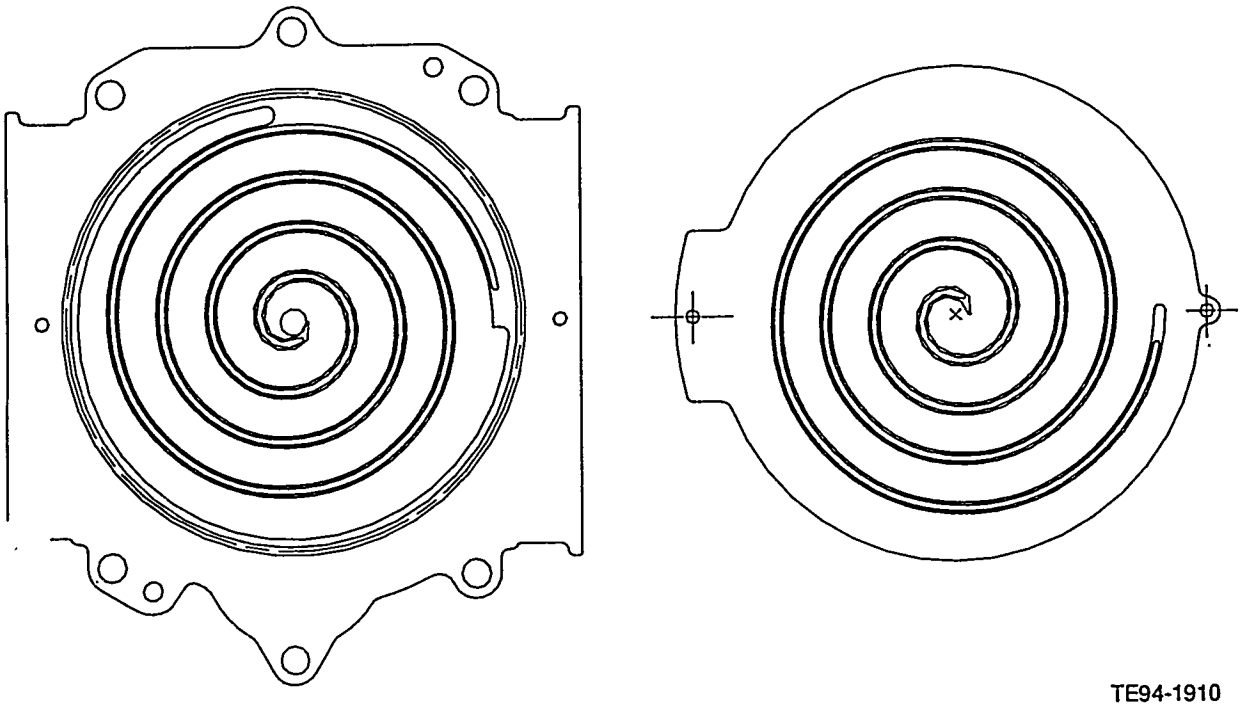

TE94-1910

Figure 6.2.2-1. Scroll compressor spiral flow paths; each portion (upper and lower) of the compressor contains one of the two spiral flow paths. One portion of the compressor remains stationary while the other orbits in a circular motion.

The reformate temperature at the exit of the PROX units is between 200 and 230°C, too high for the inlet of the fuel cell. When the reformate is cooled, the dew point of the mix is quickly reached, causing condensation. Therefore, the Mark II system utilizes a condenser capable of lowering the temperature of the reformate to about 30°C while collecting all the condensed water as a reusable product. The condenser design is presented in Figure 6.2.2-2. The fuel cell stack produces warm (about 90°C) air and reformate exhaust that is heavily laden with water. In the absence of an expander, unit identical condensers to the one used on the fuel processor exhaust are utilized to cool these exhausts and remove the water. All of these condensers possess designed-in capability to adjust both their condensing gas temperature and condensing capacity according to the desired operating condition. For example, 80°C moisture laden reformate gas could be delivered to the stack anode inlet if that were a desirable operating condition. The water collected from any of the condensers can be reused in the fuel cell system.

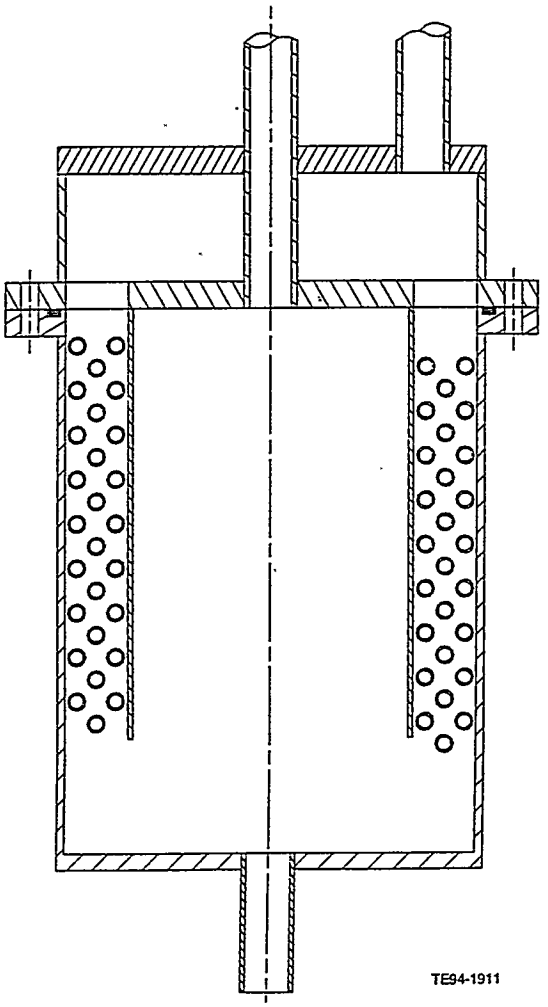


Figure 6.2.2-2. Typical condenser assembly design to adjust gas temperatures and/or remove water. These condensers are utilized at several locations within the system (see text) and have designed in capability to adjust both the temperature of the condensing gas and the condensing capacity according to the desired operating condition.

The fuel processor PROX components will not properly operate if their inlet temperatures are not held within tightly controlled limits. This PROX inlet temperature control is accomplished in the Mark II system by using gas-liquid tube-in-tube intercool heat exchangers. The heat exchanger liquid (water) flow rates are adjusted to yield a predetermined gas inlet temperature for each sequential PROX. As currently configured, the exchangers are capable of providing steady-state and some transient temperature control over the complete system operating range.

During Phase II, more self-contained heat exchanger concepts will be designed. Cooling and heating fluids for the exchangers will come from within the system, rather than being externally supplied. Exchangers will be designed for full transient operation, complementing the capabilities of the control system planned for Phase II.

## 6.3 POWER SOURCE SYSTEM SENSOR/CONTROLS

### 6.3.1 Introduction

The sensors and control system for the 10-kW power source system are integral parts of the overall system. Total system operation is dependent on proper calibration and function of the sensors with the control system. The control system monitors sensor inputs, performs appropriate computations based on this data, then sends out control signals that adjust component and ancillary operation to maintain system operation.

Development of algorithms used within the control system utilizes results of the long term experimentation conducted on the Mark II system. This experimentation is leading to an understanding of the principles which govern the operation of the power source component subsystems. Control algorithms dictate each sensor type, placement within the system, and required accuracy. Other measures of the interaction of sensors and the control system include: 1) the amount of elapsed time between sensor input and information flow into the control system, 2) the amount of sensor input filtering to remove noise or other anomalies inherent in the system design, and 3) any accumulated inaccuracies produced due to the sensor sampling frequency.

Once algorithms have processed the sensor input data, the control system can then control the power source via the actuators, MFCs, pressure regulators, and temperature controllers within the system. Some of these devices have built in sensors which provide a closed loop feed back to the control system to ensure adequate control. This constant cycle of sensor input, algorithmic processing of the input to determine the current state of the power source, and manipulation of various devices that manage the power source comprises the central focus of the control development effort

The VME-Bus based control system was also chosen in order to provide a reliable system for the engineers to use for development; it is also expandable, simply by the addition of an industry standard off-the-shelf computer or interface board. The VME-Bus system also has the benefit of available off-the-shelf hardware and software that are compatible with the RTOS chosen software package.

An RTOS was chosen in order to shorten the development time to write application software. Having an off-the-shelf RTOS significantly reduced the total development time. pSOS+, a particular RTOS, was chosen after an evaluation of all available RTOSs. This choice was made using a long list of evaluation criteria, and personal contacts with current and past users of all of the RTOSs in the final list. In several cases, users of competing RTOSs gave personal accounts of changing from their previous RTOS to pSOS+

The power source control system has a multitude of variables to monitor, including; temperatures, pressures, flow rates, currents, voltages, battery state-of-change, and reactant storage levels, etc. Variables and locations where each of these devices are monitored are summarized below.

- Temperatures (including thermocouples):

  1) Vaporizer inlet and outlet
  2) Reformer inlet and outlet
  3) Shifter stages, inlet and outlet
  4) PROX units, inlet and outlet
  5) Fuel cell stack cooling water, inlet and outlet
  6) Fuel cell stack anode and cathode inlets and exhaust outlets
  7) Burner outlet exhaust and inlets to several heat exchangers in the system

Each of the fuel processing locations are necessary in order to precisely control the reforming of methanol to produce a minimum of carbon monoxide (CO).

- Pressures:

  1) Inside the vaporizer
  2) Fuel cell anode and cathode inlet
  3) Fuel cell anode and cathode exhaust
  4) Burner inlet and exhaust
  5) Turbocompressor inlet and exhaust

Each of these pressures need to be monitored and to provide proper fuel, air, and coolant flow throughout the power source system.

- Flow rates using MFMs:

  1) Methanol flow into the vaporizer
  2) Water flow into the vaporizer
  3) Reformate flow into the fuel cell anode
  4) Air flow into the fuel cell stack cathode
  5) Water flow into the second stage shifter
  6) Air injection into the PROX units
  7) Air injection into the fuel cell anode
  8) Coolant water flow into and out of the fuel cell stack
  9) Coolant water flow into shifter heat exchangers and PROX unit intercoolers

Other measurements required for proper system control include the following:

- A current shunt input which indicates fuel cell stack current
- A current shunt input which indicates battery pack current
- Battery pack voltage
- Fuel cell stack individual cell voltages
- Methanol storage level
- Water storage level

Each of these device inputs, along with temperatures, pressures, and flow rates, are used by control algorithms to precisely control the power source system.

The outputs from the control system to the power source include the following:

1) Mass flow control, regulating the following:
   a) Air injection into the PROX units
   b) Air injection into the fuel cell anode
   c) Fuel cell anode cathode exhaust flows
2) Injector flow control, regulating the following:
   a) Methanol into the vaporizer
   b) Water into the vaporizer
   c) Water into the second stage shifter
3) Proportional valve control, regulating the following:
   a) Fuel cell stack coolant flow
   b) Coolant water flow through the PWM load
   c) Coolant water flow into shifter heat exchangers and PROX unit coolers
4) PWM analog signal to control the electrical current flow through the load
5) PWM analog signal to control the electrical current flow out of the battery pack
6) PWM analog signal to control the electrical current flow into the battery pack for state-of-charge (SOC) control

### 6.3.2 Description of Control Strategies

A block diagram of the control hardware and its general signal line interfaces are presented in Figure 6.3.2-1. The primary control hardware is rack mounted, 120 VAC, equipment. All signal lines (both input and output) from the rack are optically isolated so as to prevent electrical (RFI and EMI) interference between the control hardware and the ECE system components. The control hardware rack currently has two user interfaces; a terminal console where all control system operator functions are performed, and an IBM-PC compatible workstation used exclusively for control software development. The PC workstation communicates with the control hardware via a high-speed network connection. All software modules are written on the PC and are then uploaded to the VME-Bus control hardware for testing and debugging. All final debugging is accomplished via the PC workstation. On system start-up, the RTOS, pSOS+, bootstraps the system and initializes all system hardware and software components.

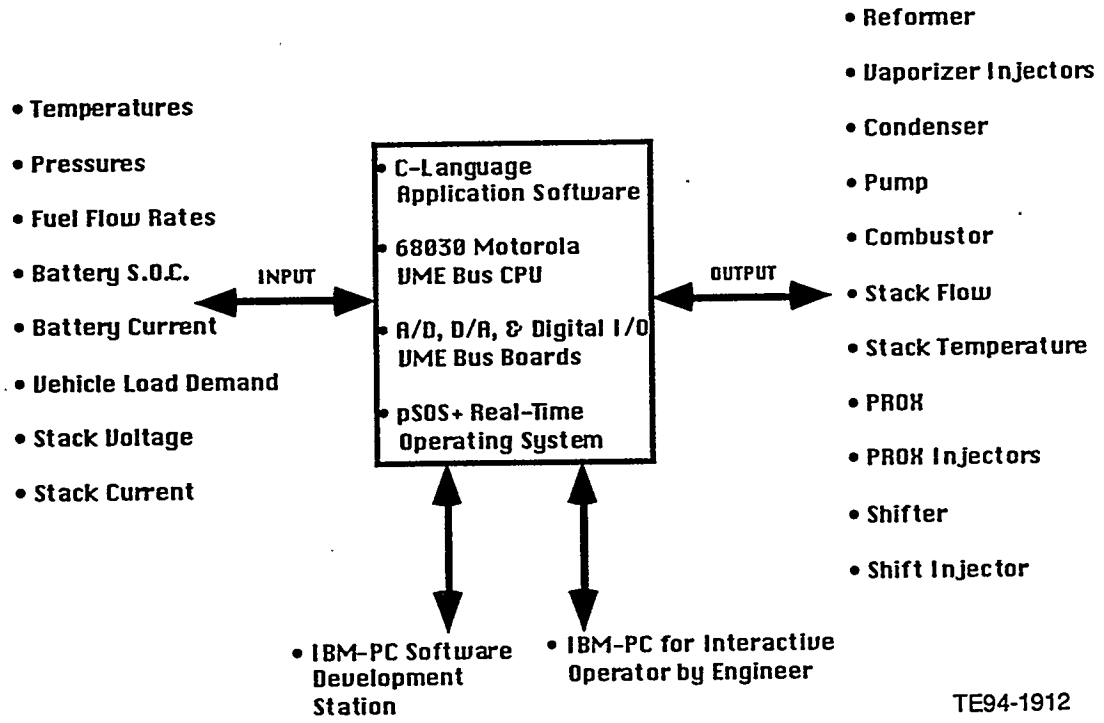


Figure 6.3.2-1. Mark II control system hardware block diagram.

pSOS+ is a versatile, multifeatured, priority-driven operating system. It is a true multitasking system; all control operations are the result of the interactions of multilayered "tasks". Each control task is a complete entity written in 'C' Language, and has one or more start execution points. Each task executes asynchronously from all other currently executing tasks. The operating system functions as a "task manager" by controlling the timing and execution of each of the tasks. All tasks execute in "time slices", small periods of time that are allotted for each task. Once a task's time slice has elapsed all data related to the task is stored and the task is put in "background" until it is called again by pSOS+.

A task is assigned a priority level when it is installed in pSOS+; pSOS+ has 256 available priority levels. Priority levels are numbered in a one-up manner, 0 to 255, with the lower priority tasks running less often than the higher priority ones. pSOS+ functions by allowing the highest numbered task, which is currently ready and available, to execute. Once this task has stopped execution, the next highest priority task is executed. pSOS+ always operates using the mode of highest priority task execution. A logical result of this mode of operation is that the most critical system and/or safety related tasks are assigned the highest priority, i.e., hydrogen gas detection, system over-current, or over-pressure detection which force the shutdown of the entire ECE system.

The control software tasks have been designed and written using a multilayered approach. The innermost tasks, as depicted in Figure 6.3.2-2, perform the "low level" functions; all underlined hardware and software tasks in Figure 6.3.2-2 have not yet been completed. Low level tasks or "device drivers" provide the communication interface between the control system hardware and all other system software.

No other tasks communicate directly with the control hardware. Generally, there are one or more low level tasks for each type of control hardware. For example, there are four low level device drivers that control and monitor the analog-to-digital (A/D) conversion hardware:

1) the initialization task, which performs the initial setup and start commands
2) the control task, which operates the circuit components directly related to the A/D converters
3) the read task, which inputs digital data from the circuitry once all A/D signal lines have been sampled
4) the write task, which commands the A/D circuitry to begin a new set of instructions once all the data from the previous conversion has been read

All of the tasks in this multilayered system communicate with each other using services provided by pSOS+. To service task-to-task communication and synchronization, three sets of pSOS+ facilities have been used, message queues, events, and semaphores.

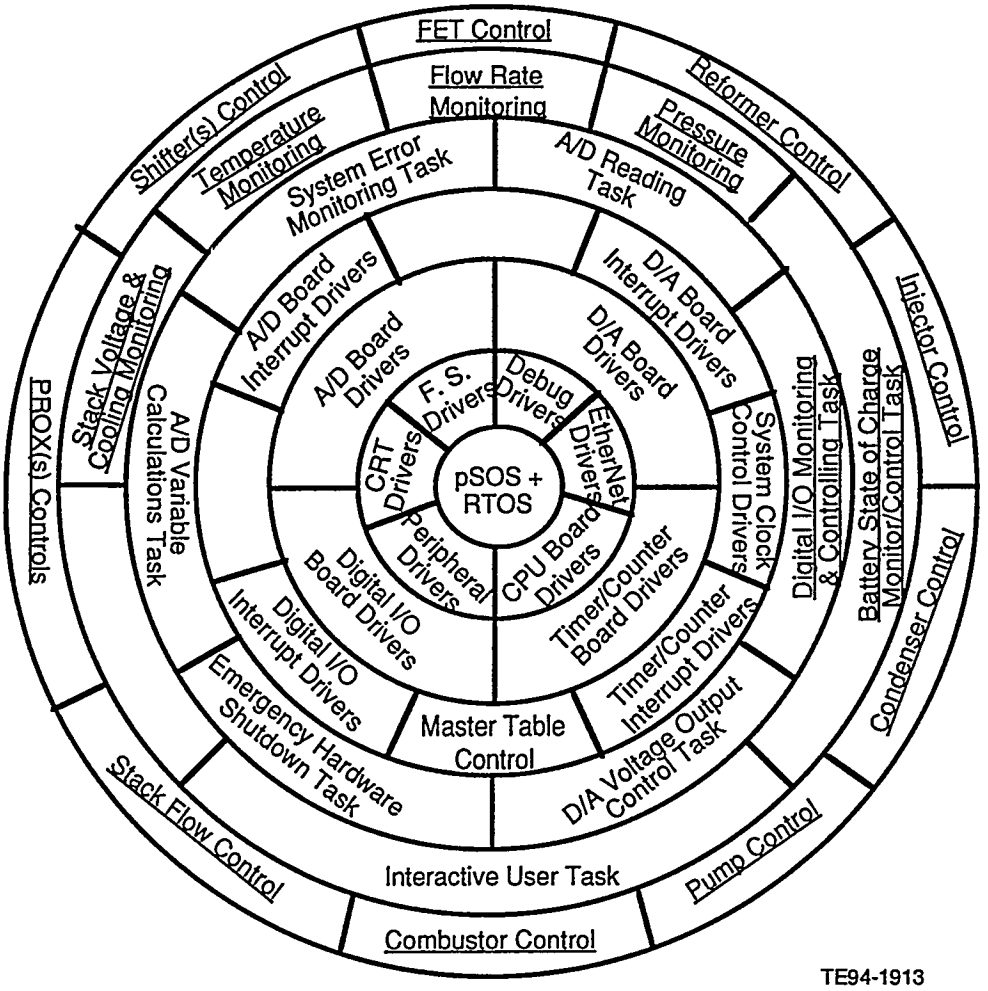


Figure 6.3.2-2. Mark II control system software block diagram.

Message queues provide a highly flexible, general-purpose mechanism for task communication and synchronization; they pass data from one task to another or from one task to many tasks. They can be used to synchronize tasks by forcing one task to suspend execution until a message is received from another. For example, a low level device driver task which controls the digital-to-analog (D/A) output signal circuitry will suspend execution until a message is received containing a D/A output channel and an analog voltage to be placed on that channel. It would be a waste of system resources to have the D/A device driver task constantly running with no data to put on the D/A signal lines. pSOS+ also provides system calls for one task to broadcast a message to several tasks. All tasks which are waiting on the message will then be readied for execution. Interrupt service routine tasks need to have a broadcast capability for informing the entire control system that an "event" has occurred. As an example, the A/D circuitry completes a set of conversions at intervals of approximately 164 milli-seconds. This is a relatively long time in terms of computer clock time. Rather than having all the A/D dependent tasks continually polling the A/D device drivers for new data, the message broadcasting system causes all of the A/D dependent tasks to halt until the a new set of instructions has been completely processed.

pSOS+ provides a set of synchronization-by-event facilities. Each task has event "flags" that control its execution; a task can be suspended until a prespecified event flag signal is received. All system events are independent of each other, and pSOS+ permits task synchronization to multi-event occurrences. Boolean functions, logical AND and OR, can be applied to the event system so that a task will synchronize to the occurrence of several events.

The third method for task communication and synchronization uses semaphore operations. Semaphores are abstract objects and are used primarily for the exclusion of system resources. Only one task can "own" a semaphore at any time. Although several tasks may simultaneously want to use a single system resource, such as a low level device driver, only one can use it, the task holding the semaphore. When the task has finished using the system resource, it releases the semaphore and another task may then take the semaphore and begin using that particular system resource.

In addition to the pSOS+ communication facilities described above, a custom "master" communication facility has been developed. This facility is used not only for passing information between tasks, but also for error checking and control software debugging. The facility is internally divided into sections; several sections are dedicated to tracking the signal analysis and throughput from the various control hardware devices (A/D, D/A, digital signal input/output). All data in the "master" communication module is stored in "packet" format; i.e., all information on a single data object is grouped together. For example, a typical A/D data packet contains the following information:

1) information on the A/D signal line which was analyzed for this packet
2) the raw, digitized signal line value
3) the processed signal line value in scaled or calibrated real-world units of temperature, pressure, flow, etc
4) a "time stamp" giving the exact control system time that the data was collected and processed (accurate to 2 milli-seconds)

5) diagnostic information on the software module that created or wrote the packet including the current loop number, critical data address values, etc

Although it is not yet fully implemented, the "master" module is able to store information on system errors (unusual or unexpected data calculation results, odd signal line levels, etc.). It is expected that an error tracking task will later be written which will list and prioritize the errors stored in the "master" module and will then pass them to a terminal or other display device. The control system operator will have almost instant access to all system errors as they are generated. When errors are detected that may result in damage to the system or risk to personnel, this task will immediately command the shutdown of the entire ECE system.

Most of the non-underlined control software tasks depicted in Figure 6.3.2-2 were written and tested while the control hardware rack resided in the JDC Technical Program Office. Near the end of Phase I, the control hardware rack was moved to the JDC Electronics Development Laboratory and electrical connections were made to the ECE system located in the adjacent room, the JDC System Laboratory. Once these connections were made, the implementation and testing of the battery SOC task was initiated. A proprietary, pseudo-code format SOC algorithm was obtained from the Delco Remy Division of General Motors Corporation (DR). This algorithm was tailored for integration into the control software/hardware package and testing began at the end of Phase I.

The SOC task provides the real-time current capacity of the battery pack. During battery discharge, the SOC parameters are updated using proprietary amp-hour integration techniques, in which the number of amp-hours used is subtracted from the total full charge, yielding the remaining current capacity of the battery pack. When the change in voltage, current, or temperature fall within a specified range, SOC is recalculated. The new SOC and the discharged amp-hour quantities are used to recalculate the total amp-hours available.

Following successful implementation of this first task the control system is now rapidly replacing most of the functions of the present limited control system composed of the HP VXI hardware and various independent controllers.

# VII. PROGRAM TASK 6: 10-kW POWER SOURCE SYSTEM INTEGRATION/DEVELOPMENT AND TEST

## 7.1 GENERAL INTRODUCTION

The key Phase I deliverable is the integrated ECE system demonstrating both the technical feasibility of various system components and that of the total system. This Phase I Mark II system deliverable maintains some utility connections. For example, as described in Section V, the device presently utilizes power from electrical connections to provide the electric resistance heating necessary to drive the fuel processing components. Cathode air is also presently supplied from a laboratory air source, rather than from an independently-driven air compressor. Consequently, the current emphasis has been on components and controls, and on the ability of the control system to develop techniques for successful transient behavior. Activities in later program phases will create ECE systems in more vehicle-compatible power densities and configurations.

- ***ECE Test Stand and Surge Battery Subsystem*** - Work progressed continuously during Phase I to build a comprehensive ECE test stand. The ECE involves simultaneous operation of both the reformer and the fuel cell stack, the test stand was also designed and built to operate either of these components individually. Control computers handle the data flow and establish the control environment. During the last half of Phase I considerable emphasis was placed on the design of full-scale shifter and PROX components. The complete Mark II fuel processing system operated well in excess of 200-hours. During repeated tests, the data indicated that the shift zone components deliver a gas stream containing nearly undetectable methanol breakthrough concentrations and a carbon monoxide concentration that is in near equilibrium with the rest of the mixture of hydrogen, water, and carbon dioxide. The PROX units, using short-residence-time designs, deliver acceptably low carbon monoxide levels. The other half of the ECE test stand supports fuel cell stack operation. Either one of the two (2) 5-kW Ballard stacks, or both, can be operated; this meets the 10-kW electrical target (20-kW when combined with a 10-kW surge battery subsystem which is described below).

- ***ECESYS Experiment*** - The first successful ECE system test occurred on 26 March 1993. The test began with simultaneous operation of the stack on synthetic reformate-air and the Mark II fuel processor at a flow rate required for the fuel cell stack current. After several hours of stable fuel processor operation with measured low carbon monoxide contamination, the anode feed was switched from the utility anode gas feed to the feed emanating from the fuel processor component. The average cell voltage on actual reformate contrasted to synthetic reformate is virtually identical. Stable operation of 0.740V at 400 amps/ft$^2$ was measured until the test was terminated. Current density operations up to 800 amps/ft$^2$ (on each of two stacks connected in a parallel configuration) have now been achieved. In general, the results closely followed data obtained with synthetic reformate.

Details regarding these developmental efforts are described in the following sections. In this report emphasis has been placed on the surge battery selection and incorporation strategies and a description of the Mark II system development pro

gram and test results. At the end of this section a brief discussion concerning the continued use of the Mark II power source in Phase II is presented.

## 7.2 SELECTION AND INCORPORATION OF SURGE BATTERIES

### 7.2.1 Introduction

The overall basic design of the ECE Power Source System not only includes the fuel processing subsystem, the fuel cell subsystem for generating direct current (DC) electricity, but also a battery subsystem to enhance the overall operating characteristics of the entire system. The battery subsystem provides certain advantages to the system including:

1) The ability to provide for cold startup (and future drive away) while the power source is warming up
2) Enhancement of the system's overall transient capability and provision of some load leveling features
3) Provision for energy storage for regenerative braking and, thus, enhance overall system efficiency
4) Provision of auxiliary power (hotel loads) for the entire system

The Initial Conceptual Design Report, discussed in Section II, contains a description of the Electric Powertrain Drive System. This information outlines the entire drive train specifications including the battery pack, the inverter, and the drive motor. The Tradeoff Analysis Report (in preparation) further refines the Electric Powertrain Drive System specification and reiterates the Initial Conceptual Design Report specifications for the surge battery.

Significant technical challenges are associated with connecting the electrochemical power source and battery pack, in parallel, to the load. One major requirement is that electrolysis inside the fuel cell never occur. A simplified block diagram in Figure 7.2.1-1 illustrates one technique of connecting either the fuel cell and/or the batteries to the load. A much more sophisticated interconnection system has been designed and is discussed in the next section.

The surge batteries procured during this contract were recommended by DR. Originally, Delco Voyager Deep Cycle Marine batteries were acquired as Delco Remy's engineers indicated that this battery closely resembled the characteristics of the then-current Impact vehicle battery, which represented the best lead-acid battery under development inside GM. Other battery types were considered, but rejected, for the Phase I effort as the lead-acid batteries were available, cheap, and could satisfy the contractual requirements. Extensive effort at the JDC was conducted to develop an accurate SOC control algorithm for these batteries. Delco Remy then informed the JDC that new, third generation Impact lead-acid battery packs, representing the latest state-of-the-art, were available on a proprietary basis.

### 7.2.2 Battery Incorporation Strategies

The performance under load of fuel cells and batteries is quite similar. A simple model of each consists of an ideal voltage source in series with an internal resistance. As more current is drawn from the device, IR losses across the resistance lower the overall system output voltage, Figure 7.2.2-1.

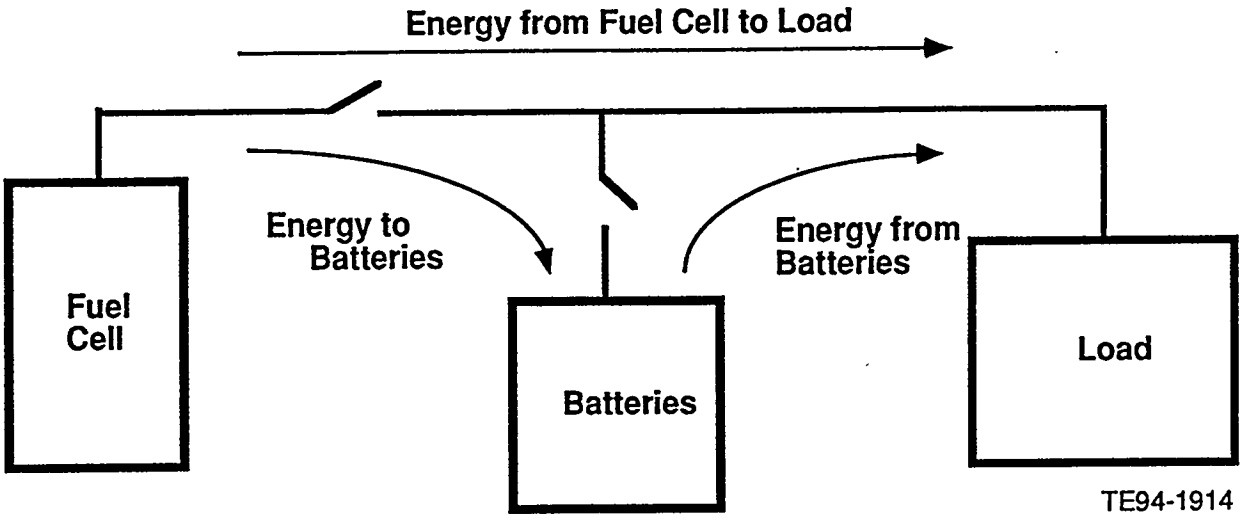


Figure 7.2.1-1. A simplified block diagram depicting the ability to selectively connect the fuel cell and/or battery pack to the load.

Combining a separate voltage source and batteries together is not an uncommon problem. Millions of automobiles around the world have such a combination; as the engine rpm increases, the alternator produces an increasing voltage output. If the battery requires charge, current flows into it. Conversely, if the battery voltage is higher than that of the alternator, the battery supplies energy (current) to the (primarily hotel) load in the case of a conventional automobile.

What makes this problem unique for a fuel cell powered vehicle is that the characteristic performance curve for the fuel cell has a much larger slope than that of the battery. Therefore, under normal use, the fuel cell operates out of the normal voltage range of the batteries. For example, the 5-kW Ballard stacks in use at the JDC range in voltage from 29-31 volts under near low-load conditions, depending on the particular stack, to around 20 volts under the presently limited continuous maximum load of 250 amps. An appropriate battery pack would operate in the range of 24 volts maximum down to nearly 21 volts at the same maximum current levels. If left connected to the fuel cell the batteries would be overcharged during most of the operating load conditions. This is clearly evident in Figure 7.2.2-2. The curves have been arbitrarily extended past actual data points at 250 amps for steady-state operation of one stack to the 300 amp level.

Combining the fuel cell and battery pack, however, is not necessarily difficult. The operating conditions of the combined system, particularly the point at which the batteries are to supply energy to the system, can, to some extent, be specified. For example, it may be desirable to have the battery pack come on line at the 50% power level of the fuel cell. The system parameters are then chosen so that the voltage of the fuel cell (at the 50% power level value) is equal to the voltage of the battery pack. If the switch connecting the battery pack is closed at this point, zero current will flow in or out of the batteries. If the load continues to increase, current is drawn out of both the fuel cell/battery system at their combined load line up to the maximum power output of the combined system.

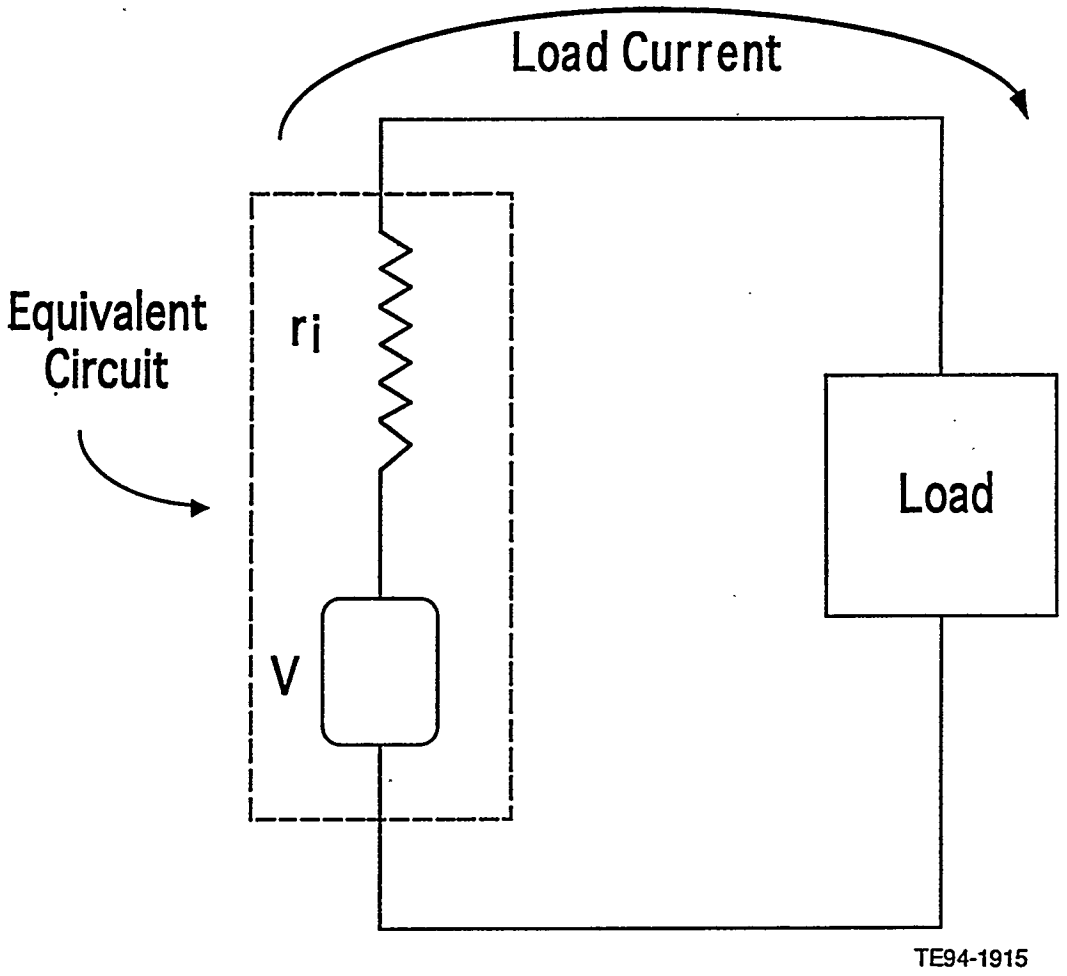


Figure 7.2.2-1. IR losses in fuel cell or battery equivalent circuits.

An actual, empirically determined combined load line of this fuel cell/battery type control option is presented in Figure 7.2.2-3. Part of the combined load is now composed of the parallel connected resistances of the fuel cell and battery.

When the load decreases, the operating characteristics continue to closely follow the combined curve. To recharge the batteries, the switch is left closed slightly past the point at which the battery pack voltage intersects the fuel cell voltage. Since the voltage of the fuel cell is now higher than that of the battery pack, current will flow into the batteries, recharging them. As the batteries approach a charged state, the charging current decreases. When this current reaches zero (a defined value) the switch is opened and the batteries are taken off-line. Control of this process is critical; cognizance of the operating conditions of the system and of the SOC of the battery pack are essential. The difference between the fuel cell voltage and battery pack voltage must be maintained within specified limits to limit current and heat flow into the batteries. This is referred to as a "serial" system configuration.

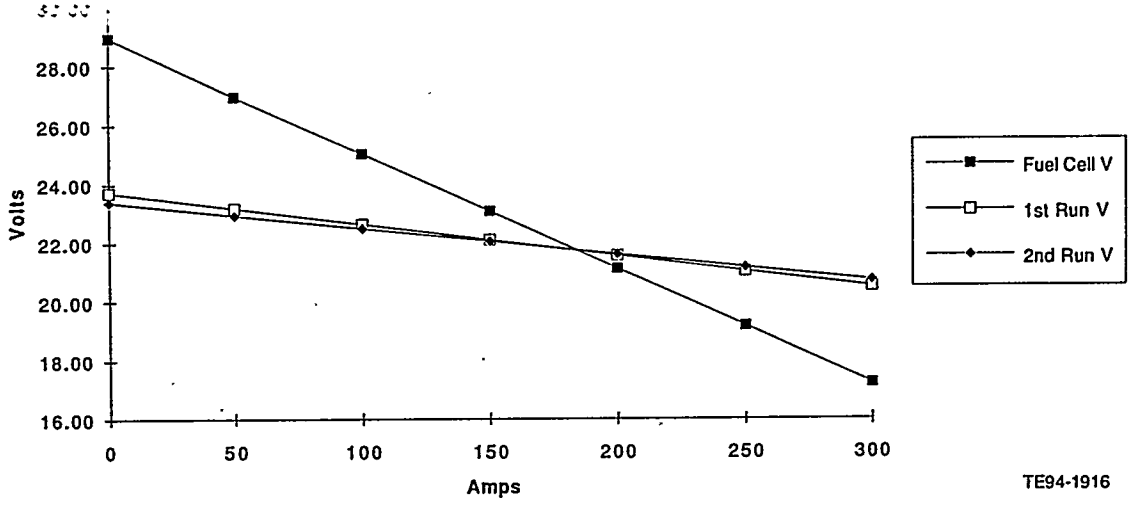


Figure 7.2.2-2. Fuel cell stack and battery pack performance polarization curves.

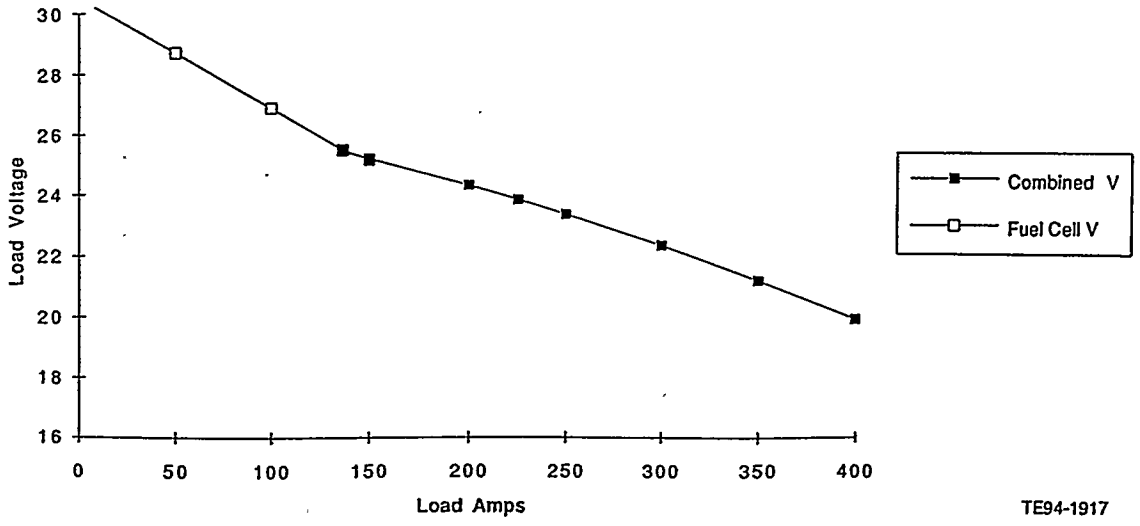


Figure 7.2.2-3. Combined fuel cell stack and battery pack performance polarization curves connected to the same load.

Further, depending upon the point at which the batteries come "on line", the battery pack can supply only a fraction of the energy required by the system. For example, using the technique described in Figure 7.2.2-3, at full system power the fuel cell is providing two-thirds of the current while the battery is providing only one-third. This may be adequate for some operational conditions, but if full power from both

the fuel cell and battery pack is desired, another approach must be utilized. This second approach depends on an adaptation of the methods presently used to vary the fuel cell load, i.e., on the function of the PWM, itself.

Output power from the system on test is transferred to a pulse width modulator, a DC switch that controls the output power level through control of the pulse width load. Electrical power that is transferred through the load is released into a water-cooled resistor, and then transferred into the laboratory chilled-water system. This PWM, which regulates the energy release from the system, is controlled by the control computer that monitors and sets system current demand. The PWM imposes a chopped DC signal on the ECE system. The currents listed in this report, therefore, are "average currents", not steady-state values. Considerable electrical engineering was conducted to determine the nature of current flow from the stacks. Results indicated that the average and chopped currents were similar, the result of very high source capacitance (the stack). Measurements attained with an integrating power meter along the transfer line from the system to the PWM are correct representations of the power produced from the system. Because of some high frequency ringing that occurs in the PWM and consequently causes some power loss in the PWM, the power deposited in the cooling water is not exactly the same as the power generated by the system. This report presents the actual system power delivery, as measured by the integrating power meter.

The PWM, used as a high-speed electronic switch, operates at about 15-kHz. During this 66.67 micro-second window, the PWM is "switched on" for a portion of time depending upon the average load current desired. For example, at a desired current load of 25% of a given water-cooled load resistor setting, the PWM is "switched on" for 25% of the time during this 66.67 micro-second window. For that 25% portion of the window the fuel cell is connected directly to the load and produces a chopped current which is as large as the fuel cell can instantaneously produce for the given resistor setting; this current flows through the PWM switch to the water-cooled load resistor. For the remaining 75% of the time, the switch is opened and the fuel cell produces (and the load receives) zero current. Since this is happening at 15-kHz, the net effect is that the fuel cell and load operate at an average current of 25% of the maximum current based on the resistance selected on the water-cooled load resistor. Further, because of the very large stack (or battery) capacitance the voltage acts as if the stack were operating at the 25% load setting. The voltage does not tend to follow steady-state polarization performance curves during the high amperage (but very short term) operation. This average current or power value can be continuously varied from 0 to 100% by an input analog signal which is proportional to the percent load desired. Now, consider a water-cooled load resistor setting, i.e., a power demand, that would require up to twice the maximum continuous output current of the fuel cell at its maximum continuous power output. Under these operational conditions, the PWM is "switched on" for about 50% of its 66.67 micro-second window; the fuel cell is operating in a "chopped current condition" at its maximum rated output current "averaged" over the whole 66.67 micro-second window. This is also the operating condition at which the fuel cell is delivering its maximum amount of power to the load, also "averaged" over this entire 66.67 microsecond window. The remaining power demanded by the load must be provided by the battery pack.

The batteries can be connected to the system by another PWM. However, the controller of this PWM must be clocked to the fuel cell PWM so that the "window" is

shared over exactly the same time frame. Just as the fuel cell PWM operates during the first 50% of the time window, the battery PWM must operate during the second 50%. The water-cooled load resistor acts as if it were receiving a continuous supply of current reflecting the combined output of the fuel cell and battery pack. In this scenario, each power source is connected to the water-cooled load resistor for 50% of the time. At the 15-kHz switching rate, each power source, due to its high source capacitance is delivering an "average" of 50% of the demanded power. Because of the chopped DC signal and high source capacitance, each power source, while delivering more instantaneous power than its steady-state rating, delivers its maximum power rating "averaged" over the whole 66.67 micro-second demand period. The total power delivered can be continuously varied from 0 to 100%, shared by the fuel cell and the battery pack, and controlled by an input analog signal to each PWM unit which is proportional to the percent power demanded of each power source.

There are several advantages to this approach. Batteries can be off-line until required. Or, for that matter, the fuel cell can be easily taken off-line (for startup, for example) and the load run directly by the batteries. The load experiences continuous current across its entire operating range. Since all switching is performed electronically (the PWM uses high-speed field effect transistors (FETs)), there is no arcing as with a mechanical relay. The FETs have negligible losses, so the system efficiency remains high.

The disadvantage of this approach is that the clocks of the two PWMs must be tied together. This is not an insurmountable problem, simply one which must be addressed. Also, battery recharge under this scenario is not as simple as with the "serial" approach. Another electronic switch, such as a PWM unit, must be used to tie the fuel cell and the batteries together, so that the charging can be accomplished during the portion of time that the power demand is significantly reduced or off-line.

A third approach, often used if the fuel cell voltage is much less than the battery or required motor voltage, utilizes a DC-DC converter between the fuel cell, battery pack, and inverter (used to convert from DC to AC for the motors). This technique simplifies battery recharging by either the fuel cell or regeneration. Additional controls are required between the fuel cell controller and the vehicle/inverter control; however, the overall fuel cell, battery, vehicle control interface is simplified. The disadvantage of this technique is the inefficiency of the DC-DC converter, particularly if more than a 2:1 step-up in voltage is utilized. The second approach described above, using very high efficiency PWMs, assumes a high output fuel cell voltage equivalent to the battery (and motor) voltage.

As all of these approaches have their advantages and disadvantages, they will continue to be studied during Phase II.

## 7.3 MARK II POWER SOURCE SYSTEM DEVELOPMENT AND TEST RESULTS

### 7.3.1 Introduction and Summary

The primary purpose for conducting all of the research and development efforts described thus far in this report, from the analytical modeling to various component developments, has been to develop and test a working breadboard ECE. This sec-

tion of the report describes the activities required to accomplish that endeavor and the test results achieved to date.

One significant challenge for PEM operation, as discussed throughout this report, is to maintain low CO concentrations in the anode feed stream. Another challenge is to develop control strategies that: 1) permit steady-state and transient operation throughout the desired power level range, and 2) recognize and correct system difficulties well before technical or safety problems occur.

First, the necessary testing facilities were fabricated, based on the test program objectives. In this case, extensive modifications of one of the JDC test cells was required. Within that area, a utilities and measurement panel was installed to provide DACQ for each component in the system, supply all of the reactant feeds, electrical power, control instrumentation, and safety monitors. Further, the panel provides for total control of experimental emissions and permits assessment regarding how the components operate as single and combined units and as part of the larger ECE system. This effort focused on fabrication and testing of the 10-kW breadboard Mark II ECE system. This particular experiment is fueled with methanol and uses air supplied from an external source. The system presently utilizes the Mark II fuel processor components which are electrically heated. The purpose of the system test was to document performance of SOA components and their interrelation when used as part of a power producing system. The system test can utilize either one (1) or two (2) Ballard Mark V-design fuel cell stacks, each built for a nominal 5-kW power production level. Future work involves the incorporation of a turbocompression system and a combustor driven fuel processor. The present experiment, however, is designed to test the following parameters:

- ***Steady-state operation between 2 and 10-kW*** - A series of tests were designed to explore operation of the system at a variety of flow and power operating conditions.
- ***Integration with Traction Battery Hardware*** - The ECE system will be coupled to a ~ 10-kW battery supply. This hybrid power system then will operate at a variety of part-load and full-load conditions. The strategy will be to maintain battery SOC throughout the load range.
- ***Transient performance*** - Load transients will be designed to simulate the FUDS, or other simulated driving scenarios. Data will focus on the ability of various ECE system components to handle specified transients.
- ***System controls*** - Specific controls and sensors, as well as control algorithms, are being addressed.

Design, evaluation, and testing of the actual ECE system continued over an 8-month period. This section of the report summarizes the scope, direction, and test results of the research and development efforts conducted to produce a working ECE.

### 7.3.2 Mark II Development Program and Test Results

#### *System Test Stand*

A schematic of the ECE system test stand is presented in Figure 7.3.2-1. This illustration demonstrates the various components and the relationship of each component to the system. The fuel processing section of the demonstrator is on the right

of the figure with the fuel cell stack, condensers, water pump, and programmable load on the left. As stated, the present experiment uses air supplied by an external source; MFCs are depicted in the schematic. The system test has been designed so that the fuel processor system and fuel cell stacks, if so desired, can be independently operated. Consequently, the system test stand can also serve to further develop the fuel processor while permitting fuel cell stack testing on synthetic reformate. When fully integrated system operation is desired the automatic control valve on the reformate exhaust is closed and the fuel valves to the fuel cells stacks are opened. Oxidant to the fuel cell stacks continues to be supplied externally through the air MFC. Automatic control valves on the anode and cathode exhausts regulate the pressure within the fuel cell stacks.

Total fuel flow is measured by an orifice flow plate in the fuel processor subsystem exhaust line. Because of the difficulty of handling two-phase flow, that measurement is performed after the fuel processing product is cooled and most of the water has been condensed. "Makeup water" to the stacks is supplied from a laboratory deionized system and is automatically fed to the stack(s). Both of the anode and cathode exhaust streams are cooled to condense water within the streams prior to their venting; the air exhaust is vented overboard while the anode (hydrogen containing) exhaust is vented to a specially designed stack. Output power from the stacks is transferred to a pulse width modulator that controls the output power level; the electrical power is transferred through the load and dissipated into a water cooled resistor.

High efficiency scroll compressors and expanders, suitable for the 10-kW demonstrator with some modification, were specified, procured, and tested. Initial results confirmed that these components were highly efficient over a very broad operating range and could be installed on the demonstrator. However, during Phase I these devices were not mounted because that task would have detracted from more critical activities. Further, the air supply systems were already totally adequate for the planned experiments. The cathode air was supplied either from a tank trailer filled with compressed air ("breathing air") or from a 250-scfm oil-free air compressor, specifically acquired and installed for this project. As previously described, air exiting from the cathode exhaust condenser can either be exhausted through a manually-controlled valve or through an automatic control valve. These valves set the pressure in the cathode compartment. A computer-controlled stepping motor actuated valve, supplied by AC Rochester and developed for automotive service, has recently been installed to parallel (and replace) the manual valve. Oxygen consumption results in decreased cathode compartment pressure; when that occurs the automatic valve maintains this pressure at a preset level, opening or closing as required. This valve is sufficiently fast that rapid load changes can occur with no loss of cathode pressure; consequently, this valve and a similar anode valve are now used to control stack operating pressures throughout all test procedures.

Fuel cell stacks require adequate temperature control; cooling of the Ballard stacks is accomplished using a closed-loop system. The stack coolant flow is set by adjusting a manual valve that determines the percentage of bypass flow around a recirculating water cooling pump. Thus, the water pump flow is essentially constant and pressures within the total loop are normally low. Desired water flow rates are 10 lpm for each stack. Thermal management is achieved by including a tube-and-shell heat exchanger in the stack cooling water system; heat from the stack(s) is transferred to the laboratory cooling water system. The closed-loop stack

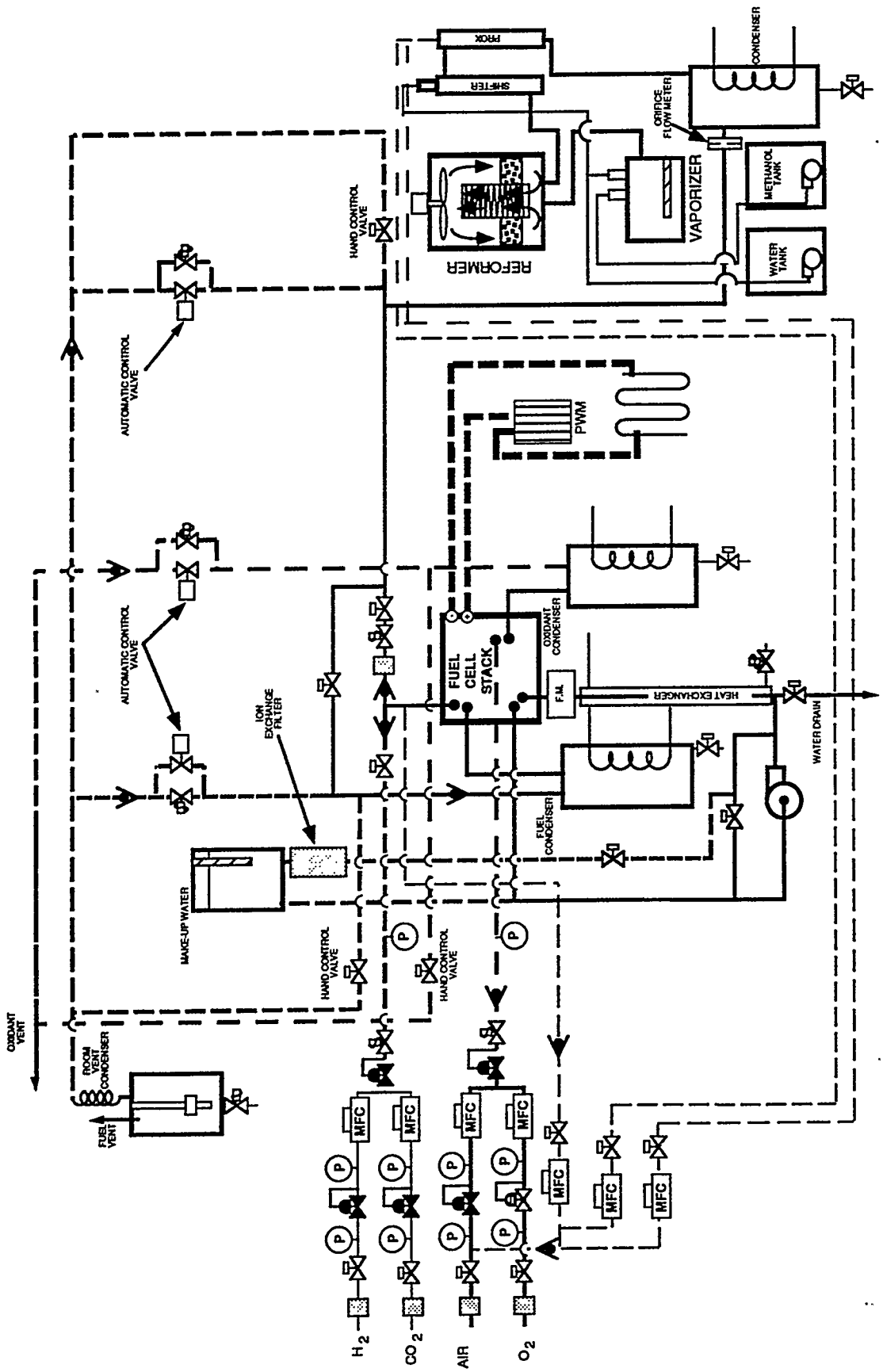


Figure 7.3.2-1. Simplified Schematic of the integrated ECE test stand. The functions of the various components are discussed in the text.

temperature is controlled by the water flow rate of the external coolant. A solenoid valve in the cooling water supply line alternatively closes and opens, as determined by the desired closed-loop temperature. A second bypass valve controls flow into the water makeup tank, where additional deionized water is added to the coolant flow as required. Because the stack coolant streams interact with both anode and cathode gas flows across various "humidifiers" during normal operation, some of these gases enter the water cooling loop. During "non normal" operation, large amounts of gas can enter the cooling loop. Both the makeup tank and special gas/liquid separators (not depicted in Figure 7.3.2-1) permit the gases to be vented from the cooling loop. Failure to do this can result in pump cavitation and degraded coolant flow. The makeup tank is located in an elevated position and provides a static pressure head.

The system stack tests were all accomplished with stacks that had first been tested with synthetic reformate (hydrogen-carbon dioxide mixtures) as anode feed. Because all test stacks demonstrated severe voltage loss on $CO_2$ containing gas feeds, it was decided to use anode air injection during all of the stack and system tests. (Later, improved Ballard stacks exhibited less voltage loss with carbon dioxide than the prototype stacks, but air injection was always beneficial. Additional improvements in anode alloy catalysts may further reduce the need for air injection; however, to date no large active area stacks produce adequate performance without some anode air injection.) The system tests described in this section all used an anode air injection feed of 2% (0.4% oxygen), metered in as a percent of the total anode flow.

### *Initial System Experimental Results*

Initial operation of the ECE system demonstrator occurred on 26 March 1993 using Ballard fuel cell stack SN-109, an early prototype. The results of this test are demonstrated in Figure 7.3.2-2 in which the switch to actual reformate (flowing from the Mark II fuel processor) is depicted. The initial comparison was performed at 100 amps (400 amps/ft$^2$); very little difference in average cell voltage compared to that for synthetic reformate-air was observed. Operation was held at 100 amps for approximately 1.2 hours; very stable performance was demonstrated. It was then decided to add some higher current tests. Stack current was increased to 125 amps and stable operation was again demonstrated. However, the PROX performance subsequently became unstable, leading to a significant CO breakthrough (1200 ppm CO); the resulting reduction in cell voltage caused an automatic "low voltage" shutdown. Since that time the demonstrator has operated up to 800 amps/ft$^2$ on one stack; a comparison of average cell voltages attained on 100% hydrogen, synthetic reformate, and actual reformate is presented in Figure 7.3.2-3. The demonstrated performance for actual reformate compared to synthetic reformate is virtually identical. The performance, is of course, considerably less than that attained on 100% hydrogen. This is primarily due to the use of an early Ballard prototype stack, SN-109, in these tests. Tests on improved stacks, such as SN-212, demonstrate little difference (40 mV) in performance between hydrogen and reformate at current levels up to 1000 amps/ft$^2$. Performance beyond 800 amps/ft$^2$ on Stack SN-109 was difficult to attain because of reductions in anode inlet pressure at higher flow rates due to excessive line and component pressure drops between the reformer and the anode compartment of the fuel cell stack. Although some design modifications to alleviate these pressure drops have been successfully implemented, reformate opera

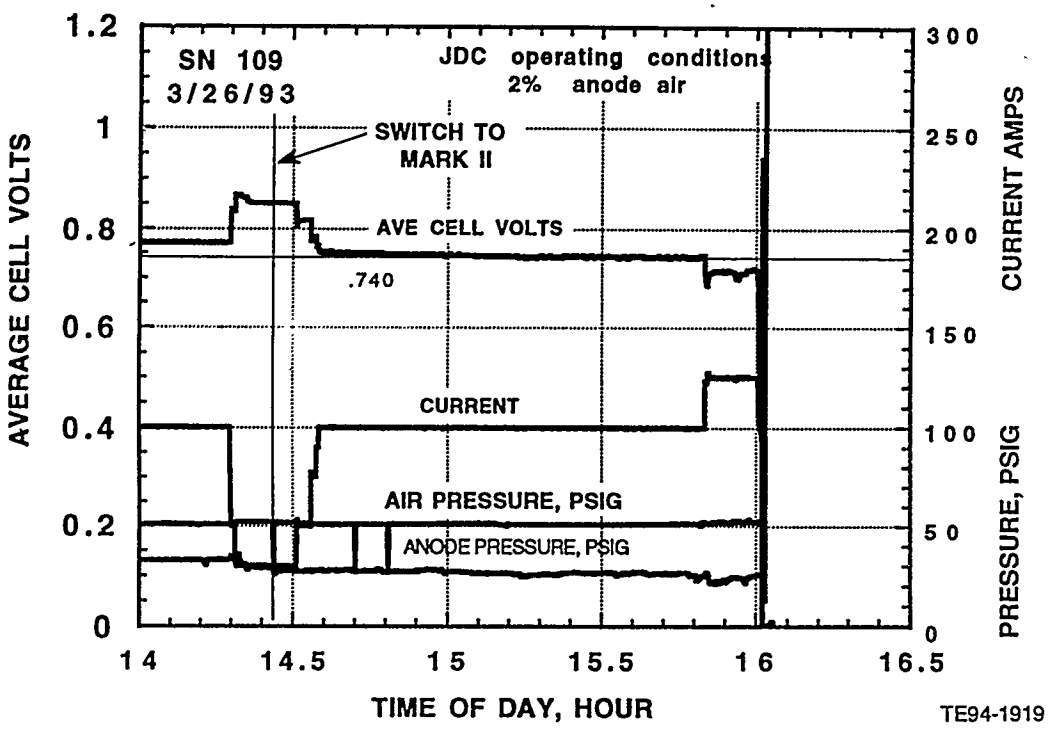


Figure 7.3.2-2. Operating data from the first integrated system test, Feeding Mark II Reformate Directly into a Ballard Power System's Prototype Stack. Stable operation was demonstrated at 100 amps (400 amps/ft$^2$).

tion beyond 800 amps/ft$^2$ on Stack SN-109 is difficult as this particular stack is very sensitive to slight changes in operating conditions at the higher current densities.

Mark II system testing intensified following the initial single stack performance test program. Subsequent effort concentrated on operational procedures and control options for the PROX units. Several different techniques were implemented to obtain uniform flow distribution into the short, wide monolith catalyst. The most successful of these incorporated tangential swirl injection in combination with an upstream piece of ceramic foam to develop a pressure drop in the gas stream, thereby forcing the total flow to spread out over the entire gas passage. Most of the effort to enhance the PROX operation, however, involved the development of better control strategies for the PROX units. Although the PROX units would initially operate successfully for several hours, successful CO conversion would suddenly cease to occur. Inadequate PROX operation was easily detected; the absence of a significant temperature gradient along the PROX flow path is one of the first indications.

It would be inappropriate to assert that all possible PROX operational conditions or control strategies have been explored. However, the most likely reason for the observed PROX unit instabilities was the result of the early strategies selected to control the fuel injection process into the vaporizer and, hence, the quality of the feed to the reformer and shifters. The injected steam to methanol ratio is now known to have experienced significant variations. At times a large fuel excess was inadvertently metered into the system, leading to a temporary very high dose of CO and/or breakthrough methanol. This CO concentration was so high exiting the shift zone

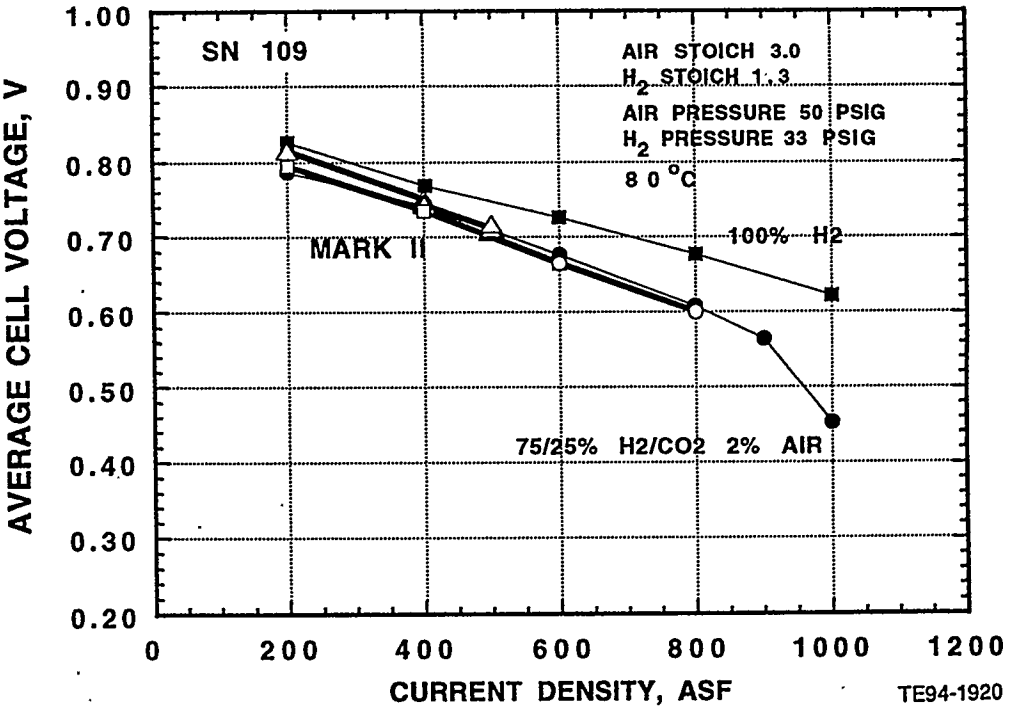


Figure 7.3.2-3. Polarization curves for the ballard power system's prototype stack used in the first integrated system test. Operation on pure hydrogen, synthetic reformate, and Mark II reformate are presented. Note that the Mark II reformate yields performance essentially the same as that obtained on synthetic reformate.

that it effectively neutralized the PROX unit platinum catalysts due to excessive CO adsorption thereby inhibiting oxidation. Clearly, if the metered air injection into the PROX units could have proportionally followed the CO increase, some level of PROX activity would have resulted. However, measurement of the "fuel flow" at the orifice could not detect sudden swings in the steam to methanol ratio. Conversely, when the steam to methanol ratio was held nearly constant, the PROX units demonstrated successful CO conversion. Consequently, considerable effort was expended to develop better control strategies for the fuel metering components. This approach was very successful, and the PROX instability process became a rare event. There are still times, however, when PROX unit instability occurs, and some of these cases are still not totally understood. One experimental difficulty is that the gas chromatograph sampling of the gases into and out of the PROX and at other points in the system takes approximately 3 minutes even with the use of sophisticated valves and multiple sample columns. A modern infra-red spectrometer (FTIR) offers the promise of far more rapid measurements; the incorporation of such an instrument in Phase II of the program will permit a definitive measurement of the relationship of CO concentration pulses and PROX operation.

As the system test program continued, increased experience and improved control strategies regarding the PROX section operation at higher chemical flow rates permitted the stack power to be increased. On 21 May 1993, the fuel cell stack as part of the system, operated at a current output of 150 amps (600 amps/ft$^2$) for an extended time period, refer to Figure 7.3.2-3. Very stable operation continued for

4.5 hours, after this time the PROX section became unstable. The PROX section was subsequently reactivated at high temperature using excess injected air for 20 minutes; stable operation was reestablished and the fuel cell current reset to 150 amps with successful operation continuing for 30 more minutes until the test was terminated. Measured CO concentrations flowing from the Mark II fuel processing PROX section during this period are presented in Figure 7.3.2-4. As is evident, most of these values were under the target level of 10 ppm except for a few high values measured during the reactivation period, near hour 14.

By 27 May 1993, successful Mark II ECE system operation was obtained at a fuel cell current of 200 amps (800 amps/ft$^2$). Average cell voltage data as a function of current density from the test conducted during that day are also presented in Figure 7.3.2-3; the results were attained using the Ballard Stack SN-109. (Recall that these early system tests were all conducted using this prototype Ballard stack, even though it did not perform well at high current densities on reformate/air reactants. Stack SN-109, however, was a proven, reliable workhorse, and at the early stages of the system tests, stressful experiments were more appropriately conducted on this stack rather than on one of the two later improved design stacks.)

### *Advanced System Test Results*

During the remainder of Phase I (fall of 1993) the Mark II system mass flow rates continued to increase; sufficient chemical flow was available to test two stacks simultaneously, but not at full power. Consequently, a second stack was added to the test stand with all of the input and output feeds connected in a parallel configuration. A single anode air injection mass flow controller was utilized to introduce air

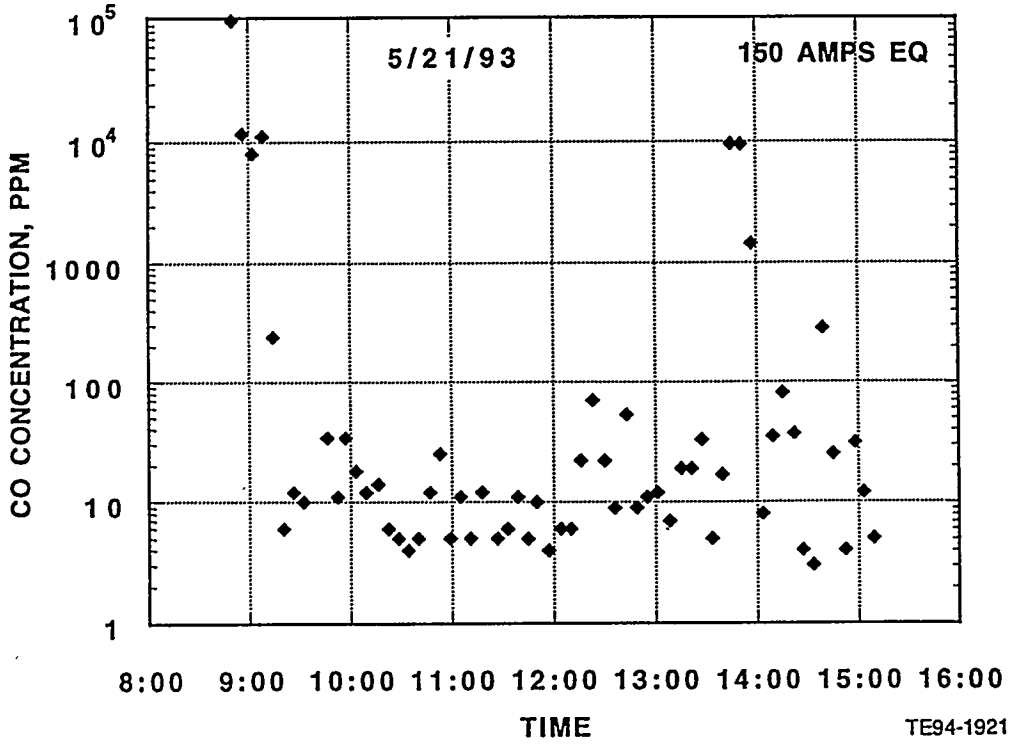


Figure 7.3.2-4. Carbon monoxide concentration at the Mark II fuel processor outlet during integrated system testing (see discussion in text).

directly into a "tee" connecting the two anode compartments. The cooling water, as well, was connected in parallel; both stacks were fully instrumented. The first two stack parallel configuration experiments were initiated on 1 August 1993 with Ballard fuel cell stacks, (SN-109 and SN-111), installed in the system. (Obviously either a parallel or series electrical stack configuration is possible; the first connection was selected so that the existing PWM could be used. The present PWM cannot accomodate the higher voltage of two stacks connected in series. Both series and parallel electrical configurations need to be tested; the parallel electrical configuration was chosen for the first experiments.) Testing of the two stacks continued for several weeks; the results of a typical experiment conducted on 1 September 1993, are presented in Figure 7.3.2-5. This particular experiment produced a total current of 300 amps (approximately 600 amps/ft$^2$ operating conditions in each stack) at 22.6 volts (each stack) achieving a gross electrical power output of 6.78-kW. Because the two stacks were connected in parallel, each stack voltage was identical; stack currents, of course, are slightly different and stack-dependent. At the 300 amp total current, the current output of Stack SN-108 was 152.6 amps while the current output of SN-109 was 147.4 amps. The average cell voltage was recorded as a function of the current setting (as controlled by the PWM) effectively producing a pseudo polarization curve; this is the data depicted in Figure 7.3.2-5. The two stacks had currents similar to each other through most of the experiment. The more common standardized performance polarization curve of these test data is presented in Figure 7.3.2-6 and compared with the performance polarization previously attained with synthetic reformate. A straightforward comparison of the results is somewhat misleading; the observed voltage reduction on actual reformate is due to a reduction in anode pressure at high fuel flow rates due to excessive line and component pressure drops between the reformer and the anode compartment of the fuel cell stack. Further, in order to maintain a reasonable pressure differential across the membrane the cathode pressure was reduced to 40 psig compared to the 50 psig utilized in the synthetic reformate tests. (Given the 6 psig reduction in the anode inlet pressure, the 10 psig reduction in cathode pressure was too severe). These prototype stacks are very sensitive to reformate pressure operating conditions. Anode pressure was decreased to a level that could be maintained for the entire polarization curve. It is anticipated that the two curves would coalesce if the actual reformate anode and cathode pressures were increased to match those for synthetic reformate data.

The last series of experiments conducted in Phase I of this program attained a total stack current (from two stacks) of 400 amps, (approximately 800 amps/ft$^2$ for each stack). The results of this test are presented in Figure 7.3.2-7 for the two Ballard stacks, SN-108 and SN-111, again connected in a parallel electrical configuration. Although the fuel processing hardware generated long term steady-state flow sufficient to power these two stacks at a total current of 350 amps, operation at 400 amps produced an average cell voltage that was not entirely stable. Although the gas chromatograph analyses indicated satisfactory, low CO levels, the anode inlet pressure was not sufficiently high to sustain stack. (It was possible to increase the fuel processor reformer pressure by increasing the vaporizer injector inlet pressure, but that procedure caused early pump failure.) Thus, while the last experiment achieved 400 amps, that condition cannot be considered continuous. The resulting performance polarization curve of this two stack experiment is presented in Figure 7.3.2-8. Again, while the synthetic reformate polarization curve appears to represent better performance results, that curve was achieved at significantly higher anode pressure. The two data sets would coalesce if the actual reformate an

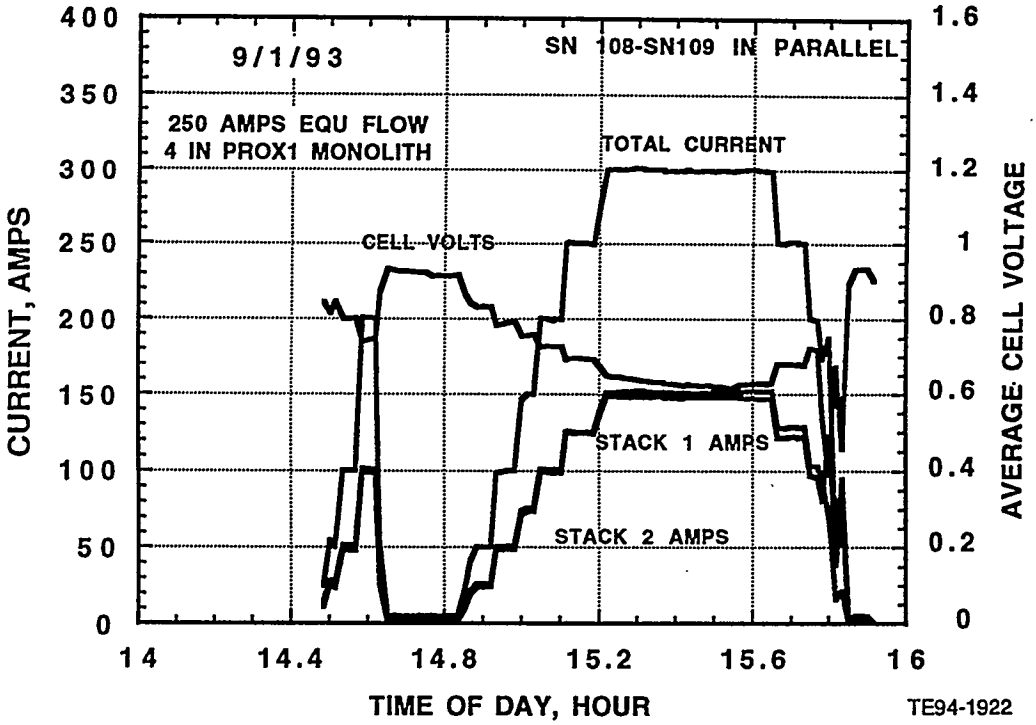


Figure 7.3.2-5. Test data for integrated system operation with two Ballard prototype stacks connected electrically in parallel. The individual stack currents were similar throughout the test.

ode and cathode pressures were increased to match the synthetic reformate data. This experiment did, however, produce a gross electrical output of 7.72 kW; the highest power output achieved during the Phase I test program.

A summary of the many experiments conducted using the Mark II ECE system is presented in Table 7.3.2-1. All of the results in the table were attained prior to modification of the Mark II fuel processor outlet flow path to include four plug flow reactors; thus, breakthrough methanol had not yet been reduced. Summary operating conditions for all major components are given from 100 to 500 amps equivalent in 50 amp steps. These data, representing results for the Mark II fuel processor and the fuel cell stacks reflect a composite data set for the latter period of the program. Gas chromatograph data were not always measured at every station when the stacks were operated on reformate. System results for the 100 and 150 amps conditions (400-600 amps/ft$^2$ equivalent each stack) were attained with a single stack (SN-109) while the higher current results were attained with two stacks operating in an electrically connected parallel configuration. The highest total current out of both stacks was 400 amps yielding a power level of 7.72-kW (gross electric).

The measured scale-weight data and resulting methanol and water flows are presented at the top of the table. The flow rate settings for vaporizer injector flows and water flow into the shift zone are presented under the entries for the affected component. Good agreement between these flow rate settings and the measured scale-weight data (which represent the actual methanol and water flows) is apparent.

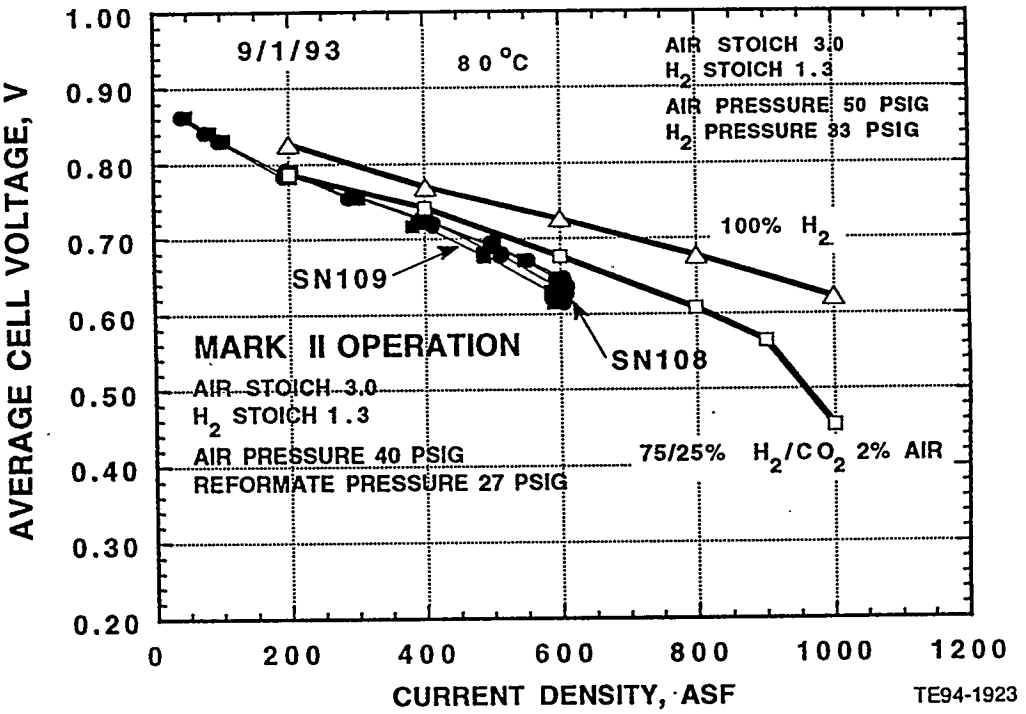


Figure 7.3.2-6. Polarization curves for integrated system operation of two Ballard prototype stacks connected electrically in parallel. Polarization curves for Stack SN-109 operating on pure hydrogen and synthetic reformate are shown for comparison. Note that the Mark II fuel processor line losses forced the stacks to run at lower anode pressures. The cathode pressure was also reduced in the system test on reformate fuel.

Data within the table demonstrate that the attempts to operate above 400 amps were not successful due to excessive methanol breakthrough (unmodified reformer and poor steam to methanol ratio control due to pump limitations) and large pressure drops within the Mark II fuel processing system. As described in Section 5.2.3, these problems are being addressed. In summary, appropriate design modifications have been completed and some of these modifications have already been successfully implemented. Because of the remaining system pressure drop limitations, steady-state operation between 2 and nearly 8-kW has been achieved. Traction battery hardware has been procured and system controls and sensors have been developed to permit the initiation of a transient performance test program.

### 7.3.3 Planned Mark II Power Source Utilization In Phase II

The overall objectives of the Phase II proposed program are the development, integration, and laboratory evaluation of the controls, sensors, ancillary interface subsystems, fuel cell stacks, methanol reformers, and surge battery subsystem(s) into a nominal 60-kW rated fuel cell power source brassboard ECE/battery-powered propulsion system. This brassboard power system includes a 30-kW fuel cell stack, 30-kW fuel processor, nominal 30-kW surge battery system, and all controls and ancillaries required to produce the nominal 60-kW rated system. As defined, approximately half of the maximum power of the system is developed by the ECE (fuel cell power source), by the surge battery subsystem. The surge battery subsystem is also

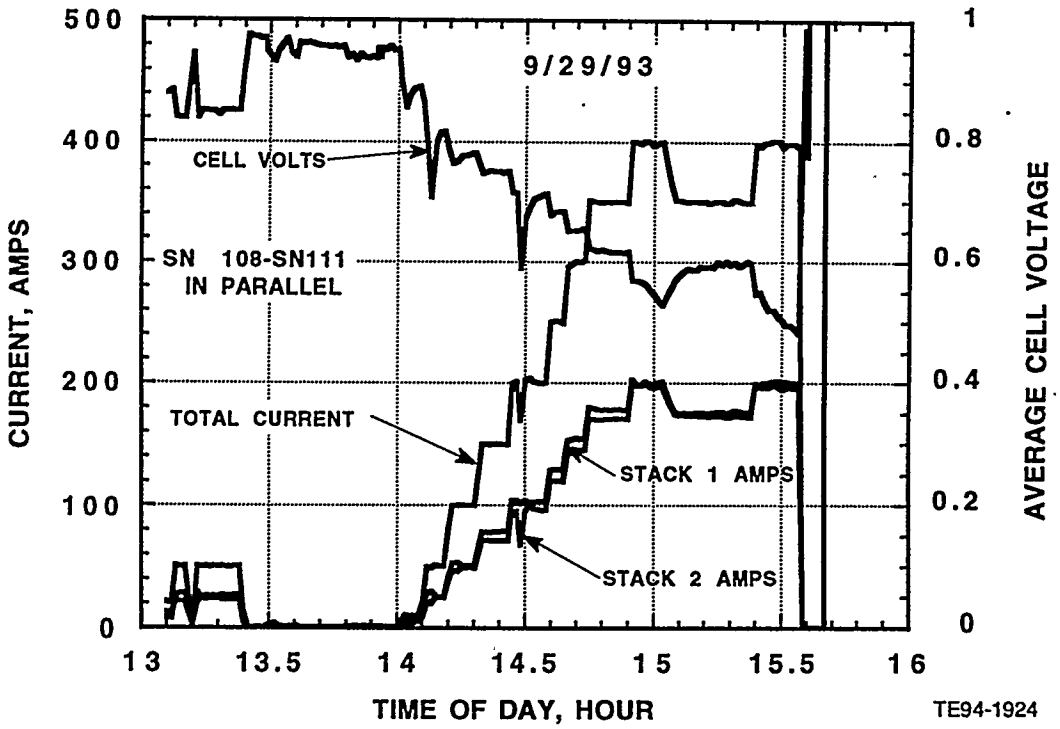


Figure 7.3.2-7. Test data for integrated system operation with two Ballard prototype stacks connected electrically in parallel. This test achieved a total current of 400 amps. Voltage could not be maintained at this level due to a low anode inlet pressure.

utilized during periods of cold-start and acts as a load leveler during transient operation. The exact ratio of ECE/battery power is not fixed but will depend on the results of reference power train design studies that are designed to evaluate the application of this unique propulsion system to automotive applications.

The Phase II, 30-month program schedule allows for early incorporation of monolith catalysts in the entire Mark II fuel processor and continuing improvements to the Mark II 10-kW system, including the incorporation of a battery subsystem, a compressor-expander subsystem, and an improved combustion driven fuel processor that incorporates monolithic catalysts. This 10-kW optimized system integration effort will be used to aid both the development and evaluation of the 30-kW fuel processor that is to be developed in this next phase and the controls, sensors, and ancillary interface subsystems that are required for the nominal 60-kW rated brassboard system.

These improvements to the existing Mark II system, combined with continuing component research and development efforts (membrane and electrode [catalyst] research, reformate/air reference fuel cell scaled prototype developments, and fuel processor catalyst design and development), lead directly to advanced 10-kW short stacks, which subsequently become 30-kW full-scale stacks, and a 30-kW multi-fuel combustor driven fuel processor. This improved Mark II system integration and optimization effort permits the fuel processor burner to be operated at least on liquid

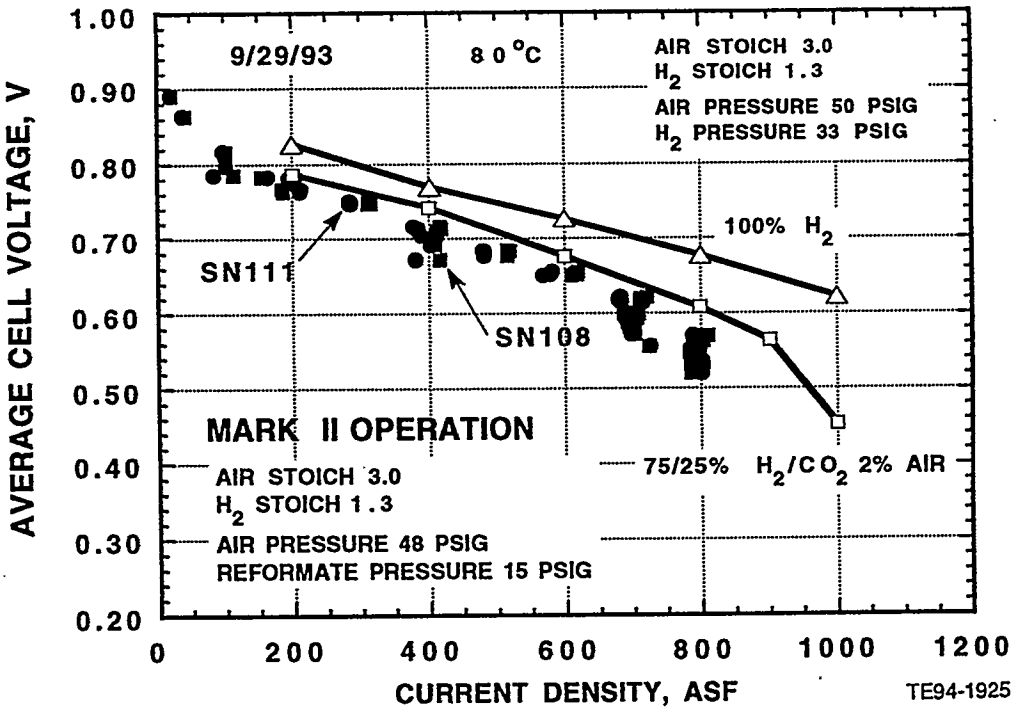


Figure 7.3.2-8. Polarization curves for integrated system operation of two Ballard prototype stacks connected electrically in parallel, with operation extended to 400 amps total (nominally 800 amps/ft² for each stack). Note that Mark II fuel processor line losses forced the stacks to run on actual reformate at much lower anode pressures at the higher current densities.

methanol fuel (not shown in the schematic) and, depending on its combustor's capability, possible on a mixture of the anode vent tail gas flowing from the fuel cell stacks and methanol. As is evident in this overall program description, the improved 10-kW system integration optimization effort plays a key role in developing the 60-kW brassboard system demonstrator.

Table 7.3.2-I.

System matrix representing operating conditions and results of the ECE integrated system test program.

| POWER LEVEL, AMPS EQU | 100 | 150 | 200 | 250 | 300 | 350 | 400 | 450 | 500 |
|---|---|---|---|---|---|---|---|---|---|
| ORIF FLOW RATE, SLPM | 43.4 | 65.5 | 87.4 | 108.2 | 131.1 | 152.8 | 174.1 | 194.8 | 216.6 |
| ORIF FLOW RATE, GM/MIN | 24.4 | 36.9 | 49.2 | 60.9 | 73.8 | 86.1 | 98 | 109.6 | 121.9 |
| SCALE MEOH FLOW RATE GM/MIN | 18.6 | 25.88 | 33.12 | 40.84 | 47.91 | 55.25 | 61.65 | 67.22 | |
| SCALE WATER FLOW RATE GM/MIN | 18.02 | 25 | 30.38 | 39.48 | 49.78 | 55.93 | 62.32 | 67.78 | |
| TOTAL STOICH | 1.72 | 1.72 | 1.63 | 1.72 | 1.85 | 1.80 | 1.80 | 1.79 | |
| VAPORIZER | | | | | | | | | |
| PRESSURE | 36 | 36.7 | 36.6 | 37.3 | 35.5 | 35.8 | 36.8 | 37.7 | 37 |
| TEMPERATURE | 125 | 123 | 120.5 | 112.8 | 118.2 | 118 | 117.5 | 111.3 | 113.8 |
| INJECTOR WATER RATE | 60 | 60 | 60 | 60 | 60 | 60 | 60 | 100 | 100 |
| INJECTOR MEOH RATE | 70 | 70 | 70 | 70 | 70 | 70 | 70 | 86 | 86 |
| WATER STOICH | 1.52 | 1.52 | 1.52 | 1.52 | 1.52 | 1.52 | 1.52 | 1.52 | 1.52 |
| REFORMER | | | | | | | | | |
| TEMPERATURE | 258.4 | 259.6 | 258.5 | 264.3 | 264.7 | 265.9 | 264.2 | 263.8 | 256.3 |
| CO PPM OUT | 14862 | 10429 | 11422 | 10166 | 16018 | 14577 | 16886 | 18799 | |
| MEOH PPM OUT | 3610 | 4768 | 7368 | 6896 | 6860 | 10641 | 17471 | 27319 | |
| SHIFT 1 | | | | | | | | | |
| TEMPERATURE | 250.7 | 244.1 | 242.5 | 254.5 | 246.4 | 242.9 | 244.6 | 228 | 214.8 |
| CO PPM OUT | 13949 | 12227 | 11132 | 13782 | 13358 | 10912 | 12421 | 12027 | |
| MEOH PPM OUT | 0 | 21 | 40 | 0 | 42 | 284 | 341 | 4760 | |
| SHIFT2 | | | | | | | | | |
| TEMPERATURE | 227.9 | 231.2 | 233.8 | 234.9 | 234.5 | 232 | 232 | 231.5 | 225.6 |
| WATER INJECTION, GM/HR | 100 | 150 | 200 | 250 | 300 | 350 | 400 | 450 | 500 |
| WATER STOICH | 0.2 | 0.2 | 0.2 | 0.2 | 0.2 | 0.19 | 0.19 | 0.19 | 0.19 |
| CO PPM OUT | 6048 | 6468 | 6777 | 8942 | 8826 | 7785 | 7725 | | |
| MEOH PPM OUT | 0 | 39 | 30 | 31 | 25 | 51 | 89 | | |
| PROX 1 | | | | | | | | | |
| CO PPM OUT | 713 | 555 | 393 | 1783 | 1785 | 944 | 1101 | | |
| MEOH PPM OUT | 0 | 0 | 0 | 0 | 0 | 0 | 0 | | |
| PROX 2 | | | | | | | | | |
| CO PPM OUT | 91 | 240 | 318 | 152 | 86 | 190 | 102 | | |
| MEOH PPM OUT | 0 | 0 | 0 | 0 | 0 | 0 | 0 | | |
| PROX 3 | | | | | | | | | |
| CO PPM OUT | 20 | 6 | 0 | 13 | 0 | 0 | 0 | | |
| MEOH PPM OUT | 0 | 0 | 0 | 0 | 0 | 0 | 0 | | |
| CONDENSER | | | | | | | | | |
| PRESSURE | 35.2 | 35.1 | 33.4 | 32.5 | 32.2 | 24.5 | 21.8 | 22.0 | 13.3 |
| TEMPERATURE | 34.9 | 35.5 | 36.5 | 36.6 | 34.7 | 38.4 | 35.7 | 35.7 | 36 |
| FUEL CELL | | | | | | | | | |
| STACK VOLTAGE, V | 26.00 | 23.30 | 25.55 | 23.80 | 22.00 | 21.63 | 19.29 | | |
| NO OF STACKS | 1 | 1 | 2 | 2 | 2 | 2 | 2 | | |
| FCELL AMPS | 100 | 150 | 200 | 250 | 300 | 350 | 400 | | |
| CELL VOLTAGE,V | 0.746 | 0.667 | 0.730 | 0.680 | 0.627 | 0.618 | 0.551 | | |
| FUEL CELL POWER KW | 2.6 | 3.495 | 5.11 | 5.95 | 6.6 | 7.5705 | 7.716 | | |
| DATE FPROC DATA OBTAINED | 10-Sep | 10-Sep | 14-Sep | 31-Aug | 1-Sep | 21-Sep | 22-Sep | 27-Sep | 24-Sep |
| DATE FCELL DATA OBTAINED | 14-May | 21-May | 14-Sep | 29-Sep | 1-Sep | 29-Sep | 29-Sep | | |

# VIII. PROGRAM TASK 7: FACILITIES AND DEVELOPMENT PLANS

## 8.1 INTRODUCTION

Phase I program activity under this task involved: (1) purchase and installation of equipment and instrumentation for use at GM sites and at the LANL JDC work-site, (2) design and construction of the initial increment of fuel cell experimental facilities at Allison's Plant 8, and (3) the formulation of a development plan for program work building on Phase I results, progressing to advanced fuel cell technology with higher system power output, improved fuel processor design, and control improvements, etc, all directed toward this program's ultimate goal of a proof-of-concept demonstration of an advanced fuel cell based power system in a fuel cell vehicle. The development plan has been detailed for the second phase of the program, and presented as a Contract Change Proposal in response to the DoE's solicitation and Statement of Work for Phase II.

The Phase II follow on effort will utilize the capabilities of the program team in developing and evaluating the advanced fuel cell/stack technology required for commercialization in vehicle applications. The primary objective of the Phase II effort will be a nominal 60-kW rated brassboard system (30-kW fuel cell stack, etc, plus a nominal 30-kW battery pack). Advanced fuel cell and fuel processor technology will be utilized at the LANL JDC work-site to produce components for the brassboard system. In addition, comprehensive evaluation of available and proposed fuel cell/stack technologies will be conducted as a basis for selecting and subsequently testing additional advanced fuel cell short stacks for comparison with the designs built at the JDC and at Ballard.

Concurrent with stack technology selection and development, the program team at the JDC will design and develop an advanced methanol fuel processor for use in the brassboard system. Phase II program efforts to optimize the Phase I 10-kW power system will result in system integration, operation, and control knowledge which will be a basis for design and integration of the brassboard system. Component research and development will continue in Phase II and serve as a basis for advanced technology in fuel processor and fuel cell design. Central to this task will be efforts directed toward improved membrane and electrode performance and improved transient response of system components.

The reference power train design and commercialization study efforts will also continue. The follow on effort will update the reference power train design based on developed capability to model transient operation of the fuel cell power system, plus additional considerations emerging during the course of vehicle analysis. The commercialization study will continue, examining a spectrum of candidate applications and affecting factors, while also focusing in depth on methanol fuel infrastructure requirements and economics, based on a methanol fuel specification developed during this program effort.

The 30-month follow on effort serves as a basis for additional effort beyond the Phase II brassboard system, leading to a power system of output and packaging characteristics matched to the needs of a selected vehicle. Integration of that sys-

tem and vehicle, plus proof-of-concept testing, will be included in post Phase II efforts.

## 8.2 FACILITIES DEVELOPMENT AT ALLISON

A major element of Allison's long term commitment to PEM Fuel Cell technology establishment is the capability to develop and test PEM Fuel Cell components and systems at Allison's Indianapolis Plant 8 Research Facility. During Phase I of the DoE PEM Fuel Cell program approximately 3200 $ft^2$ of floor space was renovated and supplemented with utilities to meet the requirements of a planned comprehensive PEM Fuel Cell laboratory. Specifications for the laboratory included requirements for electric power, HVAC, lighting, $CO_2$ fire safety and suppression, flammable gas detection, exhaust venting, explosion pressure venting panels, and stainless steel pipe routing of various gases, and water to test bench locations, etc.

The completed laboratory floor space is now ready for equipment installation that will eventually provide Allison with an on-site capability consisting of the following:

- PEM fuel cell materials development
- bipolar plate development
- reference fuel cell testing
- PEM fuel cell membrane and electrode development
- full scale PEM fuel cell stack R&D
- full scale PEM fuel cell stack testing
- catalyst material development
- PROX bench testing
- reformer and shifter bench testing
- vaporizer and combustor bench testing
- Mark II system testing
- controls and DACQ for all of the above

Allison's plan for Phase II of the DoE PEM Fuel Cell program includes installation of equipment necessary to achieve the following capability during calendar year 1994 and 1995:

- combustor bench testing
- full-scale PEM Fuel Cell 30-kW stack testing
- controls and DACQ for the above

## 8.3 PLANNING FOR FUTURE POWER SOURCE/VEHICLE POWERTRAIN INTEGRATION

As part of the Task 7.0 effort in the first program phase, a detailed plan for a 30-month Phase II effort was prepared and presented as a Contract Change Proposal for follow on effort under this contract. The planned Phase II effort includes evaluation and selection of advanced PEM fuel cell and fuel processor technology, and system integration improvements based on work with the Phase I 10-kW system.

The Phase II program schedule allows for early incorporation of monolith catalysts in the entire Mark II fuel processor and continuing improvements to the Mark II

10-kW system, including the incorporation of compressor-expander and surge battery subsystems and advanced sensors and controls. These improvements to the existing Mark II 10-kW system combined with continuing component research and development efforts (membrane and electrode [catalyst] research, reformate/air reference fuel cell scaled prototype developments, and fuel processor catalyst design and development) lead directly to advanced 10-kW short stacks, which subsequently become 30-kW full-scale stacks, and a combustor driven fuel processor. An improved 10-kW fuel processor will first be integrated into the existing Mark II system. As is evident in this overall program description, the 10-kW optimized system integration optimization effort plays a key role in developing the 60-kW brassboard system demonstrator. It permits early advanced smaller scale fuel processor and system controls developments that evolve into the 60-kW brassboard system.

Task 7.0 also calls for identifying future R&D needs, preparation of a plan for scale-up to a full-size system, and a refinement of the methods for achieving system cost reductions. The plan shall include a description of the required tasks with a multi-year time schedule and an estimate of the technical effort required to complete the scale-up and integration of a PEM fuel cell powered propulsion system into a test-bed vehicle.

GM views the Phase II effort as the second step of a multiphase eight year program that develops an advanced reformate/air PEM fuel cell power plant and culminates in an actual fuel cell/hybrid vehicle demonstration. A general milestone schedule for this multiphase effort is shown in Figure 8.3-1. Allison will continue the establishment of a new fuel cell facility during the course of this program. This includes acquisition of facilities, manpower, and capability to transform the current PEM fuel cell SOA from R&D to a commercial, practical power plant capability. Because of the forward planning nature of this task, its sub-tasks are discussed together.

The first phase initiated with the letter contract award for the first phase of this program and extended over a 38-month period. The primary objectives of this first phase have been the development of a 10-kW power source system evaluator and delivery of an Initial Conceptual Design Study and a Trade-Off Analysis Report for the automotive application of PEM fuel cells (the latter denoted as RPD on Figure 8.3-1).

The second phase of the program will extend over a 30-month period. The primary objective of this phase is the development of a 60-kW brassboard power plant. The second phase builds on the fuel cell and fuel processor R&D and system integration knowledge evolved from the first phase activities. Both the 30-kW fuel cell and fuel processor are expected to directly result from the component activities initiated in the first phase. Other activities occurring during this second phase include system optimization of the 10-kW power source system.

The third phase of effort depicted in Figure 8.3-1 involves both resizing the system to achieve vehicle-required power output (versus brassboard system) and packaging the power system to meet vehicle size requirements. Simultaneous achievement of these goals in the time frame shown is an aggressive goal; Phase II effort is planned in such a way as to reduce the risk and additional effort involved in the Phase III activity.

GM's proposed power plant characteristics for the fuel cell powered vehicle demon

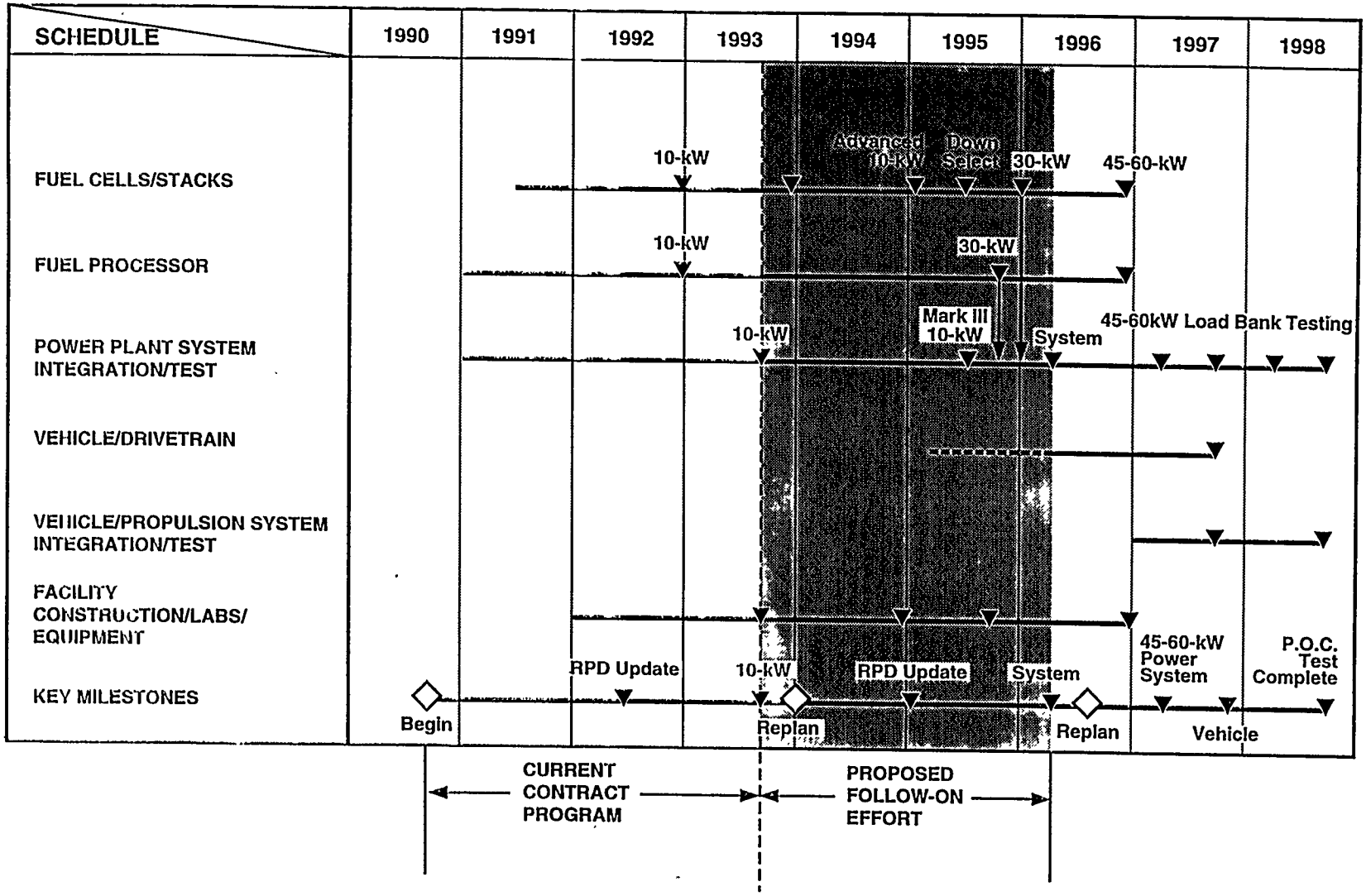


Figure 8.3-1. Preliminary multiphase milestone schedule.

VS93-1138A
TE93-878

strator are ambitious and based on emerging technology. The proposed power plant will have: minimal onboard battery requirements, fast system transients, rapid start-up and shut-down times, cold temperature survivability, wide power range with low idle power, high efficiency with minimal pollution, and power density and packaging similar to current engines. Technology goals include an installed 90% energy efficiency improvement (accompanied by a 40% reduction in $CO_2$) with a concurrent 90% reduction in regulated emissions as compared to today's internal combustion engines.

## 8.4 ALTERNATIVE APPLICATIONS

While this program is directed primarily toward a proof-of-concept application of the PEM fuel cell power system in a selected passenger vehicle, the key technologies to be developed and demonstrated are applicable to a variety of other transportation applications, plus stationary applications which are also the target of other DoE studies and initiatives. The passenger vehicle application requires high density packaging, vibration/shock tolerance, low temperature survivability, and low cost mass market applications. These requirements suggest that a PEM fuel cell power system meeting the goals of this program would meet or exceed the requirements of many other applications. The basic technological advances developed in this program would then be applicable across the whole spectrum of system designs for alternative applications.

### 8.4.1 Phase I Investigations

A fuel cell locomotive application was considered during Phase I in concert with the emphasis placed on this application by California's South Coast Air Quality Management District (SCAQMD). SCAQMD and the railroads, along with locomotive builders, recognize that there are many problems (design, infrastructure, etc) to be solved in accomplishing fuel cell applications to one or several types of locomotives. At the same time it appears that there is some general consensus that locomotives may provide an early transportation application for fuel cells, and that fuel cells are the only technology that can offer a 90% to 100% emissions reduction for Los Angeles Basin Rail Operations.

Furthermore, the cost to develop and demonstrate a small fleet of prototype fuel cell locomotives would be roughly in the range of $25 to $80 million; such a program could only be supported by a public-private partnership with major emphasis on federal funding. Clearly, the locomotive and railroad industries must be intimately involved in a fuel cell locomotive program.

Important considerations exploring fuel cell technology applications for locomotive power include the fact that locomotives require durable, very long-life power plants, and are relatively few in number. Therefore, locomotives alone are unlikely to drive the market for transportation fuel cell applications; however, locomotives can help absorb and amortize the higher initial costs of fuel cell power-plants compared to cars and trucks. It is also anticipated that fuel cell application success with locomotives would have major implications for other fuel cell powered ground transportation systems.

Looking specifically at the Los Angeles basin, railroads are a relatively small, but significant, source of $NO_x$ emissions (about a 4% contribution to the basin). Therefore, air quality considerations alone are unlikely to drive the market for fuel cell locomotives. Further, the Los Angeles basin locomotive market probably could not produce its own fuel infrastructure. SCAQMD, however, has brought to focus the consideration of fuel cell power in locomotives; its priority mandate is to determine whether the Air Quality Management Plan target of 90% emissions reduction can be met with fuel cell locomotives. Among the remaining issues involving fuel cell application to locomotives are:

- ***What are the most appropriate fuel cell technologies?*** There appears to be an inverse relationship between the technological and commercial maturity of the candidate fuel cells and their long-term viability as locomotive power-plants. PEM and Solid Oxide fuel cell technologies are the least mature, but offer the best performance and packaging prospects.

- ***What are the most appropriate fuels?***

- ***What are the relative merits of demonstrating the following?***
  single-axle power unit
  two-axle, 1-MW mule
  four-axle, 2-MW switcher
  four or six-axle, 5-MW line haul

- ***Should conversions of existing locomotives initially be pursued, or do only "ground-up" new designs make sense?***

- ***What are the relative merits of major propulsion system changes (e.g., AC drive, regenerative braking, etc.), and when is the best time to incorporate them?*** These technological advances and their application to locomotives are attracting substantial attention.

### 8.4.2 Phase II Considerations

As noted in Section 8.4.1, the technology advances developed in this transportation applications program are, in general, common to other successful applications of PEM fuel cell power systems. Considering the system size and justifiable cost, the locomotive is a logical first market for fuel cell propulsion. The SCAQMD fuel cell locomotive program is underway and will likely result in a funded program for the design and development of a demonstration locomotive.

Fuel cells are also of interest in the bus market due to their potential to reduce emissions and eliminate the smell of diesel exhaust. The federal government provides the majority of the funding (usually 80%) for urban buses. Only a few thousand buses are built per year so this market alone would not justify the development of a fuel cell propulsion system. Fortunately, the same fuel cell engines should be useful for heavy trucks. If the cost of such fuel cell propulsion systems were on the order of $200/kW fuel cells could probably be able to capture a significant portion of the Class 7 or 8 truck markets, on the order of 10,000 units per year (assuming long life, and low maintenance and fuel costs). If the price were on the order of $100/kW the sales to smaller commercial vehicles could establish a commercially viable market.

The DoE projects that by the year 2010 the energy consumption (and presumably pollution) of commercial vehicles will exceed that of private cars. It is likely that this phenomena will be accompanied by aggressive limitations on the emissions from trucks and other commercial vehicles. This may require changes to new engine technologies, such as fuel cells, as there is little to be gained by improvements in vehicle aerodynamics or structures since the empty weight of today's vehicles represent a smaller portion of their gross weight.

Several additional alternative application possibilities for fuel cell propulsion and power generation should also be considered. These include maritime, military, electric power generation, recreation and even small appliances. While the design details and packaging will differ for each of these applications it should be possible to develop a common technology which can be adapted for each of the markets. Major system elements might include two or three sizes of fuel cell elements such as individual sizes for:

- small appliances and other applications involving a fraction of a kilowatt or more of power
- intermediate power levels (10 to 50-kW)
- high power applications (100+ kW).

Different numbers of fuel cells could be grouped in stacks to provide the incremental power size of growth within each family of fuel cell systems.

Another critical element in the ability to provide the needs for diverse markets involves the development of a family of reformers which would enable the electrochemical power systems to utilize a wide range of fuels. The design of the "balance of plant" of the system should be configured in a manner which provides simple intermediate power levels at low cost.

While the major attention at the federal level has been on fuel cell powered passenger cars, because of the emphasis on reducing their emissions and energy consumption, commercial vehicles may be a more attractive first market. The truck companies and railroads will pay for lower life cycle costs and increased reliability.

Fuel cells are a logical choice for marine propulsion if they can use a fuel which is both inexpensive and easily transported. There is one existing (planned) project for a fuel cell powered mega-cruise ship. It would use three (3) power-plants, each delivering nearly 35 megawatts; this very ambitious project has received significant visibility.

The main military market, at least to date, still involves tank propulsion and field power. These requirements still exist, although probably in different forms than usually envisioned. Reformers capable of accepting a wide range of fuels would significantly increase the interest of the military in fuel cells. The military is still chiefly interested in diesel fuel, but utilization of this fuel involves very difficult fuel processing problems for use in low-temperature fuel cells.

Electric power generation, another area of fuel cell system application, can be divided into three areas of interest:

- ***Utility*** - The largest potential market for fuel cells is in utility power. DoE forecasts indicate that by the end of the century utilities will be spending from $50 to $100 billion per year on new electrical generating capacity (assuming $1,500/kW). The phosphoric acid fuel cell is not a major candidate for these markets since combined cycle power-plants can provide higher efficiency, are more fuel tolerant, and are probably less expensive. IFC quotes $1,500/kW; an Allison/GM economics study (1986) indicated that the cost of combined cycle power-plants could be as low as $750/kW.

  The PEM fuel cell could be particularly attractive for use in distributed power installations, which the utilities are finding to be less costly (reduction of the need to upgrade distribution networks) but difficult to locate, because of noise and environmental considerations; fuel cells would eliminate or minimize these considerations.

- ***Industrial*** - Increased requirements for electrical power by industry and commercial companies has led to the acquisition of independent power by many large companies. "Cogeneration" plants provide high total efficiencies by using the "waste heat" of the cogenerator (e.g. gas turbine) for process or space heating. Fuel cells could provide similar advantages and may be more economical in small units than gas turbines or diesels. The primary competitor may be the Stirling engine.

  The size of this very competitive market is not well defined but may exceed $20 billion per year.

- ***Residential*** - If fuel cells costs are decreased to under $100/kW the installation of a fuel cell in a home, where it could provide both electrical power and heating, could become very attractive, particularly in new developments where the utility is not yet providing adequate power.

  The market for fuel cell energy conversion devices for the basic new home market may be on the order of $2 to $4 billion per year. However, if the prices were on the order of $50/kW a large retrofit market could develop which would lead to a high volume sales during the retrofit period.

  Fuel cell advocates have also noted the recreational application potential for fuel cells. Examples include electrical power for back packers and onboard power for yachts where the noise of current energy conversion devices can be objectionable. The opportunity that this market provides to demonstrate and obtain field experience in the application of fuel cell technology may be as important as any direct commercial benefit to the suppliers.

An additional area of application for fuel cells is that of small appliances. This is exemplified by one suppliers response to the need for electrical power for TV cameramen; currently they have to carry many heavy batteries. Other high value fuel cell applications include power for lap top computers and for the increasing amount of electronics carried by the Army infantry. The fuel cell power concept for these applications involves a small cell which is fueled by hydrogen. The hydrogen is sup-

plied in small pressurized containers which can be discarded or recharged after use. Fuel cell power for other small appliances includes powered tools for carpenters and others who work at remote sites, lawn mowers, home tools, etc., particularly for regional areas which do not meet air quality standards.

## LIST OF ABBREVIATIONS

| | |
|---|---|
| BOP | balance of plant |
| CO | carbon monoxide |
| CO2 | carbon dioxide |
| DACQ | data acquisition |
| DOE | Department of Energy |
| ECE | electrochemical engine |
| ECESYS | electochemical engine system |
| FCSYS | fuel cell system |
| FET | field effect transistor |
| F.S. | full scale |
| GM | General Motors Corporation |
| JDC | Joint Development Center |
| LANL | Los Alamos National Laboratory |
| LHV | lower heating value |
| MEA | membrane and electrode assemblies |
| MFC | mass fuel controller |
| MFM | mass flow meter |
| NAO R&D | North American Operations Research and Development |
| PEM | proton-exchange membrane |
| PFSA | sulfonic acid functionalized fluoropolymer |
| PROX | preferential oxidation |
| PTFE | polytetrafluoroethylene |
| PWM | pulse width modulator |
| R&D | research and development |
| RPD | reference power train development |
| RTOS | real time operating system |
| SCAQMD | South Coast Air Quality Management District |
| SOA | state-of-the-art |
| TASC | The Analytical Sciences Corporation |
| T.B. | test bench |
| ULEV | ultra-low emission vehicle |
| VSIM | vehicle simulation model |

# IX. REFERENCES


2.1-1 Stroh, K. R., Hedstrom, J. C., Vanderborgh, N.E., and Inbody, M. A., "Phase I Final Report: Performance Analysis of the Electrochemical Engine", Los Alamos National Laboratory Report to General Motors, in Preparation and Review.

2.1-2 Stroh, K. R., McFarland, R. D., Hedstrom, J. C., Inbody, M. A., and Vanderborgh, N. E., "FCSYS: A Steady-State Simulation Code for Fuel-Reforming and Fuel Cell Power Systems", Los Alamos National Laboratory Report to General Motors, in Preparation and Review.

2.1-3 "Initial Conceptual Design Report," Allison Gas Turbine Division of General Motors Corporation, Allison EDR 16194, dated November 30, 1993, also published as DoE Report DoE/CH/10435-01.

2.1-4 "Trade-off Analysis Report," Allison Gas Turbine Division of General Motors Corporation, (Allison EDR to be published), (DoE Report to be published).

2.1-5 "Fuel Cell Infrastructure and Commercialization Study," Albert Sobey and Associates, Allison Gas Turbine Division of General Motors Corporation, Allison EDR 17080, dated September 29, 1994, currently under revision by GM, (DoE Report to be published).

2.2.2-1 Springer, T. E., Murray, H. S., and Vanderborgh, N. E., "Methanol Reformer System and Design for Electric Vehicles," 20th Intersociety Energy Conversion Engineering Conference, August 18-23, 1985, Miami Beach, FL (LA-UR-85-1810).

2.2.2-2 Vanderborgh, N. E., Spirio, C. A., and Huff, J. R., "Advanced Fuel Systems for Transportation Applications," PEO Fuel Cell Seminar, October 26-29, 1987, The Hague, Netherlands (LA-UR-87-2893).

2.2.2-3 Vanderborgh, N. E., and Guante, J., "Methanol Fuel Processing for Low Temperature Fuel Cells," National Fuel Cell Seminar, October 1988, Long Beach, CA.

2.2.2-4 McCullough, J. E., and Hirschfeld, F., "The Scroll Machine - An Old Principle With a New Twist," Mechanical Engineering, December 1979, pp. 46-51.

3.3 Swathirajan, S., and Mikhail, Y. M., U.S. Patent No. 5,272,017, December 21, 1993, "Membrane-Electrode Assemblies for Electrochemical Cells."

5.1-1 "Device for Staged Carbon Monoxide Oxidation," N. E. Vanderborgh, et al., Allison Gas Turbine Division of General Motors Corporation, U.S. Patent No. 5,271,916, dated December 21, 1993.